

# UC Berkeley

## UC Berkeley Electronic Theses and Dissertations

### Title

Sub-nanometer Porous Membrane Based on Cyclic Peptide-Polymer Conjugate and Block Copolymer

### Permalink

<https://escholarship.org/uc/item/9hb6f82f>

### Author

Zhang, Chen

### Publication Date

2015

Peer reviewed|Thesis/dissertation

Sub-nanometer Porous Membrane Based on Cyclic Peptide-Polymer Conjugate and  
Block Copolymer

By

Chen Zhang

A dissertation submitted in partial satisfaction of the

requirements for the degree of

Doctor of Philosophy

in

Engineering - Materials Science and Engineering

in the

Graduate Division

of the

University of California, Berkeley

Committee in charge:

Professor Ting Xu, Chair

Professor Fiona Doyle

Professor Kevin Healy

Professor Jeffrey Long

Summer 2015

Sub-nanometer Porous Membrane Based on Cyclic Peptide-Polymer Conjugate and Block Copolymer

Copyright © 2015

by

Chen Zhang

# Abstract

Sub-nanometer Porous Membrane Based on Cyclic Peptide-Polymer Conjugate and Block Copolymer

By  
Chen Zhang

Doctor of Philosophy in Materials Science and Engineering

University of California, Berkeley

Professor Ting Xu, Chair

Membrane separation is a field of both industrial and academic importance. Current technology is largely based on polymeric materials, and to a less extent other inorganic materials such as ceramics and metals. While developments in materials properties and membrane structures are constantly evolving, there are two challenges that need to be circumvented for better performance, i.e. the control over the pore structure and the chemical flexibility in modifying pore surface. “Bottom-up” approach to construct composite membranes using nanotubes in polymeric matrix is an effective route in fabricating membranes with well-defined architecture and tunable pore surface chemistry. This dissertation focuses on characterization and evaluation of cyclic peptide nanotubes (CPNs), a natural protein channel mimetic, in constructing sub-nanometer composite membranes with a cylinder-forming block copolymer (BCP) matrix in thin films. The fundamental understanding of the self-assembly of the CPNs from the building blocks establishes the foundation in utilizing the unique feature of CPNs to ensure precise structural control over the dimensions of the 1D nanotubes. The knowledge gained from the co-assembly of CPNs and BCP matrix in thin films allows further processing of the nanotubes to form well-aligned transport channels, establishing the guidelines in fabricating sub-nanometer porous membranes with and without surface chemistry modification. By identifying the key parameters in the membrane fabrication processes, design features for creating high-performance CPN based membranes can be determined and expanded. This indeed provides many exciting opportunities in developing new composite membranes with superior separation performances.

The self-assembly of cyclic peptide (CP) subunits forming high aspect ratio nanotubes is driven by strong intermolecular hydrogen bonding. To modulate and tune the growth of CPNs, polymers are conjugated to the exterior of the peptide subunits,



resulting in the formation of polymer covered-CPNs (pc-CPNs). Due to the restriction of intermolecular hydrogen bonding, the conjugated polymer chains enter a confined space set by the hydrogen bonding distance. The entropic penalty associated with deforming the conjugated polymers serves as an opposing force destabilizes nanotube structure, while the enthalpic hydrogen bonding drives the nanotube formation. A delicate balance between the enthalpic driving force and the entropic destabilizing force enables one to modulate the growth of the nanotubes. Thus, the dimensions of the resultant pc-CPNs can be supervised simply by regulating the extent of the entropic penalty from the conjugated polymer chains.

In co-assembling CPNs and BCP matrix in thin films, both thermodynamic and kinetic parameters are critical to ensure homogeneous thin film morphology with well-aligned CPN channels at the center of the cylindrical microdomains of the BCP oriented normal to the substrate surface. The balance between the enthalpic interactions between the pc-CPNs and BCP and the entropic cost of polymer chain deformation gives rise to only one nanotube in the cylindrical microdomain. Due to the dynamic nature of CPN formation, preaggregation of the nanotubes causes defects of lay-down nanotubes at the membrane surface, hence compromising membrane quality and integrity. As a result, controlling the kinetic pathway of the co-assembly process is vital to fabricate high quality membranes for separation. Two simple approaches targeting two separate aggregation contributors have been developed to effectively prevent preaggregation of CPNs, resulting in high quality membranes suitable for molecular separation.

With the advancement in incorporating functional groups to the constituting peptide subunits, the interior surface of the CPNs can be further functionalized. Membranes have been fabricated using both the unmodified and modified CPNs, in which gas separation of CO<sub>2</sub>/CH<sub>4</sub> mixture and hydronium ion transport were performed. In general, the incorporation of the CPNs improves the overall performance of the membranes, likely by providing additional pathways for the permeating molecules. Differences in the separation behaviors of the regular CPNs and the methyl-modified CPNs are observed for both gas separation and hydronium ion transport, where higher selectivity for CO<sub>2</sub> over CH<sub>4</sub> is seen for the methyl-modified CPNs. The local dipole interactions with CO<sub>2</sub> molecules as well as the reduction in pore size are speculated to induce the differences in the performances of unmodified and unmodified CPNs.

These studies indeed establish the foundation in fabricating sub-nanometer porous membranes using self-assembled CPNs and BCP matrix in thin films. A delicate balance between the enthalpic and entropic contributions results in precise control over the structures of the nanotubes and the membranes. This unique “bottom-up” strategy demonstrates to be an effective platform in constructing new family of membranes for chemical separations.

# Sub-nanometer Porous Membrane Based on Cyclic Peptide-Polymer Conjugate and Block Copolymer

## Table of Contents

|   |           |
|---|-----------|
| <b>Chapter 1 Challenges and Opportunities in Membrane Technology .....</b>                    | <b>1</b>  |
| § 1.1 Introduction .....  | 2         |
| § 1.2 Membrane Technology.....  | 2         |
| 1.2.1 Membrane Separation.....  | 2         |
| 1.2.2 Membrane Material .....   | 4         |
| 1.2.3 Membrane Structure .....  | 5         |
| § 1.3 Transport Channels.....   | 12        |
| 1.3.1 Biological Channels .....   | 12        |
| 1.3.2 Synthetic Channels.....   | 18        |
| § 1.4 Cyclic Peptide Nanotubes .....  | 23        |
| 1.4.1 Cyclic Peptide Sequence Design and Synthesis.....                                       | 25        |
| 1.4.2 Cyclic Peptide Conjugates.....  | 29        |
| § 1.5 Conclusion and Outlook.....   | 35        |
| § 1.6 General Approach and Synopsis for Subsequent Chapters .....                             | 35        |
| <br>  |           |
| <b>Chapter 2 Self-assembly of Cyclic Peptides and Cyclic Peptide-Polymer Conjugates .....</b> | <b>37</b> |
| § 2.1 Introduction .....  | 38        |
| § 2.2 Results and Discussion.....   | 40        |
| § 2.3 Conclusion.....   | 47        |
| § 2.4 Experimental .....  | 47        |
| 2.4.1 Materials.....  | 47        |
| 2.4.2 Peptide synthesis and PEG conjugation.....  | 48        |
| 2.4.3 Reversed-Phase High-Pressure Liquid Chromatography (RP-HPLC).....                       | 49        |
| 2.4.4 Fourier Transfer Infrared Spectroscopy (FTIR).....                                      | 49        |
| 2.4.5 Formation of pc-CPNs .....  | 49        |
| 2.4.6 Statistical Analysis of pc-CPN Length.....  | 49        |

|   |               |
|---|---------------|
| <b>Chapter 3 Co-assembly of Cyclic Peptide-Polymer Conjugate and Block Copolymer in Thin Films.....</b> | <b>50</b>     |
| § 3.1 Introduction .....  | 51            |
| § 3.2 Results and Discussion.....   | 52            |
| § 3.3 Conclusion.....   | 59            |
| § 3.4 Experimental .....  | 59            |
| 3.4.1 Materials.....  | 59            |
| 3.4.2 Reversed-Phase High-Pressure Liquid Chromatography (RP-HPLC).....                                 | 60            |
| 3.4.3 MALDI-TOF Mass Spectrometry .....   | 60            |
| 3.4.4 Grazing Incident Small Angle X-ray Scattering (GISAXS) .....                                      | 60            |
| 3.4.5 Dynamic Light Scattering (DLS) .....  | 60            |
| 3.4.6 Fourier Transfer Infrared Spectroscopy (FTIR).....  | 60            |
| 3.4.7 Nuclear Magnetic Resonance Spectroscopy (NMR).....  | 61            |
| 3.4.8 Thin Film Fabrication.....  | 61            |
| <br><b>Chapter 4 Interiorly Modified Cyclic Peptide and Its Assembly Behavior.....</b>                  | <br><b>62</b> |
| § 4.1 Introduction .....  | 63            |
| § 4.2 Methyl-modified Cyclic Peptide and Conjugates .....   | 65            |
| § 4.3 Co-assembly in Block Copolymer Thin Films.....  | 71            |
| § 4.4 Conclusion.....   | 77            |
| § 4.5 Experimental .....  | 78            |
| 4.5.1 Materials.....  | 78            |
| 4.5.2 Synthesis of Mba-8CP .....  | 78            |
| 4.5.3 Reversed-Phase High-Pressure Liquid Chromatography (RP-HPLC).....                                 | 79            |
| 4.5.4 MALDI-TOF Mass Spectrometry .....   | 79            |
| 4.5.5 Fourier Transfer Infrared Spectroscopy (FTIR).....  | 79            |
| 4.5.6 Dynamic Light Scattering .....  | 79            |
| 4.5.7 Co-assembly Thin Film Fabrication.....  | 79            |
| <br><b>Chapter 5 Transport Behavior of Sub-nanometer Porous Membranes .....</b>                         | <br><b>80</b> |
| § 5.1 Introduction .....  | 81            |
| § 5.2 Membrane Transport .....  | 83            |
| 5.2.1 Gas Transport Mechanism.....  | 83            |
| 5.2.2 Gas Transport Measurement .....   | 87            |

|   |            |
|---|------------|
| 5.2.3 Hydronium Ion Transport.....                    | 97         |
| § 5.3 Conclusion.....                                 | 99         |
| § 5.4 Experimental .....                              | 101        |
| 5.4.1 Membrane Preparation .....                      | 101        |
| 5.4.2 Gas Transport Measurement .....                 | 101        |
| 5.4.3 Hydronium Ion Transport Measurement.....        | 101        |
| <b>Afterword.....</b>                                 | <b>103</b> |
| <b>References.....</b>                                | <b>105</b> |
| <b>Appendix.....</b>                                  | <b>128</b> |
| Appendix 1: Supporting Information for Chapter 2..... | 129        |
| Appendix 2: Supporting Information for Chapter 3..... | 139        |
| Appendix 3: Supporting Information for Chapter 4..... | 143        |
| Appendix 4: Supporting Information for Chapter 5..... | 149        |

## Acknowledgments

First of all, I would like to thank my research advisor, Prof. Ting Xu, for her indispensable guidance and enormous support throughout my graduate studies. Her creativity and enthusiasm in tackling challenging problems in science has been truly inspiring and I am very fortunate to be able to work with her and learn from her for the past few years. Her emphasis on having a big picture of the field has really transformed my way of thinking, not only in science and research, but also in other aspects of life. Critical thinking as she always stresses has also benefited me in pushing the projects forward and in developing my own independent thinking about the world and life. I have learned how to think, how to act and how to write as a scientist from her. Needless to say, I am extremely grateful for her support even during the challenging time when the project was “stagnant”. All the training and advices that she has given to me really makes me grow and mature much, and prepares me well for the future challenges. I extremely appreciate her help and encouragement during my entire graduate studies. I am sure I will miss her and her word enlightenment in the future. Thank you Ting for everything.

I would also like to thank my colleagues and friends who have helped me in all aspects of life for the past years. I would like to thank Dr. He Dong in helping me get started in the group. Her generous support and thorough knowledge of the field beyond her own project has inspired me in my own research. I would also like to thank Dr. Yunfeng Qiu whom I had worked with closely. Valuable discussions with him had indeed allowed me to look at my project from different angles to move the project forward. Lastly, I would like to thank my friends Nikhil Dube, Joseph Kao, Peter Bai, and Kari Thorkelsson for all the good times. We have shared joys and tears, supported each other for years. It is such a memorable period of time in my life that I will cherish forever. My close friends Qiliang Xu and Lu Li, and their daughter Ivy, all have helped me and supported me during difficult times. I wish them all the best for their future endeavors and thank you all for everything.

Last but not least, I would like to thank my family for their endless love and support. My parents, my aunt and my cousin, my bother and my grand parents, whom are always so proud of me no matter what. They are indeed my biggest strength and I will not be who I am now without them. They have provided me the best opportunity for exploring myself and the world, for allowing me to live freely, and for guiding me throughout my life. I am deeply bonded with them even though I have not lived with them for the past 15 years. Thank you all for everything they have done for me and we are indeed a big family.

# Chapter 1

## Challenges and Opportunities in Membrane Technology

|              |   |           |
|--------------|---|-----------|
| <b>§ 1.1</b> | <b>Introduction.....</b>  | <b>2</b>  |
| <b>§ 1.2</b> | <b>Membrane Technology.....</b>                                   | <b>2</b>  |
|              | 1.2.1 Membrane Separation.....                                    | 2         |
|              | 1.2.2 Membrane Material .....                                     | 4         |
|              | 1.2.3 Membrane Structure .....                                    | 5         |
| <b>§ 1.3</b> | <b>Transport Channels.....</b>                                    | <b>12</b> |
|              | 1.3.1 Biological Channels.....                                    | 12        |
|              | 1.3.2 Synthetic Channels .....                                    | 18        |
| <b>§ 1.4</b> | <b>Cyclic Peptide Nanotubes.....</b>                              | <b>23</b> |
|              | 1.4.1 Cyclic Peptide Sequence Design and Synthesis .....          | 25        |
|              | 1.4.2 Cyclic Peptide Conjugates.....                              | 29        |
| <b>§ 1.5</b> | <b>Conclusion and Outlook.....</b>                                | <b>35</b> |
| <b>§ 1.6</b> | <b>General Approach and Synopsis for Subsequent Chapters.....</b> | <b>35</b> |

## § 1.1 Introduction

In Oxford Dictionary, membrane is defined as “A pliable sheetlike structure acting as a boundary, lining, or partition in an organism.” While this definition originates from anatomy and zoology, its meaning is now extended to be any barrier between two phases. Relative low production cost and ease of processing and configuration have made membranes attractive in industrial uses. Now they are widely used in various industrial processes including solution phase filtrations and gas phase separations.

Developments in membrane science have a long history dated back to the 18<sup>th</sup> century in which osmosis was first discovered by Abbé Nollet in 1748.<sup>1</sup> One century later in 1855, Fick’s phenomenological laws of diffusion were published, setting the foundation in describing diffusion process that is still used today across many disciplines.<sup>2</sup> Just a few years later in 1861, another milestone was achieved by Graham who not only performed first experiments of dialysis, but also extended the diffusion study to gas species.<sup>3-5</sup> Around the same period of time, Traube, Pfeffer and van Hoff studied osmotic pressure, leading to van Hoff’s equation for ideal dilute solutions.<sup>6-9</sup> From early 20<sup>th</sup> century, membrane science and technology became a prevalent area of study with improvements in pore size control of the membranes developed in the Europe.<sup>10-14</sup> Then there came the first significant application of membranes in filtration, especially drinking water filtration at the end of World War II in Europe.<sup>15</sup> Subsequently microfiltration was explored by Millipore Corp., which still remains as the largest microfiltration membrane producer.<sup>15, 16</sup> From 1960, modern concept of membrane science and technology had evolved around new designs of membrane materials and structures along with advancements in synthetic capabilities.<sup>15, 17-19</sup> 20 years of development resulted in the emergence of membrane technology from small-scale laboratory use to large-scale industry use in the 1980s.<sup>15-18, 20, 21</sup> Since then, new module designs and more recently bio-inspired materials and hybrid materials have attracted much attention and constituted a very important discipline of membrane technology serving specific purpose in different separation processes.

## § 1.2 Membrane Technology

### 1.2.1 Membrane Separation

Membranes are being used in a variety of different disciplines and chemical separation processes. As one of the major applications, membranes are widely applied in filtration process in which a solution containing dissolved or suspended solids is forced through a membrane filter.<sup>15, 22, 23</sup> Depending on the size of the pores of the membrane used, filtration can be further categorized into microfiltration (pore size 0.1-10  $\mu\text{m}$ ),

ultrafiltration (pore size 1-100 nm), and reverse osmosis (pore size 0.2-2 nm).<sup>15, 22</sup> Separation takes place mainly on the basis of size exclusion principle in which particles smaller than the pore size would remain in solution and larger particles are filtered out. Figure 1.2 outlines the differences based on the pore size of filtration processes and some of the common materials being separated by these processes.

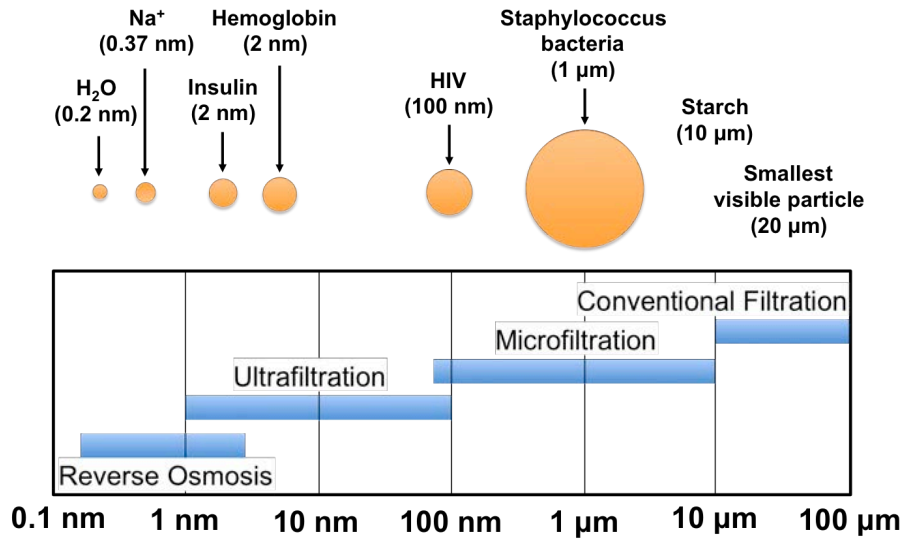


**Figure 1.1.** Different types of filtration processes and typical filtrate sizes. Adapted with permission from reference [15]. Copyright (2001) John Wiley & Sons, Inc.

Another important industrial application when membranes are heavily involved is on gas separation and is the focus of the application studies in this dissertation.<sup>15, 17, 18, 21</sup> Gas separation has become an area of study that has drawn a considerable amount of attention in the last 30 years and it is still growing rapidly due to its important in many industries.<sup>17</sup> As the first large-scale industrial application, membranes were used to separate hydrogen from nitrogen, methane and argon in ammonia purge gas streams.<sup>17, 21, 24</sup> Another common use of membranes in gas separation is in air separation where nitrogen and oxygen are being separated.<sup>21</sup> Due to the small size difference between nitrogen and oxygen, it is difficult to separate the two and many efforts have been devoted to develop more efficient membranes.<sup>25-28</sup> In parallel, natural gas processing is another area where membranes are widely used to remove acid gas such as carbon dioxide.<sup>15, 16</sup> Cellulose acetate and polyimide are the dominating material selections for separating carbon dioxide from methane and other hydrocarbons.<sup>29</sup> Air and gas dehydrogenation, polyolefin plant resin degassing, alkane/alkene separation are some of the other common industries that membranes are heavily involved, and the market for membranes is growing rapidly worldwide.<sup>15, 21</sup>



## 1.2.2 Membrane Material

A wide range of materials is used to make synthetic membranes. In terms of the material type, membranes can be broadly categorized into inorganic, organic and hybrid composite. While the vast majority of commercial membranes used are polymer-based, inorganic membranes were developed long before their organic counterparts, with early use for military purpose or nuclear application.<sup>15, 17, 23</sup> Typically, inorganic membranes are more mechanically robust and can withstand more harsh environments compared to organic membranes. As one of the mostly used inorganic materials, ceramic membranes such as glass, alumina, silicon nitride are commonly used as porous membranes for microfiltration and ultrafiltration in which solvent resistance and thermal stability are required.<sup>15, 18</sup> Metal and metal alloys are also often used for gaseous separation processes, for example Palladium in hydrogen separation.<sup>15</sup> More recently, requirements in precise pore size control and high selectivity have also triggered fast developments in silica, zeolites and carbon membranes in which molecular sieving effect can be achieved for gaseous species.<sup>15, 16</sup> In comparison, polymers are the more commonly used materials for making membranes due to their relatively low cost and high processability. Although there are a large number of polymers being developed and investigated, only a limited has been in commercial systems. In particular, eight to nine polymer materials have been used to make 90% of the membranes for gas separation.<sup>15, 18</sup> Lastly, inorganic-organic hybrids especially in the form of composite membranes are another area of interest. Mixed matrix membrane (MMM),<sup>30-33</sup> nanoparticle/polymer,<sup>30, 34</sup> and carbon nanotube (CNT)/polymer<sup>35-37</sup> composites have drawn a considerable amount of attention in research in the past years owing to their potential applications in specific applications.<sup>38</sup> Table 1.1 lists some of the most common membrane materials used in industry, as well as some recent developments in new membrane materials discovered in laboratories that can be potentially used in the future.

**Table 1.1.** List of common membrane materials

|           | <b>Material</b>                                 | <b>Remark</b>  | <b>Application</b>   |
|-----------|---|--|--|
| Inorganic | Ceramic<br>e.g. glass, alumina, silicon nitride | High mechanical strength;<br>Good chemical resistance        | Microfiltration;<br>Ultrafiltration;<br>High temperature application |
|           | Metal/metal alloy                               | High mechanical strength;<br>Low fouling rate                | Palladium in hydrogen separation                                     |
|           | Silica/Zeolites/Carbon                          | Precise pore size control;<br>High selectivity               | Gas separation with molecular sieving effect                         |
| Organic   | Cellulose Acetate (CA)                          | Glassy polymer;<br>Decent mechanical strength and durability | Liquid phase separation, RO membrane, gas separation                 |

|        |  |   |   |
|--------|--|---|---|
|        | Polysulfone(PSf)/Polyethersulfone(PES) | Glassy polymer;<br>Stability at high temperature (< 180°C)  | Liquid and gas separation   |
|        | Polyimide                              | Glassy polymer;<br>Stability and heat resistance  | Gas separation  |
|        | Polycarbonate (PC)                     | Glassy polymer;<br>Heat resistance;<br>Track-etched PC membrane with precise pore control           | Liquid and gas separation   |
|        | Polyvinylidene fluoride (PVDF)         | Crystalline polymer;<br>Mechanical strength and chemical resistance                                 | Liquid and gas separation;<br>Artificial membrane in protein immunoblot |
|        | Polyethylene (PE)/Polypropylene (PP)   | Low cost  | Gas separation  |
|        | Poly(dimethylsiloxane) (PDMS)          | Rubbery polymer;<br>High permeability   | Gas separation  |
| Hybrid | Mixed Matrix Membrane (MMM)            | Combining superior separation performance of inorganic particles with polymer's easy processability |   |
|        | Carbon Nanotube-polymer composite      | Gas flow rate 1-2 orders of magnitude faster  |   |

### 1.2.3 Membrane Structure

Based on the structures, membranes can be generally categorized as porous and dense (non-porous) as shown in Figure 1.1.<sup>15</sup> A dense membrane usually consists of a dense film in which the permeants pass through the membrane by diffusion. External driving force such as pressure difference, concentration gradient, etc is used to drive the transportation process.<sup>15</sup> Therefore, separation across a dense membrane depends on the rate of transport of the permeants, which in turn is related to the diffusivity and the solubility of the permeants in the membrane material. A detailed discussion about transport mechanism is presented in Chapter 5. In contrast, porous membranes contain continuous passages for permeants to go through, typically in the form of randomly distributed but interconnected voids and in some cases direct channels.<sup>15, 17, 18</sup> The size of the pores for conventional membranes is on the order of 0.01-10  $\mu\text{m}$ .<sup>15, 22</sup> Permeants pass through the membranes usually by size-exclusion rule in which particles larger than pores get ejected. Thus, separation of permeants is mainly based on the size of the particles and the pore size distribution of the membrane.<sup>22</sup> Depending on the pore size distribution,

porous membranes can be further divided into two different structures, namely symmetric and asymmetric as shown in Figure 1.1. While symmetric membranes tend to be more homogeneous in pore sizes, asymmetric membranes typically have different pore size distributions across the membrane thickness.<sup>15</sup> To obtain high enough flux across for economic reasons, it is desirable to make membranes as thin as possible so that fast transport can be achieved. However, mechanical stability and defects are two main concerns with thinner membranes, with additional constraint of fabrication limitation.<sup>15</sup> Asymmetric membranes were therefore developed to address these issues. They consist of a functional layer which usually serves the purpose of separation on a mechanically strong support layer.<sup>15</sup> The advantage of higher flux with good mechanical support makes the asymmetric membrane an ideal candidate for almost all commercial processes.<sup>15, 22</sup> Regardless of the internal structure of the membrane, one critical factor which affects the transport performance is the pore size. Both the channel diameter as well as the size distribution need to be precisely controlled to allow superior yet consistent performance across the membrane. Various approaches have been developed to ensure well control over the pore size and using block copolymer is one appealing methods as the microdomain size can be precisely controlled, forming uniform pores in the membrane.

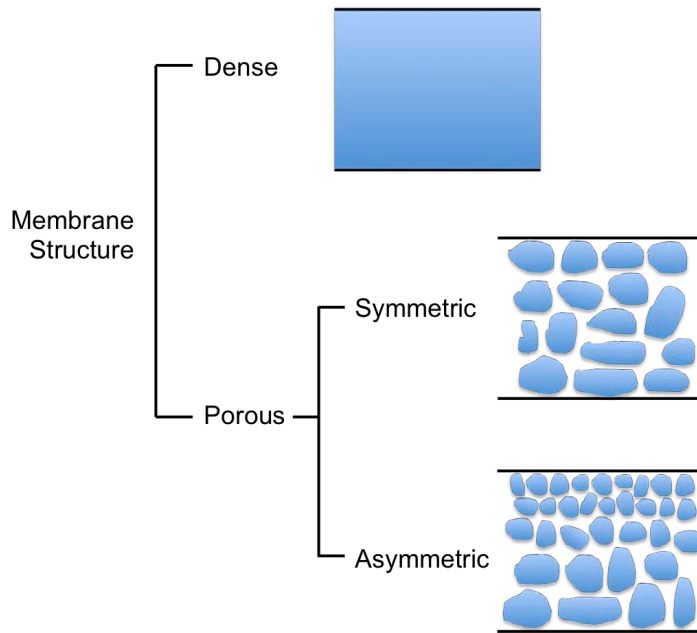


**Figure 1.2.** Different types of membranes based on the internal structure.

Block copolymers (BCPs), consisting of two or more chemically different polymer chains that are covalently connected, can self-assemble into a variety of different

morphologies. Membranes fabricated using BCPs offer narrow pore size distribution in nanometer scale as the structure of the membrane can be well controlled via microphase separation of the BCP. The tendency for BCPs to microphase separate reflects the energetic balance between various segments both enthalpically and entropically.<sup>39,40</sup> To understand why BCPs microphase separate, the classic Flory-Huggins theory of polymer blends would build the foundation for the thermodynamic principle of separation for polymers. In an A-B polymer blend, the Gibbs free energy of mixing is defined as:<sup>39</sup>

$$\Delta G = \Delta H - T\Delta S$$

where  $\Delta H$  and  $\Delta S$  are change in enthalpy and entropy due to mixing and  $T$  is the temperature. Adopting statistical mechanics, the entropy of mixing can be re-expressed in terms of the volume fraction of A and B,  $\phi_A$  and  $\phi_B$ , as well as the degree of polymerization of A and B,  $N_A$  and  $N_B$  respectively:

$$\Delta S = -k_B(N_A \ln \phi_A + N_B \ln \phi_B)$$

and the enthalpy of mixing can be re-written as:

$$\Delta H = k_B T N_A \phi_B \chi_{AB}$$

in which  $\chi_{AB}$  is the Flory-Huggins interaction parameter which measures the enthalpic interaction between A and B:

$$\chi_{AB} = \left( \frac{z}{k_B T} \right) \left[ \varepsilon_{AB} - \frac{1}{2}(\varepsilon_{AA} + \varepsilon_{BB}) \right]$$

where  $z$  is the number of nearest neighbors,  $k_B T$  is the thermal energy, and  $\varepsilon_{AB}$ ,  $\varepsilon_{AA}$  and  $\varepsilon_{BB}$  are the interaction energies between AB, AA and BB monomer pairs, respectively. From statistical mechanics, the entropy of the system is related to the volume fraction of A. Combining the contributions from both enthalpy and entropy, the overall energy landscape of the system becomes:

$$\Delta G = k_B T (N_A \ln \phi_A + N_B \ln \phi_B + N_A \phi_B \chi_{AB})$$

Phase separation is favored if the change in free energy is negative. However, for an AB diblock copolymer, this is prohibited since the blocks are covalently connected. Thus, instead of macrophase separation, a phenomenon called microphase separation takes place if A and B are incompatible.<sup>40,41</sup> For such an AB diblock copolymer, the phase behavior of the system ultimately depends on three parameters: 1) the volume fraction of segment A (or B),  $f$ ; 2) the overall degree of polymerization,  $N$ ; and 3) the A-B segment interaction parameter,  $\chi_{AB}$ .<sup>41</sup> The overall interaction enthalpy of the AB diblock is given by the product of the pair-wise interaction parameter and the total number of monomers,  $\chi_{AB} N$ . Seminal work from Hashimoto et al. investigated thoroughly model polystyrene-polyisoprene (PS-PI) diblock copolymer systems with different morphologies<sup>42-48</sup> and Figure 1.3 represents the phase diagram of the PS-PI diblock.

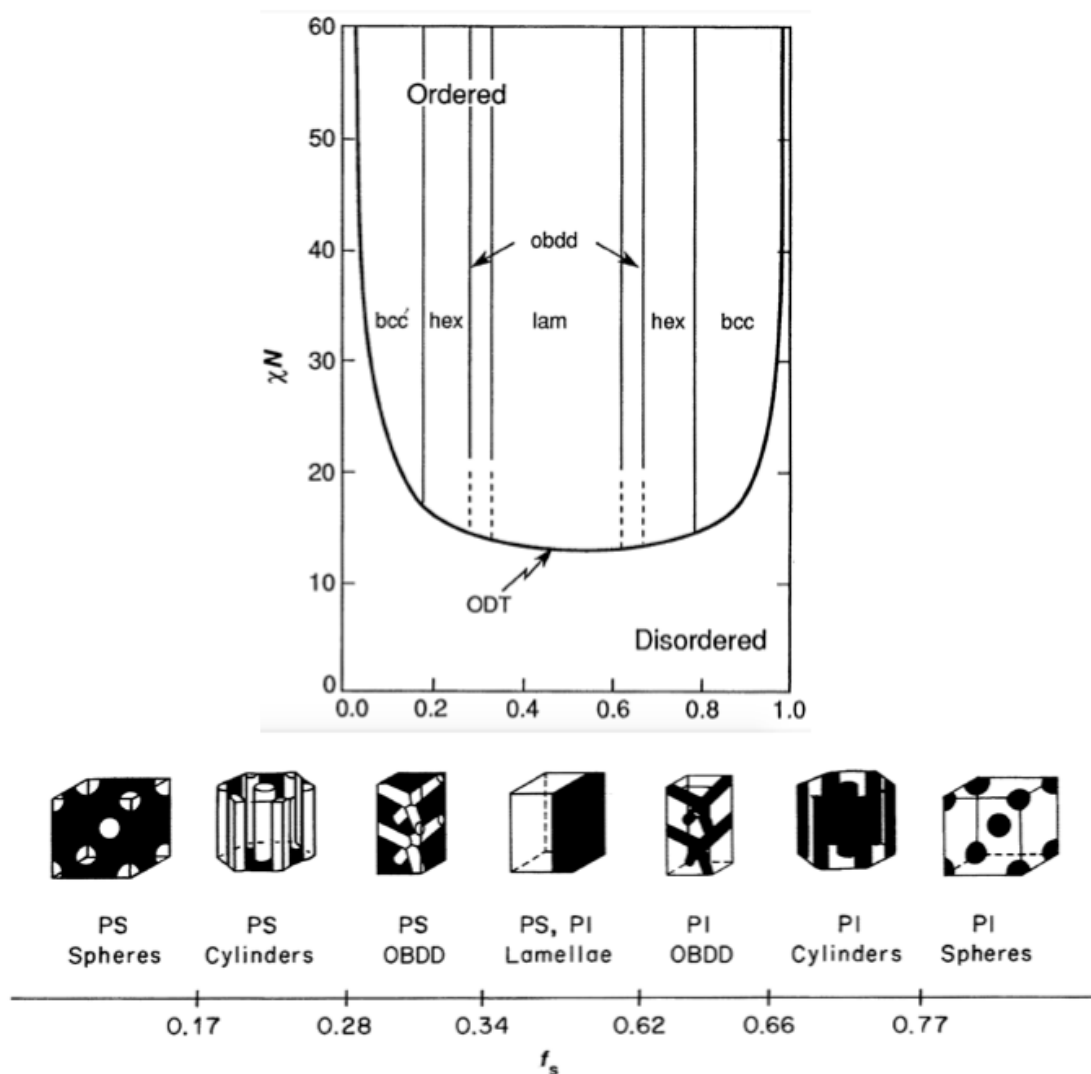


**Figure 1.3.** Phase diagram and various morphologies of PS-PI diblock copolymer. When  $\chi N < 10.5$ , no microphase separation takes place and PS-PI is in a disordered state. When  $\chi N > 10.5$ , as volume fraction of the PS block varies from 0 to 1, the morphology of the diblock changes from PS spheres (body centered cubic, “bcc”), to PS cylinders (hexagonally packed cylinders, “hex”), to PS gyroids (ordered bicontinuous double diamond, “OBDD”), to lamellae phase (“lam”) around  $f_s \sim 0.5$ , and the inverse PI analogues. Reprinted with permission from reference [40]. Copyright (1991) AAAS.

With developments in polymer synthesis, more complicated polymer architectures are now readily available. For example, a three-component ABC triblock terpolymers can microphase separate to a much wider variety of morphologies that extend the BCP library.<sup>49</sup>

Among the available morphologies, the hexagonally packed cylindrical phase and the bicontinuous phase are particularly interesting morphologies for membrane

application as both morphologies offer continuous paths of one phase which is one critical requirement for transport membranes.<sup>50, 51</sup> In particular, the bicontinuous phase provides non-directional pathways in all 3 directions in bulk, and well-oriented cylinders provide direct pathways from one side to the other. By selectively removing the segment forming the continuous phase using both physical and/or chemical method, membranes with uniform pore size can be obtained. Regardless of the morphology, one important criterion for the use of BCP as membrane material is to ensure the consistency of the morphology with well controlled spacing. Thus, the self-assembly of the BCPs must be well controlled to ensure uniform morphology across the sample. Numerous efforts have been dedicated in fabricating BCP based membranes and the following paragraphs give an overview of some significant achievements in the area.

For bicontinuous gyroid structure, the exact alignment of the microdomains is trivial but the formation of the gyroid itself poses some challenges since this bicontinuous phase only exists within a vary narrow range as seen in Figure 1.3. Several approaches have been taken to achieve gyroid structure using various BCPs. For example, Hashimoto *et al.* successfully fabricated membranes using a diblock copolymer polystyrene-*b*-polyisoprene (PS-*b*-PI) blended with homopolymer PS to attain the right volume fraction of PS.<sup>52</sup> The PI block was subsequently removed by ozonolysis and the nanochannels were plated with nickel for catalytic activities. Improvements on the mechanical stability were later developed by crosslinking the PI block with 1,4-diiodobutane using a slightly different system of blends of poly(2-vinylpyridine)-*b*-polyisoprene (P2VP-*b*-PI) with homopolymer PI.<sup>53</sup> Similar approach of achieving gyroid structure was used in other BCP systems and Hillmyer *et al.* pioneered the use of polylactic acid (PLA) based BCPs in fabricating membranes that are mechanically robust with show transport properties. Using polynorbornenylethylstyrene-*b*-polylactic acid (P(N-s-S)-*b*-PLA) system, membranes with 14 nm pore and 40% void fraction showing high performance for ultrafiltration were fabricated as PLA could be selectively etched away by a dilute base as shown in Figure 1.6b).<sup>54, 55</sup> A different approach was taken by Uehara *et al.* in the fabrication of bicontinuous BCP membrane. The system they used was polyethylene-*b*-polystyrene (PE-*b*-PS) in which the isothermal crystallization of the PE block induces the formation of the bicontinuous phase.<sup>56</sup> 5-30 nm pore could be obtained by etching the amorphous PS block by fuming nitric acid and the remaining crystalline PE was mechanically strong as illustrated in Figure 1.4a). They successfully demonstrated the potential use of an implantable glucose sensor as glucose molecules could pass through the nanochannels but not larger albumin molecules.<sup>57</sup> Another novel approach was developed by Zhou *et al.* which utilizes bicontinuous microemulsion using blends of BCP with corresponding homopolymers as shown in Figure 1.4c).<sup>58</sup> From a bicontinuous microemulsion precursor of blends of polystyrene-*b*-polyisoprene (PS-*b*-PI), PS and PI were co-dissolved and dried to form the bicontinuous structure. The PI block was subsequently cross-linked with sulfur monochlorite vapor and PS block was then removed by hexane. Other than diblock copolymer, triblock terpolymers have also been used to create bicontinuous structures.<sup>59-62</sup>

Comparing to the bicontinuous structure, cylindrical morphology offers directional pathways and straight channels often give rise to high flux. However, ensuring the proper orientation of the cylinders to be perpendicular to the membrane surface is complicated. Elaborate efforts have been dedicated to methods to self-assemble various BCPs with perpendicular cylinder orientation, especially in thin films. Two powerhouses in the area of fabricating nanoporous membranes based on BCP are Hillmyer's group that focuses on polylactic acid based BCP; and Russell's group that works with polystyrene-*b*-poly(methyl methacrylate) (PS-*b*-PMMA) systems.<sup>51, 59</sup> Early work from Hillmyer's group was based on PS-*b*-PLA diblock copolymer in which perpendicular orientation of the BCP was achieved by carefully controlling the thin film thickness. As the surface energy of PS is similar to that of PLA, perpendicular alignment of the PLA cylinders was achieved and a nanoporous template was thus constructed by selectively etching the PLA block by dilute base.<sup>63</sup> External electric field could also be used to align the PLA cylinder as demonstrated in poly (4-fluorostyrene)-*b*-polymer(D,L-lactide) (PFS-PLA) diblock copolymer.<sup>64</sup> The PS-*b*-PLA diblock system was later expanded to triblock terpolymer systems for adding functional groups to the pore surface. In this regard, polystyrene-polydimethylacrylamide-poly lactide (PS-PDMA-PLA) with PS matrix and PLA cylinder core with PDMA block in the middle was obtained by high temperature extrusion method as demonstrated in Figure 1.4e).<sup>65</sup> Etching the PLA would expose PDMA to the free surface, which was later hydrolyzed to produce carboxylic acid groups as PDMA was converted to poly(acrylic acid). In parallel, inspired by Park *et al.*'s work of creating holes or dots with PS-PB and PS-PI BCP via reaction ion etching (RIE), triblock terpolymer was also used in attempt to create more complex structures. Using two etchable blocks, PS-PI-PLA triblock system was assembled into two different morphologies by varying the volume fractions of each of the block.<sup>66, 67</sup> PLA and PI were removed by dilute base treatment and ozonolysis separately, leaving on the PS block. Depending on the morphology, cylindrical channels in PS matrix or empty PS cylinders could be constructed.<sup>65</sup> Based on this PS-PI-PLA system, the gas and water transport had been investigated.<sup>68</sup> The diffusion coefficients for He, Ar, N<sub>2</sub> and O<sub>2</sub> gases calculated accounting for 0.26 pore fraction and pore diameter ~ 14 nm were in quantitative agreement with Knudsen diffusion, and water flow fluxes were consistent with the results of pore size ~ 13 nm. Although the results from gas and water measurements were consistent, the actual pore size measured from microscopy method and inferred from scattering indicated that the pore size was ~ 17 nm. The discrepancy was attributed to non-ideal pore geometry but nonetheless the results together with later extend work suggest potential application of using the membranes in ultrafiltration.<sup>68, 69</sup>

As one of the most well studied BCP, PS-*b*-PMMA has been widely applied in nanotechnology such as etching masks in nanolithography,<sup>70</sup> templates for creating nanostructures,<sup>71</sup> and membranes for ultrafiltration.<sup>51, 59</sup> Russell and co-workers developed an effective method to assemble thin films of PS-*b*-PMMA with microdomains oriented perpendicular to the substrate through chemically modifying the substrate surface with a neutral brush layer of crosslinked PS-PMMA based random

copolymer (PS-*r*-PMMA).<sup>72, 73</sup> Membranes were fabricated by using blends of PS-*b*-PMMA with homopolymer PMMA, in which the homopolymer assembled at the center of the perpendicularly oriented PMMA cylinders was subsequently removed by acetic acid wash as illustrated in Figure 1.4d).<sup>74</sup> High flux and high selectivity for human rhinovirus type 14 (HRV14) were observed using these nanoporous membranes with pore size ~ 30 nm.<sup>74, 75</sup> Advantages of these membranes include tunable pore size from 10-40 nm by changing the molecular weight of the homopolymer PMMA,<sup>76, 77</sup> and good mechanical strength and excellent resistance to organic solvents due to crosslinking of the PS block.<sup>74, 75</sup> More recently, single-file diffusion of different protein drugs was observed by tuning the pore size by Au deposition to achieve long-term controlled release of protein drugs.<sup>78</sup>

In addition to the above-mentioned PLA based BCP and PS-*b*-PMMA, other BCPs have also showed potential for fabricating nanoporous membranes for transport and filtration. For example, Peinemann *et al.* developed a very interesting approach to fabricate integral asymmetric membranes from polystyrene-*b*-poly(4-vinylpyridine) (PS-*b*-P4VP) in one step via non-solvent induced phase separation.<sup>79</sup> 250 nm thick nanoporous layer was formed on top of a disordered support layer with much larger pore structure as shown in Figure 1.4f). Polystyrene-*b*-poly(ethylene oxide) (PS-*b*-PEO) had also been successfully assembled via solvent annealing<sup>80</sup> and channel die extrusion<sup>81</sup>, respectively to construct nanoporous membranes. In parallel, it is worth noting that the application of BCP based membrane is not limited to transport and filtration. As shown by Yang *et al.*,<sup>78</sup> the BCP nanoporous membrane can also be used as drug delivery vehicle. Kim and co-workers had also demonstrated the potential use of nanoporous membrane as anti-reflection coating.<sup>82</sup> In summary, BCP indeed offers many advantages in constructing nanoporous membranes as the pore size distribution can be limited to a very narrow range, and the channels size can be tuned easily. The vastly available BCP systems also expands the fabrication methods of nanoporous membranes and offers various approaches to functionalize the pores. However, there are still several challenges that need future improvements. Firstly, the pore size from BCP membrane is usually > 5 nm, as limited by the self-assembly of the BCP as well as the subsequent etching. Thus, achieving small channel size using BCP, especially in the sub-nm range which is needed for molecular separation, seems to be an extremely difficult task with current technology. Moreover, the nanochannel surface for BCP membrane is another area that needs more investigation and improvements. Current etching method may result in imperfect channel wall and high surface roughness, which are undesirable for transport and separation. Other criteria such as mechanical strength and chemical robustness need also to be considered as polymers are inherently less tough than their inorganic counterparts such as ceramics and metals. Nevertheless, the use of BCP as membrane materials indeed is an area of interest and great efforts as well as developments have been made to improve the performance of BCP membranes.



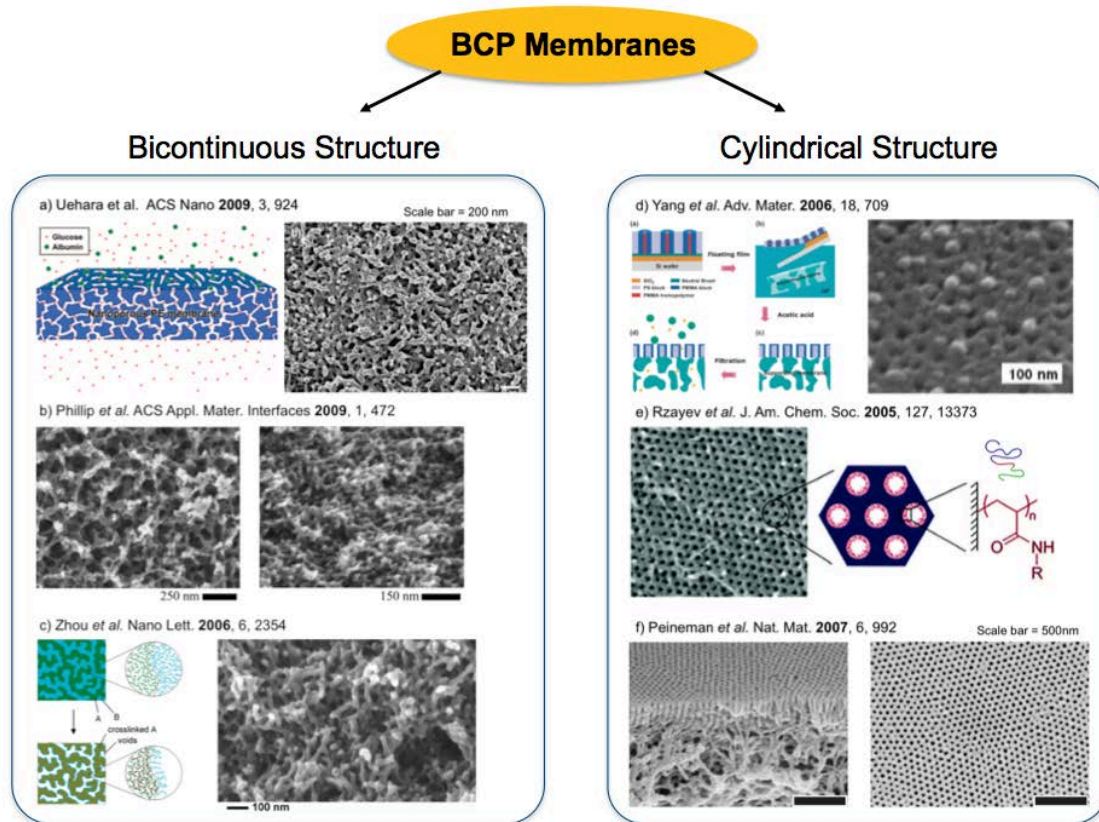


**Figure 1.4.** BCP Membranes fabricated showing bicontinuous structure and perpendicularly aligned cylindrical structure from different approaches. a), b), c) and e) are adapted with permission from references [57], [55], [58], and [65], respectively. Copyright (2009) (2009) (2006) (2005) American Chemical Society. d) is adapted with permission from reference [74]. Copyright (2006) John Wiley & Sons, Inc. f) is adapted with permission from reference [79]. Copyright (2007) Macmillan Magazines Ltd.

## § 1.3 Transport Channels

### 1.3.1 Biological Channels

While current synthetic membranes regardless of the membrane materials and membrane structures show some shortcomings and limitations, natural membranes on the other side offer some insights in designing next-generation membranes.<sup>83</sup> Biological membranes, also referred as cell membranes, are much more superior in their transport performances than synthetic membranes in terms of efficiency, selectivity and

precision.<sup>84, 85</sup> Furthermore, biological membranes are capable of self-regulating, self-correcting and self-healing, and responding to various external stimuli that are extremely challenging for synthetic membranes.<sup>85</sup> Unlike the synthetic membrane, cell membrane is a multicomponent system with very complex structure that is dynamic in nature.<sup>84, 86</sup> There are protein molecules embedded in the cell membrane, serving the critical role of facilitating transport across the cell membrane.<sup>85, 87, 88</sup> These natural biological channels are very specific to various transport processes but their efficiencies are insurmountable by synthetic materials.

Transport across the cell membrane can be generally categorized into three modes: simple diffusion, facilitated diffusion, and active transport.<sup>85</sup> Particles with the right size and hydrophobicity may diffuse through the phospholipid bilayer directly through simple diffusion. Facilitated diffusion via integral proteins is another common mechanism for the exchange of many substances across the cell membrane. As an example, water molecules move across cell membranes through the water channel proteins called the aquaporins.<sup>85</sup> There are more than 10 types discovered in the aquaporin family with similar tetramer structure and monomer motif of 3 amino sequence NPA (Asn-Pro-Ala) forming 6 transmembrane  $\alpha$ -helices in each monomer.<sup>89-91</sup> Figure 1.5 shows the structure for the monomer motif (a) and the tetramer structure (b) of aquaporin 1, consisted of a 29 kDa polypeptide.<sup>89, 92-94</sup> Superior selectivity for only water molecules, even rejecting hydronium ( $\text{H}_3\text{O}^+$ ) ions is speculated to arise from two principal mechanisms, namely the size exclusion and dipole interaction.<sup>89, 95-97</sup> The AQP1 channel narrows down to 2.8 Å slightly above the mid-plane of the membrane, thus only permitting water molecules with size 2.75 Å to pass through. In addition, dipoles from the NPA motifs interact with water molecules, preventing them from hydrogen bonding to other water molecules; and therefore restricting the movements of  $\text{H}^+$ . The combination of size exclusion and charge restriction indeed gives rise to superior performance of aquaporin channels, highlighting two important parameters of channel size and channel-permeants interaction in the effort to fabricate high performance membrane by mimicking natural transport channels.

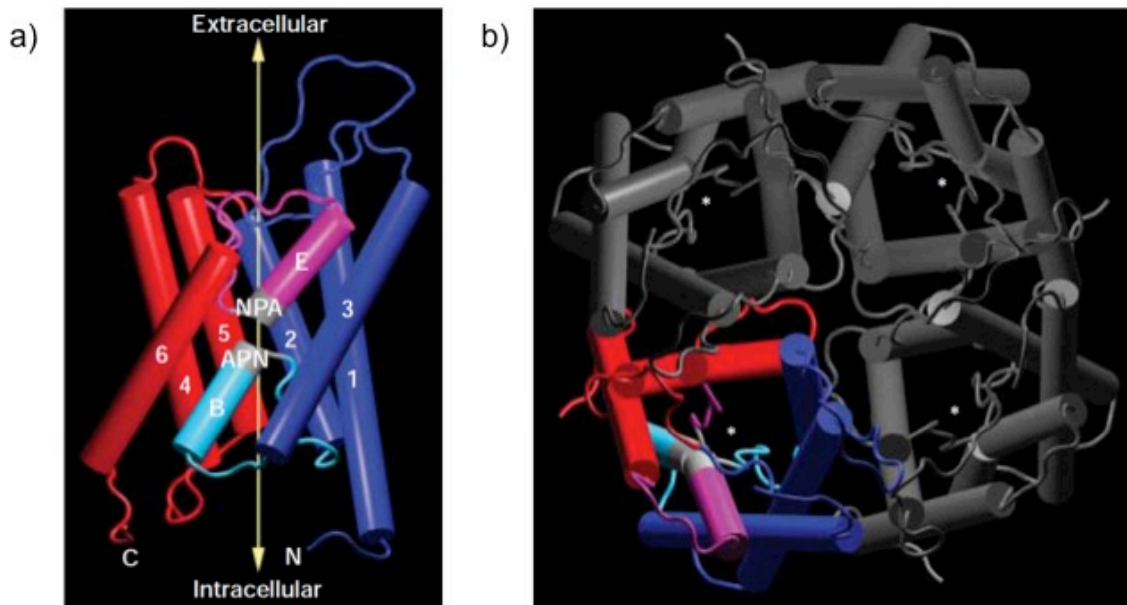


**Figure 1.5.** Schematic showing the structure of a) aquaporin-1 (AQP1) monomer, and b) AQP tetramer seen from above. Rods numbered 1-6 in a) represent 6 helices that span the cell membrane. The amino-terminal half of the molecule is shown in purple and light blue, and the carboxy-terminal half is shown in red and pink. Loops B and E, which fold into the membrane to form the pore, are labeled, as are the conserved NPA motifs (shown in light grey). Reprinted with permission from reference [89]. Copyright (2004) Macmillan Magazines Ltd.

Another example of integral protein channel made of  $\beta$ -barrel structure is the porin channel in Gram-negative bacteria and some Gram-positive bacteria, and mitochondria and cytoplasm for the transport of small metabolites such as ions and sugar molecules.<sup>98-101</sup> The  $\beta$ -barrel structure usually consists of  $\beta$ -sheets, varying from 8 strands to 22 strands, that are arranged in an anti-parallel fashion,<sup>100, 102</sup> and Figure 1.6 shows some examples of  $\beta$ -barrel structures. Schematic representation of Maltoporin, an example of the trimeric  $\beta$ -barrel porins that are either nonspecific or facilitated transporters in the outer membranes of Gram-negative bacteria, is shown in a) with side view (upper) and bottom view (lower).<sup>103</sup> Each trimeric porins have 16 or 18 strands, which comprise three separate barrels in the trimer. Each of the barrels contains a narrow, central channel. b) shows the structure of FepA, an Fe-siderophore transporter which uses active transport to channel Fe ions through via active interactions with inner pores protein groups.<sup>104, 105</sup> c) shows the structure of TolC, a unique  $\beta$ -barrel structure that comprised of a trimeric, 12-stranded single barrel in which each monomer contributes four strands to the barrel.<sup>106</sup> The pore of the  $\beta$ -barrel is connected to the pore of a hollow  $\alpha$ -helical bundle that extends across the periplasmic space to the inner membrane. d) shows the structure of toxin  $\alpha$ -hemolysin from bacteria *S. aureus* with side view (upper) and bottom view (lower) of the heptameric pore.<sup>107</sup> This toxin is secreted as a monomeric unit that

subsequently assembles into a heptameric pore on the membrane, each contributing one  $\beta$ -hairpin to the 14-stranded barrel that is inserted into the membrane, ultimately leads to osmotic cytolysis.<sup>108</sup> Last but not least, (e) shows the structure of OmpLA, an outer membrane phospholipase that consists of a dimer of 12-stranded  $\beta$ -barrel.<sup>109</sup> Interestingly, the dimer interface is mostly nonpolar and accommodates both active centers. There are many other  $\beta$ -barrel structures present in the outer membrane of bacteria, mitochondria and cytoplasts and Figure 1.6 only lists a few of them. Nevertheless, variations on the structures have demonstrated the versatility of this family of protein channels in transporting different molecules via different mechanisms. Thus, in combination with the knowledge gained from aquaporin,  $\beta$ -barrel structure with precise pore size control and appropriate pore surface chemistry seem to be a suitable candidate for constructing high performance man-made membrane channels.

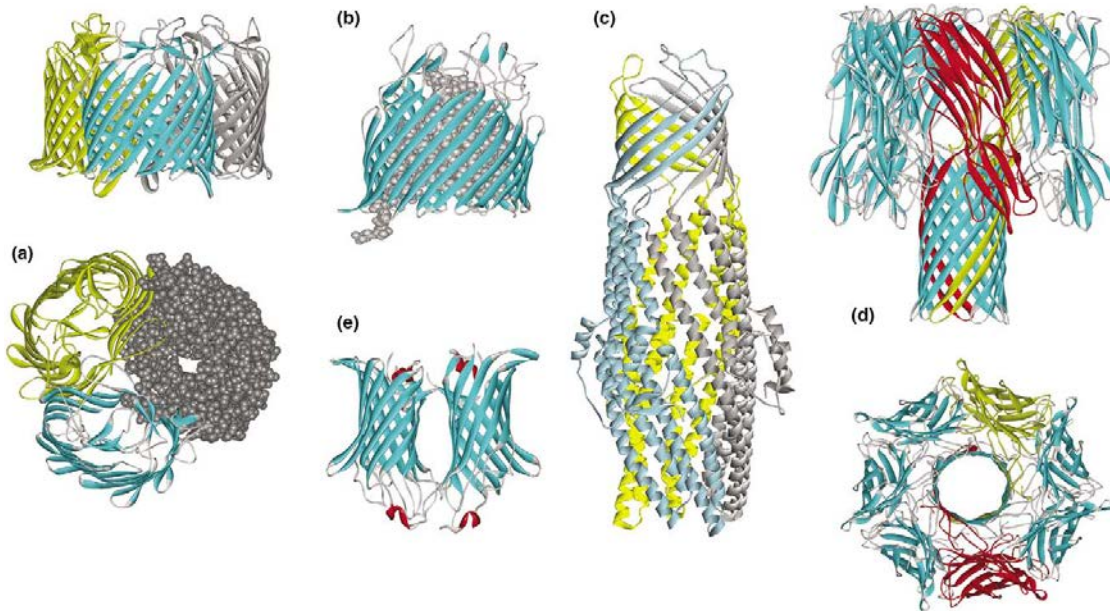


**Figure 1.6.** Schematic representations of various  $\beta$ -barrel membrane protein structures. a) Maltoporin, b) FepA, c) TolC, d)  $\alpha$ -hemolysin, and e) OmpLA. Reprinted with permission from reference [102]. Copyright (2003) Elsevier Ltd.

In many cases, simple and facilitated diffusions are insufficient since substances need to be transported against their electrical or chemical gradient to maintain specific concentrations inside or outside the cell.<sup>85</sup> Active transport across cell membranes is a vital process for many of the cellular activities and continues to a topic of research interests for many years. The sodium-potassium pump (also known as “ $\text{Na}^+$ ,  $\text{K}^+$ -ATPase”) is one of the well-known protein channels for movement of  $\text{Na}^+$  and  $\text{K}^+$  along with hydrolysis of ATP.<sup>110, 111</sup> Typically  $\alpha$ - and  $\beta$ -subunits make up the protein structure but in certain cases a third  $\gamma$ -subunit may also be present.<sup>90, 112, 113</sup> Figure 1.7 schematically

represents the architecture of  $\text{Na}^+$ ,  $\text{K}^+$ -ATPase consists of  $\alpha$ -,  $\beta$ -,  $\gamma$ -subunits. The crystal lattice consists of layers of membrane-spanning segments oriented in a certain direction . The  $\beta$ -subunit in the extracellular regions do not contribute to the interlayer contact, but rather point into large solvent filled channels of the structure. The  $\alpha$ -subunits adopt a topology similar to that of the  $\text{Ca}^{2+}$ -ATPase with three characteristic cytoplasmic domains, namely the actuator (A), nucleotide-binding (N) and phosphorylation (P) domains.<sup>112</sup> In this particular case, as shown in Figure 1.7a), there are ten transmembrane segments of  $\alpha$ -subunits,  $\alpha\text{M1}$ –  $\alpha\text{M10}$ . The  $\text{Na}^+$ ,  $\text{K}^+$ -ATPase is one of the most important transport channels in regulating normal cellular activities by regulating the resting potential of the cell membrane, enabling the transport of  $\text{Na}^+$  and  $\text{K}^+$  ions and maintaining appropriate cell volume. With the energy released from the hydrolysis of ATP, 3  $\text{Na}^+$  ions are transported out of the cell and subsequently 2  $\text{K}^+$  ions are transported in, both against their concentration gradients. The  $\text{Na}^+$ ,  $\text{K}^+$ -ATPase is very effective in the transport of  $\text{Na}^+$  and  $\text{K}^+$  ions and comparable efficiency has not been achieved by man-made materials. However, constant evolvments in the field still provides useful insights in designing high performance transport channels, revealing the importance of the internal channel structure and specific binding and interactions with not only the permeants but also other facilitating molecules.



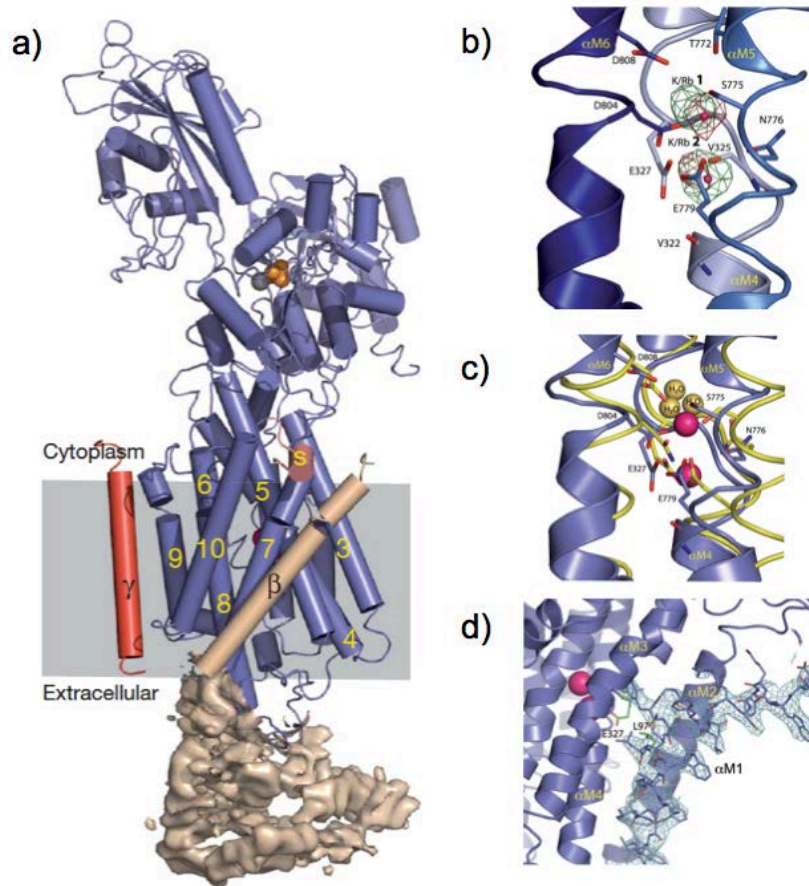


**Figure 1.7.** Schematic of the structure of Na<sup>+</sup>, K<sup>+</sup>-ATPase  $\alpha\beta\gamma$  complex. a)  $\alpha$ -,  $\beta$ -, and  $\gamma$ - subunits are represented by blue, ivory, and red, respectively; while  $\alpha$ -helices are represented by cylinders and  $\beta$ -strands by arrows. The transmembrane segments of the  $\alpha$ -subunit are numbered in yellow, starting with the most N-terminal, and the small C-terminal helix (S, for switch) is colored in light red. Mg<sup>2+</sup>, MgF<sub>4</sub><sup>2-</sup> and Rb<sup>+</sup> ions are in grey, orange and pink, respectively. b) shows the positions of Rb<sup>+</sup> and K<sup>+</sup> ions, respectively within the complex. d) shows the alignment of Na<sup>+</sup>, K<sup>+</sup>-ATPase (blue) with SERCA (yellow) in E2•MgF<sub>4</sub><sup>2-</sup> form. Yellow and magenta spheres represent water molecules in SERCA and K<sup>+</sup>/Rb<sup>+</sup> ions in Na<sup>+</sup>, K<sup>+</sup>-ATPase, respectively. d) shows the interaction between Glu 327 ( $\alpha$ M4) and Leu 97 ( $\alpha$ M1).<sup>114</sup> Adapted from reference [112]. Copyright (2007) Macmillan Magazines Ltd.

In summary, biological channels are indeed superior in their transport performance specific to the process. The structures of these protein-based channels can vary but the major constituting subunits are  $\alpha$ -helices and  $\beta$ -barrels. The specific sequence of the polypeptides and the folding of the proteins allow for very precise control over the channel size and the microenvironment inside the channel. Nevertheless, despite the superior performance, these biological channels are not suitable for use in membrane technology because stability and durability are two important considerations in real applications. Biological channels are very subjected to denaturation and therefore

environmental changes, such as high temperature, extreme pH or ionic strength, as the secondary, tertiary and quaternary structures of proteins and polypeptides can be significantly changed, and therefore it is difficult to process the biological channels with conventional techniques. As a result, novel materials need to be developed that not only mimic the superior performance of the natural channels, but also can be processed and applied to large-scale industry.

### 1.3.2 Synthetic Channels

In searching for appropriate channel materials, synthetic nanotubes are an attractive candidate as they can fulfill the two critical requirements for high performance transport channels, i.e. appropriate channel diameter in the nanometer to sub-nanometer range, and tunable channel surface chemistry with functional groups. Moreover, synthetic channels tend to be more mechanically and chemically stable than the biological channels, thus suitable for use in industrial separation processes. The following section will discuss in details some of the advantages in using synthetic channels in membranes, as well as some drawbacks and challenges that need to be overcome.

Inorganic nanotubes typically are composed of metal oxides, various sulfides, and most importantly carbon based materials.<sup>115, 116</sup> As one of the most well studied nanochannels, carbon nanotubes (CNTs) have demonstrated exceptional properties for a wide range of applications,<sup>117, 118</sup> including nanotube/fiber reinforced nanocomposites for their high mechanical strength,<sup>119, 120</sup> in electronic applications such as flexible electronics and sensors and transistors for their excellent electrical conductivity and carrier mobility,<sup>121-125</sup> in biotechnology and biomedical applications,<sup>126-129</sup> and as transport channels in membrane technology.<sup>36, 37</sup> Exceptional fast mass transport better or comparable to Knudsen diffusion of water and gas molecules have been achieved using CNTs,<sup>35</sup> and ion exclusion as high as 98% was achieved with sub-2 nm CNTs.<sup>130</sup> However, it still remains a significant challenge to synthesize CNTs with controlled dimensions and functionalities, limiting the application of CNTs in membrane technology.<sup>120, 131</sup>

In contrast, organic nanotubes (ONTs) are very appealing as they offer better control over the CNTs in terms of the assembly process and the surfaces as well as interior and exterior functionalities can be easily tuned by modifying the constituting subunits.<sup>132-136</sup> Various motifs such as amphiphiles, macrocycles, and peptides have been used to construct ONTs through self-assembly process.<sup>132-135, 137, 138</sup> The following sections will give an overview of each of these self-assembling ONTs and discuss some of the issues associated with each of the ONTs.

Amphiphilic molecules, consisted of both hydrophobic and hydrophilic moieties, are one of the most common building blocks for constructing tubular structures through molecular self-assembly.<sup>134, 135</sup> As shown in Figure 1.8, there are 4 common mechanisms

for nanotube formation. Chiral self-assembly typically involves low-molecular-weight amphiphilic molecules self-assemble into helical ribbon or tape structures due to spontaneous twisting of the molecules as an intermediate, and later form a tubular structure as the solution cools down.<sup>135</sup> Theories have been developed to explain the origin of the molecular packing of the chiral amphiphiles<sup>135, 139, 140</sup> and experimental observations for example using phospholipid molecules<sup>141, 142</sup> both demonstrated the formation of nanotubes. Achiral amphiphiles can also self-assemble into tubular structures through packing-directed self-assembly. Israelachvili has pioneered in the field in which cylindrical micelle is would form if the packing parameter,  $P$ , is between  $\frac{1}{3}$  and  $\frac{1}{2}$ .<sup>143</sup> A third mechanism called molecular sculpting is commonly found in polymer amphiphiles and later extended to other systems.<sup>144-146</sup> For instance, a triblock copolymer is made to self-assemble into cylinders first, followed by crosslinking of the outer layer and removal of the inner block typically by ozonolysis.<sup>144</sup> Last but not least, a nanoporous template, such as anodic alumina oxide (AAO) and polycarbonate (PC) membranes, can be used to template nanotube formation from amphiphiles, polymers and metal species.<sup>147-151</sup> ONTs constructed from amphiphilic molecules generally are in tens and hundreds of nanometers range and a considerable amount of effort has been made to well control their morphology and the dimension. However, due to the nature of the subunits and the assembly mechanism, ONTs based on amphiphiles suffer a significant drawback as their structures are very sensitive to the environment.<sup>135</sup> Changes such as the pH, ionic strength, temperature may induce changes in the morphology and hence disassembly of the amphiphiles, restricting the use of ONTs only to limited conditions.

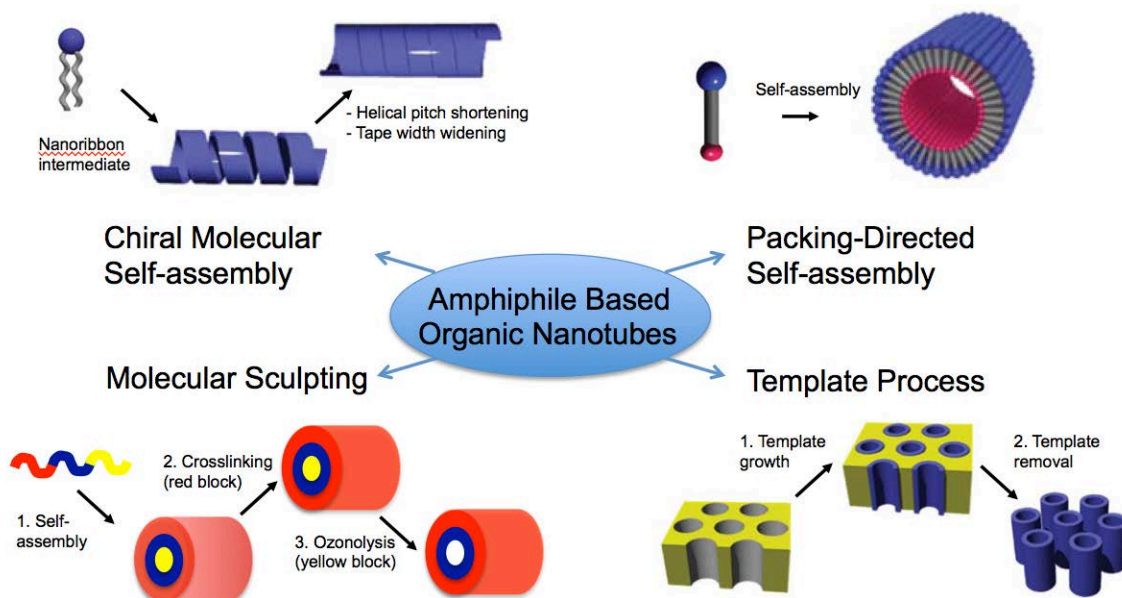


**Figure 1.8.** Schematic showing four common self-assembly mechanisms for ONTs constructed from amphiphilic building blocks. Adapted with permission from reference [135]. Copyright (2005) American Chemical Society.



An alternative strategy in forming tubular structure is through stacking hollow disc-like cyclic subunits, typically via a self-assembly process. Figure 1.7 demonstrates a few examples of different macrocycles capable of forming tubular structures with various dimensions. The driving force for nanotube formation varies with different subunits, some of the common ones include but not limited to  $\pi$ - $\pi$  interactions, Van der Waals forces, hydrogen bonding, electrostatic interactions, etc. One interesting family of macrocycles that have attracted a considerable amount of attention is shape-persistent macrocycle.<sup>138, 152</sup> As shown in Figure 1.9a), Moore et al. successfully synthesized shape-persistent phenylacetylene macrocycles with the planar phenol groups on the backbone favoring the formation of nanotube through  $\pi$ - $\pi$  interaction.<sup>153, 154</sup> Additional contributions from Van der Waals forces and electrostatic interactions may also be responsible for nanotube formation.<sup>153-155</sup> Changing the R side groups to hydrogen bonding moieties such as -OH groups allow further 2D hydrogen bonding network with maintained registry between the subunits.<sup>156</sup> With these shape-persistent macrocycles, it is indeed possible to design and construct nanotubes with well-defined pores and the registry between the subunits allows presentation of different functional groups at very specific sites. Great efforts have been made to improve the synthesis strategy and yields of various macrocycles, especially when subunits contain interior functionalities. In this regard, templated cyclization of macrocycle monomers is commonly used. Instead of non-covalent interaction such as metal coordination and electrostatic interactions, Höger developed the strategy of using an ester linkage to successfully incorporate hydroxyl functionalities in the macrocycle pores with nearly quantitative yield (Figure 1.9b).<sup>157-159</sup> Recently, an interesting strategy of one-step synthesis of oligoamide macrocycles was developed by Gong et al as shown in Figure 1.9c).<sup>160</sup> They same group later investigated the directional assemblies of their oligoamide macrocycles and found that the individual nanotubes formed further organized into a hexagonal lattice with highly efficient ion transport through the nanotubes due to hydrophilic pores.<sup>161</sup> ONTs constructed from macrocycles are robust due to cooperative force of stacking individual subunits and the size of the nanotubes as well as functionalities can be the easily tuned. However, aggregation of macrocycle based ONTs in solution and on solid support is one big issue while processing these nanotubes, preventing the use of ONTs in applied fields.

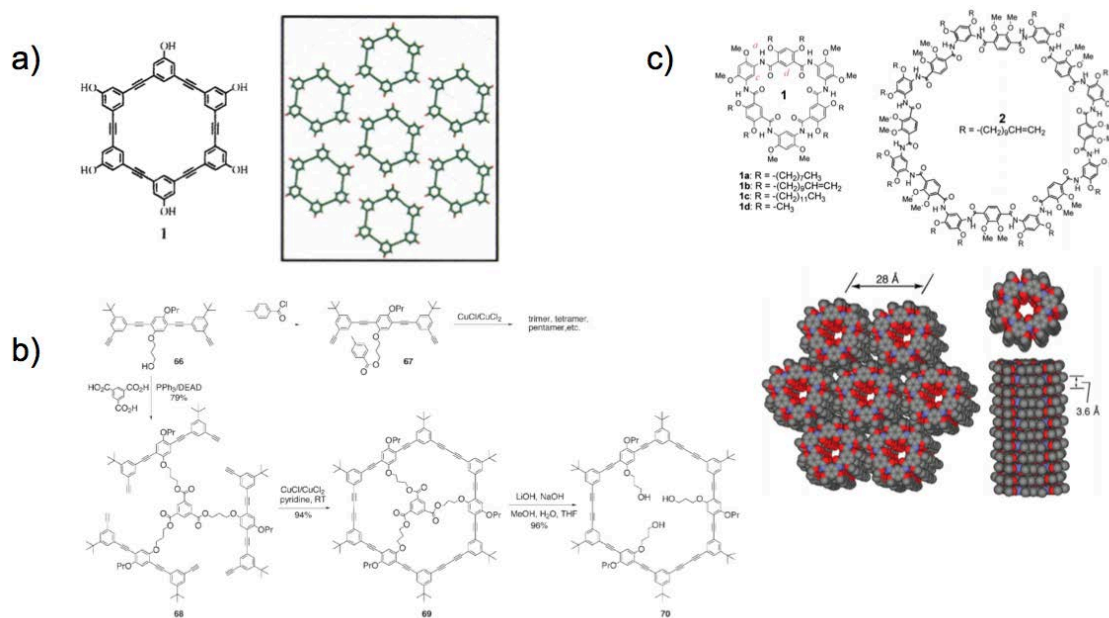


**Figure 1.9.** a) chemical structure and proposed stacking of shape-persistent macrocycles from phenylacetylene molecules; b) hydroxyl-functionalized macrocycle synthesized via templated cyclization; c) one-step synthesis of oligoamide based macrocycles and proposed hexagonal packing of larger macrocycle **2**. a) is adapted with permission from reference [156], copyright (1994) Macmillan Magazines Ltd. b) is adapted with permission from reference [159], copyright (1999) John Wiley & Sons, Inc. c) is adapted from reference [161], copyright (2011) American Chemical Society.

Inspired by the superior performance of the naturally occurring transport channels in biological membranes, channels mimicking the structures of these transmembrane proteins are very attractive and become an interesting area of research. A number of different designs and approaches have been developed to construct artificial protein channels, and peptide-based ONTs with their biodegradability and biocompatibility are a very appealing family of materials to be used as transport channels. Three broad categories of peptides, namely amphiphilic peptide, linear peptide and cyclic peptide have been demonstrated to self-assemble into tubular structures.<sup>133, 136, 162</sup> As discussed previously, amphiphilic building blocks are capable of forming nanotubes with appropriate design and their assemblies can be tailored by varying experimental conditions. The same principle can be applied to peptide-based amphiphiles in which hydrophobic alkyl chains can be attached to hydrophilic peptide heads to form tubular structures.<sup>163</sup> The design of the peptide amphiphile directly determines the self-assembled structure as well as various functions of the resultant ONTs. For instance, as shown in Figure 1.10a), Hartgerink *et al.* designed a peptide amphiphile with 5 regions with the alkyl chains forming the hydrophobic core, cysteine residues for di-sulfide bridge for structural stability, glycine residue for hydrophilicity and flexibility, serine for interaction

with  $\text{Ca}^{2+}$  ions and RGD domains for cell recognition, respectively.<sup>164</sup> Versatility in the selection of various functionalities gives rise to diverse applications of these peptide ONTs in such as drug encapsulation and templated growth of nanowires, etc.<sup>162, 165-167</sup> Nevertheless, structural stability as well as robustness of peptide-amphiphile based ONTs are two areas that still need significant improvements. Another type of building blocks for forming peptide nanotubes is linear peptide. As one of the most studied natural fiber-like structures, amyloid fiber that is responsible for Alzheimer's disease and Parkinson's disease has been investigated and evaluated in details in terms of the constituents and assembly behavior.<sup>168, 169</sup> It is discovered that specific amino acid residue sequences, typically capable of inter- and intra- molecular hydrogen bonding in forming  $\beta$ -sheet structures, are responsible for tubular aggregation and fibrillization of the polypeptide.<sup>170, 171</sup> De novo designs of peptides with fiber-inducing amino acid sequences have been developed to construct various forms of nanotubes as shown in Figure 1.10b).<sup>172, 173</sup> In addition,  $\beta$ -sheet-type helical structures can also be formed using linear D, L-peptide, as inspired from natural pore forming peptide gramicidin A as shown in Figure 1.10c).<sup>133, 174</sup> However, despite of the structural stability due to cooperative  $\beta$ -sheet hydrogen bonding for these linear peptides, poor processability is one serious drawback limiting the use of resultant ONTs for real application since peptides are very subjected to environmental changes such as high temperature, extreme pHs, etc.

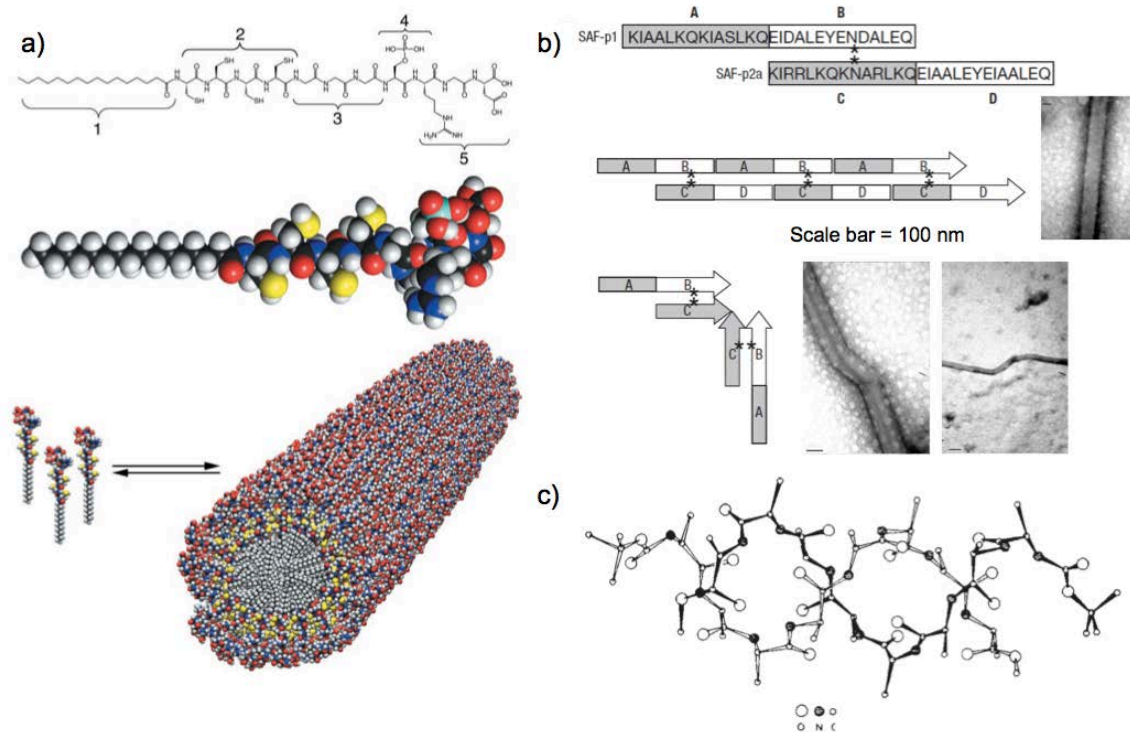


**Figure 1.10.** a) ONTs constructed from 5-component peptide amphiphiles. The alkyl chain (region 1) gives rise to the hydrophobic core while the other 4 peptide-based regions serve various functions. Reprinted with permission from reference [164]. Copyright (2001) AAAS. b) *De novo* designs of ONTs based on linear peptide inspired from the critical  $\beta$ -sheet hydrogen bonding peptide sequence from amyloid fiber.

Reprinted with permission from reference [173]. Copyright (2003) Macmillan Magazines Ltd. c) A double helix ONT structure constructed from linear D, L-oligopeptide. Reprinted with permission from reference [174]. Copyright (1979) Macmillan Magazines Ltd.

Although there are still remaining challenges that need to be circumvented, peptide-based ONTs do offer several insights for the requirements for an ideal candidate for constructing tubular structures as transport channels. While precise structural control on the dimensions of the nanotubes such as the aspect ratio and polydispersity is one of the most critical factor, versatility in synthesis for incorporating different functionalities as well as good processability of the nanotubes are two other important factors to consider for extending the applications of nanotubes in different disciplines. With these criteria in mind, a third type of peptide building blocks, called cyclic peptide, becomes a very attractive candidate for constructing tubular structures which fulfill the three above mentioned requirements. The next section will discuss in details how cyclic peptides form nanotubes and recent achievements in the development of cyclic peptides nanotubes for various applications.

## § 1.4 Cyclic Peptide Nanotubes

Nanotubes assembled from cyclic peptide motif are indeed a promising family of ONTs that can be used as transport channels since they not only offer high performance by mimicking natural cell membrane ion channels, but their structural stability as well as processability with conventional fabrication methods also enable potential use in large scale industrial application. In addition, synthesis and post-modifications of cyclic peptide based motifs are relatively manageable compared to other motifs so that large-scale production is possible.<sup>175-179</sup> History of cyclic peptide motifs can be traced back to 1974, as suggested by De Santis et al. in their theoretical analysis, alternating D, L-amino acids could for closed rings and the peptide rings are capable of stacking to form tubular structures.<sup>180</sup> Based on this design principle, Ghadiri had elegantly synthesized cyclic peptides (CPs) that self-assembled into cyclic peptide nanotubes (CPNs) via extensive intermolecular hydrogen bonding.<sup>176</sup> In his design, CPs are consisted of an even number of alternating D- and L- amino acids. In order to minimize side chain-side chain and side chain-backbone interactions, the CP subunit would adopt a flat ring-like structure where the backbone amide functionalities are approximately perpendicular to the CP ring plane.<sup>176, 181</sup> Therefore, the backbone amides bonds can hydrogen bond with other CP monomers when they are aligned as shown in Figure 1.11. Transmission electron microscopy and electron diffraction clearly demonstrated the structure of CPNs both in bundles and as individual nanotubes.<sup>176</sup> The stacking of the CP monomers is later derived

to be anti-parallel  $\beta$ -sheet structure based on the ring conformation of the CP subunits.<sup>182</sup>  
183

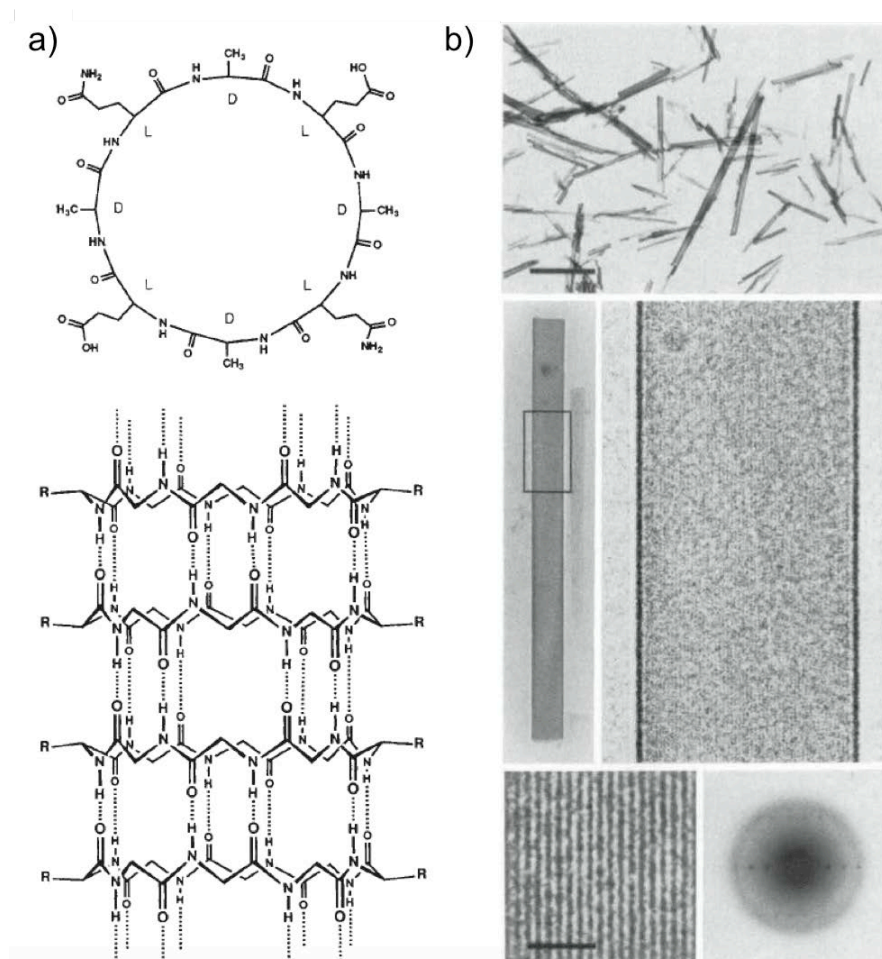


**Figure 1.11.** a) Chemical structure of cyclic peptide and 2D representation of the formation of nanotube through intermolecular hydrogen bonding, b) TEM images of the nanotubes. The top right image shows nanotubes tend to aggregate and form bundles (scale bar = 1  $\mu\text{m}$ ). The bottom right image shows a higher resolution image of individual nanotubes (scale bar = 10 nm) and the electron diffraction pattern of a single nanotube. Reprinted with permission from reference [176]. Copyright (1993) Macmillan Magazines Ltd.

The CPN structure of  $\beta$ -helices from the self-assembly of CP subunits is also found in natural pore-forming peptides such as gramicidin A, making CPN an attractive candidate for artificial ion channels.<sup>184, 185</sup> The synthesis of CPs alone is relatively simple in which standard Fmoc based solid phase peptide synthesis is usually used.<sup>186</sup> Furthermore, due to the constriction of amino acid backbone, the side groups on the amino acids will project outward away from the CP rings.<sup>176, 181</sup> This makes post-synthesis modifications possible with selected amino acid side chains so that various bioconjugates can be made.<sup>187-190</sup> A detailed discussion of CP-polymer conjugates is

presented in the next section. In addition, the nanotube diameter as well as chemical surface properties can be easily tuned by modifying the primary amino acid sequence. CPNs with different diameters had been successfully made, and various artificial subunits had been incorporated into the peptide sequence to make CPNs with different surface properties and interior functionalities. Unlike natural ion channels which are made of proteins, CPNs with extensive inter-CP hydrogen bonds are relatively stable against changes in pH, temperature, ionic strength, etc. As a result, CPNs formed by the self-assembly of CP monomers are indeed an attractive materials in mimicking natural transport channels. The following section outlines and discusses some of the developments in the design and synthesis of various cyclic peptides.

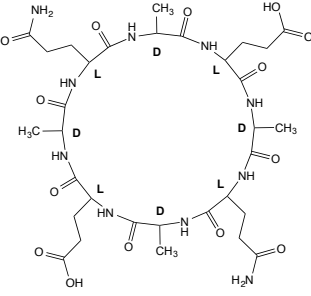
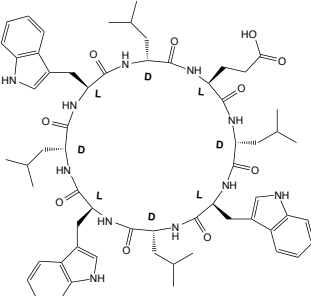
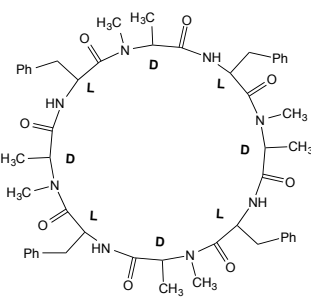
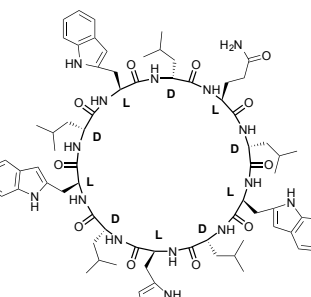
### 1.4.1 Cyclic Peptide Sequence Design and Synthesis

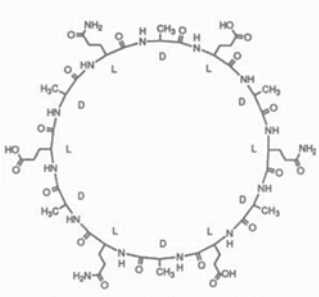
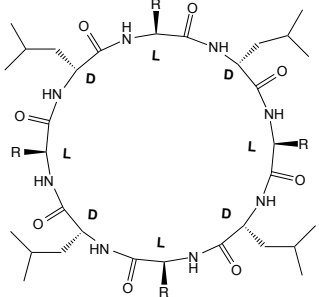
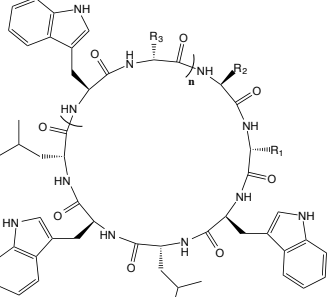
Depending on the constituting amino acid structures, various CPs have been successfully made and Table 1.2 presents a summary of some notable examples of the CPs.  $\alpha$ -amino acids, the most common form of amino acids, was what Ghadiri used to make the very first CPN with the 8-mer peptide sequence *cyclo*(D-Ala-L-Glu-D-Ala-L-Gln)<sub>2</sub>.<sup>176</sup> Similar D, L- $\alpha$ -cyclic peptides with 10 and 12 amino acid subunits have been successfully synthesized, giving rise to bigger ring size of 1.0 nm and 1.2 nm, respectively.<sup>191, 192</sup> In parallel, changes in the constituting amino acid sequences as well as amino acid side groups have been made for specific purpose. For example, tryptophan and leucine have been incorporated to the primary peptide sequence so that the exterior of the resultant CPN is hydrophobic and can be inserted to lipid bilayer to form ion channels.<sup>175</sup> Using N-methylated alanine subunit, CPN formation is limited to only dimer formation and the  $\beta$ -sheet structure of CPN is therefore confirmed.<sup>183</sup> Arginine has also been included in the CP sequence and the resultant CPN can act as adapters for the pore-forming protein staphylococcal  $\alpha$ -hemolysin ( $\alpha$ -HL) to tune the conductance across the pore.<sup>193</sup> Antibacterial activity has also been observed for CPNs with 6 or 8 amino acid sequences of arginine or lysine.<sup>194</sup>

Taking one step further,  $\beta$ -amino acids can also be used to make  $\beta$ -cyclic peptides that are still capable of self-assembling into nanotubes. Due to the extra carbon from the  $\beta$ -amino acid, 4 subunits would be sufficient to make a flat CP ring adopting a C<sub>4</sub> structure.<sup>195-197</sup> The alignment of the amide and carbonyl groups generates a net dipole moment, possibly affecting the nanotube conductance.<sup>196</sup> A third variation can be made when  $\gamma$ -amino acids are used to substitute  $\alpha$ -amino acids to make  $\alpha$ ,  $\gamma$ -CPs, 3 $\alpha$ ,  $\gamma$ -CPs, and  $\gamma$ -CPs.<sup>198</sup> This design gives the inner cavities of CPNs certain hydrophobicity, resulting in a rich variety of tubular structures with various ion transport performance.<sup>199</sup> In particular, the very first CP with interior functional group (methyl functionality) was successfully synthesized and proved to form long aspect ration nanotubes.<sup>200</sup> Last but not least,  $\epsilon$ -amino acids with triazole functionalities have also been incorporated into the CP backbone to tune the physical properties of the nanotube interior.<sup>201</sup>

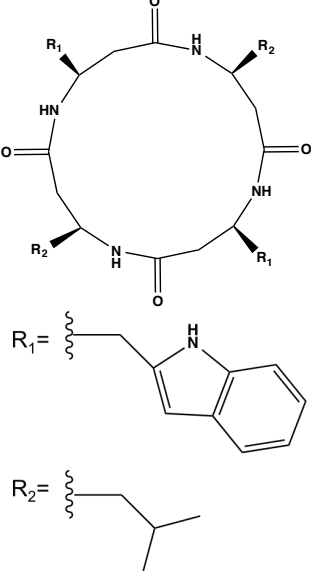
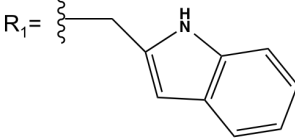
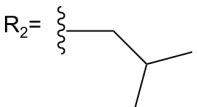
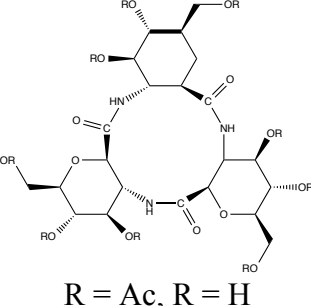
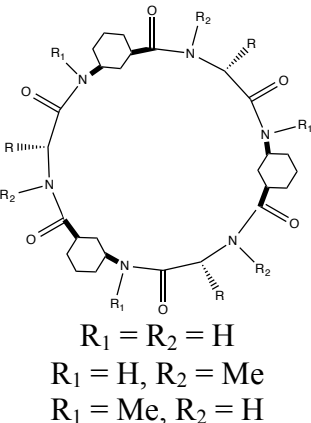
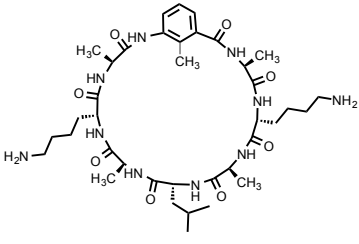


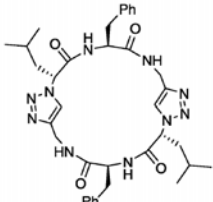
**Table 1.2.** Structures and properties of selected cyclic peptides

| Structure   | # of units | Amino acids                            | Remark  | Ref. |
|---|------------|--|---|------|
|  <p><i>cyclo</i>[D-Ala-L-Glu-D-Ala-L-Gln]<sub>2</sub></p>    | 8          | All $\alpha$                           | First report of D, L- $\alpha$ cyclic peptide forming nanotubes                                 | 176  |
|  <p><i>cyclo</i>[(L-Trp-D-Leu)<sub>3</sub>-L-Gln-D-Leu]</p> | 8          | All $\alpha$                           | Nanotubes as ion channels incorporated in lipid bilayer membrane                                | 175  |
|  <p><i>cyclo</i>[L-Phe-D-N-MeAla]<sub>4</sub></p>          | 8          | (4) $\alpha$<br>(4) N-methylated D-Ala | Dimer formation due to N-methylation; Confirmation of $\beta$ -sheet formation of the nanotubes | 183  |
|    | 10         | All $\alpha$                           | 10-residue peptide sequence with 10 Å channel size; Display glucose transport                   | 191  |

|   |        |              |   |     |
|---|--------|--------------|---|-----|
| <p><i>cyclo</i>[L-Gln-(D-Leu-L-Trp)<sub>4</sub>-D-Leu]</p>  |        |              |   |     |
|  <p><i>cyclo</i>[(L-Gln-D-Ala-L-Glu-D-Ala)<sub>3</sub>]</p>  | 12     | All $\alpha$ | 12-residue peptide sequence with 13 Å diameter still forms nanotubes  | 192 |
|  <p>R= Arg, R= Glu<br/><i>cyclo</i>[(L-Arg/Glu-D-Leu)<sub>4</sub>]</p>  | 8      | All $\alpha$ | Nanotubes act as adapters for the pore-forming protein staphylococcal $\alpha$ -hemolysin ( $\alpha$ -HL); Charge selectivity of $\alpha$ -HL altered by peptide; Conductance of $\alpha$ -HL reduced by 53% when R=Arg | 193 |
|  <p>n = 0<br/>R<sub>1</sub> = R<sub>2</sub> = Lys<br/>R<sub>1</sub> = R<sub>2</sub> = Arg<br/>n = 1<br/>R<sub>1</sub>, R<sub>2</sub>, R<sub>3</sub> = Lys, Glu, Arg; Lys, Ser, Lys; Lys, Lys, Lys; Arg, Arg, Lys</p> | 6 or 8 | All $\alpha$ | Antibacterial behavior against Gram-positive and/or Gram-negative bacterial by increasing permeability and collapsing potential gradient across the cell membrane   | 194 |
|   | 4      | All $\beta$  | 4-residue $\beta$ -peptide sequence adopting C <sub>4</sub> ring structure, forming nanotubes via hydrogen bonding  | 196 |



|   |   |   |  |     |
|---|---|---|--|-----|
|  <p> <math>R_1 =</math> <br/> <math>R_2 =</math>  </p> |   |   |  |     |
|  <p><math>R = \text{Ac}, R = \text{H}</math></p>  | 3 | All $\beta$                             | 3-residue $\beta$ -peptide sequence adopting $C_3$ ring structure forms nanotubes  | 197 |
|  <p> <math>R_1 = R_2 = \text{H}</math><br/> <math>R_1 = \text{H}, R_2 = \text{Me}</math><br/> <math>R_1 = \text{Me}, R_2 = \text{H}</math> </p>  | 6 | (3) $\alpha$<br>(3) $\gamma$            | $\alpha, \gamma$ -cyclic peptide forming nanotubes with inner cavities due to the cyclohexane groups in the primary sequence | 198 |
|    | 8 | (7) $\alpha$<br>(1) $\gamma$ derivative | $\alpha, \gamma$ -cyclic peptide forming nanotubes with methyl group projected to the interior of the peptide ring           | 200 |

|   |   |                                |  |     |
|---|---|--------------------------------|--|-----|
|  | 4 | (2) $\alpha$<br>(2) $\epsilon$ | $\alpha$ , $\epsilon$ -cyclic peptide forming nanotubes with tunable nanotube interior physical properties | 201 |
|---|---|--------------------------------|--|-----|

## 1.4.2 Cyclic Peptide Conjugates

Although cyclic peptide nanotubes have demonstrated many advantages over other materials for mimicking natural transport channels, one major drawback for cyclic peptides is its poor solubility due to high tendency to form bundles of CPNs in micrometer sizes.<sup>176</sup> This tendency to aggregate as a result of extensive intermolecular hydrogen bonding prevents easy processing of the CPNs and thus limits their uses. Moreover, although there have been much progress in constructing functional nanotubes, more advancements are needed to expand the functionalities of the CPNs so that this platform can be applied to other disciplines.<sup>202</sup> As a result, various molecules have been conjugated to the peripheral of the CP rings to improve the processability of the CPNs and to expand the functionalities for various applications. For example, cationic 1,4,5,8-naphthalenetetracarboxylic diimide (NDI) derivatives were attached to D, L- $\alpha$ -CPs and the resultant conjugates self-assembled into nanotubes in aqueous solution.<sup>203</sup> The self-assembly of the CPs mediated the alignment of the NDI units and the nanotubes possessed delocalized electronic states.<sup>203</sup> Furthermore, fullerenes could also be attached to the exterior of the CPs, in which the formation of CPNs would template the alignment of the C<sub>60</sub> units to form 1D fullerene arrangement.<sup>187, 204</sup> Due to the delocalized electrons from fullerenes and the NDI units, CPN conjugates can therefore be potentially used for electronic applications. More recently, a double nanotube structure has been achieved using pre-formed CNT with self-assembled CPN in which CPNs tend to bind to semiconducting CNTs rather than metallic CNTs.<sup>205</sup> With electrical conductivity from CNTs, the double nanotube hybrid may be used for optical and electrical applications.

Cyclic peptide-polymer conjugates are a very important family of CP based conjugates. The conjugated polymer chains not only wrap around the individual nanotubes to prevent aggregation of the CP subunits, but also add more functionalities to the CPs to help process the nanotubes in different environments.<sup>188, 189, 206, 207</sup> To conjugate polymer chains to the peptide nanotubes, both convergent and divergent approaches have been used and demonstrated successful attachment of various polymers to the exterior of the CP subunits. Biesalski's group first adopted the "graft-from"

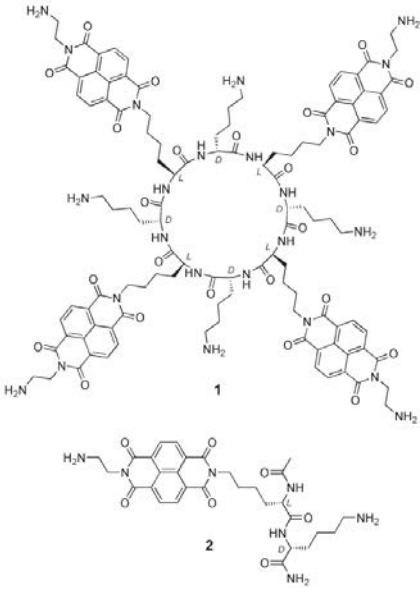
method in which side groups of specific amino acids were modified with functional groups to initiate atom-transfer radical polymerization (ATRP) of *N*-isopropylacrylamide (NIPAM).<sup>188</sup> In the process, CP subunits with initiators were assembled into nanotubes first and PNIPAM were grown on the nanotube surface. A homogeneous shell of PNIPAM chains on the CPN surface prevents 2D aggregation of bare CPs. In subsequent studies, three polymers (polystyrene, poly(*n*-butyl acrylate), and poly(*N*-isopropylacrylamide)) were grown from the CP exterior with controlled degrees of polymerization.<sup>208</sup> It was found that with increasing mass of the grafted polymers, there was an increase in resultant nanotube diameter but a decrease in length due to excluded volume of the grafter polymer chains. This indeed demonstrates that the dimensions of CPNs can be fine tuned through polymer conjugation. On the other side, “graft-to” method was used by Börner’s group in which carboxylated poly(*n*-butyl acrylate) were covalently conjugated to the amine functionality of the lysine side chains of the cyclic peptide sequence.<sup>189</sup> The conjugates could interact laterally to further organize into weak networks. Both approaches demonstrated that CPs could still self-assemble into tubular structures despite the steric hindrance of confining the conjugated polymer chains to inter-CP hydrogen bonding distance which destabilizes the nanotube structure.

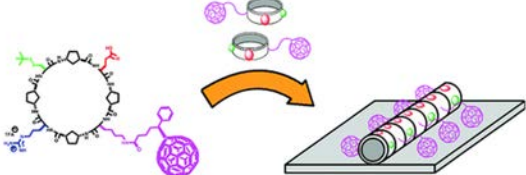
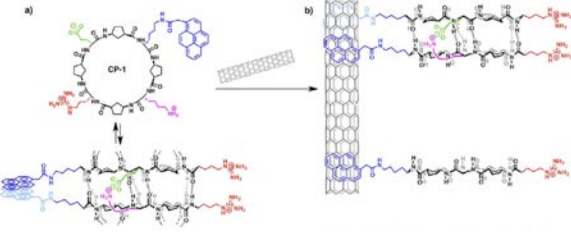
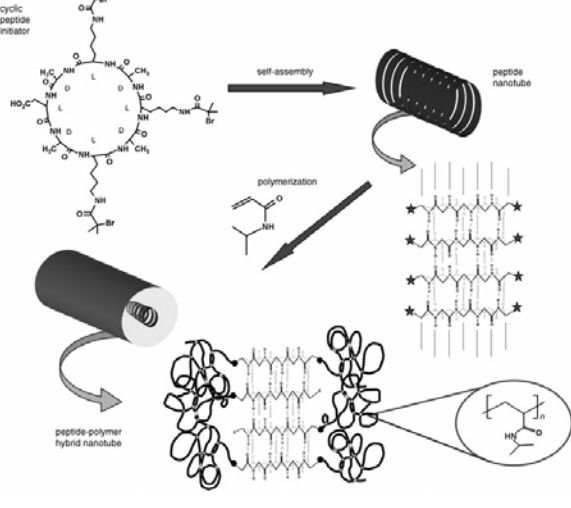
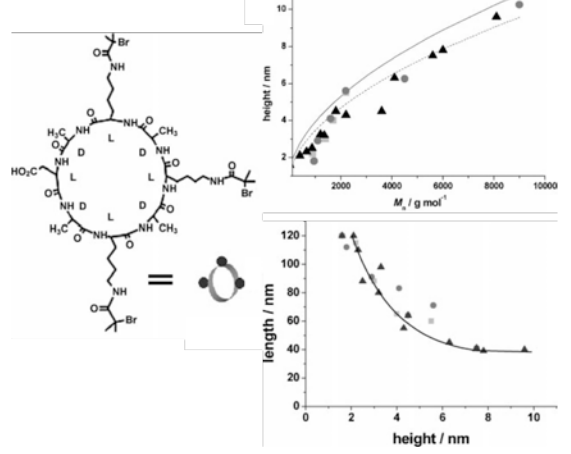
More recently, Perrier’s group has been very successful in attaching polymer chains of different functionalities to cyclic peptide using copper catalyzed “click” chemistry and reversible addition-fragmentation chain transfer (RAFT).<sup>190, 207, 209-211</sup> The ability to grow polymer chains with very narrow molecular weight distribution enables them to perform fundamental studies on the self-assembly of CPNs with different polymer shells. Using neutron scattering, *in-situ* investigation had been performed on the assembly of poly(butyl acrylate)-conjugated CPNs in solution.<sup>211</sup> Due to the chemical nature of the polymer and steric repulsion of the conjugated chains, the dimensions of polymer-conjugated CPNs can therefore be controlled by varying the solvent conditions and/or polymer chain length. More complex tubular structure can be constructed with variations in the conjugated polymer chains. Two polymer chains of different chemical natures were conjugated to the same cyclic peptide back so that the conjugates would self-assemble into a demixed Janus-like nanotubes or mixed polymer wrapped nanotubes depending on the environment.<sup>190</sup> It is demonstrated that in the demixed state, the Janus-like nanotubes can further organize to form a bigger artificial pore in phospholipid bilayer.<sup>190</sup> This design not only offers dual functionalities on the nanotube surface, but also provides insights in creating natural protein channel mimetics. Furthermore, multi-shell cyclic peptide nanotube can also be attained when conjugating block copolymer arms to the CP backbone, allowing potential further processing the nanotubes to form anisotropic nanocapsules.<sup>207</sup> On the other hand, Xu et al. has developed a novel approach in using cyclic peptide nanotubes as transport channels in a polymeric membrane. They showed that the polymer side chains could modulate the growth of the cyclic peptide nanotubes through polymer-polymer interactions with different components of a block copolymer (BCP) matrix, thus confining the nanotubes to be at the center of the cylindrical block of the BCP matrix and creating channels with sub-nanometer pores.<sup>206</sup>

This novel approach indeed opens a new strategy in fabricating membranes containing sub-nanometer channels for different transport processes and molecular separation. Using an interiorly functionalized CP, they have also demonstrated the conjugated polymer chains have allowed further processing of the nanotubes to be compatible with conventional polymer processing.<sup>200</sup> Using solvent annealing which is typically used for polymers, poly(ethylene oxide)-conjugated CPNs can be broken down into shorter tubelets. As a result of thermo-reversibility of hydrogen bonding, the short fragments can be re-merged to form longer nanotubes upon controlled heating and cooling. This approach demonstrates the advantage of polymer conjugation in facilitating control over the CPN nanostructures. Table 1.3 summarizes the structures and highlights important findings for the selected cyclic peptide nanotubes conjugated with various compounds.

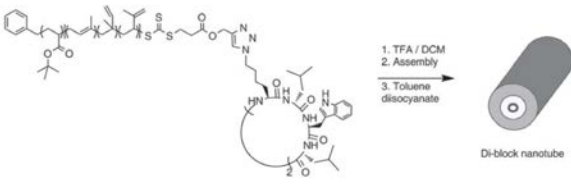
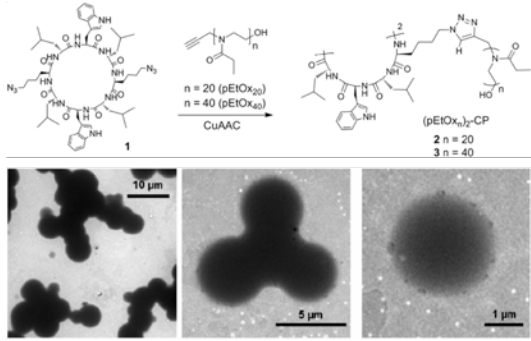
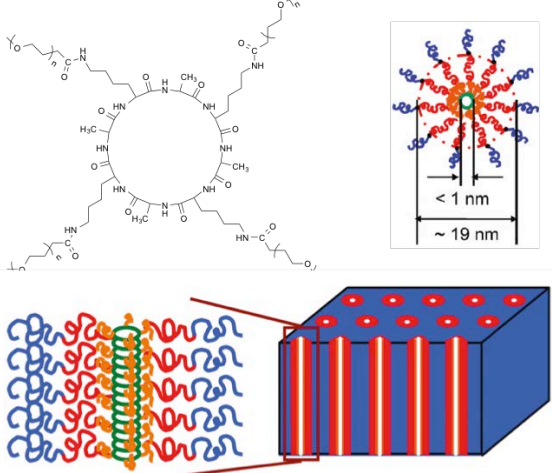
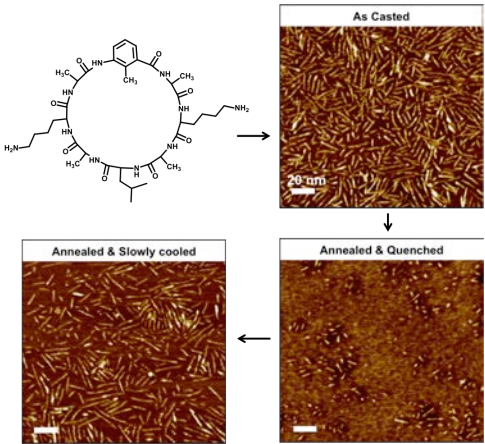
In summary, CPNs with their stability and robustness are attractive family of materials potentially useful for various applications. Various materials have been conjugated to the exterior of the nanotubes, serving various functions. In particular, polymer conjugation has set many advancements in fine-tuning the dimensions of the resultant nanotubes, constructing complex tubular nanostructures, and allowing further processing of the nanotubes with conventional processing techniques used for polymers.

**Table 1.3** Summary of selected cyclic peptide conjugates and their properties

| Structure/Scheme  | Conj. units                | Remark   | Ref        |
|---|----------------------------|--|------------|
|  <p>1</p> <p>2</p> | <p>NDI and derivatives</p> | <p>Delocalized electrons from NDI side groups results in CPNs possessing highly delocalized electron states potentially useful in optical and electronic devices</p> | <p>203</p> |

|   |  |   |     |
|---|--|---|-----|
|    | Fullerene  |   | 187 |
|    | CNT  | Double nanotube structure of inorganic CNT and self-assembled CPN is achieved, and the hybrid displays electrical conductivity                                  | 205 |
|   | Polymer: N-isopropylacrylamide [PNIPAM]  | Polymer coated CPN is constructed by adopting “graft-from” strategy to grow PNIPAM arms off from CP backbone  | 188 |
|  | Polymer: styrene, or <i>n</i> -butyl acrylate, or N-isopropylacrylamide [PS, PnBA, and PNIPAM] | PS/PBA/PNIPAM coated CPNs are constructed, demonstrating an inverse relationship between the dimensions of the CPNs with the mass of the grafted polymer chains | 208 |

|   |            | <p>Polymer: <i>n</i>-butyl acrylate [PnBA]</p>                    | <p>Polymer wrapped CPNs constructed using “graft-from” method by directly conjugating polymer chains to CP backbone</p> | <p>189</p>      |    |     |  |  |    |     |  |  |    |     |     |     |    |     |     |      |     |     |     |     |     |     |     |     |  |            |            |            |    |     |  |    |     |  |    |     |     |    |     |     |     |     |     |     |     |     |                                      |  |            |
|---|------------|---|---|-----------------|----|-----|--|--|----|-----|--|--|----|-----|-----|-----|----|-----|-----|------|-----|-----|-----|-----|-----|-----|-----|-----|--|------------|------------|------------|----|-----|--|----|-----|--|----|-----|-----|----|-----|-----|-----|-----|-----|-----|-----|-----|--------------------------------------|--|------------|
| <p>Total Length (Å) vs Polymer DP</p> <table border="1"> <thead> <tr> <th>Polymer DP</th> <th>DMF</th> <th>TFA / CDCl<sub>3</sub> (1:9)</th> <th>TFA / THF (1:9)</th> </tr> </thead> <tbody> <tr><td>16</td><td>177</td><td></td><td></td></tr> <tr><td>30</td><td>261</td><td></td><td></td></tr> <tr><td>70</td><td>231</td><td>413</td><td>444</td></tr> <tr><td>90</td><td>275</td><td>421</td><td>1500</td></tr> <tr><td>108</td><td>303</td><td>407</td><td>306</td></tr> <tr><td>195</td><td>326</td><td>307</td><td>326</td></tr> </tbody> </table> | Polymer DP | DMF   | TFA / CDCl <sub>3</sub> (1:9)   | TFA / THF (1:9) | 16 | 177 |  |  | 30 | 261 |  |  | 70 | 231 | 413 | 444 | 90 | 275 | 421 | 1500 | 108 | 303 | 407 | 306 | 195 | 326 | 307 | 326 | <p>Total length (Å) vs Polymer DP</p> <table border="1"> <thead> <tr> <th>Polymer DP</th> <th>DMF - 25°C</th> <th>DMF - 70°C</th> </tr> </thead> <tbody> <tr><td>16</td><td>229</td><td></td></tr> <tr><td>30</td><td>216</td><td></td></tr> <tr><td>70</td><td>237</td><td>218</td></tr> <tr><td>90</td><td>275</td><td>241</td></tr> <tr><td>108</td><td>300</td><td>273</td></tr> <tr><td>195</td><td>307</td><td>307</td></tr> </tbody> </table> | Polymer DP | DMF - 25°C | DMF - 70°C | 16 | 229 |  | 30 | 216 |  | 70 | 237 | 218 | 90 | 275 | 241 | 108 | 300 | 273 | 195 | 307 | 307 | <p>Polymer: butyl acrylate [PBA]</p> | <p><i>In-situ</i> investigation on the assembly of polymer covered CPNs in solution. Control over the nanotube dimension can be achieved by varying the solvent conditions and/or polymer chain length</p> | <p>211</p> |
| Polymer DP  | DMF        | TFA / CDCl <sub>3</sub> (1:9)                                     | TFA / THF (1:9)   |                 |    |     |  |  |    |     |  |  |    |     |     |     |    |     |     |      |     |     |     |     |     |     |     |     |  |            |            |            |    |     |  |    |     |  |    |     |     |    |     |     |     |     |     |     |     |     |                                      |  |            |
| 16  | 177        |   |   |                 |    |     |  |  |    |     |  |  |    |     |     |     |    |     |     |      |     |     |     |     |     |     |     |     |  |            |            |            |    |     |  |    |     |  |    |     |     |    |     |     |     |     |     |     |     |     |                                      |  |            |
| 30  | 261        |   |   |                 |    |     |  |  |    |     |  |  |    |     |     |     |    |     |     |      |     |     |     |     |     |     |     |     |  |            |            |            |    |     |  |    |     |  |    |     |     |    |     |     |     |     |     |     |     |     |                                      |  |            |
| 70  | 231        | 413   | 444   |                 |    |     |  |  |    |     |  |  |    |     |     |     |    |     |     |      |     |     |     |     |     |     |     |     |  |            |            |            |    |     |  |    |     |  |    |     |     |    |     |     |     |     |     |     |     |     |                                      |  |            |
| 90  | 275        | 421   | 1500  |                 |    |     |  |  |    |     |  |  |    |     |     |     |    |     |     |      |     |     |     |     |     |     |     |     |  |            |            |            |    |     |  |    |     |  |    |     |     |    |     |     |     |     |     |     |     |     |                                      |  |            |
| 108   | 303        | 407   | 306   |                 |    |     |  |  |    |     |  |  |    |     |     |     |    |     |     |      |     |     |     |     |     |     |     |     |  |            |            |            |    |     |  |    |     |  |    |     |     |    |     |     |     |     |     |     |     |     |                                      |  |            |
| 195   | 326        | 307   | 326   |                 |    |     |  |  |    |     |  |  |    |     |     |     |    |     |     |      |     |     |     |     |     |     |     |     |  |            |            |            |    |     |  |    |     |  |    |     |     |    |     |     |     |     |     |     |     |     |                                      |  |            |
| Polymer DP  | DMF - 25°C | DMF - 70°C  |   |                 |    |     |  |  |    |     |  |  |    |     |     |     |    |     |     |      |     |     |     |     |     |     |     |     |  |            |            |            |    |     |  |    |     |  |    |     |     |    |     |     |     |     |     |     |     |     |                                      |  |            |
| 16  | 229        |   |   |                 |    |     |  |  |    |     |  |  |    |     |     |     |    |     |     |      |     |     |     |     |     |     |     |     |  |            |            |            |    |     |  |    |     |  |    |     |     |    |     |     |     |     |     |     |     |     |                                      |  |            |
| 30  | 216        |   |   |                 |    |     |  |  |    |     |  |  |    |     |     |     |    |     |     |      |     |     |     |     |     |     |     |     |  |            |            |            |    |     |  |    |     |  |    |     |     |    |     |     |     |     |     |     |     |     |                                      |  |            |
| 70  | 237        | 218   |   |                 |    |     |  |  |    |     |  |  |    |     |     |     |    |     |     |      |     |     |     |     |     |     |     |     |  |            |            |            |    |     |  |    |     |  |    |     |     |    |     |     |     |     |     |     |     |     |                                      |  |            |
| 90  | 275        | 241   |   |                 |    |     |  |  |    |     |  |  |    |     |     |     |    |     |     |      |     |     |     |     |     |     |     |     |  |            |            |            |    |     |  |    |     |  |    |     |     |    |     |     |     |     |     |     |     |     |                                      |  |            |
| 108   | 300        | 273   |   |                 |    |     |  |  |    |     |  |  |    |     |     |     |    |     |     |      |     |     |     |     |     |     |     |     |  |            |            |            |    |     |  |    |     |  |    |     |     |    |     |     |     |     |     |     |     |     |                                      |  |            |
| 195   | 307        | 307   |   |                 |    |     |  |  |    |     |  |  |    |     |     |     |    |     |     |      |     |     |     |     |     |     |     |     |  |            |            |            |    |     |  |    |     |  |    |     |     |    |     |     |     |     |     |     |     |     |                                      |  |            |
| <p>demixed mixed</p>  |            | <p>Polymer: <i>n</i>-butyl acrylate and styrene [PnBA and PS]</p> | <p>Janus-like cyclic peptide-polymer nanotubes can be formed in appropriate solvents and in phospholipid bilayer</p>    | <p>190</p>      |    |     |  |  |    |     |  |  |    |     |     |     |    |     |     |      |     |     |     |     |     |     |     |     |  |            |            |            |    |     |  |    |     |  |    |     |     |    |     |     |     |     |     |     |     |     |                                      |  |            |

|   |  |  |            |
|---|--|--|------------|
|    | <p>Polymer:<br/>isoprene and<br/>acrylic acid<br/>BCP [PI-<i>b</i>-<br/>PAA]</p> | <p>Multi-shell cyclic<br/>peptide-polymer<br/>nanotubes by<br/>conjugating BCP<br/>chains to CP<br/>backbone</p>   | <p>207</p> |
|    | <p>Polymer:<br/>poly(2-ethyl-2-<br/>oxazoline)<br/>[PEtOx]</p>                   | <p>LCST behavior of<br/>PEtOx causes<br/>resultant CPNs<br/>reversibly<br/>transformed into<br/>microparticles at<br/>temperature &gt;<br/>cloud point in<br/>water</p>  | <p>212</p> |
|   | <p>Polymer:<br/>ethylene<br/>oxide [PEO]</p>                                     | <p>PEO-conjugated<br/>CPN incorporated<br/>into BCP<br/>cylindrical<br/>microdomains to<br/>form sub-<br/>nanometer<br/>channels<br/>demonstrating<br/>high gas transport<br/>performance</p>  | <p>206</p> |
|  | <p>Polymer:<br/>ethylene<br/>oxide [PEO]</p>                                     | <p>Conjugated PEO<br/>arms allow further<br/>processing of the<br/>CPNs. Nanotubes<br/>are broken down<br/>upon solvent<br/>annealing due to<br/>high PEO<br/>mobility, and can<br/>be reformed with<br/>thermal heating<br/>and slow cooling.</p> | <p>200</p> |

## § 1.5 Conclusion and Outlook

Membranes are widely used in separation and purification processes and polymeric membranes are very attractive materials due to their relative low cost and ease of fabrication. However, polymeric membranes do suffer from a trade-off between permeability and selectivity as exemplified by the upper boundary in Robeson's plot for gas separation. Furthermore, as the size of the permeates continues to go down, high performance membrane often requires very small pore size and narrow pore size distribution. Thus, novel designs for polymer-based membranes are needed to meet the demand for high performance that balance the permeability and selectivity trade-off and maintain well-controlled pore size. In this regard, self-assembled cyclic peptide nanotubes in comparison to other nanotubes offer many advantages as transport channels for molecular separation. They have a strong tendency to form high aspect ratio nanotubes with very well defined pore size as a result of extensive hydrogen bonding between subunits. The antiparallel stacking of constituting subunits mimics the  $\beta$ -barrel structure of natural protein channels, which show very high performance in ion transport. The small channel size in the range of 0.8-1.2 nm also allows the possibility for molecular separation and the size is tunable simply by varying the number of amino acid subunits in the peptide primary sequence. Moreover, functionalities can be incorporated to the interior of the channel to improve the selectivity for certain species. However, one major drawback of using cyclic peptide nanotubes for transport channels is its strong tendency to aggregate in organic solvents. To circumvent this problem, polymer conjugation proves to be an effective way to prevent aggregation of CPs. The conjugated polymer chains not only wrap around individual nanotubes to prevent aggregation in the lateral direction, but they may also offer certain control over the length of the polymer-conjugated nanotubes. Furthermore, the conjugated polymers also mediate the interactions of the CPs to the environment so that the CP-polymer conjugates can be processed with block copolymers. This indeed expands the use of the self-assembled CPNs not only as ion channels in phospholipid bilayer, but also as transport channels in conventional membranes for different chemical species.

## § 1.6 General Approach and Synopsis for Subsequent Chapters

The general strategy to fabricate sub-nanometer porous membrane is to utilize the self-assembly of cyclic peptides and align the resultant cyclic peptide nanotubes in a controlled manner. It is important to gain a fundamental understanding of the behavior of polymer-conjugated cyclic peptides and how the added polymers affect the interactions between the nanotubes with the environment. Chapter 2 discusses in details how different degrees of polymer conjugation could affect the self-assembly of the cyclic peptides and how the growth of the nanotubes can be to controlled and modulated within a processing



window. With the understandings from the assembly behavior of polymer-conjugated cyclic peptide nanotubes and the control over the dimensions of the nanotubes, we can then focus on fabricating membranes using the nanotubes as transport channels. Block copolymer (BCP), which self-assembles into a cylindrical morphology, is used as the matrix to confine and orient the cyclic peptide nanotubes. Chapter 3 describes in details the fundamentals (i.e. thermodynamic and kinetic contributions) governing the co-assembly of cyclic peptide-polymer conjugates and block copolymer matrix in thin films. Cyclic peptide-polymer conjugates are firstly sequestered in the cylindrical microdomain of the BCP matrix due to the interactions with the individual blocks of the BCP, and the nanotubes are then re-grown within the cylindrical microdomains to form well-aligned channels. Fine details of how to control the kinetic pathway in the co-assembly process to ensure high quality membrane are revealed in Chapter 3. Taking a step further, a new type of cyclic peptide with interior functionality (methyl group) has also been synthesized successfully. Chapter 4 reveals the self-assembly as well as co-assembly behaviors of the methyl modified cyclic peptides with BCP, focusing on the key parameters in processing new type of nanotubes to fabricate sub-nm channels with interior functionalities. Upon successful fabrication of membranes containing sub-nm pores with and without functionalities, gas transport behavior is investigated for both the unmodified and modified cyclic peptides. Furthermore, preliminary studies on the ion transport of the sub-nanometer membranes are also investigated. Both investigations offer valuable insights for utilizing cyclic peptide nanotubes as transport channels in membrane technology for different separation processes.

## Chapter 2

# Self-assembly of Cyclic Peptides and Cyclic Peptide-Polymer Conjugates

|              |   |           |
|--------------|---|-----------|
| <b>§ 2.1</b> | <b>Introduction.....</b>  | <b>38</b> |
| <b>§ 2.2</b> | <b>Results and Discussion.....</b>                                      | <b>40</b> |
| <b>§ 2.3</b> | <b>Conclusion .....</b>   | <b>47</b> |
| <b>§ 2.4</b> | <b>Experimental .....</b>   | <b>47</b> |
|              | 2.4.1 Materials.....  | 47        |
|              | 2.4.2 Peptide synthesis and PEG conjugation.....                        | 48        |
|              | 2.4.3 Reversed-Phase High-Pressure Liquid Chromatography (RP-HPLC)..... | 49        |
|              | 2.4.4 Fourier Transfer Infrared Spectroscopy (FTIR).....                | 49        |
|              | 2.4.5 Formation of pc-CPNs .....  | 49        |
|              | 2.4.6 Statistical Analysis of pc-CPN Length.....                        | 49        |

Partial material has been submitted for publication: C. Zhang and T. Xu, submitted to *JACS* (2015).

*Self-assembling cyclic peptide nanotubes (CPNs) offer unique advantage in constructing high aspect ratio tubular structures with surface functionalities that are relatively stable. However, it is challenging to control the growth of the CPNs, which naturally tend to further aggregate to form bundles of nanotubes. Polymer conjugation on the exterior of the CPNs prevents lateral aggregation by shielding individual CPNs to form polymer-covered nanotubes (pc-CPNs), in which the growth of the pc-CPNs is restricted mainly due to steric hindrance. We demonstrate here an alternative simple design to tune the growth of pc-CPNs by varying the position of the conjugated polymer chain to destabilize the nanotube structure as a result of the entropic penalty associated with chain deformation. The resultant pc-CPN length is correlated to the degree of polymer conjugation, or the number of polymer chains anchored, and the solution concentration. A theoretical framework is developed to capture the underlying thermodynamic basis of pc-CPN growth. The entropic effect of polymer conjugation combined with enthalpic monomer concentration give us multiple handles in modulating the growth of pc-CPNs, extending the experimental approach to control the spatial organization 1D nanotubes with varying interior and exterior features for various applications.*

## § 2.1 Introduction

Tubular nanostructures have gained growing attention as their unique properties may be exploited for many applications such as molecular transport and separation, biosensing, controlled drug release, fiber-reinforced nanocomposites, etc.<sup>1-7</sup> As one of the most well-studied 1D nanostructures, carbon nanotubes (CNTs) have demonstrated exceptional mechanical, electrical, biomedical and transport properties.<sup>8-17</sup> However, it is still nontrivial to synthesize CNTs with controlled aspect ratio, and to tune the exterior and interior functionalities.<sup>18-20</sup> In contrast, organic nanotubes (ONTs), constructed from various motifs such as macrocycles,<sup>21, 22</sup> amphiphiles,<sup>23, 24</sup> and peptides through self-assembly process,<sup>25-27</sup> are very appealing as they circumvent these limitations with facile chemistry of monomer synthesis forming nanotubes with desirable functionalities and the possibilities to control the nanostructures.<sup>23-25, 28</sup> However, macrocycle-based ONTs have high tendency to aggregate,<sup>29</sup> and amphiphile-based ONTs suffer from low structural stability since amphiphilic self-assemblies are very subjected to the environmental changes such as pH, temperature, ionic strength, etc.<sup>23, 30</sup> As a result, although the nanotube diameter can be well controlled in the sub-nanometer to nanometer range, precise control over the nanotube length, the dispersion of the nanotubes, and the stability of the nanotubes remain as significant challenges for ONT processing.

Cyclic peptide nanotubes (CPNs), constructed from the self-assembly of alternating D, L- cyclic peptides (CPs) via multi-pair inter-CP hydrogen bondings,<sup>31-33</sup> offer unique advantages of stability and robustness against environmental changes.<sup>25, 34, 35</sup> Through interior modifications on the building blocks which reduces the strength of inter-CP hydrogen bonding, processability with conventional materials such as polymers can be achieved via reversible self-assembly and disassembly of the nanotubes.<sup>36</sup> Developments in the exterior functionalization of CPNs, in particular conjugation with polymers, have permitted dispersion of high aspect ratio CPNs which tend to aggregate and solubility in various organic solvents incompatible with polar peptides.<sup>37-40</sup> Successful construction of individual polymer-covered CPNs (pc-CPNs), as well as the capability to grow them in block copolymer (BCP) matrix have now set the stage for several advances in the design of artificial nanochannels and complex tubular nanostructures.<sup>34, 41-43</sup> To better control the dimensions of the pc-CPNs, it is important to evaluate the underlying physics governing the assembly by delaminating the entropic contribution from the enthalpy of association. Scrutinizing on the conjugated polymer chains, steric repulsions due to polymer chain conformation have been otherwise explored extensively in various polymer brush systems in which polymers anchored to a surface with high enough grafting density tend to be stretched.<sup>44-46</sup> Similar concept may be applied to pc-CPN systems where the conjugated polymers chains tend to avoid coil overlapping when their size (i.e. radius of gyration,  $R_g$ ) is larger than the separation distance between two chains (i.e. CP-to-CP distance). The stretching of the polymer chains contribute to an entropic penalty to nanotube formation, hence modulating the length of the pc-CPNs. Restricted growth of CPNs with polymer conjugation was first reported by Biesalski's group, and later Börner's and Perrier's groups where a general correlation of decreasing pc-CPN length on solid support and/or in solution with increasing mass of grafted polymer chains was observed.<sup>37-40, 47</sup> While previous reports rely mainly on manipulating the molecular weight of the grafted polymer chains to control the pc-CPN length, here we demonstrate an alternative approach to tune the growth of the nanotubes by varying the position of the conjugated polymer chains and the monomer concentration for a delicate balance between entropy and enthalpy within the processing window.

In this contribution, a model system of *cyclo*(D-Ala-L-Lys)<sub>4</sub> (called "8CP") conjugated with  $n$  poly(ethylene glycol) (PEG,  $M_w=2,000$  Da) chains per CP ring ( $n=2, 3$  and 4, called " $n$ -arm") was designed to closely investigate the self-assembly of pc-CPNs. Constrained by hydrogen bonds, the CP-to-CP distance is  $\sim 0.47$  nm,<sup>31</sup> much less than the  $R_g$  of the conjugated PEG chains( $\sim 1.6\pm 0.3$  nm).<sup>48</sup> Drawing an analogy to comb-like polymers or cylindrical molecular brushes, we speculate that the steric repulsions between the conjugated arms lead to the stretching of the brush backbone and give rise to an entropic penalty which opposes nanotube formation.<sup>49, 50</sup> Fig. 1 shows the speculated stacking configurations for the designed conjugate systems. For simplicity, only a pair of dimers is shown. To minimize the entropic penalty, we hypothesize that configurations with fewer PEG chains in close proximity are more preferred since high stacking density

results in high entropic penalty. 1-arm and 2-arm can potentially alternate the positions of PEG chains but not the 4-arm conjugates. When other conditions are kept constant, 4-arm conjugates are speculated to form the shortest pc-CPNs due to high entropic penalty.

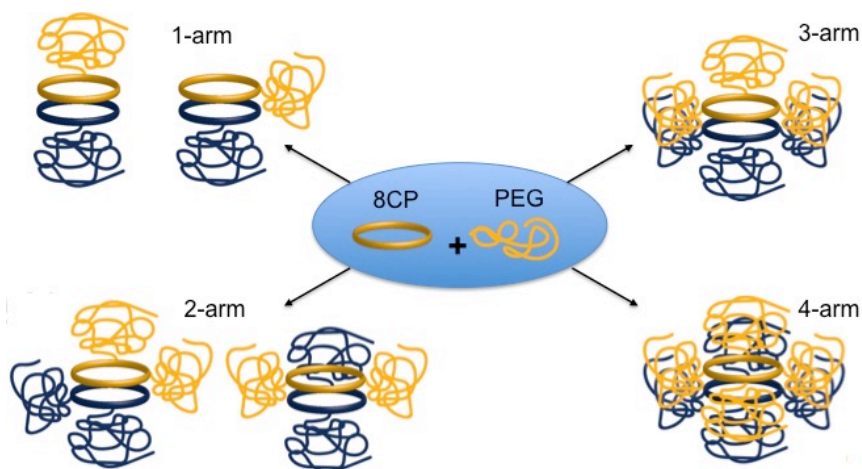


**Figure 1.** Schematic showing possible stacking scenarios for conjugates with different PEG chains attached.

## § 2.2 Results and Discussion

To validate our design, different conjugates were synthesized and purified by liquid chromatography as shown in Figure A.1.1 of the Appendix. The extent of the entropic penalty can be quantitatively realized by evaluating the strength of inter-CP hydrogen bonding using Fourier Transform - Infrared Spectroscopy (FTIR). Fig. 2.2 shows the FTIR spectra of amide A band of various conjugates and at room temperature. A clear left-shift in the peak position to higher wavenumber is observed as the  $n$  increases from 0 to 4, indicating the weakening of inter-CP hydrogen bonds as more PEG chains are attached. In particular, the difference between 8CP/2-arm and 3-arm/4-arm, is very small ( $\sim 0.2 \text{ cm}^{-1}$ ) compared to the difference between 2-arm/4-arm ( $\sim 3.2 \text{ cm}^{-1}$ ), reflecting the stacking configurations of the different systems. From the analysis of N-H stretching distance with the wavenumber, the N-to-O distance from two adjacent CP rings can be estimated to be  $\sim 2.97 \text{ \AA}$  for 4-arm and  $2.96 \text{ \AA}$  for 2-arm, or CP-to-CP distance of  $4.86 \text{ \AA}$  for 4-arm and  $4.85 \text{ \AA}$  for 2-arm, respectively.<sup>51</sup> Based on this, 2-arm and 4-arm were used to closely examine the effect of PEG arms on the growth of pc-CPNs.

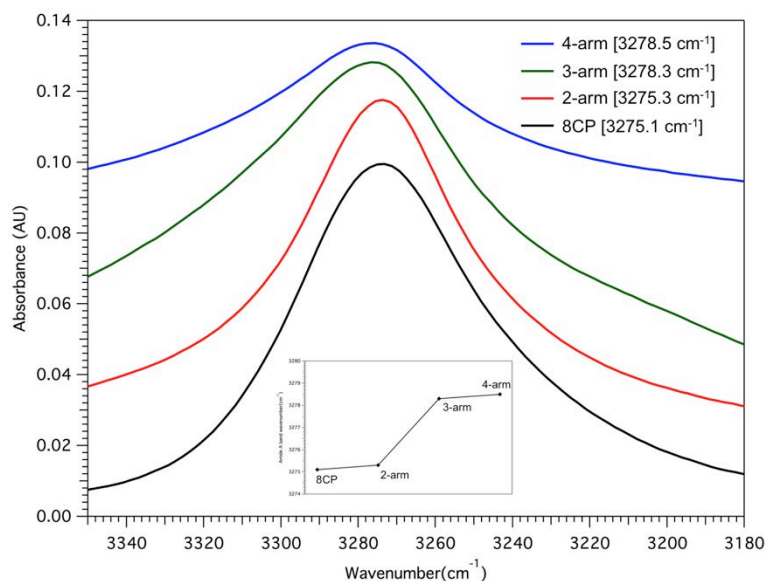


**Figure 2.2.** FTIR spectra showing amide A band for 8CP and 2-, 3-, and 4-arm conjugates. The inset in b) clearly shows the change in the amide A peak position to higher wavenumber as more PEG chains are attached.

Figure 2.3 shows the amide A peak position of 8CP, 2-arm and 4-arm conjugates as a function of temperature. A general increase in peak wavenumber with temperature indicates that the hydrogen bonds are weakened upon heating. While the entropic penalty of the conjugated PEG arms clearly destabilize the nanotube, the same effect can be achieved by weakening the inter-CP hydrogen bonds through thermal heating. On average, a shift factor of  $\sim 20$  °C is seen between the 4-arm and 2-arm conjugates. This result suggests a superposition behavior between the entropic penalty and temperature, i.e. the entropic effect is equivalent to thermal melting in destabilizing the nanotube structure.

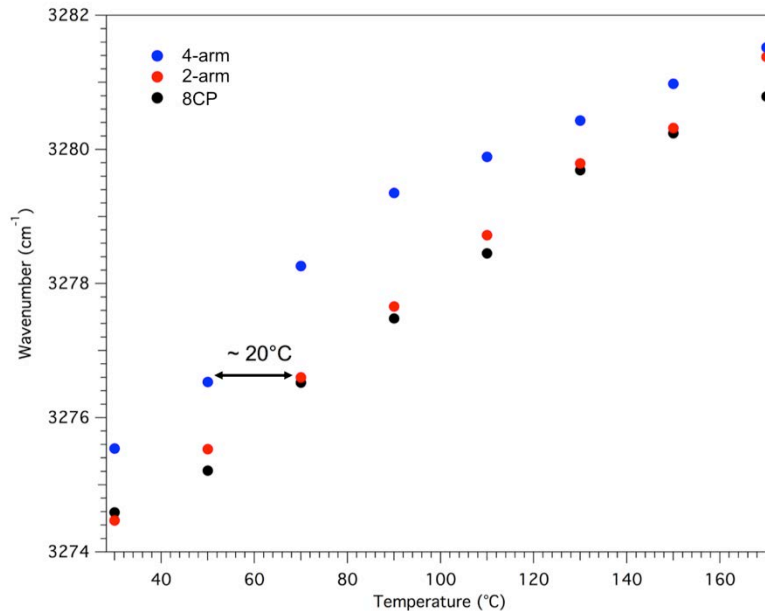


**Figure 2.3.** Amide A band peak position of bare 8CP, 2-arm and 4-arm as a function of temperature, showing a shift factor of  $\sim 20$  °C between the 4-arm and 2-arm conjugates.

The growth of pc-CPNs is evaluated by characterizing the lengths of pc-CPNs as a function of  $n$  and the solution concentration,  $C$ . We realized that the formation of pc-CPN on solid support from solution is rather complicated in which other parameters such as the growth kinetics, polymer conjugate-solvent interaction and the spin-casting process all play a role. Aware of the restrictions and limitations, we kept the conditions consistent by regulating the solvent removal rate, and keeping the conjugate concentration low to prevent aggregation in solution. Figure 2.4 a-c) shows representative phase-contrast Atomic Force Microscopy (AFM) images of 2-, 3-, and 4-arm conjugates spin-casted on Si substrate with  $\sim 2$  nm native oxide layer from 10  $\mu$ M toluene solutions and the corresponding statistical analysis of the pc-CPNs length. An inverse relationship between the pc-CPN length and its distribution with the value of  $n$  is observed, validating our design in which the growth of pc-CPNs can be tuned by varying the number of the conjugated polymers. 2-arm conjugates with the lowest entropic penalty forms the longest pc-CPNs  $\sim 64$  nm with the widest distribution, and 4-arm conjugates with very high steric repulsion forms pc-CPNs almost 5-fold shorter  $\sim 14$  nm and narrow length distribution, with 3-arm pc-CPNs lie in between.

However, the growth of pc-CPNs is not solely determined by entropy, but also depends on the enthalpic interactions, allowing length modulation through varying the monomer concentration. When there is sufficient amount of monomers available, longer pc-CPNs may be formed even for 4-arm conjugates since the entropic penalty does not prevent the formation of inter-CP hydrogen bonds but rather destabilizes the

nanostructure. Figure 2.4 d-f) shows the AFM images of 4-arm conjugates casted from toluene with different solution concentration,  $C$ . Longer pc-CPNs are formed when  $C$  increases from 20  $\mu\text{M}$  to 50  $\mu\text{M}$ , with no significant change beyond 50  $\mu\text{M}$ . We speculate that the limited surface area is one possible reason prohibiting the growth of longer nanotubes. The highlighted region in Figure 2.4 e) shows that there is a distribution of pc-CPN lengths within a patch of nanotubes with similar orientation, suggesting that longer nanotubes can be formed if there is available space for growth. Similar concentration dependence has also been observed for 2-arm conjugates and the AFM images and statistical analyses are included in Figure A. 1.3, A. 1.4, and A. 1.5 of the Appendix.) summarizes the results for both 4-arm and 2-arm systems, in which the growth of pc-CPNs reflects the energetic competition between two contributions, i.e. the enthalpy of inter-CP hydrogen bonding which drives the nanotube formation, and the entropy associated with PEG chain deformation which destabilizes the nanotubes. 2-arm with lower entropic penalty forms longer pc-CPNs than the 4-arm conjugates even at the plateau point, highlighting the effect of the entropic contribution from the conjugated polymer chains which may be overtaken by higher solution concentration. This indeed gives us multiple handles to modulate the self-assembly process and to tune the length of the pc-CPNs.



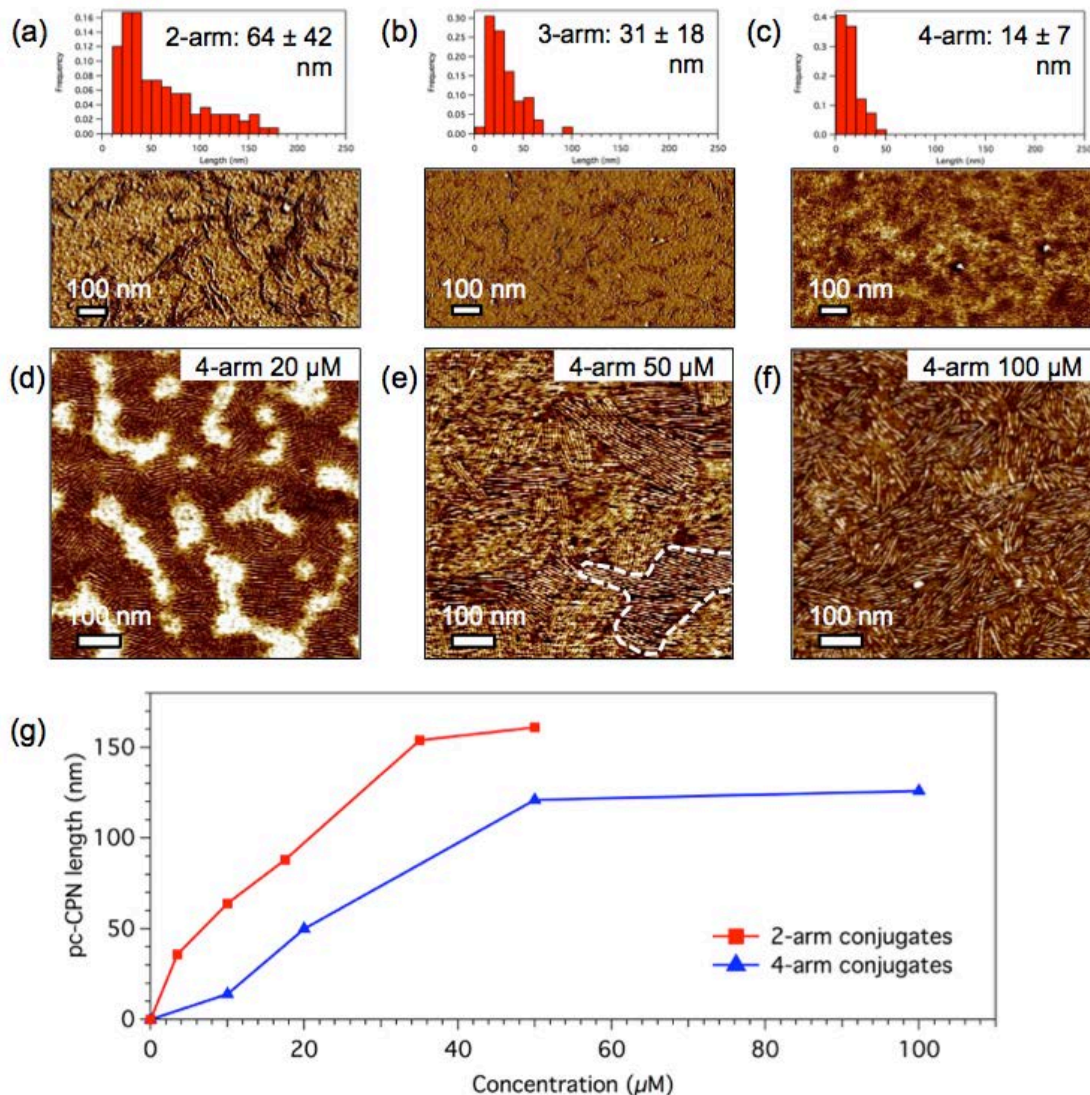


**Figure 2.4.** AFM phase images of pc-CPNs casted from toluene solutions for (a) 2-arm at 10  $\mu\text{M}$ , (b) 3-arm at 10  $\mu\text{M}$ , and (c) 4-arm at 10  $\mu\text{M}$ , (d) 4-arm at 20  $\mu\text{M}$ , (e) 4-arm at 50  $\mu\text{M}$ , (f) 4-arm at 100  $\mu\text{M}$ , respectively. (g) summary of the concentration dependence of the lengths of pc-CPNs with concentration for 2-arm and 4-arm conjugates. Statistical analysis was performed to the AFM images to obtain the lengths of pc-CPNs as shown in (a)-(c). The length of pc-CPNs is inversely related to the degree of PEG conjugation but proportional to the solution concentration. 2-arm with the low entropic penalty tend to for longer pc-CPNs. The growth of pc-CPNs eventually becomes limited by the available space as indicated by the plateau for both conjugates in (g).

A novel theoretical framework that relates the net binding free energy between the CPs with the length of the nanotubes has been established. It is well-known that 1D rod-like supramolecular assemble in a fashion that could be considered as cylindrical

micelles.<sup>49</sup> The nanotubes will grow to an average length,  $\langle L \rangle$ , depending on two factors:  $\Delta F$ , the net binding energy between two monomers; and  $C$ , the monomer concentration. The average length will then scale such that  $\langle L \rangle = \sqrt{C \cdot \exp(-\Delta F/k_B T)}$  (see ref. 49 for a full-derivation and assumptions). Keeping  $C$  constant, the ratio of  $i$ -arm and  $j$ -arm can be written as  $R_{i/j} = \langle L \rangle_{i\text{-arm}} / \langle L \rangle_{j\text{-arm}} = \exp[(\Delta F_{j\text{-arm}} - \Delta F_{i\text{-arm}})/k_B T]$ . The net binding energy simplifies to a linear relationship,  $\Delta F = P_1 \cdot n$ , for low molecular weights because in plane conjugation is negligible, where  $P_1$  is a constant that depends on the molecular weight, molecular details of the polymer and the solvent conditions (e.g. excluded volume). The ratio then becomes  $R_{i/j} = P_3 \exp(\Delta n)$ , where  $\Delta n$  is the difference in the degree of conjugation and  $P_3 = \exp(P_1/k_B T)$  (detailed explanation included in the *Supporting Information*). From the experiments at 10  $\mu\text{M}$  (Figure 2.4), the ratios are estimated to be  $R_{2/3} \approx 2.1$ ,  $R_{3/4} \approx 2.2$ ,  $R_{2/4} \approx 4.6$ . Constant  $P_3$  is calculated to be  $0.77 \pm 0.1$  from fitting the theoretical relation to the experimental data. The theoretical prediction shows a reasonable agreement with the experimental results (Figure 2.5), suggesting the proposed theoretical framework, which predicts an approximate linear scaling of the free energy penalty with the number of arms, captures the physics underlying the conjugation effects on the length of the pc-CPNs accurately with a single physical parameter. Remarkably, it explains the experimental observation that the ratio of the pc-CPN length of 2-arm/3-arm is roughly the same as 3-arm/4-arm since the free energy difference is predicted to be identical in these two cases.

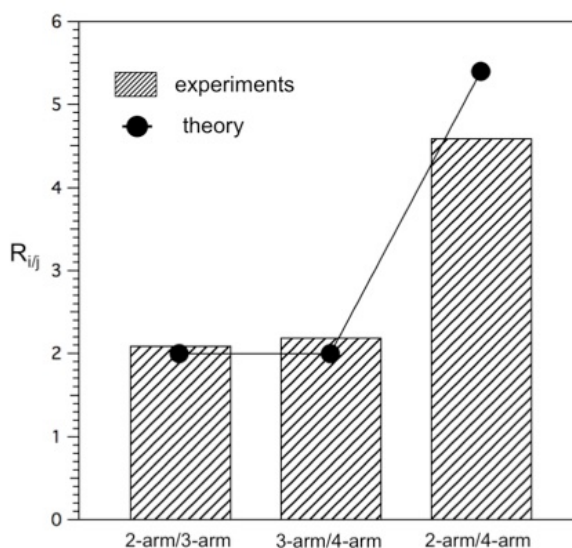


**Figure 2.5.** Comparison of the ratios of the lengths of various conjugates between experimental observation and proposed theoretical framework.

Combing both contributions from the net binding energy and monomer concentration, Figure 2.6 summarizes the correlation of pc-CPN length with degree of PEG conjugation and conjugate solution concentration below the surface coverage limit. It can be observed that 2-arm follows reasonably well with theoretical scaling predicted by micelle theory,  $\langle L \rangle_{2-arm} \sim C^{1/2}$  at any given concentration below the surface coverage limit. A similar trend of increasing pc-CPN length with concentration is observed for 4-arm conjugates, but surprisingly the correlation deviates from the micelle theory with a stronger dependence on concentration,  $\langle L \rangle_{4-arm} \sim C^2$ . We speculate that the difference in the scaling behavior might suggest that in addition to thermodynamic contributions, kinetic contributions should also be considered. We hypothesize that the rate of diffusion, which is molecular weight dependent, is the other critical kinetic parameter that influences the growth of pc-CPNs. Due to faster rate of diffusion, coalescence of dimers or larger oligomers is more easily attained for 2-arm, resulting in pc-CPNs with wider length distribution. On the other side, 4-arm with slower rate of diffusion grows in a more homogeneous manner and its growth demonstrates a  $\sim C^2$  dependence, resembling a self-catalyzed step-growth polymerization process. While it is challenging to definitively explain the physics behind the growth of various pc-CPNs and to come up with an exact model to predict their lengths, we can still obtain many insights from present study in which multiple approaches can be adopted to control and modulate the growth of pc-CPNs.

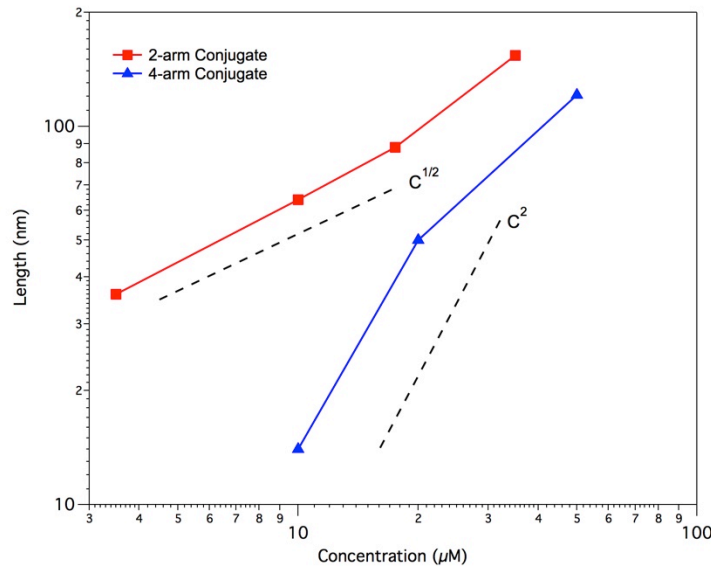


**Figure 2.6.** Summary of the different pc-CPNs length casted from different solutions. A correlation of pc-CPN length with the solution concentration can be seen for all pc-CPNs.

## § 2.3 Conclusion

Using the designed system, we found that regardless of the  $n$  value, all conjugates self-assemble into homomeric nanotubes and pc-CPN length is inversely proportional to the degree of PEG conjugation. High entropy of 4-arm conjugates results in pc-CPN length 5-fold shorter than 2-arm conjugates under the same condition. Furthermore, the growth of pc-CPNs also demonstrates concentration dependence below the saturation point, allowing conjugates with different degrees of conjugation to form pc-CPNs with similar lengths. From the experimental observations, a theoretical framework from atomistic and coarse-grained molecular dynamics simulations is developed to correlate the growth of pc-CPNs to the degree of PEG conjugation ( $n$ ) and the monomer concentration ( $C$ ), where the length of pc-CPN  $\sim nC$ . These results suggest that the growth of pc-CPNs can be tailored and modulated using two different approaches, i.e. controlling the entropic penalty of PEG conjugation and/or monomer concentration. In addition to the thermodynamic origin of the destabilization effect and concentration dependence, there is also the kinetic factor in which the growth of the pc-CPNs is likely to be diffusion limited. Although it is very challenging to decouple thermodynamic contributions from kinetic factors, we can still obtain some insights in the self-assembly of polymer conjugated cyclic peptides which allow us to have multiple handles in tuning the growth process of pc-CPNs. Our analysis indeed paves the way for extending the experimental approach to control the spatial organization of self-assembling organic nanotubes with varying interior and exterior features for constructing 1D tubular structures for different applications.

## § 2.4 Experimental

### 2.4.1 Materials

Propylphosphonic anhydride (T3P), N,N-Diisopropylethylamine (DIPEA), 1-ethyl-3-(3-dimethylaminopropyl) carbodiimide (EDC), 2-(N-Morpholino)ethanesulfonic acid sodium salt (MES) were purchased from Sigma Aldrich. Fmoc-D-Ala-OH, Fmoc-L-Lys(Boc)-OH, polystyrene-(2-chlorotrityl) resin (loading: 1.5 mmol/g), and 2-(6-Chloro-1H-benzotriazole-1-yl)-1,1,3,3-tetramethylaminium hexafluorophosphate (HCTU) were purchased from Nova Biochem. Carboxylic acid-terminated PEG (Mw=2K, PDI 1.2) was purchased from RAPP Polymere. Dimethylformamide (DMF), piperidine and toluene were purchased from Fisher Scientific. All reagents were purchased with the highest purity and used as received unless otherwise noted.

## 2.4.2 Peptide synthesis and PEG conjugation

2-Chlorotrityl chloride resin was swelled for two hours in dry DMF (5 mL). Fmoc-D-Ala-OH (2 eq.) was dissolved in dry DMF (5 mL) and added to the solution, followed by DIPEA (4 eq.) addition. The amino acid mixture was added to the resin suspension and stirred for two hours to manually load the first amino acid to the resin. Methanol was then added to block remaining chloride residues and quench the reaction. The resin was filtered and washed with DMF, DCM and methanol and left to dry under vacuum overnight. The loading was assessed using UV-vis by monitoring the absorbance at 290 nm of free Fmoc group after deprotection. All consequent coupling reactions were performed using the automated solid phase synthesizer (Prelude) using standard 9-fluorenylmethoxycarbonyl (Fmoc) protocol for solid-phase peptide synthesis.

To cleave the linear sequence H<sub>2</sub>N-L-Lys-D-Ala-L-Lys-D-Ala-L-Lys-D-Ala-L-Lys-D-Ala-OH, the peptide loaded resin (400 μmol) was gently stirred in a solution (20 mL) of 1% v/v TFA, 5% v/v TIS in DCM for 60 minutes. The solid residue was then removed by vacuum filtration and washed with DCM. The filtrate volume was reduced under vacuum to near dryness, and the product redissolved with a minimum of DCM and precipitated using cold ether (50 mL). The mixture was centrifuged, and ether was then decanted. This step was repeated twice, resulting in a transparent gel-type precipitate. The solid residue was dried under vacuum to yield 0.35 g (75%). MALDI-TOF for the deprotected linear peptide using 100% TFA Calculated: 815 [M+H]<sup>+</sup>; Found 814 [M+H]<sup>+</sup>, 838 [M+Na]<sup>+</sup>, 852 [M+K]<sup>+</sup>.

To form *cyclo*(L-Lys-D-Ala-L-Lys-D-Ala-L-Lys-D-Ala-L-Lys-D-Ala), the linear sequence H<sub>2</sub>N-L-Lys-D-Ala-L-Lys-D-Ala-L-Lys-D-Ala-L-Lys-D-Ala-OH (0.3 g, 490 μmol) was dissolved in dry DMF (800 mL). The solution was cooled to 0 °C in an ice bath. T3P (50% w/w in DMF), (2.25 mL, 3.4 mmol) was slowly added to the solution mixture while stirring at 0 °C. DIPEA (450 μL, 3.4 mmol) was added slowly to the mixture. The reaction mixture was left to stir for 2 hours at 0 °C and then at room temperature for 1 day. An equal amount of T3P was added, and left stirring for another two days at room temperature. Cyclized product precipitated out and settled to the bottom of the reaction flask during the cyclization reaction. Remaining DMF was removed by rotovap at 70 °C, resulting in a gel-like residue. Boc protecting groups on the lysine side chains were removed from the crude product by dissolving the later in 10 mL of 95% v/v TFA, 2.5% v/v TIS and 2.5% v/v H<sub>2</sub>O. The mixture was left to stir for two hours at room temperature. The deprotected product was then precipitated twice using cold ether (100 mL) to yield a white precipitate. The product was then dissolved in H<sub>2</sub>O (10 mL), and lyophilized giving an off-white fluffy solid. The cyclization efficiency was found to be greater than 95% using analytical HPLC.

For PEG polymer conjugation, the cyclized product (“*cyclo*(D-Ala-L-Lys)<sub>4</sub>”) or “AK<sub>4</sub>”) was dissolved in pH 6.5 MES buffer. Carboxy-terminated PEG (4 mol. Eq.) was added and stirred until complete dissolution. EDC (4 mol eq.) was added and the solution was sonicated for a few minutes. The reaction was left to proceed for 4 hr and an additional 8 molar eq. of EDC were added and the reaction was left for another 24 hr. After every addition, the pH was adjusted, so as to maintain it around pH 6.5. The

solution was injected directly into the preparatory HPLC for purification. Salts and other small molecules eluted first, and the conjugates. Different fractions were collected and lyophilized immediately.

#### **2.4.3 Reversed-Phase High-Pressure Liquid Chromatography (RP-HPLC)**

The reaction mixture from conjugation was purified by RP-HPLC (Beckman Coulter) to obtain AK<sub>4</sub>-PEG conjugates with various PEG arms with reasonable purity using a C4 column (Vydac 22 mm x 250 mm) at a flow rate of 8 mL min<sup>-1</sup>. Conjugates were eluted with a linear AB gradient, where solvent A consisted of water containing 0.1% (v/v) TFA and solvent B consisted of acetonitrile (ACN) containing 0.1% (v/v) TFA. A linear gradient of 20 to 65% solvent B over 45 min was used and the elution was monitored using a diode array detector at wavelengths of 200 nm and 220 nm. 2-arm conjugates were eluted at ~47-48% ACN, 3-arm conjugates at ~50-51%, and 4-arm conjugates around 52-53%.

#### **2.4.4 Fourier Transfer Infrared Spectroscopy (FTIR)**

FTIR measurements were performed using the Perkin Elmer Spotlight 200 FTIR Microscope System. The samples were casted from toluene solutions between two NaCl pellets for KA<sub>4</sub>-PEG conjugates, and from aqueous solution between two CaF<sub>2</sub> pellets for the bare CP AK<sub>4</sub>. For *in-situ* FTIR, the samples were being heated from 30 °C to 250 °C and back to 30 °C under nitrogen environment. Spectra were collected 5 minutes after reaching the targeted temperature at a 20 °C interval.

#### **2.4.5 Formation of pc-CPNs**

After obtaining pure conjugates from HPLC (2-arm, 3-arm and 4-arm), the powders were dissolved in MilliQ H<sub>2</sub>O respectively to make stock solutions with 1mg/mL concentration. Appropriate amount of stock solution was then re-lyophilized to obtain dry powder of pc-CPs. Toluene dried with molecular sieves was then added to the dry powder of pc-CPs. Finally the toluene solution was deposited onto Si wafer (pretreated with Piranha solution to remove impurities on the surface) at 1000 rpm for 15 seconds to form various pc-CPNs.

#### **2.4.6 Statistical Analysis of pc-CPN Length**

Statistical analysis was performed by manually counting 100 pc-CPNs and measuring the lengths by ImageJ.

## Chapter 3

# Co-assembly of Cyclic Peptide-Polymer Conjugate and Block Copolymer in Thin Films

|              |  |           |
|--------------|--|-----------|
| <b>§ 3.1</b> | <b>Introduction.....</b>   | <b>51</b> |
| <b>§ 3.2</b> | <b>Results and Discussion.....</b>                                       | <b>52</b> |
| <b>§ 3.3</b> | <b>Conclusion .....</b>  | <b>59</b> |
| <b>§ 3.4</b> | <b>Experimental .....</b>  | <b>59</b> |
|              | 3.4.1 Materials .....  | 59        |
|              | 3.4.2 Reversed-Phase High-Pressure Liquid Chromatography (RP-HPLC) ..... | 60        |
|              | 3.4.3 MALDI-TOF Mass Spectrometry .....                                  | 60        |
|              | 3.4.4 Grazing Incident Small Angle X-ray Scattering (GISAXS).....        | 60        |
|              | 3.4.5 Dynamic Light Scattering (DLS).....                                | 60        |
|              | 3.4.6 Fourier Transfer Infrared Spectroscopy (FTIR) .....                | 60        |
|              | 3.4.7 Nuclear Magnetic Resonance Spectroscopy (NMR) .....                | 61        |
|              | 3.4.8 Thin Film Fabrication.....   | 61        |

This material has been submitted for publication: C. Zhang and T. Xu, submitted to *Nanoscale* (2015).

*Directed co-assembly of polymer-conjugated cyclic peptide nanotube (CPN) and block copolymer in thin films is a viable approach to fabricate sub-nanometer porous membranes without synthesizing nanotubes with identical length and vertical alignment. Here we show that the process is pathway dependent and successful co-assembly requires eliminating CPN larger than 100 nm in solution. Optimizing polymer-solvent interaction can improve conjugate dispersion to certain extent, but this limits thin film fabrication. Introduction of a trace amount of hydrogen-bond blockers, such as trifluoroacetic acid by vapor absorption is more effective to reduce CPN aggregation in solution and circumvents issues with solvent immiscibility. This study provides critical insights for guided assemblies within nanoscopic frameworks toward sub-nanometer porous membranes.*

### § 3.1 Introduction

Membranes with uniform pore size less than 1 nm are desirable for molecular separation.<sup>1, 2</sup> Organic nanotubes such as cyclic peptides nanotubes (CPNs) are advantageous because the channel diameter and interior functionality can be molecularly tailored.<sup>3-11</sup> The guided growth of CPNs within cylindrical block copolymer (BCP) in thin films opened a viable approach to generate porous membrane with vertically aligned, uniform sub-nanometer channel with interior functionalization.<sup>12</sup> It overcame challenges of reducing pore size in nanoporous BCP membranes,<sup>13-17</sup> and synthesizing high aspect ratio nanotubes with controlled length and vertical alignment.<sup>18, 19</sup> In the guided CPN growth process, it was proposed that cyclic peptides (CPs) or short CPN tubelets need to be first selectively incorporated into BCP cylinders, and subsequently reassembled into high aspect ratio CPNs.<sup>12</sup> However, CPs and CPN tubelets tend to aggregate due to multi-pair inter-CP hydrogen bonding.<sup>3, 20</sup> When the aggregate size exceeds the periodicity of the BCP, the conjugate cannot be distributed uniformly within the preferred BCP microdomain, similar to what have been observed in nanoparticles/BCP blends.<sup>21-23</sup> The presence of large aggregates also compromises membrane quality and integrity, analogous to defects due to inorganic particles in composite membranes.<sup>24, 25</sup> Therefore, it is a requisite to develop systematic understanding in the kinetic pathway of the co-assembly process and to control CPN aggregation.

Here, we present a systematic study on the co-assembly of *cyclo*(D-Ala-L-Lys) (AK<sub>4</sub>) conjugated with four chains of PEG with molecular weight 2,000 Da (AK<sub>4</sub>-4P2k) and cylindrical PS-*b*-PMMA in thin films, focusing on the control of the kinetic pathway



which proves to be the critical factor in governing the co-assembly process. CPNs and their polymer conjugates tend to aggregate in solution due to two contributions: namely the unfavorable interactions between the conjugated polymers and the solvent, and the multi-pair, highly directional hydrogen bonds between cyclic peptides. Large aggregates cannot be distributed in the preferred BCP microdomains and need to be first broken down, requiring high activation energy that cannot be provided by thermal annealing. To prevent the formation of large aggregates, we developed two approaches to address each of the aggregation contributors to facilitate thin film fabrication, i.e. optimizing polymer-solvent interaction and adding small molecule hydrogen bond blocker. We are particularly intrigued by the effect of the latter, in which the presence of a trace amount of trifluoroacetic acid (TFA) overcomes the incompatibility issue between the conjugate and the solvent in addition to preventing extensive intermolecular hydrogen bonding. This approach not only facilitates the co-assembly of CPNs and BCP, but is also applicable to many organic systems since it eliminates the limitation on solvent selection. Present study indeed provides critical insights for fabricating sub-nanometer porous membrane through guided assemblies of organic nanotubes within nanoscopic frameworks.

### § 3.2 Results and Discussion

Polymers attached to the CPN exterior greatly affect CPN formation and its solubility in different media.<sup>11, 12, 20, 26-30</sup> However, previous studies are based on CP-polymer conjugate mixtures with different number of polymer chains attached.<sup>12</sup> The CP-polymer conjugates are purified via dialysis and there could be some trace amounts of chemical impurities. Here we developed purification procedure using Reversed-Phase High-Pressure Liquid Chromatography (RP-HPLC) to obtain model CP-polymer conjugates with high purity. To ensure the conjugate used contains well-defined architecture, PEG with molecular weight 2,000 Da was selected as other molecular weights resulted in either incomplete conjugation reaction or difficulty in purification. The conjugate purity was confirmed using analytical HPLC and mass spectroscopy (Figure 3.1) and the RP-HPLC spectrum of the reaction mixture is shown in Figure A.2.1, Appendix. Only a single peak can be observed in Fig. 3.1b), confirming the purity of the conjugate. Cylindrical BCP, polystyrene (57 kDa)-block-poly(methyl methacrylate) (25 kDa) (PS-*b*-PMMA) was used as the nanoscopic framework to guide CPN growth.

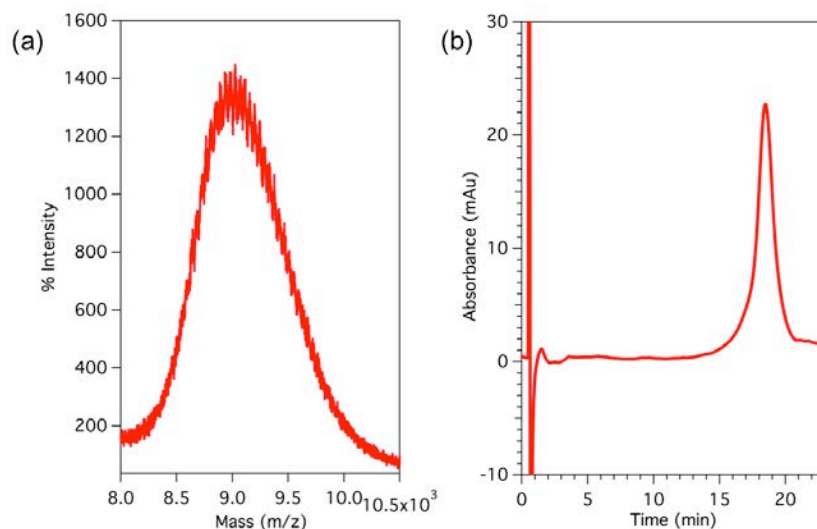


**Figure 3.1.** Characterization of purified KA<sub>4</sub>-4P2K conjugate. a) MALDI-TOF spectrum and b) corresponding RP-HPLC spectrum of the isolated KA<sub>4</sub>-4P2k, confirming the purity of materials used in this study

Thin films ~40 nm thick were prepared from toluene solution with constant BCP concentration at 10 mg/mL and varying conjugate concentration to tailor the fraction of AK<sub>4</sub>-4P2K,  $f$ . As shown previously, there is a reasonable agreement between the Atomic Force Microscopy (AFM) image and High-angle Annular Dark Field-Scanning Transmission Electron Microscopy (HAADF-STEM) results in terms of CPN formation in thin films.<sup>12</sup> Considering the limited area scanned and the time required to obtain high quality HAADF-STEM, present studies rely on AFM, in-plane TEM, and Grazing Incident Small-angle X-ray Scattering (GISAXS) for structural characterization. Figure 3.2 shows the AFM and TEM images of thin films containing different fraction of AK<sub>4</sub>-4P2K after thermal annealing at 180°C for 4hr in vacuum. At 0.8 wt%, homogeneous morphology is observed where cylindrical PMMA microdomains are oriented normal to the substrate. Dark circular areas ~3-5 nm, which are confirmed previously to be the PEG-covered CPNs can be seen at the center of some PMMA cylinders,<sup>12</sup> indicating that only a fraction of PMMA microdomains contains CPNs. At 2 or 4 wt%, CPNs are seen in most vertically aligned PMMA cylinders. However, there are aggregates of PEG-covered CPNs on the surface for both films. At  $f = 8$  wt%, the top-view TEM image shows the film contains a large fraction of PEG-covered CPNs laying parallel to the surface. GISAXS was used to characterize the in-plane ordering and to quantify the average lateral periodicity ( $L_0$ ). As  $f$  increases, the first order peak shifts to a lower  $Q$  (scattering vector) value, and  $L_0$  increases from 38.4 nm for BCP alone, to 39.5 nm and 40.6 nm for 0.8 and 2 wt%, respectively. This, in conjunction with the AFM results and previous HAADF-STEM studies, indicates the incorporation of PEG-covered

CPNs in the PMMA cylinders. The diffraction peak also broadens as  $f$  increases, implying less in-plane ordering. The ordered cylinder morphology is largely lost when  $f > 4$  wt%, consistent with the TEM result.

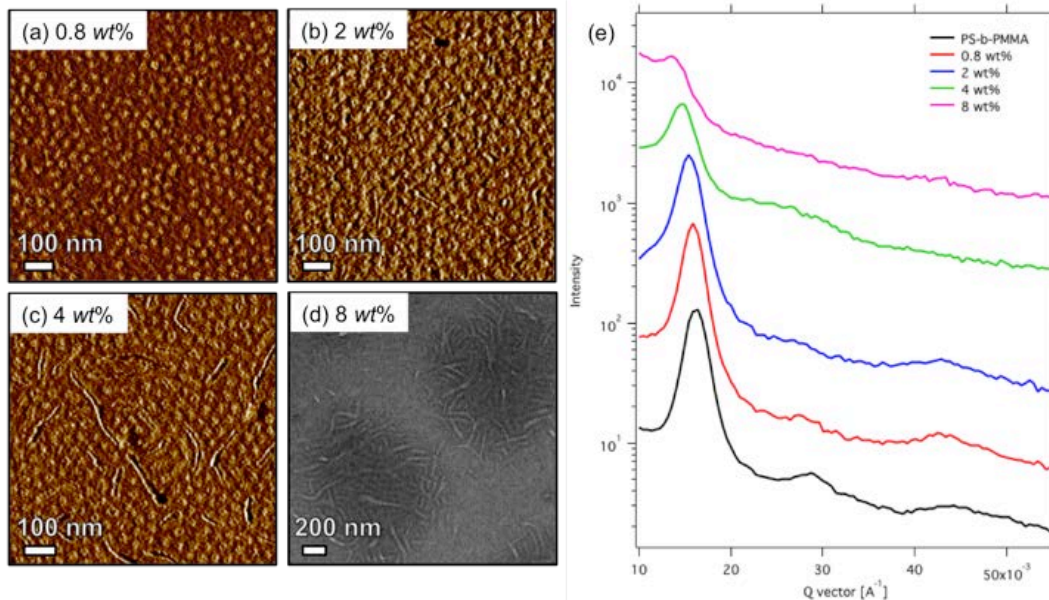


**Figure 3.2.** AFM phase images of blends of AK<sub>4</sub>-4P2K conjugate and PS-*b*-PMMA in thin films with  $f$  at (a) 0.8 wt%, (b) 2 wt%, (c) 4 wt%, and (d) TEM image at 8 wt%. (e) shows the GISAXS profiles of the films. A left-shift in the first order peak position indicates the incorporation of AK<sub>4</sub>-4P2K conjugate. The BCP lateral ordering deteriorates for thin films containing 8 wt% AK<sub>4</sub>-4P2K.

A simple model shown in Figure 3.3 is used to investigate the loading limit of the system. More than one CPN in one PMMA microdomain is not considered here due to high-energy cost to deform PMMA cylinders and rearrangement of cylindrical BCPs.<sup>31</sup> The critical  $f$  value for one PEG-covered CPN per PMMA cylinder is  $\sim 2.6$  wt%. However, aggregates (darker regions) are still seen at 2 wt% film (Figure 3.2b). Thus, the aggregation cannot be explained by the CPN loading limit within PMMA cylinder alone.

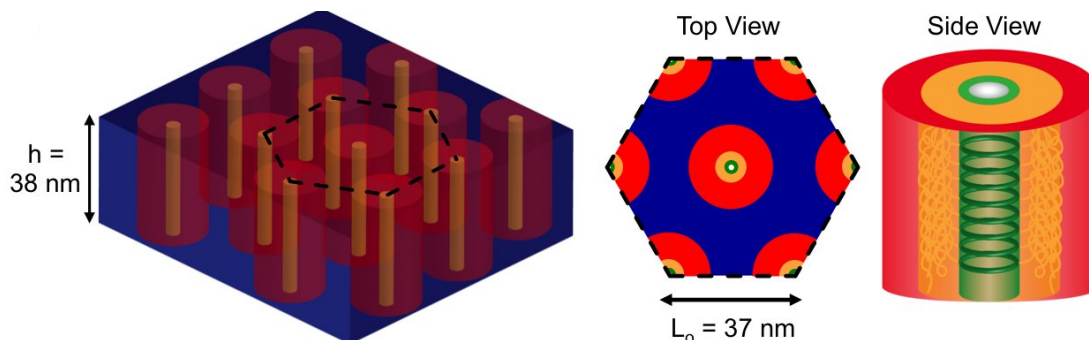


**Figure 3.3.** Schematic illustrating the estimation of  $AK_4-4P2k$  loading limit in cylindrical BCP. Using a hexagonal prism as a unit cell, the amount of BCP is  $M_{BCP} = \rho \cdot \frac{3\sqrt{3}}{2} L_o^2 \cdot h$ , where  $\rho$  is the density and  $L_o$  is the periodicity of the BCP respectively, and  $h$  is the film thickness. Under the constraint of the hydrogen bond distance and known film thickness, each PMMA cylinder contains  $\sim 8$  cyclic peptides stacked vertically. The amount of  $AK_4-4P2k$  in the unit cell become  $M_{AK_4-4P2k} = 3 \frac{h}{d_{H\ bond}} \cdot m_{AK_4-4P2k}$ , in which  $d_{H\ bond} = 4.7 \text{ \AA}$  and  $m_{AK_4-4P2k}$  is the mass of one conjugate molecule. The ratio of the conjugate to the BCP gives an estimate of the loading limit  $\sim 2.6 \text{ wt\%}$ .

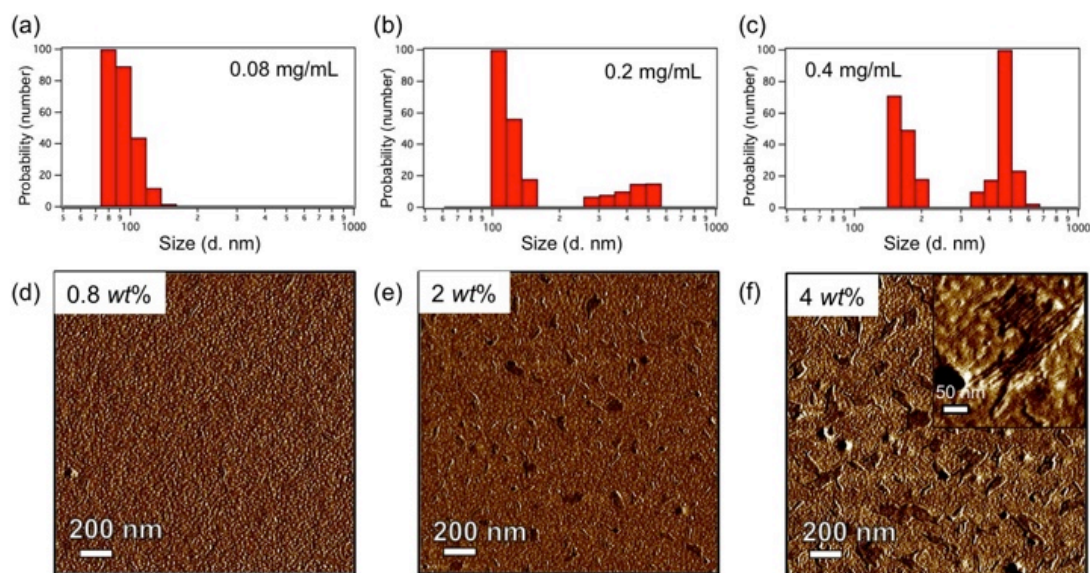


**Figure 3.4.** DLS results of  $AK_4-4P2K$  conjugates in toluene at various concentrations (a) 0.08 mg/mL, (b) 0.2 mg/mL, (c) 0.4 mg/mL; and corresponding AFM phase images of as-casted  $AK_4-4P2K$  conjugates in BCP at  $f =$  (d) 0.8 wt%, (e) 2 wt%, and (f) 4 wt%, respectively. Increasing solution concentration of  $AK_4-4P2K$  conjugates results in larger

aggregates in toluene. The insert of (f) shows the details of the AK<sub>4</sub>-4P2K aggregates consisted of bundles of PEG-covered CPNs.

Dynamic light scattering (DLS) studies (Figure 3.4) confirm that the AK<sub>4</sub>-4P2K conjugates pre-aggregate in toluene prior to thin film formation. The sizes increase from ~ 100-400 nm at 2 wt% to ~200-600 nm at 4 wt%. After further annealing at 245°C (Figure 3.5), the CPN aggregates are only partially broken. More PEG-covered CPNs are incorporated into PMMA cylinders but defects still remain on the surface. Although the study clearly demonstrates the exceptional thermal stability of polymer-covered CPNs,<sup>11, 12</sup> the surface defects due to CPN aggregation are undesirable and need to be eliminated.

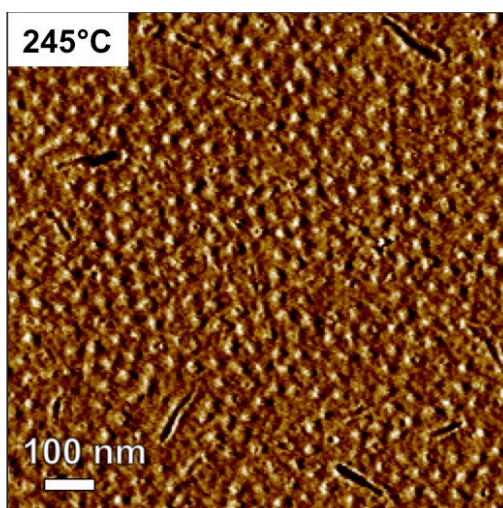


**Figure 3.5.** AFM image of 2 wt% (AK)<sub>4</sub>-4P2K/PS-*b*-PMMA blend thermally annealed at 245°C below the degradation temperature of the BCP matrix. The film remains intact with no obvious thermal degradation. Less CPN aggregates are seen on the surface comparing to the sample annealed at 180°C (Fig. 3.2b). However, surface defects of lay-down PEG covered CPNs are not completely broken down.

The CPN aggregation can be attributed to two factors: strong hydrogen bonding between CP rings,<sup>3</sup> and interactions between the attached polymers and the solvent.<sup>20</sup> Molecular dynamic simulation studies show there are 7-8 pairs of hydrogen bonds between CPs,<sup>11, 32, 33</sup> which are the main force stabilizing CPN and contributors to the insolubility of CPNs in most organic solvents. Polymers covalently attached to the CPN exterior can improve solubility and modulate CPN growth.<sup>20, 26-28</sup> While toluene, with solubility parameter  $\delta=8.9$  (calcm<sup>-3</sup>)<sup>-1/2</sup>, is good for preparing smooth thin films of PS-*b*-PMMA, it is not a good solvent for PEG ( $\delta=9.9$ ), leading to aggregation of PEG-covered CPNs in solution.<sup>34</sup> DLS studies (Fig. 3.6 a,b) show that benzene ( $\delta=9.1$ ) and chloroform ( $\delta=9.2$ ) are more effective in solubilizing AK<sub>4</sub>-4P2K and reducing the aggregate size



down to  $\sim 70$  nm and  $\sim 200$ - $300$  nm, respectively. In contrast, poor solvent such as o-xylene ( $\delta=8.85$ ) results in aggregates of a few micrometers (Fig. 3.6 c). For benzene and chloroform, homogeneous as-cast films are obtained at 2 wt% and well-aligned CPNs at the center of PMMA cylinder can be seen post thermal annealing (Fig. 3.6 d,e).

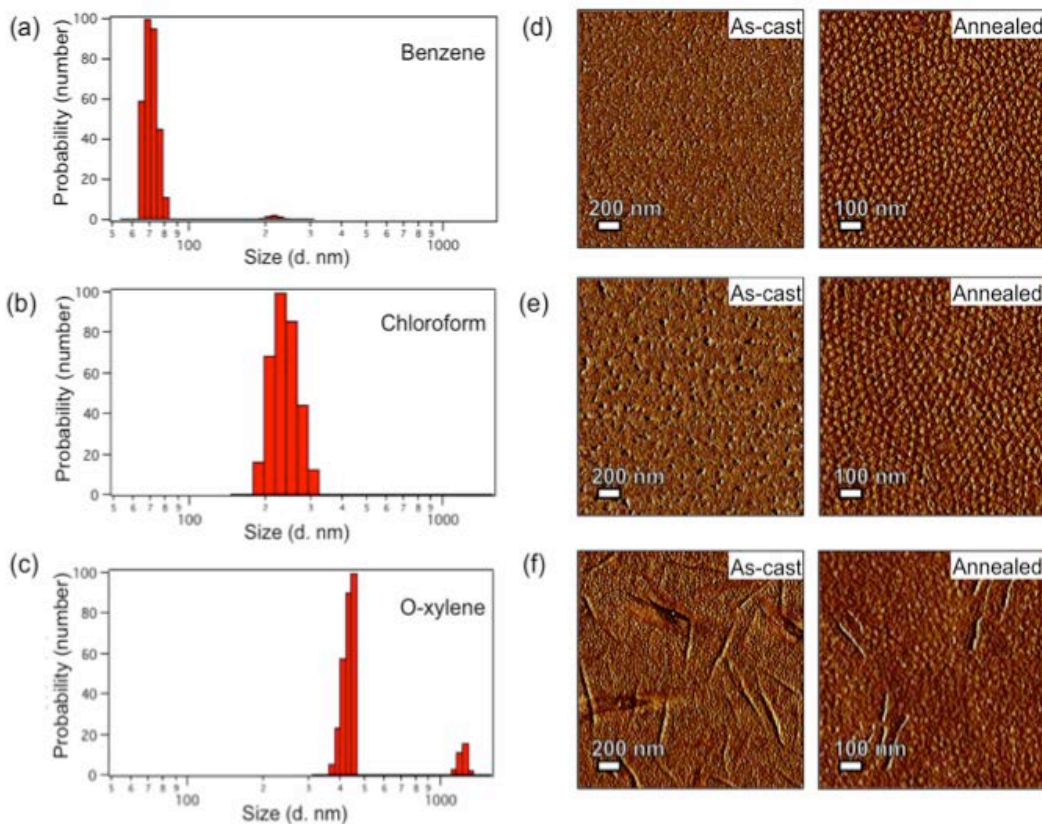


**Figure 3.6.** DLS results of 0.4 mg/mL AK<sub>4</sub>-4P2K conjugate solutions in (a) benzene, (b) chloroform, (c) o-xylene; and AFM phase images of as-casted and annealed AK<sub>4</sub>-4P2k/BCP blends at  $f = 2$  wt% casted from (d) benzene, (e) chloroform, and (f) o-xylene, respectively. Favorable PEG-solvent interactions result in better dispersion of AK<sub>4</sub>-4P2K conjugates in solution.

Although tailoring solvent-polymer interaction is effective, it limits solvent selection and benzene is not ideal due to its toxicity. An alternative approach was developed to reduce inter-CP hydrogen bonds during thin film fabrication. Trifluoroacetic acid (TFA) is one of the very few polar solvents used to dissolve CPs.<sup>3, 20, 26</sup> In prior solution studies, TFA was mixed with polar solvents such as DMF to disperse CP or CP-polymer conjugates in solution.<sup>20, 35</sup> However, none of these polar solvents are suitable for polymer processing, and TFA is incompatible with many organic solvents. To overcome the miscibility issue, we developed a simple yet effective route to introduce

TFA as co-solvent. The freshly lyophilized AK<sub>4</sub>-4P2K powder was first exposed to TFA vapor and then co-dissolved in toluene with PS-*b*-PMMA, and the solution remained clear. Fourier Transform Infrared spectra (FTIR) of samples pre-/post treatment are shown in Fig. 3. 7 a. The characteristic peak  $\sim 1200\text{ cm}^{-1}$  corresponding to C-F bond can be clearly seen for AK<sub>4</sub>-4P2K and PEG post TFA exposure. To quantitatively estimate the amount of TFA absorbed, <sup>19</sup>F Nuclear Magnetic Resonance spectroscopy (NMR) was used. Shown in Fig. A.2.3a of the *Appendix*, using 2,2,2-trifluoroethanol (TFE) as reference, 1 mg of AK<sub>4</sub>-4P2k absorbs  $\sim 0.394$  mg of TFA. Based on FTIR spectra, we speculate that PEG chains molecularly absorb TFA, and act as a local TFA reservoir. The amount of TFA present is sufficient to prevent CPN aggregation in toluene. The DLS result in Fig. 3.4b shows the size of CPN aggregate is  $\sim 200$  nm in TFA treated toluene, while large aggregates  $\sim 400$  nm are seen in untreated solution. Thermal annealing removes most TFA molecules to the level below the detection limit as indicated by the disappearance of the C-F peak after heating (Fig. 3.7 a, solid blue trace), and the lack of TFA peak in NMR spectrum (Fig. A.2.3 b, *Appendix*). More importantly, no CPN aggregates are seen in the as-cast film (Fig. 3.7 c), and well-aligned CPN channels are formed in PMMA cylinders post thermal annealing (Fig. 3.7 d).

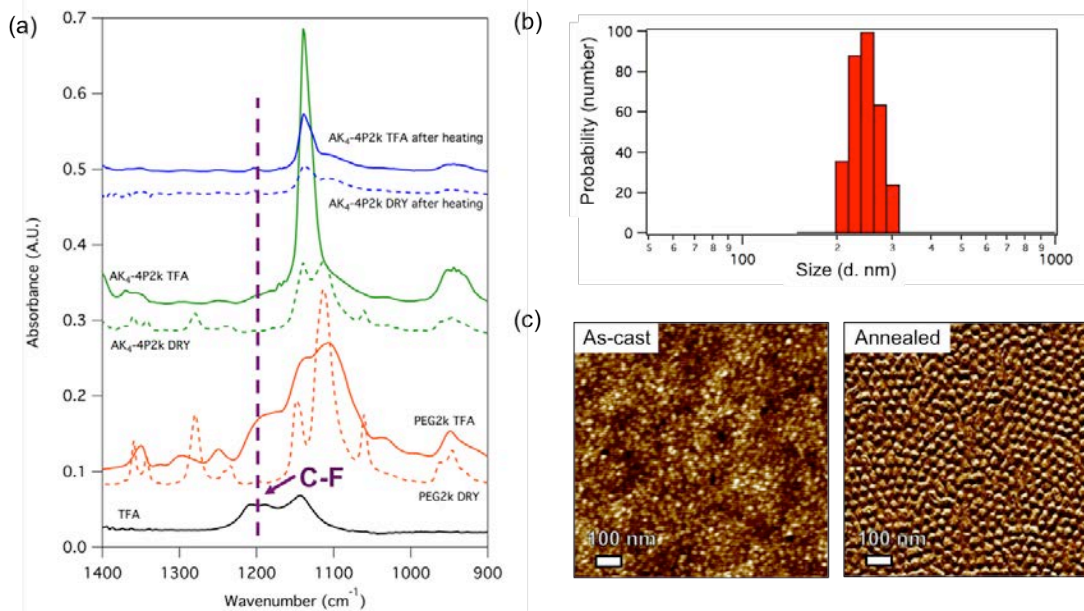


**Figure 3.7.** a) FTIR spectra of various samples at room temperature, (b) DLS result of 0.4 mg/mL AK<sub>4</sub>-4P2k post TFA treatment in toluene, and (c) AFM images of (b) blended with BCP at  $f=2$  wt%. The appearance of the characteristic peak of C-F bond  $\sim 1200\text{ cm}^{-1}$  indicates the absorption of TFA molecules after exposing to vapor for 2 minutes, which are removed by thermal heating. DLS result and AFM images further support the effect of TFA in reducing aggregation in toluene, resulting in well aligned CPNs at the center of PMMA cylinders after annealing.

### § 3.3 Conclusion

Guided growth of organic nanotube in polymeric matrix opens a viable route to fabricate sub-nanometer membranes by eliminating the need to control the nanotube diameter, length, and vertical alignment. However, CPNs tend to aggregate, preventing formation of through channels and compromising the membrane quality. Using well-defined CP-PEG conjugate with high purity, we systematically investigated the kinetic pathway of co-assembling the conjugate and cylindrical BCP in thin films and highlight important parameters to obtain high quality membrane. Thermal annealing at 245°C is ineffective in dispersing aggregates > 300 nm. Two routes were developed to overcome the membrane processing challenges. Using favorable solvents of PEG can reduce conjugate aggregation, thus improving the uniformity of vertically aligned CPN. The more effective route is to introduce a trace amount of small molecule hydrogen bond blocker, such as TFA to interfere with the inter-CP hydrogen bonding. Good nanotube dispersion is achieved even using non-optimal solvents for the polymer-covered nanotubes. The introduction of removable small molecule opens up a simple and yet viable route to modulate organic nanotube assembly during the fabrication process.

### § 3.4 Experimental

#### 3.4.1 Materials

The linear sequence of octapeptide [D-Ala-L-Lys]<sub>4</sub> (KA<sub>4</sub>) was synthesized following the standard 9-fluorenylmethoxycarbonyl (Fmoc) protocols for solid-phase peptide synthesis using 2-chlorotrityl chloride resin preloaded with Fmoc-D-Ala-OH. The linear peptide was then cleaved from the resin and cyclized head-to-tail using propylphosphonic anhydride (T3P) and N,N-Diisopropylethylamine (DIPEA) in DMF. Boc-protecting groups on the lysine residues were subsequently removed by 95% TFA to expose the free amines. Carboxylic acid-terminated PEG (Rapp Polymere) was conjugated to KA<sub>4</sub> by carboxy-amine coupling to the ε-amino groups of lysine residues at a mixing ratio of 4 equivalents of PEG to 1 equivalent of cyclic peptide. 1-ethyl-3-(3-dimethylaminopropyl) carbodiimide (EDC) was used as the coupling reagent and the reaction was run in a phosphate buffer solution at pH 6.5. Fmoc-D-Ala-OH, Fmoc-L-Lys(Boc)-OH, polystyrene-(2-chlorotrityl) resin (loading: 1.5 mmol/g), and 2-(1H-benzotriazole-1-yl)-1,1,3,3-tetramethyluronium hexafluorophosphate (HBTU) were



purchased from Nova Biochem. 2 Propanephosphonic acid anhydride (T3P) in DMF was purchased from Advanced ChemTech. Polystyrene-*block*-poly(methyl methacrylate) (PS-*b*-PMMA) with molecular weight **57K-25K (PDI 1.07)** was purchased from Polymer Source. Carboxylic acid-terminated poly(ethylene glycol) (PEG) (**Mw=2,000 Da, PDI 1.2**) was purchased from RAPP POLYMERE. All reagents were purchased with the highest purity and used as received unless otherwise noted. The random copolymers of styrene and methyl methacrylate with 2% reactive benzocyclobutene (BCB) [P(S-*r*-BCB-*r*-MMA)] (**Mw= 45K PDI 1.3**) was provided by T. P. Russell at the University of Massachusetts, Amherst.

### **3.4.2 Reversed-Phase High-Pressure Liquid Chromatography (RP-HPLC)**

The reaction mixture from conjugation was purified by RP-HPLC (Beckman Coulter) to obtain KA<sub>4</sub>-4P2K with reasonable purity using a C4 column (Vydac 22 mm x 250 mm) at a flow rate of 8 mL min<sup>-1</sup>. Conjugates were eluted with a linear AB gradient, where solvent A consisted of water containing 0.1% (v/v) TFA and solvent B consisted of acetonitrile (ACN) containing 0.1% (v/v) TFA. A linear gradient of 20 to 65% B over 45 min was used and the elution was monitored using a diode array detector at wavelengths of 200 nm and 220 nm. AK<sub>4</sub>-4P2K conjugates were eluted at ~55% ACN.

### **3.4.3 MALDI-TOF Mass Spectrometry**

The identity and purity of the isolated AK<sub>4</sub>-4P2K conjugates were verified by MALDI-TOF MS using  $\alpha$ -cyano-4-hydroxycinnamic acid matrix. Mass spectrum was recorded on an Applied BioSystems Voyager-DE Pro.

### **3.4.4 Grazing Incident Small Angle X-ray Scattering (GISAXS)**

DLS was performed using Brookhaven BI-200SM at a wavelength of 637 nm with the scattering angle at 90°. The solvent used (can't filter the solution because of the aggregation problem) was filtered using 0.1  $\mu$ m PTFE filters.

### **3.4.5 Dynamic Light Scattering (DLS)**

Measurements were performed at beamline 8-ID Advanced Photon Source (APS) at Argonne National Lab with x-ray wavelength 1.240 nm. An X-ray beam was directed at the sample at a grazing incident angle slightly above the critical angle of the polymer film.

### **3.4.6 Fourier Transfer Infrared Spectroscopy (FTIR)**

FTIR measurements were performed using a Perkin Elmer Spotlight 200 FTIR Microscope System. The samples were casted between two NaCl pellets.

### 3.4.7 Nuclear Magnetic Resonance Spectroscopy (NMR)

NMR experiments were performed using Bruker AVQ-400 with 5mm QNP probe. Chemical shifts were taken relative to  $\text{CFCl}_3$  at 0 ppm and  $\text{D}_2\text{O}$  was used as the solvent. 2,2,2-trifluoroethanol was added as the reference to estimate the amount of trifluoroacetic acid in solution.

### 3.4.8 Thin Film Fabrication

Si wafers were modified using a random copolymer of styrene and methyl methacrylate as described previously.<sup>36</sup> A ~ 12-14 nm layer of BCB was deposited onto the wafer and subsequently heated to 250°C for 20 minutes to anchor the polymer chains to the substrate and also to crosslink the chains randomly. This brush layer was then rinsed with toluene three times at 3000 rpm to remove any uncrosslinked chains.  $\text{AK}_4\text{-4P2k}$  conjugates and PS-*b*-PMMA BCPs were dissolved in toluene at 1 % w/v and the solutions was sonicated for 30 minutes. Thin films were prepared by spin casting the sonicated solution at 2500 rpm at room temperature. For the benzene thin films, the preparation was similar except the solution was spin casted at 8000 rpm instead of 2500 rpm. All films were annealed in vacuum for 4 hours and slowly cooled down to room temperature by placing the films in a Styrofoam box. A schematic outlining the thin film preparation process is included in Figure A.2.2. Freestanding films were also prepared for TEM in which the thin films were prepared on special Si wafers with 200nm thermal oxide layer. After annealing, the films were immersed in a 5 wt % HF in  $\text{H}_2\text{O}$  solution to etch away the thermal oxide layer and then transferred to a DI water bath to float the films off the substrates. Finally, freestanding films were transferred onto copper grids for TEM measurements.

## Chapter 4

# Interiorly Modified Cyclic Peptide and Its Assembly Behavior

|       |  |    |
|-------|--|----|
| § 4.1 | Introduction.....  | 63 |
| § 4.2 | Methyl-modified Cyclic Peptide and Conjugates.....                       | 65 |
| § 4.3 | Co-assembly in Block Copolymer Thin Films.....                           | 71 |
| § 4.4 | Conclusion .....   | 77 |
| § 4.5 | Experimental .....   | 78 |
|       | 4.5.1 Materials .....  | 78 |
|       | 4.5.2 Synthesis of Mba-8CP .....   | 78 |
|       | 4.5.3 Reversed-Phase High-Pressure Liquid Chromatography (RP-HPLC) ..... | 79 |
|       | 4.5.4 MALDI-TOF Mass Spectrometry .....                                  | 79 |
|       | 4.5.5 Fourier Transfer Infrared Spectroscopy (FTIR) .....                | 79 |
|       | 4.5.6 Dynamic Light Scattering.....                                      | 79 |
|       | 4.5.7 Co-assembly Thin Film Fabrication .....                            | 79 |

Partial material has been previously published:

R. Hourani, C. Zhang, R. Weegen, L. Ruiz, C. Li, S. Keten, B. Helms and T. Xu, JACS, 2011, 133, 15296-15299

*An 8-mer cyclic peptide (CP) with a methyl group projected to the interior has been successfully synthesized. The self-assembly of the conjugates is evaluated to gain fundamental understandings on the nanotube formation for CPs with non-ideal stacking structure. Despite the reduced number of inter-CP hydrogen bonds, both the methyl modified CP and its poly(ethylene glycol) (PEG) conjugates form high aspect ratio cyclic peptide nanotubes (CPNs) and PEG-covered CPNs respectively. The conjugated PEG chains allow further processing of the nanotubes to be compatible with conventional polymer processing. The co-assembly of the methyl modified CP conjugates with block copolymer in thin films is thoroughly investigated and a general protocol is thus developed in co-assembling different cyclic peptide nanotubes with block copolymer matrix in thin films. Controlling the kinetic pathway is the critical factor in which good dispersion of the conjugates prior to thin film fabrication is required. These studies indeed establish the foundation for fabricating membranes containing molecularly defined pores with various functionalities for specific separation processes.*

## § 4.1 Introduction

In the previous chapters, we have focused on simple cyclic peptides (CPs) consisting of 8-mer *cyclo*(D-Ala-L-Lys)<sub>4</sub> (“AK<sub>4</sub>”) and its poly(ethylene glycol) (PEG) conjugates (“AK<sub>4</sub>-PEG conjugates”). Great efforts have been made to understand the assembly behaviors of this simple AK<sub>4</sub>-PEG conjugate system in which the self-assembly has been systematically investigated in Chapter 2, and the co-assembly with polystyrene-*b*-poly(methyl methacrylate) (PS-*b*-PMMA) in thin films is carefully evaluated in Chapter 3. Nevertheless, for applications in transport and membrane technology, additional interactions with various chemical species are often needed to facilitate the separation process and to enhance the membrane performance.<sup>1-5</sup> For example, the NPA (Asn-Pro-Ala) motifs in aquaporins (biological protein channels) are speculated to facilitate the transport of water through dipole interactions with H<sub>2</sub>O molecules in addition to size exclusion principle.<sup>6-9</sup> Thus, although simple CPs fulfill the requirement for pore size, there is a need to extend the current simple CPs to specially designed CPs to enrich the available library of 1D nanotubes with added functionalities. The focus of this chapter is really to take a step further in exploring and assessing the feasibility in synthesizing special CPs with functional groups projected inside the CP ring, and systematically studying the self-assembly as well as co-assembly of the modified CPs under different environments.

There have been several attempts to modify nanotube interior by incorporating artificial amino acids containing cyclohexanes and aromatic rings, or unsaturated amino

acids at multiple positions in the primary CP sequence to project a specific chemical functionality towards the nanotube interior.<sup>10-12</sup> A minimalist approach to synthesize CPs with interior functionalities was developed by Dr. Rami Hourani and Mr. Robert van der Weegen.<sup>13</sup> As an initial demonstration, a methyl group was introduced although other functional groups might also be incorporated following the same approach. This was achieved by substituting one of the amino acid in the primary 8-mer peptide sequence with an aromatic amino acid carrying the desired functionality (methyl). As a result of this substitution, the symmetry in the inter-CP hydrogen bonding is broken and the estimated number of hydrogen bonds in between two CP rings is reduced from  $\sim 7.3$  to  $\sim 5.9$  pairs.<sup>13</sup> Nevertheless, we found that the modified CP subunits still self-assembled into large aggregates with sizes in the micrometer range, similar to what has been observed for unmodified CPs.<sup>13-17</sup> Two PEG chains had been successfully conjugated to the methyl-modified CP so that the assembly process can be tuned and controlled. The conjugated PEG chains not only break the lateral aggregations of methyl-modified CPs to individual PEG covered cyclic peptide nanotubes (CPNs),<sup>18</sup> but also serve to direct and modulate the growth of the nanotubes in a more controllable manner.<sup>19-22</sup>

The co-assembly of methyl-modified CP-PEG conjugates and block copolymer (BCP) in thin films was also systematically investigated. It is found that the co-assembly of the methyl-modified CP is similar to its unmodified counterpart in which the process is governed by both thermodynamic and kinetic contributions. A general protocol can therefore be developed for co-assembling different cyclic peptides and BCP matrix in thin films. Thermodynamically, there exists a loading limit of a maximum of one nanotube in one cylindrical microdomain whereas excessive conjugates in the form of PEG covered nanotubes tend to aggregate to the free surface, resulting in defects at the polymer/air interface. Kinetically, ensuring good dispersion of CP-polymer conjugates is required prior to thin film fabrication because the co-assembly is pathway dependent. Therefore, a careful selection of processing solvents needs to be evaluated before casting. However, due to the differences in chemical nature and solubility, the introduction of hydrogen bonding blocker (i.e. small molecules) is less effective in preventing pre-aggregation of the conjugates comparing to the unmodified CP system in toluene. Nevertheless, a combination of introduction of hydrogen bond blockers coupled with greater driving force of higher annealing temperature can be used to achieve homogeneous thin film morphology of well-aligned nanotubes. From the knowledge gained in these studies and from previous investigations, we have derived that there are two pre-requisites for successful co-assembly process, namely the thermodynamic loading limit and kinetic pathway due to CP aggregation. This general protocol indeed establishes the foundation for co-assembling cyclic peptides and block copolymers, and can be extended to other systems for the fabrication of high quality membranes with various functionalities for different separation processes.

## § 4.2 Methyl-modified Cyclic Peptide and Conjugates

Before the detailed discussion about the interiorly modified cyclic peptide, I would like to emphasize that this study was a collaborative effort between previous group member, Dr. Rami Hourani, Mr. Robert van der Weegen and me. In particular, Dr. Hourani had developed this minimalist approach of incorporating an artificial subunit with methyl functionality in the linear peptide sequence. All the synthetic work was performed by Dr. Hourani and Mr. van der Weegen with structural characterization using various techniques including molecular simulation, and my contribution is mainly focused on the investigation of the assembly behavior of the modified cyclic peptides and its conjugates. Detailed work was published in *Journal of American Chemical Society*, **2011**, 133, 15296-15299. I would like to express my great appreciation to Dr. Hourani for providing me the modified cyclic peptide for my subsequent studies.

The *L*-Leu in the primary sequence of a prototypical 8-mer CP sequence *cyclo(L-Lys-D-Ala-L-Leu-D-Ala)<sub>2</sub>* (“8CP”) was substituted by a single aromatic amino acid, 3-amino-2-methylbenzoic acid ( $\gamma$ -Mba-OH). The detailed synthesis is outlined in Section 4.5.2 and the chemical analysis is presented in Figure A. 3.1 of the Appendix. The chemical structure of the Mba-modified cyclic peptide, *cyclo(L-Lys-D-Ala-L-Leu-D-Ala-L-Lys-D-Ala- $\gamma$ -Mba-D-Ala)* (“Mba-8CP”), is also shown (Figure 4.1 a and b) for comparison. Molecular dynamics (MD) simulations were carried out to compare the structure and stability of the assemblies of Mba-8CP and the unmodified 8CP. The simulations were performed using the COMPASS force field. Top-views and side-views of the equilibrated structures obtained from MD simulations are shown in Figure 4.1 c-f). For Mba-8CP, due to the substitution of the  $\gamma$ -Mba subunit, the methyl group is forced to be presented to the interior of the pore. This mutation reduces the radius of the nanotube to  $\sim 4.7$  Å (Figure 4.1 c), a 38% reduction in size from  $\sim 7.6$  Å pore size for the 8CP nanotube (Figure 4.1 d). The aromatic rings of  $\gamma$ -Mba-OH are oriented to one side of the nanotube, implying the methyl groups are stacked along the nanotube with slight tilts. The lateral views (Figure 4.1 e and f) of the formed nanotubes showed that the mutation disproportionately elongates the ring structure and disrupts the symmetry of its backbone amide bonds. This affects the carbonyl and amide groups which hydrogen bond in an anti-parallel fashion for 8CP without the mutation. As a result, the number of hydrogen bonds between adjacent cyclic peptide rings is reduced from an average of 7.3 hydrogen bonds for 8CP to 5.9 for Mba-8CP. The average inter-ring distance is  $\sim 4.8$  Å in both cases (Appendix, Figure A. 3.3).

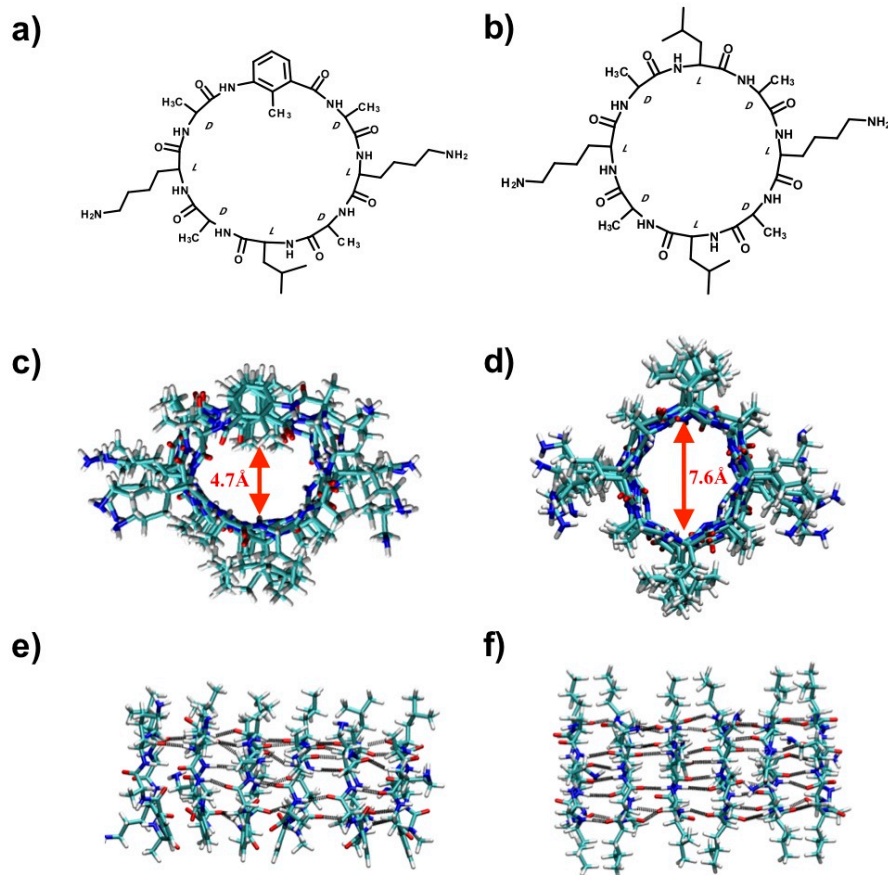


**Figure 4.1.** Chemical structures of (a) Mba-8CP and (b) its conventional analogue 8CP; Snapshots of equilibrium structures calculated from molecular dynamics (MD) simulations, showing cross-sectional (c, d) and lateral (e, f) views of Mba-8CP and 8CP nanotubes respectively. The radii of Mba-8CP and unmodified 8CP are  $\sim 4.7$  and  $7.6$  Å, respectively.

Based on the understandings from the self-assembly behavior of unmodified cyclic peptide and its conjugates (Chapter 2), we know that the strength of inter-CP hydrogen bonding is the critical driving force for nanotube formation. Therefore, it is important to ensure the reduction of hydrogen bonding pair for Mba-8CP does not compromise the formation of high aspect ratio nanotubes. A systematic investigation was therefore performed on the self-assembly of the modified Mba-8CP, and its PEG 2-arm conjugates, Mba-2P2k to evaluate the inter-CP hydrogen bonding strength. Fourier Transformed Infrared spectroscopy (FTIR) was therefore performed on Mba-8CP and Mba-2P2k conjugates to confirm the intermolecular hydrogen bonds in forming  $\beta$ -sheet structures. The amide A band peak at  $3282.3\text{ cm}^{-1}$  for Mba-8CP and at  $3286.2\text{ cm}^{-1}$  for Mba-2P2k conjugates at  $30^\circ\text{C}$  both verify the formation of inter-CP hydrogen bonding for both systems, and therefore nanotube formation. However, the amide A band peaks for the methyl-modified CP and its conjugate are shifted to higher wavenumbers than

their unmodified CP counterparts (i.e. AK<sub>4</sub> and AK<sub>4</sub>-2P2k), in which the peak positions are 3275.1 cm<sup>-1</sup> for AK<sub>4</sub> and 3275.3 cm<sup>-1</sup> for AK<sub>4</sub>-2P2k conjugates respectively (Figure 2.1 of Chapter 2). This is a reflection of weakened inter-CP hydrogen bonding as a result of the mutation in the primary CP structure. Moreover, the difference between the naked CP and 2-arm PEG conjugates for the methyl-modified system is ~ 20 folds larger than the unmodified system (3.9 cm<sup>-1</sup> vs. 0.2 cm<sup>-1</sup>), indicating less stable nanotube structure due to weakened inter-CP hydrogen bonds. Nevertheless, similar temperature dependence is observed since the driving force of inter-CP hydrogen bonding for nanotube formation is the same in both cases. Upon heating, the amide A band peak position shifts to higher wavenumber, demonstrating the weakening of the inter-CP hydrogen bonds as hydrogen bonds are sensitive to thermal perturbation. Upon cooling, reformation of hydrogen bonds is seen as indicated by the change of the amide A band peak back to lower wavenumber. The observed thermoreversibility for both Mba-8CP and Mba-2P2k conjugates indeed allows further processing of the methyl-modified nanotubes to be compatible with conventional polymer processing.

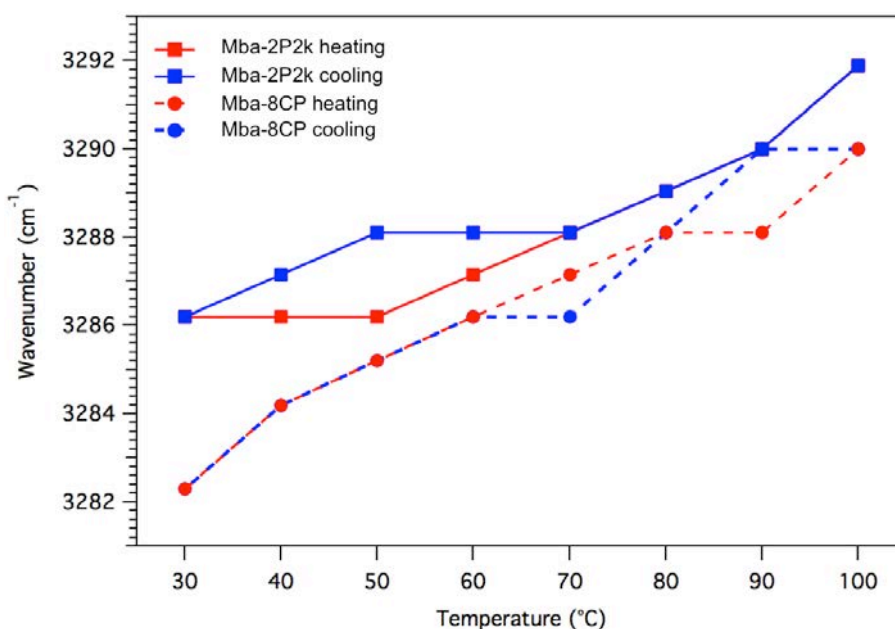


**Figure 4.2.** Plots showing the Amide A band peak wavenumbers of Mba-8CP and Mba-2P2k conjugates as a function of temperature. Samples were prepared by casting on the NaCl plates from DMF solutions and kept under vacuum with desiccant overnight at 25 °C. Changes in the Amide A band peak position to higher wavenumbers indicate the weakening of the inter-CP hydrogen bonding upon heating. Thermoreversibility of hydrogen bonding is observed for both the Mba-8CP and the 2-arm PEG conjugate.

Upon spin casting onto silicon substrate with ~2 nm native oxide layer, both the Mba-8CP and Mba-2P2k conjugates would form high aspect ratio CPNs and PEG



conjugated-CPNs (called “pc-Mba-CPNs”) as shown in Figure 4.3 a) and b). In this case, tetrahydrofuran (THF) was used to process CPs and the conjugates because of proper solubility. No obvious difference in nanotube sizes were seen for the conjugates casted at different spinning speeds, as demonstrated in Figure A. 3.5 of the Appendix. This is probably due to very fast removal rate of THF. The AFM results again confirm that the driving force for nanotube formation, i.e. the remaining ~6 pairs of hydrogen bonds, is strong enough to overcome the mutation in the Mba-8CP sequence so that the subunits could stack to form a tubular structure. Similar to the unmodified counterpart, PEG conjugation prevents lateral aggregation of the naked CPs as individual PEG covered nanotubes ~ 5 nm can be seen with lengths ~ 50-150 nm in Figure 4.3b), whereas bundles of bare nanotubes with lengths ~ 500-1000 nm are seen for naked Mba CPNs in Figure 4.3a). Furthermore, the conjugated PEG chains also improve the overall solubility of the conjugates in many organic solvents, making further processing possible.

Like the unmodified AK<sub>4</sub> system, the conjugated PEG arms indeed allow further manipulation of the growth of pc-Mba-CPNs due to the added interactions between the PEG chains with the environment. In addition to the entropic penalty of confining the PEG arms to the inter-CP hydrogen bonding distance of ~ 4.7 Å,<sup>13</sup> movements of PEG chains can potentially cause more interruption to the nanotube structure compare to the AK<sub>4</sub> system because the overall inter-CP hydrogen bonding is reduced. Inspired by conventional treatments for polymer processing, solvent annealing was performed to the Mba-2P2k conjugates. From Figure 4.3 c), it is clear that longer Mba-pc-CPNs are broken down into shorter nanotubes/tubelets after THF solvent treatment. It is speculated that under high THF vapor, the PEG chains likely would be in a rubbery state in which the chain mobility is very high. The movement of the PEG chains acts as an opposing force to the inter-CP hydrogen bonding, destabilizing the nanotube structure. Furthermore, polar THF molecules may directly interact with the hydrogen bonding and reduce the number of effective hydrogen bonds, similar to the function of hydrogen bonding blocker (trifluoroacetic acid) as described in Chapter 3. A combined effect of these two destabilizing contributions cause long pc-Mba-CPNs being broken down into shorter tubelets < 20 nm under the influence of THF molecules. The capability to manipulate the length of the nanotubes is critical in future processing of these nanotubes with block copolymers for the fabrication of sub-nm membranes with functionalized transport channels.

Remarkably, due to the reversibility of hydrogen bonding, longer nanotubes can be reconstructed from the shorter fragments through the reformation of inter-CP hydrogen bonds on solid support. As shown in Figure 4.3 d), upon thermal annealing followed by slow cooling, high aspect ratio pc-Mba-CPNs can be indeed re-grown. It is speculated that the added thermal energy gives the PEG chains enough mobility to move around and slow cooling allows the building blocks to adjust and orient in the right direction, resulting in the re-formation of inter-CP hydrogen bonds and therefore long aspect ratio nanotubes. This reversible transition indeed enables one to modulate and

manipulate the nanotube formation to be compatible with polymer processing window, which is needed for membrane fabrication.

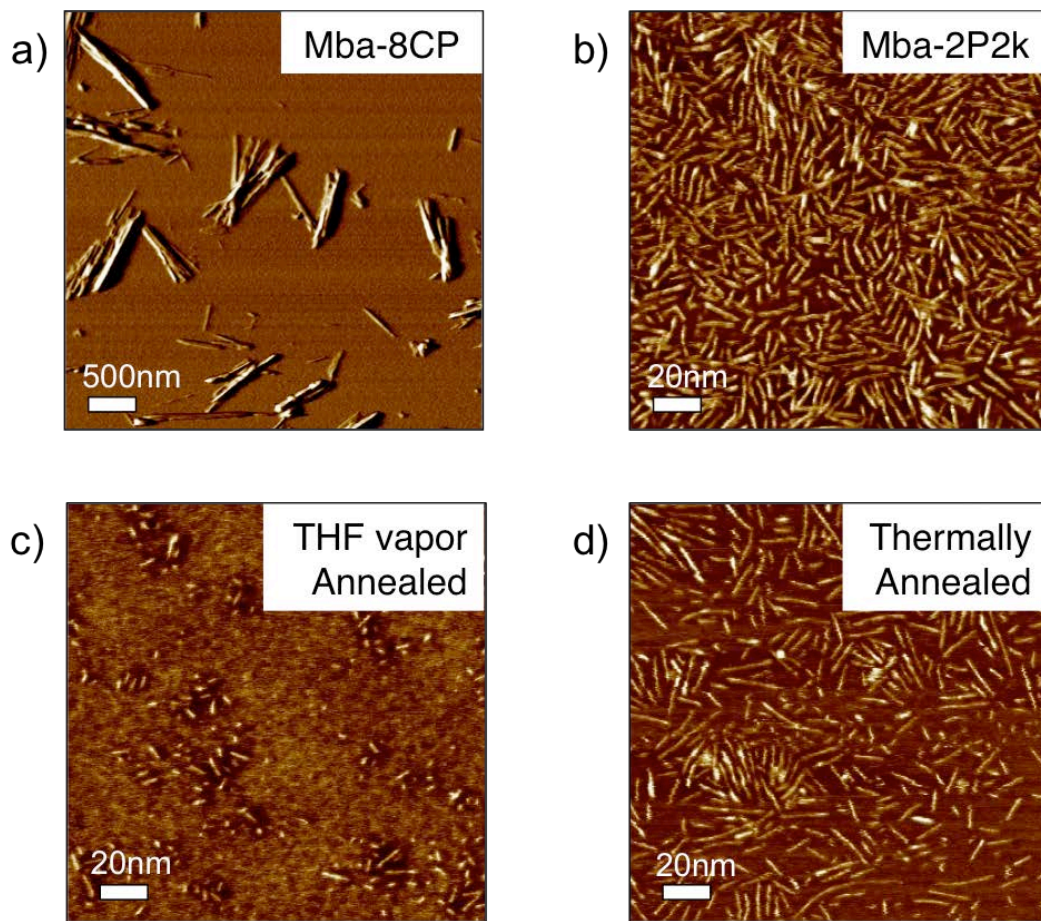


**Figure 4.3.** AFM images of a spin-cast 0.1 mg/mL THF solution of a) Mba-8CP, b) Mba-2P2k conjugates, c) sample b) treated with THF vapor, and d) sample (c) heated to 80 °C for 1 hr and slowly cooled down to room temperature. Bundles of high aspect ratio Mba nanotubes of ~500-1000 nm in length are broken down to individual polymer covered nanotubes with much lower aspect ratio through PEG conjugation. Reversible growth of high aspect ratio Mba-pc-CPNs can be achieved using a combination of solvent annealing and thermal annealing.

The results from Chapter 2 reveal that the growth of PEG conjugated CPNs can be indeed tuned and modulated via two simple approaches without additional annealing process, i.e. varying the position of the PEG arms and/or varying the solution concentration. Since the underlying thermodynamics of nanotube formation does not differ much for the methyl-modified CPs, similar behavior is expected for the Mba-PEG conjugates. Due to difficulty in purification, the position of the PEG arm was not

evaluated. However, by varying the solution concentration of Mba-2P2k conjugates, useful information about the growth of methyl modified CPNs could still be extrapolated. Figure 4.4 shows the phase-contrast AFM images of Mba-2P2k conjugates spin-cased from THF from 15  $\mu\text{M}$  and 30  $\mu\text{M}$  solutions respectively. The average length of pc-Mba-CPNs is  $\sim 29.7 \pm 18.9$  nm for 15  $\mu\text{M}$ , and  $\sim 67.7 \pm 31.4$  nm for 30  $\mu\text{M}$ . Similar to the unmodified AK<sub>4</sub>-PEG systems, the growth of pc-Mba-CPNs is directly related to the solution concentration. However, the length for the modified CPN tends to be shorter than its unmodified counterpart. There are two speculated reasons for the observed difference. First, the driving force for nanotube formation is reduced for the case of Mba-2P2k since the effective number of inter-CP hydrogen bonds is decreased due to the mutation in the CP sequence. Additionally, the entropic penalty associated with conjugated PEG chains is likely to be higher for Mba-2P2k since the stacking of the Mba-8CP results in PEG chains in close proximity with one another from the adjacent CPs according to our simulation result (Figure 4.1 c). The combined effect from lower driving force and higher entropic penalty likely will result in shorter pc-Mba-CPNs. Another possible reason for shorter nanotubes may be due to the casting solvent. Toluene was used as the casting solvent for AK<sub>4</sub>-PEG systems, whereas THF was used for Mba-2P2k conjugates. Being a much volatile solvent, THF evaporates much faster than toluene, allowing less time for nanotube formation. Due to the dynamic nature of CPN formation, slight difference in solvent removal rate may result in differences in the growth of CPNs, hence the nanotube length. Nevertheless, similar concentration dependence is observed for both cases, indicating that the growth of polymer covered CPNs can be indeed tuned and modulated just like the unmodified AK<sub>4</sub> system.

Through systematic investigation on the self-assembly of Mba-8CP and Mba-2P2k conjugates, and comparison with the unmodified AK<sub>4</sub> and AK<sub>4</sub>-PEG systems, we do have a basic understanding of the behavior of the resultant nanotubes or PEG-covered nanotubes with a functional group inside the pore. Although the mutation in the primary CP sequence causes a reduction in the effective number of inter-CP hydrogen bonds, the formation of nanotubes and PEG-covered nanotubes are similar to the unmodified counterparts, and specifically the growth process for the PEG-covered nanotubes can be tuned and modulated. While solution concentration is one parameter that we can play with to modulate the length of the nanotubes, conventional techniques compatible with polymer processing such as solvent annealing and thermal treatment can be applied to the Mba-2P2k conjugates to manipulate the length of the nanotubes. These conclusions and studies are critical for subsequent investigations to assess the feasibility of fabrication membranes containing interiorly functionalized sub-nanometer channels via co-assembly the modified CPNs with block copolymer matrix in thin films.

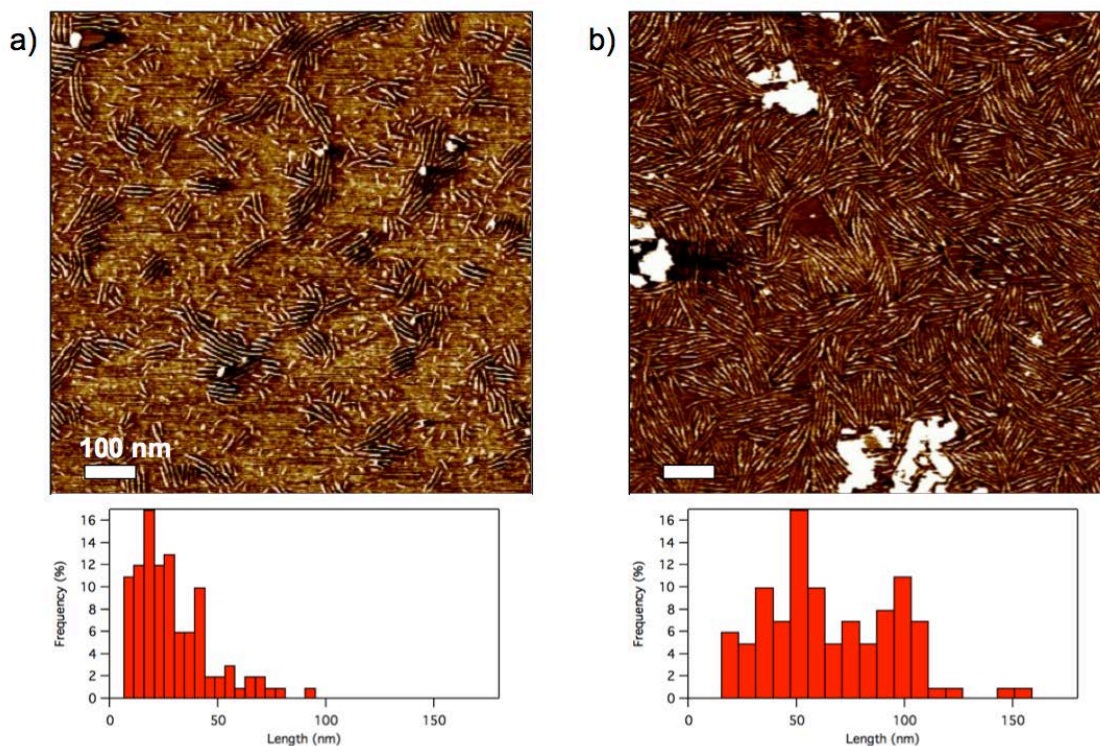


**Figure 4.4.** AFM phase images and corresponding statistic length analyses of PEG covered Mba-CPNs spin casted from THF solutions at a) 15  $\mu\text{M}$  and b) 30  $\mu\text{M}$ .

### § 4.3 Co-assembly in Block Copolymer Thin Films

As discussed earlier in Chapter 3, the guided co-assembly of cyclic peptide-polymer conjugates and block copolymer (BCP) in thin films is a viable approach to fabricate sub-nanometer porous membranes containing high-density arrays of through channels. The study on unmodified cyclic peptide-PEG conjugates indeed allows us to have a basic understanding of the factors affecting the co-assembly process of the conjugates and BCP in thin films and set the foundation for processing the cyclic peptide nanotubes in BCP framework to make membranes for various applications. With the successful synthesis of the interiorly modified cyclic peptide, we can now move one step further to possibly have a library of different functional groups inside the nanotube channel to facilitate the overall transport across the membrane.

From previous section on the self-assembly of Mba-8CP and Mba-2P2k systems, we know that the effective number of hydrogen bonds between two CP rings is reduced to  $\sim 5.9$  pairs. This may be advantageous for co-assembling Mba-2P2k conjugates with BCP as the tendency for disfavored pre-aggregation in solution is reduced. However, the

overall solubility of the Mba-2P2k conjugates in processing solvents such as toluene is being compromised as only 2 PEG chains were conjugated to the Mba-8CP, whereas 4 PEG chains were conjugated to AK<sub>4</sub> system for the investigations on the co-assembly process described in chapter 3. Different number of PEG chains will affect how different conjugates behave in solution and/or interact with the BCP matrix. Therefore, it is important to investigate the co-assembly of the Mba-2P2k conjugates and cylinder-forming polystyrene-*b*-poly (methyl methacrylate) (PS-*b*-PMMA) in thin films alone and to develop a specific processing condition for various cyclic peptides due to the slight differences in the chemical nature and the nanostructures.

Pre-aggregation of CPNs in solution prior to thin film fabrication has been shown to be the biggest challenge preventing the formation of high-quality membranes suitable for separation. Thus, systematic studies have been performed to the Mba-2P2k conjugates targeting the two contributors to the preaggregation separately. The first parameter of solvent quality was tested by dissolving Mba-2P2k conjugates in a number of organic solvents and study their solution behaviors. In this case, THF was not selected due to poor processability of PS-*b*-PMMA although it dissolves Mba-2P2k conjugates reasonably well and was used for the previous self-assembly studies. Dynamic light scattering (DLS) was used to gauge the extent of CPN aggregation and the results are presented in Figure 4.5. Similar to the case of the unmodified AK<sub>4</sub>-4P2k conjugates, toluene with solubility parameter  $\delta_{\text{toluene}}=8.9 \text{ (calcm}^{-3}\text{)}^{-1/2}$  is a poor solvent for PEG ( $\delta_{\text{PEG}}=8.9 \text{ (calcm}^{-3}\text{)}^{-1/2}$ ) and therefore Mba-2P2k conjugates aggregate strongly in toluene with sizes beyond 1  $\mu\text{m}$  (Figure 4.7c). In comparison, chloroform and benzene with solubility parameter  $\delta_{\text{chloroform}}=9.2 \text{ (calcm}^{-3}\text{)}^{-1/2}$  and  $\delta_{\text{benzene}}= 9.1 \text{ (calcm}^{-3}\text{)}^{-1/2}$  respectively can disperse Mba-2P2k conjugates reasonably well with most conjugate sizes  $\sim 100\text{-}200 \text{ nm}$ . Despite the reduced number of hydrogen bonds for Mba-8CP in comparison to unmodified CP, the tendency for Mba-2P2k conjugates to aggregate in solution is still very strong, possibly due to reduced number of PEG arms as the average size of AK<sub>4</sub>-4P2k conjugates in benzene is only  $\sim 70 \text{ nm}$  (Figure 3.6, Chapter 3). With only 2 PEG chains conjugated, not only the overall solubility of the conjugate is reduced, the entropic penalty due to PEG chain deformation in destabilizing the nanotube structure is also lowered. The combined effect of lower solubility and lower entropic penalty compromises the reduced hydrogen bonds, resulting in preaggregation of Mba-2P2k conjugates in non-favorable solvents such as toluene.



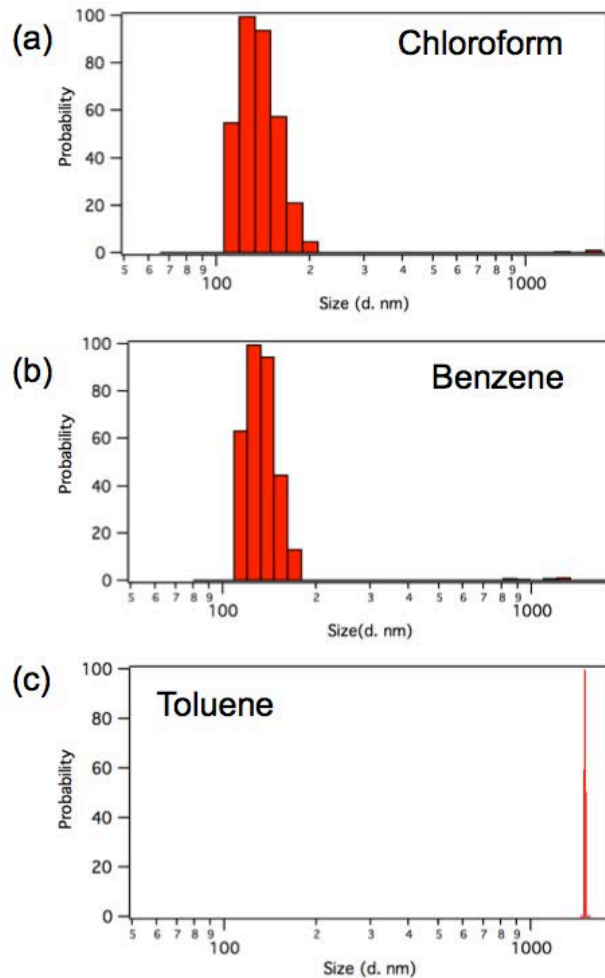


**Figure 4.5.** DLS results of 0.1 mg/mL Mba-2P2k conjugates in a) chloroform, b) benzene, and c) toluene. Good solvents for PEG such as chloroform and benzene can disperse the conjugates reasonably well, while large aggregates  $> 1 \mu\text{m}$  are seen in poor solvent toluene.

Nevertheless, CPN aggregates can be broken upon heating. Thermal annealing treatment during membrane fabrication process has been shown to break some of the aggregations for AK<sub>4</sub>-4P2k conjugates. With reduced hydrogen bonding strength for Mba-2P2k conjugates, some aggregation may be tolerated by the system. Therefore, thin films were fabricated using both good and poor solvents and the morphologies of the annealed films were characterized by atomic force microscopy (AFM) shown in Figure 4.6. At 1 wt% loading, homogeneous thin films with mostly well-aligned Mba-CPNs inside the PMMA microdomains oriented normal to the surface can be obtained using good solvent chloroform and benzene (Figure 4.6 a) and b). This result reveals several important pieces of information about the interiorly modified CPN/BCP blends. Firstly, with only 2 PEG chains, the net result of unfavorable interaction between PEG and PS

and the favorable interaction between PEG and PMMA is sufficient to sequester Mba-2P2k conjugates at the center of PMMA microdomains, similar to the case of AK<sub>4</sub>-4P2k conjugates. Secondly, thermoreversibility of inter-CP hydrogen bonding allows the nanotubes to be re-grown within the PMMA microdomains, resembling the self-assembly behavior of Mba-2P2k conjugates as shown in Figure 4.3 d). Lastly, despite of slightly larger sizes of conjugates in solution prior to thin film fabrication (~ 100-200 nm, Figure 4.5 a) and b), thermal annealing at 180 °C provides sufficient driving force to break larger conjugates and to sequester them in the PMMA microdomains, leading to homogeneous thin film morphology. In contrast, AK<sub>4</sub>-4P2k system with stronger inter-CP hydrogen bonding only allows conjugates < 100 nm to be dispersed well in the matrix (Figure 3.6, Chapter 3). The reduction in the number of inter-CP hydrogen bonds compensates for the reduced number of conjugated PEG chains, even slightly broadens the processing window for Mba-2P2k/PS-*b*-PMMA system.

However, when the conjugate sizes are beyond the limit of the thermal energy in breaking large aggregates into smaller pieces, defects of lay-down nanotubes can be seen at the polymer/air interface as seen for the thin film processed from toluene solution (Figure 4.6 c). This reflects our previous finding that controlling the kinetic pathway of pre-aggregation in solution is indeed a critical factor in ensuring the membrane quality and integrity. Since both chloroform and benzene can disperse the Mba-2P2k conjugates reasonably well, chloroform with lower toxicity was used as the preferred solvent to fabricate thin films. In order to better characterize the morphology of the thin films, Fast-Fourier Transform (FFT) was performed to all the AFM images and the results are shown as the insets. By back calculating the radii of the circles, the average periodicities for all the samples are obtained as the following: 39.87 nm for a), 39.93 nm for b), and 42.53 nm for c). Comparing all the 1 wt% thin films, the periodicity of the toluene sample is much larger than the chloroform and benzene samples, likely due to the surface defects. Moreover, the FFT circle for toluene sample is more diffused in terms of the thickness, indicative of less ordering in the nanostructure. Homogeneous thin films can be obtained using favorable solvents such as chloroform and benzene, which show very similar periodicity without much pre-aggregation. When loading goes beyond the critical value of one CPN in one PMMA cylinder (i.e. ~1.3 wt%), surface defects of lay-down nanotubes can be seen clearly at the polymer/air interface as shown in Figure 4.8 d). FFT of d) gives a periodicity of 41.10 nm, slightly larger than the 1 wt% sample. Similar to the case of the toluene sample, overloading causes surface defects of lay-down nanotubes and less ordering of the nanostructure as indicated by the thickness of the FFT circle. From the past experience in structural characterization and agreement among the results obtained different techniques such as AFM, transmission electron microscopy (TEM), and x-ray scattering, AFM results are very accurate in depicting the surface morphology of the thin films, and in-plane information can then be deduced. Combing the results from Figure 4.6 and our understandings on the co-assembly of the unmodified AK<sub>4</sub>-4P2k and PS-*b*-PMMA blends, we tentatively conclude that the co-assembly of methyl-modified CP-PEG conjugates and PS-*b*-PMMA in thin films is similar to the case of unmodified

AK<sub>4</sub>-4P2k conjugates in which both thermodynamic and kinetic factors are important to ensure thin film morphology and membrane quality.

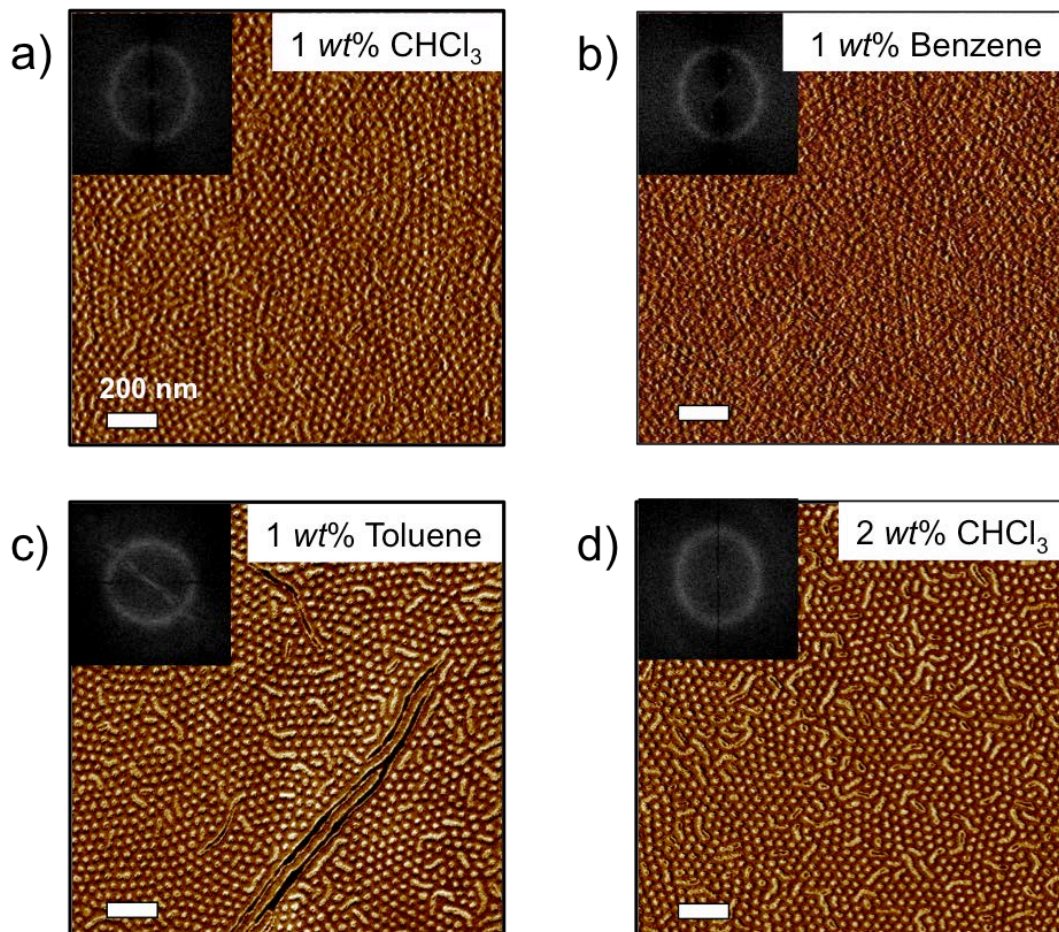


**Figure 4.6.** AFM phase images of Mba-2P2k co-assembled with PS-*b*-PMMA at a) 1 wt% casted from chloroform solution, b) 1 wt% casted from benzene solution, c) 1 wt% casted from toluene solution, and d) 2 wt% casted from chloroform solution. The inset shows the FFT of each of the AFM images. The co-assembly process for methyl modified CP is similar to the unmodified CP in which the thermodynamic loading limit of 1.3 wt%, as well as the kinetic pathway dependence of pre-aggregation of conjugates in solution are both observed.

In Chapter 3, another more effective strategy of using hydrogen bonding blockers was developed to disperse the conjugates in non-favorable solvent so that the kinetic pathway can be carefully controlled. The same method was applied to Mba-2P2k conjugates to evaluate the effectiveness of this alternative route of introducing hydrogen bond blocker of trifluoroacetic acid (TFA). Experimentally, freshly lyophilized Mba-2P2k conjugates powder was exposed to TFA vapor for 2 minutes. Subsequently,



appropriate amount of PS-*b*-PMMA in toluene was added and the solution mixture was sonicated for 30 minutes before spin casting the thin films. We highly speculate that TFA molecules are absorbed to the conjugates and interact with the amide groups on the CP backbone, interrupting the formation of inter-CP hydrogen bonding and preventing pre-aggregation of the conjugates in toluene. This hypothesis can be supported by evaluating the sizes of the conjugates in toluene before and after TFA treatment. Shown in Figure 4.9 a), DLS result reveals that the sizes of Mba-2P2k conjugates are reduced by more than 50% to less than 500 nm post TFA exposure while the untreated conjugates aggregate beyond 1  $\mu\text{m}$  (Figure 4.7 c). Better dispersion in solution results in more homogeneous morphology of the thin film after annealing in which most of the Mba-2P2k conjugates are well aligned in the center of the PMMA microdomains (Figure 4.9 b). However, a few defects of lay-down nanotubes are still seen at the free surface. This is because there still exist conjugates with sizes around 400-500 nm in toluene and thermal annealing at 180  $^{\circ}\text{C}$  is insufficient to break aggregates with these sizes. Although the strength of the inter-CP hydrogen bonding is reduced for Mba-2P2k, other factors compromise the reduced number of hydrogen bonds and therefore similar TFA treatment becomes less effective comparing to AK<sub>4</sub>-4P2k system. Looking at the DLS results alone pre-/post TFA treatment for Mba-2P2k (Figure 4.6 c) and 4.7 a) and AK<sub>4</sub>-4P2k conjugates (Figure 3.7), the sizes of the aggregates are reduced by 50% for both cases. We speculate that while the inter-CP hydrogen bonds are weaker for Mba-2P2k conjugates, less TFA molecules are absorbed since only 2 PEG chains are attached. In addition, the overall solubility of Mba-2P2k conjugates in toluene is much lower comparing to AK<sub>4</sub>-4P2k conjugates as indicated by the aggregate size in pure toluene. The subtle differences in the solubility and conjugated PEG chains result in TFA treatment being more effective for AK<sub>4</sub>-4P2k/BCP blends. While simple TFA vapor exposure alone does not completely prevent preaggregation of the conjugates in toluene, higher temperature thermal treatment may provide extra energy needed to break the aggregates and to disperse smaller fragments well in BCP. As shown in Figure 4.9 c), when thermal annealing was performed at 245  $^{\circ}\text{C}$  to TFA treated Mba-2P2k/BCP blends, well-aligned nanotubes can be incorporated at the center of the preferred PMMA microdomains. These results demonstrate that the processing window varies for different CP systems as the strength of inter-CP hydrogen bonding, the solubility of the conjugates in casting solvent, the amount of TFA molecules absorb would vary according to the structure of individual CP-PEG conjugates. Thus, it is important to make adjustments accordingly even though the underlying principle of co-assembly remains the same.

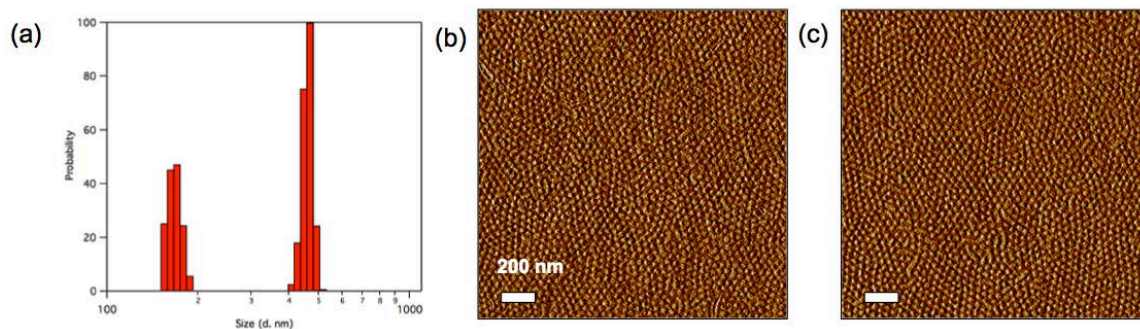


**Figure 4.7.** a) DLS of TFA vapor treated Mba-2P2k conjugates in toluene at 0.1 mg/mL, b) AFM of TFA vapor treated 1 wt% Mba-2P2k/ BCP blends thermally annealed at 180 °C, and c) AFM image of b) thermally annealed at 245 °C.

## § 4.4 Conclusion

In summary, interiorly modified cyclic peptide was successfully synthesized by incorporating an artificial amino acid in the primary peptide sequence. The mutation results in reduced number of intermolecular hydrogen bonds, but sufficient for nanotube formation. Self-assembly of the modified cyclic peptide and its conjugates was thoroughly investigated, in which polymer conjugation enables further processing of the nanotubes. The co-assembly process of the conjugates was also carefully revealed, where the behavior of the conjugates is generally similar to its unmodified counterpart with subtle differences in processing window for the two systems. There is a thermodynamic loading limit of one nanotube in each cylindrical microdomain, and the co-assembly is pathway dependent where good dispersion of the conjugates in solution prior to thin film fabrication is required. From the systematic investigations on both the unmodified AK<sub>4</sub> system and methyl modified Mba system, a general protocol in co-assembling different cyclic peptides with PS-*b*-PMMA in thin films can be drawn to make membranes with various functionalities. Controlling the kinetic pathway is the critical factor in ensuring homogeneous film morphology and good membrane quality. Good dispersion of CP-polymer conjugates in solution is required and this can be achieved by careful selection of the solvent system, TFA vapor absorption, high thermal annealing temperature, and/or a combination of the three. This general protocol of controlling kinetic pathway and loading estimation sets the foundation for fabricating membranes with different cyclic peptides, enabling one to explore the transport behavior of membranes made from different cyclic peptides with various functionalities for specific applications.

## § 4.5 Experimental

### 4.5.1 Materials

Fmoc-*D*-Ala-OH, Fmoc-*L*-Lys(Boc)-OH, Fmoc-*L*-Leu-OH, polystyrene-(2-chlorotriptyl) resin (loading: 1.5 mmol/g), and 2-(6-Chloro-*1H*-benzotriazole-1-yl)-1,1,3,3-tetramethylammonium hexafluorophosphate (HCTU) were purchased from Nova Biochem. 3-amino-2-methylbenzoic acid (**B**), Carboxylic acid-terminated polyethylene glycol (PEG) (CH<sub>3</sub>-PEG-NHCOCH<sub>2</sub>CH<sub>2</sub>COOH) (M<sub>w</sub>=2000 g/mol) were purchased from Rapp Polymere. PEG-covered CPNs of Mba-8CP and unmodified 8CP were synthesized using 2 equivalents of PEG to the 1 equivalent of the cyclic peptide. 2-Propanephosphonic acid anhydride (T3P) in 50/50 DMF, *N,N*-Diisopropylethylamine (DIPEA), ethyl-3-(3-dimethylaminopropyl) carbodiimide (EDC), *N*-(9-fluorenylmethoxycarbonyloxy)succinimide (Fmoc-OSu), and all other reagents were purchased from Sigma Aldrich without further purification. All solvents used were of HPLC grade. Polystyrene-*block*-poly(methyl methacrylate) (PS-*b*-PMMA) with molecular weight 57K-25K (PDI 1.07) was purchased from Polymer Source. The random copolymers of styrene and methyl methacrylate with 2% reactive benzocyclobutene (BCB) [P(*S-r*-BCB-*r*-MMA)] (M<sub>w</sub>= 45K PDI 1.3) was provided by Prof. T. P. Russell at the University of Massachusetts, Amherst.

### 4.5.2 Synthesis of Mba-8CP

The synthesis of Mba-8CP was performed by Dr. Rami Hourani and Mr. Robert van der Weegen and details are outlined in reference [13]. The substituting subunit of Sy3-(9-Fluorenylmethoxycarbonyl)amino-2-methylbenzoic acid (Fmoc- $\gamma$ -Mba-OH) was prepared from 3-amino-2-methylbenzoic acid and *N*-(9-fluorenylmethoxycarbonyloxy) succinimide (Fmoc-OSu) in 80% yield in large quantities (~ 2g). The synthesis of Mba-8CP is very similar to the unmodified AK<sub>4</sub> in which standard Fmoc solid phase peptide synthesis was first performed to obtain the linear peptide sequence, followed by cleavage of the linear peptide from 2-chlorotriptyl chloride resin and head-to-tail cyclization at high dilution using propane phosphonic acid anhydride (T3P) in DMF (85% yield). After deprotection of the Boc groups on the lysine to expose the free amine groups, the crude materials were purified using preparative HPLC in an overall yield of 30%. A through-space 2D NOESY experiment was carried out to determine the orientation of the substituent at the 2-position of the aromatic amino acid in the modified CP (Appendix Figure A.3.2). The methyl group of  $\gamma$ -Mba-OH at  $\delta$  2.19 ppm showed distinctive through-space interactions with each of the amide resonances in the CP backbone between 7.80 and 9.20 ppm. This correlation was absent for the aromatic protons, except for the two neighboring amide protons on either side of the aromatic ring. These results confirmed that the methyl group was directed towards the inside of the CPN, while the aromatic protons were outwards. Thus, by simply inserting this single aromatic amino acid into the primary sequence of the cyclic peptide 8-mer, its

associated functional groups were presented in the interior of the nanotubes without compromising the formation of high aspect ratio assemblies. PEG conjugation was performed following a similar procedure outlined in Section 2.4.2, chapter 2.

#### **4.5.3 Reversed-Phase High-Pressure Liquid Chromatography (RP-HPLC)**

The reaction mixture from PEG conjugation was purified by RP-HPLC (Beckman Coulter) to obtain Mba-2P2k with high purity using a C4 column (Vydac 22 mm x 250 mm) at a flow rate of 8 mL min<sup>-1</sup>. A linear AB gradient, where solvent A consisted of water containing 0.1% (v/v) TFA and solvent B consisted of acetonitrile (ACN) containing 0.1% (v/v) TFA was used. Conjugates were eluted with a gradient of 20 to 65% B over 45 min and the elution was monitored using a diode array detector at wavelengths of 200 nm and 220 nm. Mba-2P2K conjugates were eluted at ~54% ACN.

#### **4.5.4 MALDI-TOF Mass Spectrometry**

The identity and purity of the isolated Mba-2P2K conjugates were verified by MALDI-TOF MS using  $\alpha$ -cyano-4-hydroxycinnamic acid matrix. Mass spectrum was recorded on an Applied BioSystems Voyager-DE Pro.

#### **4.5.5 Fourier Transfer Infrared Spectroscopy (FTIR)**

FTIR measurements were performed using a Perkin Elmer Spotlight 200 FTIR Microscope System. The samples were casted between two NaCl pellets. The heating experiments were performed with a ramping rate of 10 °C/min and readings were collected 5 minutes after reaching the targeted temperature.

#### **4.5.6 Dynamic Light Scattering**

DLS was performed using Brookhaven BI-200SM at a wavelength of 637 nm with the scattering angle at 90°. The solvent used was filtered using 0.1  $\mu$ m PTFE filters.

#### **4.5.7 Co-assembly Thin Film Fabrication**

Si wafers were first modified using a random copolymer of styrene and methyl methacrylate with 2% reactive benzocyclobutene (BCB) [P(S-*r*-BCB-*r*-MMA)] (Mw= 45k Da, PDI=1.3, provided by T. P. Russell at the University of Massachusetts, Amherst).<sup>23</sup> Thin films were fabricated according to the previously described methods (Chapter 3, Section 3.4.8), in which appropriate amount of freshly lyophilized powders of Mba-2P2k conjugates were added to stock solutions of PS-*b*-PMMA in various solvents right before thin film fabrication. To ensure proper thin film thickness, the solution concentrations for PS-*b*-PMMA in toluene and in chloroform were 10 mg/mL and 6 mg/mL respectively. After obtaining the thin films, thermal annealing in vacuum was performed immediately for 4 hours at 180 °C, followed by slow cooling by turning off the vacuum oven.

## Chapter 5

# Transport Behavior of Sub-nanometer Porous Membranes

|              |   |                                     |
|--------------|---|-------------------------------------|
| <b>§ 5.1</b> | <b>Introduction.....</b>                        | <b>81</b>                           |
| <b>§ 5.2</b> | <b>Membrane Transport .....</b>                 | <b>83</b>                           |
|              | 5.2.1 Gas Transport Mechanism.....              | 83                                  |
|              | 5.2.2 Gas Transport Measurement.....            | 87                                  |
|              | 5.2.3 Hydronium Ion Transport.....              | <b>Error! Bookmark not defined.</b> |
| <b>§ 5.3</b> | <b>Conclusion .....</b>                         | <b>Error! Bookmark not defined.</b> |
| <b>§ 5.4</b> | <b>Experimental .....</b>                       | <b>Error! Bookmark not defined.</b> |
|              | 5.4.1 Membrane Preparation.....                 | <b>Error! Bookmark not defined.</b> |
|              | 5.4.2 Gas Transport Measurement.....            | <b>Error! Bookmark not defined.</b> |
|              | 5.4.3 Hydronium Ion Transport Measurement ..... | <b>Error! Bookmark not defined.</b> |

*Cyclic peptide nanotubes offer unique advantages of precise control over nanotube size, versatility in synthesis and post modification, compatibility with polymeric materials, and processability with conventional fabrication techniques, thus suitable to be used as nanochannels for various transport processes. Gas transport and ion transport have been performed to membranes consisting of block copolymer matrix and cyclic peptide nanotubes with and without interior functional groups. In ion transport, the presence of well-aligned nanotubes provides additional pathways for various ion species to diffuse through, and thus improves the overall permeability across the membrane. In gas transport, a typical “trade-off” between permeability and selectivity for carbon dioxide/methane gas pair is observed. The incorporation of the nanotubes improves the overall selectivity for carbon dioxide molecules at the expense of lower permeability. Slight differences in transport behaviors of the nanotubes with and without interior functionality are speculated to be due to the reduction in pore size with presence of functional groups and the local dipole interactions of the functional groups with permeating molecules. The preliminary investigation using cyclic peptide nanotubes/block copolymer blends indeed proves that this is a viable approach in fabricating nanoporous membranes with well-defined channel orientation and channel size and functionalities for molecular separation.*

## **§ 5.1 Introduction**

Membranes are widely used for chemical separations in a large range of disciplines from large-scale industrial uses such as natural gas processing and water desalination, to smaller-scale laboratory uses for purification and synthesis.<sup>1-6</sup> Among all the applications, gas separation remains a mature and yet constantly evolving area for membrane technology.<sup>1, 2, 7, 8</sup> In gas separation, the applications are focused mainly on certain separation processes because the number of gases with industrial importance is rather limited.<sup>2, 9</sup> As a result, specific technologies are designed and developed for various separation processes. There are two general requirements for membranes to exhibit excellent separating performance. Firstly, most gas molecules are very small with similar kinetic diameters.<sup>10</sup> This implies that the molecular separation process of a particular gas pair requires extremely small pore size and very narrow pore size distribution. Moreover, chemically modifying the pore surface with functional groups for better affinity for various molecules is often needed to improve the transport performance, especially the selectivity of the membranes.<sup>4</sup>

It remains a significant challenge to fabricate membranes with uniform pore sizes at sub-nanometer range for effective sieving effect that is desirable for molecular separation.<sup>2-4</sup> There have been several approaches developed using synthetic materials

such as 3-dimensional zeolites and metal-organic frameworks, and 1-dimensional carbon nanotubes (CNTs), embedded in polymeric matrix to form so called “mixed-matrix membranes” (MMMs).<sup>11-18</sup> However, it is still a synthetic challenge to obtain homogenous membranes of porous components with uniform dimensions and monodispersed pore sizes. Moreover, the interface between the dispersed inorganic phase and the continuous polymeric matrix is of critical importance to the separation performance. Due to genuine incompatibility between the two types of materials, ensuring a good contact surface without air gap is required for high performance. Thus, rather than inorganic materials, organic nanotubes are more suitable as they are inherently compatible with polymer matrix and their synthesis and post-modification are relatively nontrivial.<sup>19-22</sup> Among all the organic nanotubes, self-assembling cyclic peptide nanotubes (CPNs) not only offers unique advantages in their structural control and modulation, but their robustness and mechanical stability also make them suitable to be used as transport channels in industrial processes.<sup>23-26</sup>

In the present study, gas separation of CO<sub>2</sub>/CH<sub>4</sub> mixture for various membranes was first investigated using blends of polystyrene-*b*-poly(methyl methacrylate) (PS-*b*-PMMA) and two different types of cyclic peptides under different conditions. The first cyclic peptide investigated is *cyclo*(D-Ala-L-Lys)<sub>4</sub> conjugated with 4 chains of poly(ethylene glycol) with molecular weight 2,000 Da (called “AK<sub>4</sub>-4P2k”). The interior pore diameter for AK<sub>4</sub>-4P2k is estimated to be around 7.6 Å.<sup>24</sup> The second cyclic peptide investigated is *cyclo*(L-Lys-D-Ala-L-Leu-D-Ala-L-Lys-D-Ala-γ-Mba-D-Ala), containing an interior functionality of a methyl group inside the channel with pore size around 4.6 Å.<sup>24</sup> Two PEG chains with molecular weight 2,000 Da were conjugated to the modified cyclic peptide and the conjugate is called “Mba-2P2k”. We found that the incorporation of CPNs in the PMMA microdomains improves the overall selectivity of CO<sub>2</sub> over CH<sub>4</sub> in comparison to BCP alone, while modified Mba-2P2k exhibits higher selectivity for CO<sub>2</sub> than unmodified AK<sub>4</sub>-2P2k. This could be due to the pore size difference between the two different cyclic peptides. Moreover, among the membranes containing cyclic peptide nanotubes, we found that the overall permeability of the membranes is higher for membranes with through channels, suggesting the well-aligned nanotubes may provide extra pathways for gas molecules to pass through. Nevertheless, these composite membranes demonstrate higher selectivity at the expense of lower permeability in comparison to the BCP matrix alone, resembling the typical “trade-off” observed for polymeric membranes.<sup>27, 28</sup> In addition, we also found that the presence of water molecules could affect the selectivity of CO<sub>2</sub> over CH<sub>4</sub>. Due to the higher solubility of CO<sub>2</sub> in water, membranes under high moisture content show higher selectivity of CO<sub>2</sub> over CH<sub>4</sub>. Adopting the simple Maxwell model, we had semi-quantitatively estimated the collective CO<sub>2</sub> permeability of the PEG wrapped CPNs for the unmodified AK<sub>4</sub> as well as the methyl modified Mba nanotubes, which are estimated to be ~10 folds and ~30 folds higher than the BCP matrix. Lastly, initial assessment on ion transport was also performed to the membranes containing different cyclic peptides, in which the presence of the through channels via the incorporation of cyclic peptide nanotubes results in more

transport of ions across the membranes. From these preliminary transport investigations, the incorporation of cyclic peptide nanotubes indeed proves to be a viable approach in fabricating polymeric membranes containing sub-nanometer channels for chemical separations.

## § 5.2 Membrane Transport

### 5.2.1 Gas Transport Mechanism

In gas separation, a mixture of gases (i.e., feed) is passed across a membrane which is typically more permeable to one component of the mixture than the other. The passing-through gas (i.e., permeate) on the other side of the membrane is thus enriched in this more permeable gas, and the remaining mixture (i.e., residue) is enriched in less permeable gases. Shown in Figure 5.1, the mechanism for the separation process is different depending on the internal structures of the membrane and the nature of the permeants.<sup>2, 29</sup> For porous membranes, the transport mechanism is ultimately dependent on the pore size. For membranes with much larger pore sizes than the permeating particles, typically 0.1 – 10  $\mu\text{m}$ , convective flow takes place and usually no separation will be observed since all permeates are able to pass through the membrane in a similar manner.<sup>2, 30</sup> When the pore size is reduced to be comparable or smaller than the mean free path of the gas molecules, Knudsen diffusion takes place in which the molecules collide with the pore wall frequently. For Knudsen diffusion, the rate of diffusion is inversely proportional to the square root of the molecular weight of a particular species. Therefore, the selectivity of two gas species is proportional to the inverse of the square root of the ratio of the two molecular weights, resulting in lighter molecules moving through nanochannels faster than the heavier molecules. In the third scenario in which the membrane pores are extremely small on the order of 0.5-2 nm, molecular sieving effect can be realized.<sup>2</sup> The principle of size exclusion applies in which molecules smaller than the channel size would pass through whereas large molecules are being filtered out. Due to the small size of gas molecules, it remains a significant challenge to fabricate membranes operating on molecular sieving effect.<sup>31</sup> In addition, the condensability of gas molecules can potentially pose another challenge of pore clogging which would affect the transport property.<sup>29, 31</sup> The actual mechanism for molecular sieving is quite complex, in which both normal diffusion (diffusion of gas phase) and surface diffusion (diffusion of adsorbed species) can potentially take place.<sup>32, 33</sup> Experimentally, high transport performance and separation behavior have been observed with carbon membranes.<sup>33-35</sup> This is still an area of active research, especially with the developments in new membrane materials such as carbon nanotubes (CNTs) and graphene oxide membranes, superior performance of high flux and high separation has been achieved.<sup>36-</sup>



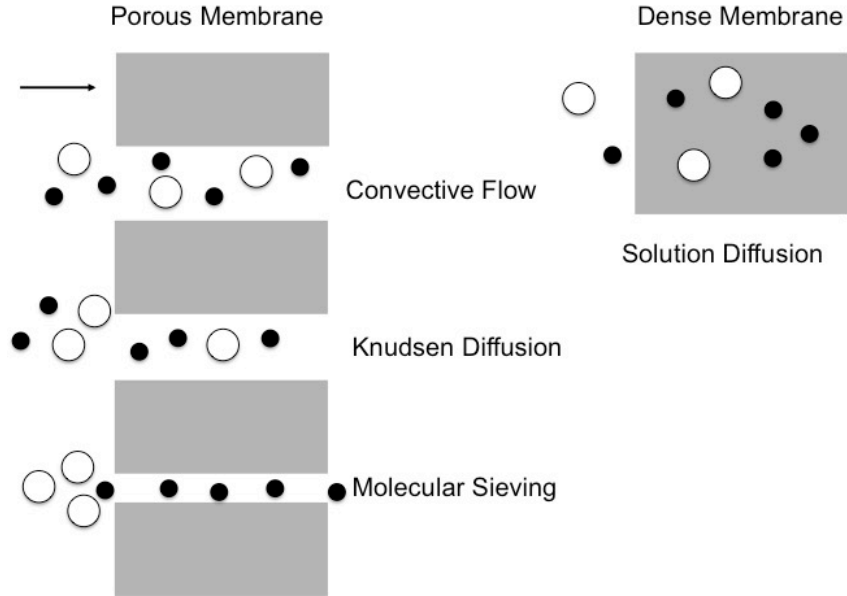


**Figure 5.1.** Transport mechanisms for porous and dense membranes. For polymeric membranes without well-defined through channels, solution-diffusion is the main mechanism in which gas molecules first get solubilized into the membrane, and then diffuse through the membrane. For membranes with through channels, depending on the sizes of the channel diameter and the gas molecules, different mechanisms may apply. For large pores, convective flow takes place without much selectivity. When the pore size is smaller than the mean free path of the diffusing gas molecule, the molecules collide frequently with the channel wall and this is known as Knudsen diffusion. Molecular sieving is based on size exclusion principle in which molecules larger than the pore size. Adapted with permission from reference [2]. Copyright (2002) John Wiley & Sons, Inc.

While microporous and nanoporous membranes continue to be a topic that attracts much research interests, all current commercial membranes for gas separation are based on the fourth mechanism, the solution-diffusion mechanism for dense membrane.<sup>2, 8</sup> In this process, molecules first adsorb and dissolve into the membrane, and then diffusion takes place within the membrane. The flux for a particular species is defined as:

$$J_i = \frac{P_i \Delta p}{l}$$

where  $P_i$  is the permeability coefficient of species  $i$ ,  $\Delta p$  is the partial pressure difference of  $i$  across the membrane, and  $l$  is the membrane thickness. The permeability coefficient in turn can be represented by the product of the diffusivity coefficient ( $D$ ) and the solubility coefficient ( $S$ ):<sup>8</sup>

$$P_i = D_i \cdot S_i \dots \dots \dots [1]$$

The ability of the membrane to separate two species is defined as the selectivity,  $\alpha_{ij}$ , the ratio of the permeabilities of species  $i$  and  $j$ :

$$\alpha_{ij} = \frac{P_i}{P_j} = \left(\frac{D_i}{D_j}\right) \left(\frac{S_i}{S_j}\right) \dots \dots \dots [2]$$

Therefore, the selectivity can be seen as the combination of two contributions, the mobility selectivity ( $D_i/D_j$ ) and the solubility selectivity ( $S_i/S_j$ ). The mobility selectivity is largely dependent on the void space of the membrane, which in turn is governed by factors such as polymer chain rigidity, intersegmental packing, etc.<sup>8</sup> Therefore, the mobility selectivity is different for glassy and rubbery polymers as shown in Figure 5.2.<sup>30, 40, 41</sup> For rubbery polymers, due to larger fraction of free volume, gas molecules diffuse through faster than glassy polymer membranes. In addition, smaller gas molecules are favored than the larger molecules due to faster rate of diffusion and interaction with less polymer segments.<sup>2</sup>

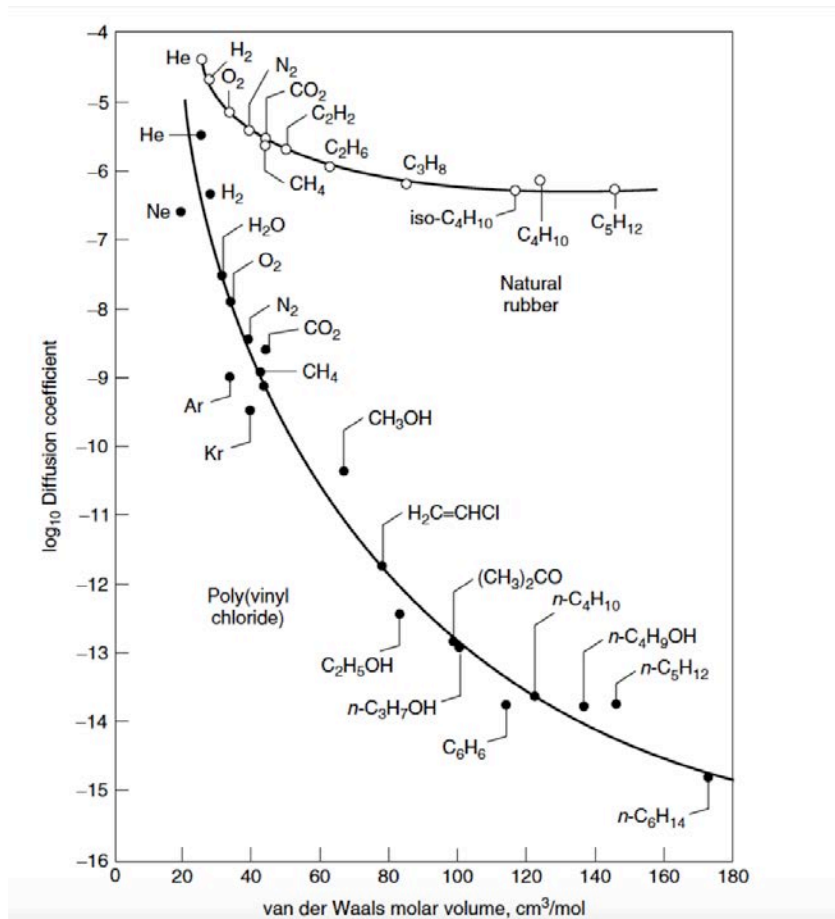


**Figure 5.2.** Diffusion coefficient as a function of molar volume for different molecules in natural rubber and in poly(vinyl chloride). Reprinted with permission from reference [40]. Copyright (1982) Elsevier B. V.

Typically, polymeric membranes show higher selectivity but relatively lower permeability comparing to porous membrane due to their low free volume.<sup>31</sup> Moreover, they also suffer a “trade-off” between permeability and selectivity in which increase in selectivity happens simultaneously with decrease in permeability.<sup>10, 28, 42</sup> Robeson, based on a large set of data for gas molecules, created the well-known Robeson’s plot which gives an “upper bound” representing the performance limit of the polymeric membranes.<sup>28, 42</sup> A general correlation between the permeability and the selectivity can be represented as:

$$P_i = k\alpha_{ij}^n$$

where  $P_i$  is the permeability of the faster gas,  $\alpha(P_i/P_j)$  is the separation factor (i.e. selectivity parameter),  $k$  is the “front factor” and  $n$  is the slope of the log-log plot. In this regard, theoretical work in predicting the empirical upper bound has also been developed by Freeman.<sup>10</sup> Based on the activation energy theory, the value of  $-1/n$  is found to be related to the difference of the molecular diameters of the gas pair,  $d_j - d_i$ :

$$-1/n = \left(\frac{d_j}{d_i}\right)^2 - 1 = \left[\frac{d_j + d_i}{d_i^2}\right] (d_j - d_i) \sim (d_j - d_i)$$

The value of  $k$  is dependent on the solubility constants of the gas molecules with the following relationship:

$$k^{-1/n} = \frac{S_i}{S_j} S_i^{-1/n} \exp\left\{\frac{1}{n}\left[b - f\left(\frac{1-a}{RT}\right)\right]\right\}$$

where  $S_i$  and  $S_j$  are the solubility constants of the gas pair;  $a = 0.64$ ,  $b_{glassy} = 11.5$  for glassy polymer and  $b_{rubbery} = 9.2$  for rubbery polymer; and  $f = 12600 \text{ cal/mol}$  to best-fit the upper bound. Over the years, with developments in material synthesis, surface modification, and fabrication techniques, new families of membranes and membrane structures have pushed the original 1991 upper bound with better performance as shown in Figure 5.3, a representative Robeson’s plot for carbon dioxide/methane separation.<sup>42</sup>

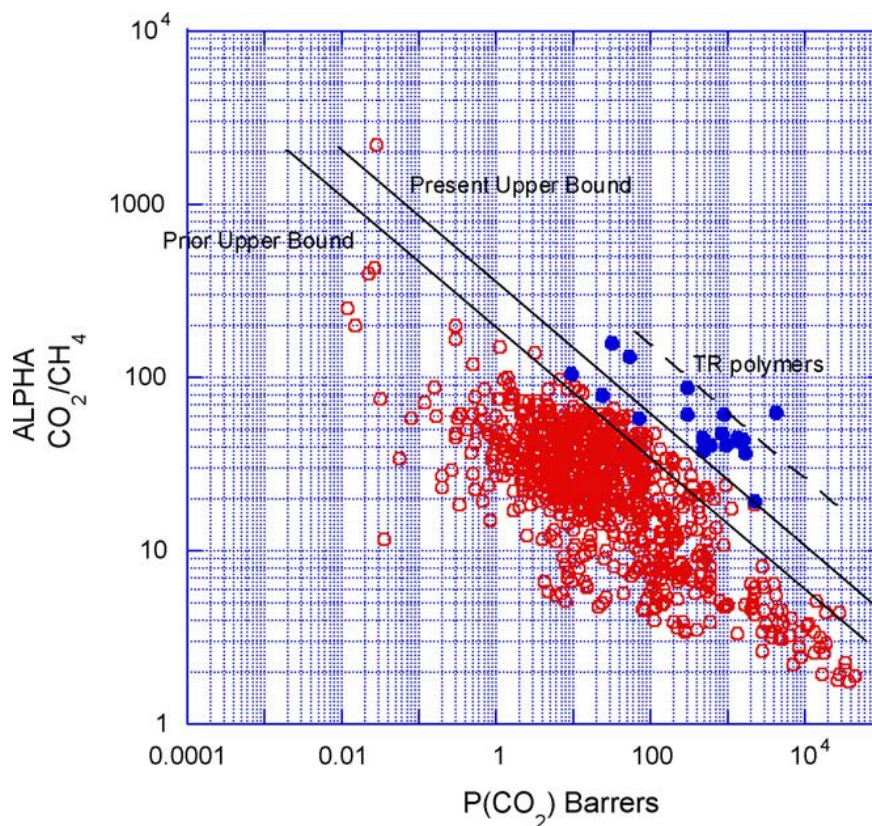


**Figure 5.3.** Robeson's plot showing the upper bound for CO<sub>2</sub>/CH<sub>4</sub> separation. Prior upper bound is based on data published by Robeson in 1991.<sup>28</sup> Thermally rearranged (TR) polymers (blue solid circles), which exhibit unique structures of very small voids in the molecular sieving range, demonstrate enhanced performance than conventional polymeric membranes.<sup>43</sup> The dotted line shows the new upper bound including the TR membrane data. Reprinted with permission from reference [42]. Copyright (2008) Elsevier B.V.

### 5.2.2 Gas Transport Measurement

Natural gas separation is one of the most important separation processes in which acidic gas such as carbon dioxide needs to be removed.<sup>7</sup> In this regard, a mixture of CO<sub>2</sub> and CH<sub>4</sub> is used to test the separation behavior of our membranes containing different types of cyclic peptides. Figure 5.4 demonstrates transport measurement setup that was used for this study. The entire setup was adapted from Dr. David Luebke's design from National Energy Technology Laboratory (NETL). Measurements were recorded under ambient conditions at room temperature and atmospheric humidity after equilibrating for 15 minutes to ensure a steady state flow. As shown in Figure 5.4b), the feed is composed of 90 mol% CH<sub>4</sub> and 10 mol% CO<sub>2</sub> premixed before passing through the testing membrane. Helium is used as the sweep gas to maintain a gradient across the membrane.

All the gases on the permeate stream are passed to gas chromatography machine (GC) for analysis. In this case, the membrane cell is a customized cell with a very small area for testing. More details for the design of the membrane cell are included in Figure A. 4.1, Appendix.

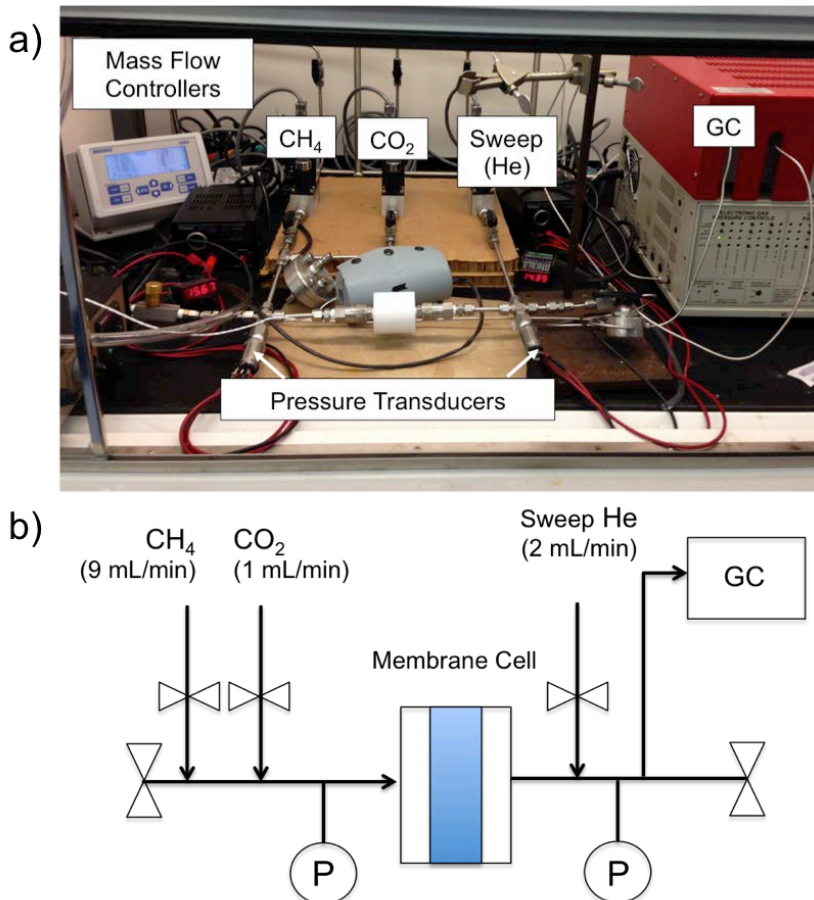


**Figure 5.4.** a) experimental and b) schematic of the gas transport measurement setup. A mixture of 90 mol% CH<sub>4</sub> and 10 mol% CO<sub>2</sub> is used as the feed and He is used as the sweep gas. Measurements are taken after equilibrating for 15 minutes to ensure steady state flow condition. Gas chromatography is used to analyze the composition of the permeate stream. Two pressure transducers are used to monitor the pressures across the membrane.

In present study, we decided to use the solution-diffusion model to evaluate the gas transport of our membranes for two reasons. Firstly, the majority of our membrane (> 99 vol%) is consisted of glassy BCP made of PS-*b*-PMMA blended with rubbery PEG chains which form the shell layer on the CPNs. Thus, the use of the solution-diffusion model for estimating the overall performance becomes more appropriate even though the transport of gas molecules within the CPN nanochannels may follow another mechanism. Furthermore, our sub-nanometer porous membrane may be viewed as analogous to a

composite membrane such as carbon nanotube (CNT) based membrane with inorganic dispersed phase embedded in a polymer matrix.<sup>18</sup> To assess the separation behavior of these composite membranes, solution-diffusion model is often used to directly compare the changes in the performance with the incorporation of the dispersed phase. Therefore, the overall permeability and selectivity of the entire membrane with and without different CPNs are calculated based on the solution-diffusion model. However, for transport inside the nanochannels, Knudsen diffusion is speculated to take place within since the CPN channel size falls in the range of Knudsen diffusion, in which the diameter of the nanotube is smaller than the mean free path of the CO<sub>2</sub> and CH<sub>4</sub> molecules.

Under steady state flow condition, we can use the following expression to calculate the permeability coefficient of CO<sub>2</sub> and CH<sub>4</sub> for various membranes according to the solution-diffusion model:<sup>44</sup>

$$P_{CO_2} = \frac{\chi_{CO_2}^p S l}{\chi_{He}^p A \Delta p_{CO_2}} \dots \dots \dots [3]$$

where  $P_{CO_2}$  is the permeability coefficient of CO<sub>2</sub>,  $S$  is the He sweep gas flow rate,  $\chi^p$  is the mole fraction of different gases in the permeate stream,  $l$  is the membrane thickness,  $A$  is the membrane area, and  $\Delta p_{CO_2}$  is the partial pressure difference of CO<sub>2</sub> across the membrane. The values for  $S$ ,  $l$ ,  $A$ , and  $\Delta p_{CO_2}$  are all known, and the value of  $\chi_{CO_2}^p / \chi_{He}^p$  can be obtained from the GC analysis. The selectivity of CO<sub>2</sub> over CH<sub>4</sub> can therefore be obtained:

$$\alpha_{CO_2/CH_4} = \frac{P_{CO_2}}{P_{CH_4}} \dots \dots \dots [4]$$

Figure 5.5 shows the selectivity vs. permeability plot for membranes containing unmodified AK<sub>4</sub>-4P2k CPNs with different loading values ( $f_{AK4-4P2K}$ ) and the reference PS-*b*-PMMA. Upon the incorporation of CPNs, the overall selectivity of CO<sub>2</sub> molecules over CH<sub>4</sub> molecules is improved comparing to just the BCP matrix; however at the expense of the permeability, reflecting the typical “trade-off” in polymeric membranes. Looking closely at all the AK<sub>4</sub>-4P2K membranes, the overall permeability increases with the loading of the CPNs,  $f_{AK4-4P2K}$ . To explain the differences, we then need to focus at the membrane morphology at different  $f_{AK4-4P2K}$  values. The calculated critical loading of the system is ~ 2.6 wt% with one CPN in each PMMA cylindrical microdomain (Chapter 3, Figure 3.3). Below the critical value, not every PMMA cylinder contains a through channel and therefore the overall permeability for the 2 wt% sample is lower. Whereas for the case of 3 wt% and 4 wt%, all the PMMA cylindrical microdomains would contain a through channel in the center, giving rise to relatively higher permeabilities for the two cases. However, at 4 wt%, the excess PEG-covered CPNs lie parallel on the polymer/air interface as shown in Figure A. 4. 2 of the Appendix. This creates defects and interfaces that further complicate the separation behavior across the membrane.

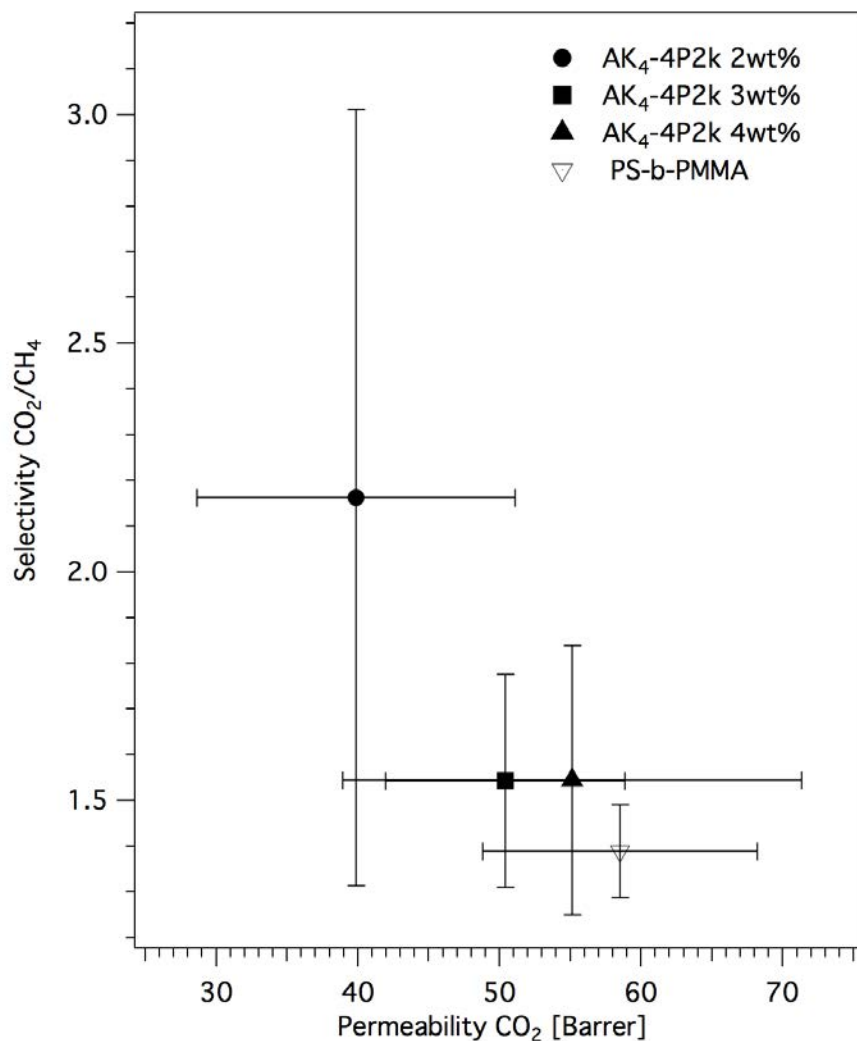


**Figure 5.5.** Gas transport performance of membranes of regular AK<sub>4</sub>-4P2k nanotubes in PS-*b*-PMMA matrix at different loading values. The incorporation of CPNs in the PMMA cylinders improves the overall selectivity of CO<sub>2</sub> over CH<sub>4</sub> compared to BCP alone. Membranes with through channels demonstrate higher permeability at the expense of lower selectivity, resembling the typical “trade-off” observed for polymeric membranes.

To closely examine the effect of the through channels in the membrane to the gas transport performance across the membrane, we then systematically investigated membranes with different morphologies with and without the through channels. In this set of experiments, AK<sub>4</sub>-4P2k conjugates were blended with PS-*b*-PMMA matrix using benzene. Transport measurements were performed to both as-casted and thermally annealed thin films and Figure 5.6 summarizes the results. Comparing the CO<sub>2</sub> transport



performance, it is clear that thermally annealed samples are more permeable to CO<sub>2</sub> molecules than the as-casted samples for both 3 wt% and 4 wt%. This implies that the presence of the through channels improves the overall permeability of CO<sub>2</sub>, likely by providing additional paths for the gas molecules to diffuse through. In addition, it is also observed that the differences in the as-casted samples for 3 wt% and 4 wt% is smaller than the annealed samples. One possible explanation for the difference is due to the internal structure of the membranes. For the as-cast samples, both the PS-*b*-PMMA matrix and the AK<sub>4</sub>-4P2k conjugates are in a disordered state in which no obvious differences are seen between the two samples (Appendix, Figure A. 4.2 a) and c). However, different thin film morphology is observed after thermal annealing (Figure A. 4.2 b) and d), Appendix). As a result of overloading, more surface defects are seen for the 4 wt% annealed sample. The additional interfaces may create extra space for the gas molecules to pass through, and therefore slightly higher permeability of CO<sub>2</sub>.

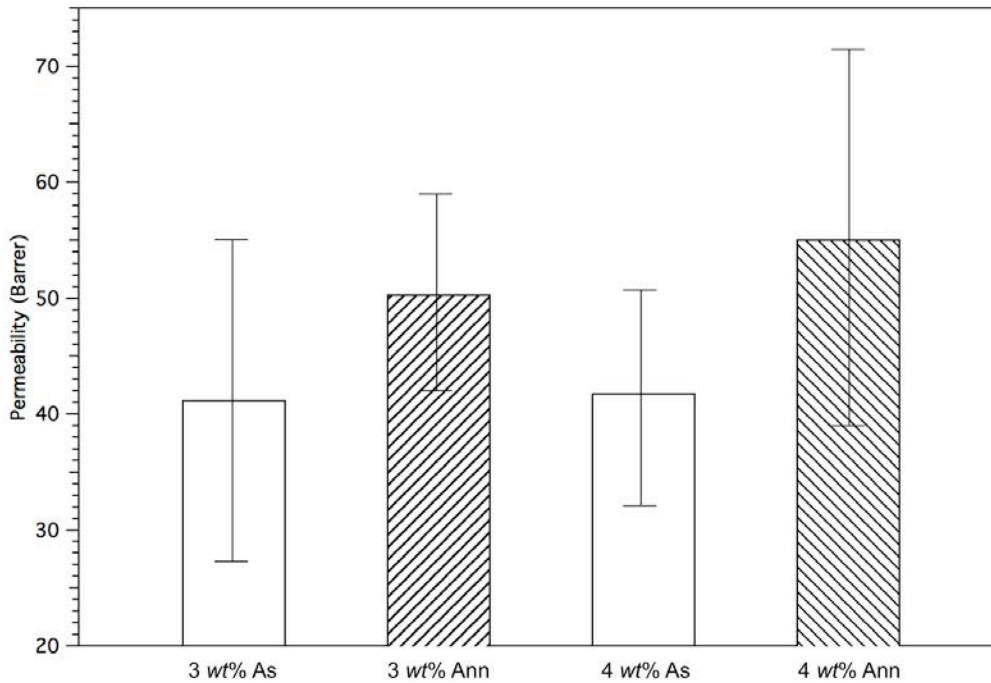


**Figure 5.6.** Permeability of CO<sub>2</sub> for as-casted (“As”) and thermally annealed (“Ann”) membranes with AK<sub>4</sub>-4P2k loading at 3 wt% and 4 wt%. Annealed films demonstrate higher CO<sub>2</sub> permeability than the as-casted films, indicating that through channels would enhance the overall permeability of the membrane.



While performing the gas transport measurements, we sometimes found a notable discrepancy between the performances of membranes with similar loading and thin film morphology. Closely looking at the membrane fabrication process, since water is involved in the last two steps, the amount of water trapped inside the membrane may greatly affect the membrane performance, especially the selectivity for CO<sub>2</sub> molecules. Figure 5.7 demonstrates the comparison between annealed membranes exposed to different moisture levels at 2 wt% and 4 wt% from the same batch. “DRY” membranes were exposed to 10% relative humidity overnight and “H<sub>2</sub>O” membranes were exposed to 85% relative humidity overnight prior to gas transport measurements. It is clear that the wet membranes exhibit higher selectivity for CO<sub>2</sub> compared to dry films regardless of the loading value. We speculate that this is due to solubility of CO<sub>2</sub> in water, in which more CO<sub>2</sub> molecules are absorbed into wet membranes.<sup>45</sup> Both the backbone cyclic peptide and the conjugated PEG chains for AK<sub>4</sub>-4P2k are hydrophilic in nature and thus water molecules can be easily trapped in these domains. Due to difference in solubility of CO<sub>2</sub> and CH<sub>4</sub> molecules in water, we speculate that more preference would be given to CO<sub>2</sub>. Thus, the value of  $\frac{S_{CO_2}}{S_{CH_4}}$  becomes larger, and hence the overall selectivity of CO<sub>2</sub>. Moreover, although the typical “trade-off” between permeability and selectivity<sup>28, 42</sup> causes the dry 2 wt% membranes exhibiting higher selectivity than the 4 wt% membrane, the difference diminishes for the wet membranes. Referring to equation [2], the selectivity of CO<sub>2</sub> essentially is the product of the ratio of the diffusivity and the ratio of the solubility of CO<sub>2</sub>/CH<sub>4</sub>. When water is present, the increase in solubility selectivity (i.e.  $\frac{S_{CO_2}}{S_{CH_4}}$ ) may dominate the diffusivity selectivity. As a result, less difference is seen for the two wet membranes.

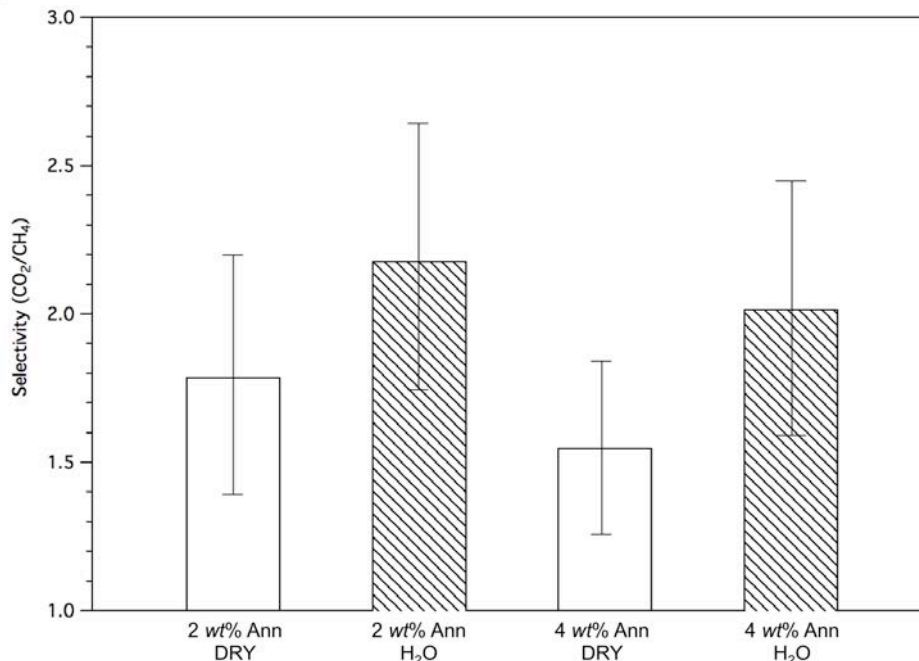


**Figure 5.7.** Selectivity of CO<sub>2</sub> molecules for different membranes under different treatments. Dry films are less selective for CO<sub>2</sub> than the wet films, likely due to the solubility of CO<sub>2</sub> molecules in water.

For gas separation application, selectivity is a critical parameter to consider. In this regard, one of the approaches to improve the selectivity is to incorporate appropriate chemical functionalities to increase the affinity between the gas molecule and the membrane.<sup>7</sup> With the goal in mind, we had successfully synthesized and studied cyclic peptide nanotubes with interior functionality of a methyl group.<sup>24</sup> Comparing the methyl modified cyclic peptide (i.e. “Mba”) with its unmodified counterpart (i.e. “AK<sub>4</sub>”), the major difference that could affect the CO<sub>2</sub>/CH<sub>4</sub> transport is the presence of the methyl group inside the channel. More specifically, the interaction between the methyl group with CO<sub>2</sub>, and/or CH<sub>4</sub> molecules will definitely affect the selectivity of the membranes. Furthermore, the presence of the methyl group also reduces the empty space inside the cyclic peptide nanotube; thus affects the overall gas transport across the membrane. Figure 5.8 summarizes the CO<sub>2</sub>/CH<sub>4</sub> gas transport performance of different membranes with regular AK<sub>4</sub>-4P2k nanotubes and the modified Mba-2P2k nanotubes at different loading amounts. The incorporation of cyclic peptide nanotubes improves the overall selectivity of CO<sub>2</sub> molecules over CH<sub>4</sub> molecules in comparison to the PS-*b*-PMMA matrix. However, the typical “trade-off” between permeability and selectivity observed for polymeric membranes are also seen in these sub-nanometer porous membranes where the permeability of CO<sub>2</sub> is being compromised by higher selectivity. In both types of nanotubes, membranes with through channels (i.e. 3 wt% and 4 wt% for AK<sub>4</sub>-4P2k and 2 wt% for Mba-2P2k) show higher CO<sub>2</sub> permeability than the lower loading membranes, indicating that the additional channels of the CPNs help the gas molecules to pass

through, likely by providing additional diffusing pathways. Comparing the transport behavior between the two different types of cyclic peptides, the methyl-modified nanotubes demonstrate much higher CO<sub>2</sub> selectivity over CH<sub>4</sub> molecules. As described earlier, the presence of methyl group inside the nanotube not only exerts additional interactions to CO<sub>2</sub> and CH<sub>4</sub> molecules, but also reduces the nanotube diameter from 7.6 Å to 4.7 Å. Local dipole in the modified Mba cyclic peptide may interact more strongly with CO<sub>2</sub> molecules, resulting in higher selectivity. Furthermore, CO<sub>2</sub> molecule (kinetic diameter = 3.3 Å) with planar structure is slightly smaller than CH<sub>4</sub> molecule (kinetic diameter = 3.8 Å) with tetrahedral structure.<sup>29</sup> With the reduction in channel diameter and differences in molecular shape, size sieving effect may also be one factor in which smaller CO<sub>2</sub> molecules can potentially pass through the smaller channels more easily.

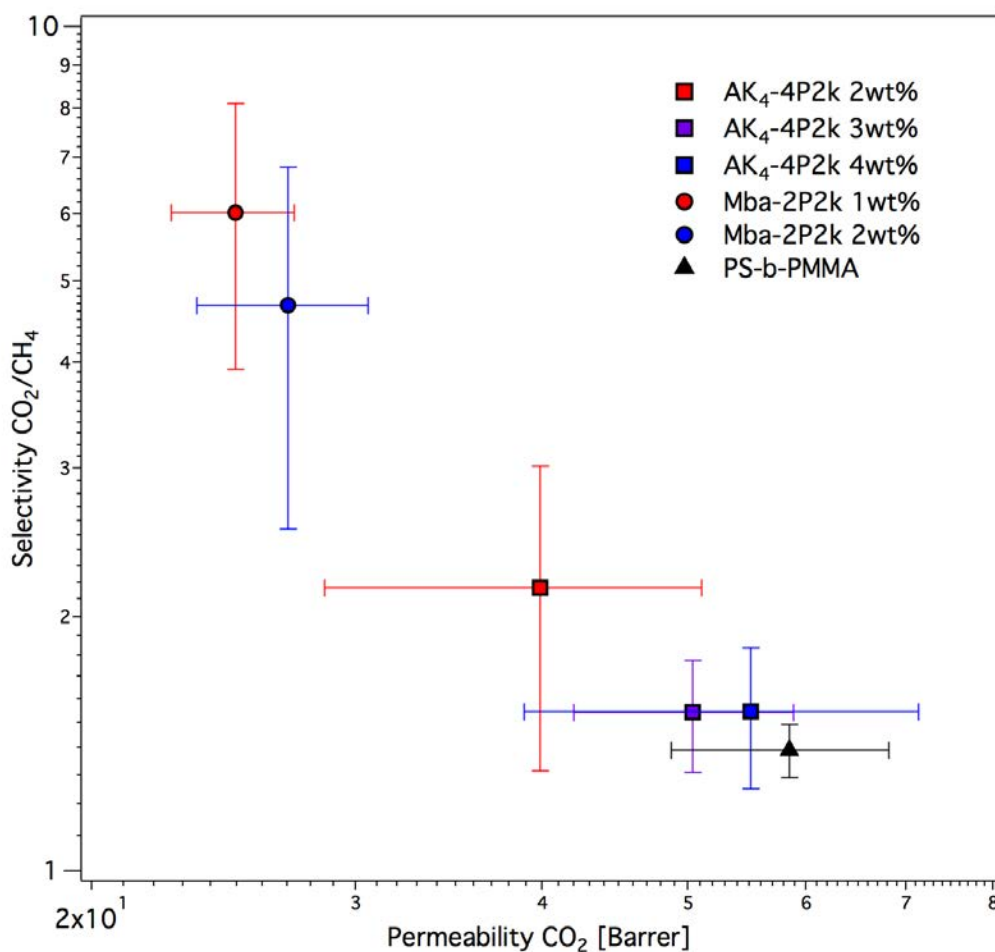


**Figure 5.8.** Summary of gas transport performance of different membranes using regular AK<sub>4</sub>-4P2k nanotubes and the modified Mba-2P2k nanotubes. Membranes with through channels (3, 4 wt% for AK<sub>4</sub>-4P2k and 2 wt% for Mba-2P2k) demonstrate higher permeability at the expense of lower selectivity, resembling the typical “trade-off” observed for polymeric membranes. The modified Mba-2P2k nanotubes with smaller channel size shows higher selectivity for CO<sub>2</sub> molecules, possibly due to the size sieving effect.

Limited by current techniques available, it is extremely challenging to measure the permeability of various gas species across the CPN nanochannels directly. However, we can alternatively estimate the permeability of the CPNs adopting a simple Maxwell model which is commonly used for mixed matrix membrane.<sup>46-48</sup> Analogous to original Maxwell equation which correlated the permittivity of dielectric material to the flux and the electrical potential across,<sup>49</sup> the effective permeability of a binary mixture membrane consisted of a continuous matrix and a dispersed phase can be represented by the following equation.<sup>47</sup>

$$P_{eff} = P_c \left[ \frac{nP_d + (1 - n)P_c - (1 - n)\phi_d(P_c - P_d)}{nP_d + (1 - n)P_c + n\phi_d(P_c - P_d)} \right]$$

where  $P_{eff}$  is the effective permeability of the membrane;  $P_c$  and  $P_d$  are the permeability of the continuous and the dispersed phase, respectively;  $\phi_d$  is the volume fraction of the dispersed phase; and  $n$  is the shape factor of the dispersed phase. In the limit of the dispersed phase made of through channels extending throughout the membrane, the shape factor becomes  $n = 0$  in the direction parallel to the channel axis. In other words, the transport across the membrane essentially becomes parallel transport made of laminated layers of the two different phases. The effective permeability when  $n = 0$  can then be rewritten as:

$$P_{eff} = P_c(1 - \phi_d) + \phi_d P_d$$

However, this simple Maxwell model only gives us a rough idea of the transport across the dispersed phase. Firstly of all, the Maxwell model assumes the penetrants do not interact with the dispersed phase, which may or may not be true for CPNs. Inter-CP hydrogen bonds from backbone amide groups may potentially interact with local dipole moment of the penetrating molecules.<sup>50</sup> Moreover, the interface between the dispersed phase and the continuous phase is ignored in the Maxwell model.<sup>18</sup> A perfect contact between the two phases is often unrealistic, especially for inorganic nanofillers in polymer matrix, leaving certain void space around the filler particles.<sup>51, 52</sup> In the case of CPNs, this problem is avoided as the nanotubes are wrapped by polymers that are very compatible with the matrix materials. However, because of the polymer shell around the CPNs, the interface between the channels and the matrix is not very sharp but rather of certain width. Various approaches have been used to account for the interface defects between the two phases. By envisioning the interface and the dispersed phase together as a pseudo-dispersed phase, the Maxwell model can be further modified.<sup>11, 53, 54</sup> More complicated models have been proposed by several groups over the years and a couple of review articles on the subject are readily available.<sup>46, 48, 51, 54, 55</sup> Nevertheless, the simple Maxwell model is used to obtain a semi-quantitative permeability parameter of the CPN based channels.

Thus, for our membranes, we assume the continuous phase to be the PS-*b*-PMMA matrix and the dispersed phase is the PEG-covered CPNs, neglecting the interface between PEG and PMMA. Using the unmodified AK<sub>4</sub>-PEG conjugates as an example. The volume fraction of the dispersed phase with one CPN in each PMMA cylinder,  $\phi_{CPN}$ , is calculated to be  $\sim 0.0093$  knowing the diameter of the dispersed phase is  $\sim 5$  nm (Chapter 3, Figure 3.2) and the lateral periodicity of the matrix PS-*b*-PMMA is  $\sim 39.5$  nm (Chapter 3, Figure 3.2). From the gas transport measurements, the average permeability of CO<sub>2</sub> for the continuous matrix phase,  $P_{PS-PMMA}$  is also known  $\sim 58.5$  Barrer. Since the calculated loading for one CPN in one PMMA cylinder is  $\sim 2.6$  wt%, the result from 3 wt% loading is therefore used. Similar approach is performed on the modified Mba system in which the size of the dispersed phase is  $\sim 5$  nm and the periodicity of the continuous BCP phase at 2 wt% loading is  $\sim 36.7$  nm (Chapter 4, Figure 4.8). The permeability parameter for CO<sub>2</sub> of the unmodified AK<sub>4</sub> nanotubes with the PEG shell is  $\sim 500$  Barrer and that of the modified Mba nanotubes with PEG shell is  $\sim 1815$  Barrer. These values in comparison with the permeability of the BCP matrix are much higher, an enhancement of  $\sim 10$  times and  $\sim 30$  times for the unmodified and modified CP systems respectively. Although the calculated values may not necessarily be a true reflection of the actual performance of the nanotubes, they still provide some valuable information regarding the transport across the CPNs. The void space of the nanotubes indeed provide additional pathways for gas molecules to pass through, in which the permeability is likely to be higher than the glassy BCP matrix. In addition, the incorporation of the methyl group at the interior of the nanotube pore seems to enhance the gas transport significantly. Although the reason for the enhancement is not clear at the moment, local dipole interaction between the methyl group with CO<sub>2</sub> molecules facilitating the transport along the nanotube wall and different transport mechanism are two speculations which need further validation. Nevertheless, like inorganic CNTs, CPNs prove to be one promising nanotube material in fabricating sub-nanometer porous membranes with high performance. Future development in the interior functionalization of the nanotube pore is expected to bring significant improvement in the gas separation performance, especially high selectivity.

**Table 1.** Approximated CO<sub>2</sub> permeability of unmodified (AK<sub>4</sub>) and modified (Mba) CP-PEG conjugates with corresponding PEG-covered CPN volume fraction in PS-*b*-PMMA matrix

|                       | AK <sub>4</sub> -4P2k @3 wt% | Mba-2P2k @2 wt% |
|-----------------------|------------------------------|-----------------|
| Permeability / Barrer | 500                          | 1815            |
| Volume Fraction       | 0.0145                       | 0.0168          |

In summary, the incorporation of cyclic peptide nanotubes improves the overall selectivity of CO<sub>2</sub> over CH<sub>4</sub> at the expense of slightly lower permeability. Membranes containing through channels show higher permeability than the less aligned membranes. Methyl modified cyclic peptide nanotubes show higher selectivity towards CO<sub>2</sub> molecules, likely due to size sieving effect that larger CH<sub>4</sub> molecules do not pass through smaller channels as easily as smaller CO<sub>2</sub> molecules.

### 5.2.3 Hydronium Ion Transport

As mentioned in Chapter 1, cyclic peptide nanotubes with  $\beta$ -sheet structure are structurally similar to some of the natural ion channels.<sup>20</sup> There have been several reports on the successful incorporation of different types of CPNs into lipid bilayer which display channel-mediated ion transport activities, mimicking the performance of natural protein channels.<sup>56-58</sup> However, most studies were performed on liquid system in which peptides or peptide-polymer conjugates solutions were added to the lipid bilayer solution, and the formation of the peptide channels simply relies on the spontaneous incorporation of the nanotube into the bilayer. In contrast, membranes fabricated using CPN/BCP blends contain well-ordered channels with known orientation and position, and can be easily tested and used in many potential applications.

Preliminary studies of hydronium ion transport were therefore performed and the setup is outlined in details in section 5.4.3. Various membranes were tested in which two phosphate buffer solutions with different pH values were placed at the two sides of the membranes. 8-Hydroxypyrene-1,3,6-trisulfonic acid (HPTS) being a pH indicator was used to monitor the change of pH of the buffer solutions and the overall performance of the membranes can be qualitatively estimated based on the pH change. The actual setup is shown in Figure A. 4.3, Appendix. The pH change was monitored by taking the fluorescence intensity of the HEPES buffer 5 minutes after placing 10  $\mu$ L of pH 2.25 buffer solution on the other side of the membranes, where higher fluorescence intensity indicates higher pH value. The original fluorescence spectra are included in Figure A. 4.4 of the Appendix. The two black traces (solid and dotted) indicate the upper and lower bounds (fluorescence spectra of just the pH 7.5 PBS and the mixture of pH 7.5 PBS with 10  $\mu$ L pH 2.25 PBS) for the change of the pH values in which the performances of different membranes vary in between the two boundaries. Taking the difference of the two boundaries, the fraction of the intensity change of various membranes is shown in Figure 5.9. The polysulfone based commercial membrane (HT Tuffryn®, Pall Corporation) used as the mechanical support shows the largest change of pH  $\sim$ 0.88, which is very close to the lower bound. Nevertheless, with the PS-*b*-PMMA based thin film placed on top of the commercial support, the performance is almost reduced by half. Similar to the case of gas transport, differences in performance can be observed for PS-*b*-PMMA matrix alone ( $\sim$ 0.36), and BCP matrix incorporated with the unmodified CPN

(~0.44) and methyl-modified CPN (~0.55). Membrane containing through channels demonstrate higher permeability, possibly due to more diffusion of ions across the membrane as indicated by greater change of pH. It is worth noting that there may be additional transports of other ions from the buffer solutions simultaneously taking place in addition to hydronium ions, which are not reflected by the change of the pH. The control sample with only PEG incorporated (~0.3) demonstrates a similar behavior to the PS-*b*-PMMA matrix, confirming that improved permeability across the membrane is likely to be due to the incorporation of the nanotubes. Based on the observation, one possible reason for improved hydronium ion transport is the additional space of the through channels that permit more diffusion. Nevertheless, other contributions such as the local and overall dipole moment of the CPNs, the change of the dissociation constant of water in local environment can also potentially contribute to the high ion conductance as seen in previous reports.<sup>56, 58-60</sup> Control experiment was therefore performed on porous PS-*b*-PMMA membranes. The PMMA microdomain of the BCP matrix can be degraded by UV exposure, leaving channels with size of the PMMA microdomain (~15 nm in diameter) in PS matrix. Comparing the UV treated PS-*b*-PMMA matrix membrane and membrane containing CPN channels (AK<sub>4</sub>-4P2k), surprisingly the transport behavior of the UV treated membrane is very similar to the membrane with high density through channels of unmodified CPNs. Despite almost 20-fold difference in channel size (15 nm vs. 0.76 nm), the extent of the transport hydronium ions across the membranes is similar. This observation suggests that in addition to the extra diffusion pathways, the inherent interaction between the ions and the cyclic peptides might be another contribution to the improved transport across the membrane. This behavior is also reflected in the transport for cyclic peptides with and without interior functionalities. The methyl-modified CP demonstrates a greater extent of hydronium ion transport as indicated by greater change of pH. One explanation for the difference could be the local dipole moment around the artificial phenol subunit with methyl functionality might slightly interact with hydronium ions, facilitating their transports along the nanotube wall, consistent with the gas transport behavior where Mba-2P2k thin films demonstrate a higher selectivity for polar CO<sub>2</sub> molecules. Based on these observations, we tentatively conclude that other than gas separation, the sub-nanometer porous membranes based on CPNs and BCP can also be potentially used for hydronium ion transport as demonstrated by improved permeability of hydronium ions across the membranes. In addition to providing diffusion pathways, local dipole interactions between the CPN and permeating ions may also contribute to the improved performance. Future efforts will be focused on investigating CPNs containing polar functional groups for even greater performance.

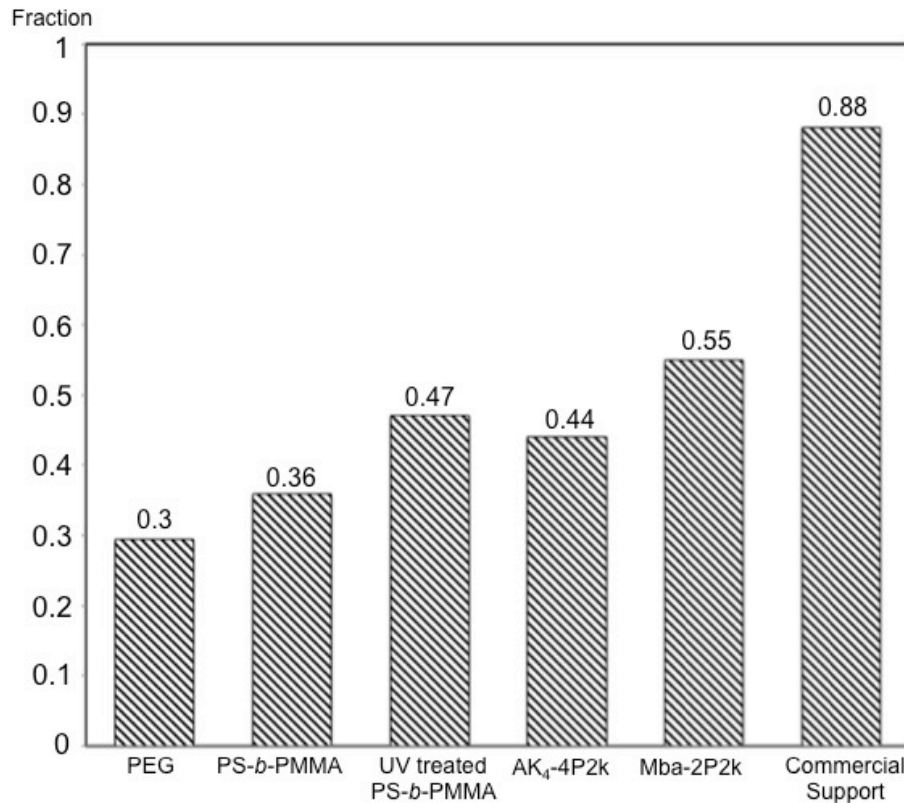


**Figure 5.9.** Summary of the change of the HEPES buffer fluorescence peak intensity for different membranes after 5 minutes. Reference is taken as the maximum change of pH by directly adding 10  $\mu$ L of pH 2.25 PBS buffer to HEPES buffer (pH 7.5). The commercial polysulfone membrane with hydrophilic nature shows the greatest permeability whereas membranes containing CPNs are more permeable than the BCP matrix alone, confirming the additional diffusion pathways from the hollow nanotubes.

### § 5.3 Conclusion

CO<sub>2</sub>/CH<sub>4</sub> separation is a critical step in natural gas processing and many approaches have been developed to remove CO<sub>2</sub> content from methane. Membrane technology is one attractive candidate for CO<sub>2</sub>/CH<sub>4</sub> separation due to low material cost and high processability. In this regard, we had successfully fabricated membranes containing sub-nanometer channels using cyclic peptide-polymer conjugates and block copolymer matrix. We found that the incorporation of CPNs in the PMMA microdomains improves the overall selectivity of CO<sub>2</sub> over CH<sub>4</sub> in comparison to BCP alone, while Mba-2P2k exhibits a higher selectivity of CO<sub>2</sub> than AK<sub>4</sub>-2P2k. This could be due to the



pore size difference between the two different cyclic peptides. Moreover, we also found that the overall permeability of the membranes increases with the incorporation of through channels for both cyclic peptides, suggesting the presence of through channels may provide extra pathways for gas molecules to pass through. Nevertheless, membranes demonstrate higher permeability at the expense of lower selectivity, resembling the typical “trade-off” observed for polymeric membranes. Furthermore, we also found that the presence of water molecules could affect the selectivity of CO<sub>2</sub> over CH<sub>4</sub>. Due to the higher solubility of CO<sub>2</sub> in water, membranes treated with water show higher selectivity of CO<sub>2</sub> over CH<sub>4</sub>. In summary, the incorporation of cyclic peptide nanotubes improves the overall selectivity of CO<sub>2</sub> over CH<sub>4</sub> at the expense of slightly lower permeability. Membranes containing through channels show higher permeability than the less aligned membranes. Lastly, we had estimated the collective CO<sub>2</sub> permeability of the nanotubes for the regular AK<sub>4</sub> as well as the methyl modified Mba nanotubes to be ~ 10 folds and ~ 30 folds higher than the BCP matrix. This is very promising as with future developments in the interior functionalization of the nanotubes, even better performance may be expected using these sub-nanometer porous membranes.

In addition to gas separation, membranes containing sub-nm channels based on cyclic peptides can also be potentially used in hydronium ion transport as CPNs being structurally similar to natural protein channels have demonstrated high ion conductance as reported previously. Using BCP as structural framework, membranes are fabricated using different types of cyclic peptides, extending the investigation on hydronium ion transport of CPN based channels to solid phase and allowing potential applications in membrane technology. Preliminary studies on the pH change of the PBS buffer solutions have demonstrated differences in the overall hydronium ion transport behaviors of membranes containing different types of cyclic peptides, and control samples with just the BCP matrix, BCP matrix containing large through pores, and BCP matrix containing PEG. We speculate that the additional diffusion paths from CPNs and the interactions between diffusing species with local dipole moments of the CP backbone groups may both contribute to the observed difference. However, further investigations are needed to validate our hypothesis, for example direct measurements of ion conductance, etc. Nevertheless, our observations using membranes fabrication with CPN/BCP blends still provide some useful insights in understanding transport across membranes containing sub-nanometer channels, in which performance can be potentially fine-tuned through interior modification of the primary cyclic peptide sequence. This opens a new route in fabricating membranes with specific purpose and selectivity for various applications such as gas separation and ion transport. With successful polar functional groups in the interior of the nanotubes, it is expected that even more enhanced separation performance will be observed. Future effects will be focused on incorporating polar functional groups such as carboxylic acid, amine, hydroxyl, etc to the cyclic peptide nanotube interior, and investigating separation behavior of both gaseous permeates and ionic species.

## § 5.4 Experimental

### 5.4.1 Membrane Preparation

The preparation of the membrane involves three steps. The first step is to prepare thin films of CPN/BCP blends. Cyclic peptide-polymer conjugates and PS-*b*-PMMA were co-dissolved in benzene, and the solution was spin-casted onto Si wafer with ~200 nm thermal oxide layer pre-modified with a neutral brush layer to form various thin films with desirable morphologies. Thermal annealing was then applied to thin films. A detailed description of this step could be found in Section 3.4.8, Chapter 3. The second step in preparing the transport membranes is to obtain free-standing thin films from the Si substrate. This was done by etching the 200 nm thermal oxide layer so that the thin film could be delaminated from the Si substrate. The annealed samples were immersed in 5% HF/95% DI H<sub>2</sub>O solution for 25 seconds, and then transferred to 100% DI H<sub>2</sub>O to float off the top layer, leaving the free-standing film floating on H<sub>2</sub>O surface. The last step in membrane preparation is to place the free-standing thin film onto a commercial polysulfone membrane (HT Hyffryn 200, Millipore) for support. The thin film/polysulfone membranes were then carefully dried under vacuum overnight, and were kept in a dry box with relative humidity ~ 10%. For the water moisture study, the dried membranes were exposed to saturated KCl solution with an estimated relative humidity ~ 85% for 12 hours. For hydronium ion transport studies, the dried membranes were carefully wetted with pH 7.5 HPTS buffer before starting the measurements.

### 5.4.2 Gas Transport Measurement

Gas transport measurements were performed using the setup shown in Figure 5.1 and Figure A. 4.1 of Appendix. A customized membrane holder was designed and made with testing area 0.0792 cm<sup>2</sup>. Calibration tests were first performed to obtain the mole fraction of various gases (CO<sub>2</sub> and CH<sub>4</sub>) in the permeate stream from the GC readings (integrated areas). Measurements were performed under ambient environment and GC readings were recorded 10 minutes after starting the gas flow to ensure steady-state flow condition. Each membrane was tested for three times, and 5 samples were measured for each sample conditions. The permeability and selectivity coefficients are calculated using the equation [3] and [4].

### 5.4.3 Hydronium Ion Transport Measurement

Experiments were performed using two phosphate buffer (PBS) solutions with different pH values using MilliQ water (Millipore Corporation, resistivity = 18.2 MΩ·cm at 25 °C). KCl, K<sub>2</sub>HPO<sub>4</sub>, KH<sub>2</sub>PO<sub>4</sub> (Sigma Aldrich, used as received) were used to make pH7.5 and pH2.25 PBS solutions with ionic strength 20 mM. Hydroxypyrene-1,3,6-trisulfonic acid (HPTS, Sigma Aldrich) was added to pH 7.5 buffer at 10 μM to monitor the pH change of the buffer solution. 270 μL of pH 7.5 HPTS buffer was first added to PDMS container, and various pre-wetted membranes were placed on top of the container with

the BCP thin film facing air. 10  $\mu\text{L}$  pH 2.25 buffer was then added and a schematic of the setup is shown in Appendix, Figure A. 4.2. After five minutes, the membranes were removed from the PDMS container and the pH value of the HPTS buffer was immediately measured using fluorometer (Perkin Elmer, LS-55). Fluorescence measurements were also measured directly on pH 7.5 HPTS buffer and the mixed solution of 270  $\mu\text{L}$  pH 7.5 and 10  $\mu\text{L}$  pH 2.25 buffer to set the two boundaries.

## Afterword

The work described in this dissertation demonstrated that self-assembled cyclic peptide nanotubes are a very promising family of materials inspired by nature in constructing complex 1D nanostructures as transport channels in membrane technology for molecular separation. Precise structural control of the cyclic peptide nanotubes within polymeric matrix allows the fabrication of membranes containing uniformly distributed sub-nanometer channels with monodispersed pore size. The capability to chemically modify the nanotube surface both exteriorly and interiorly enables the design of the cyclic peptide nanotubes for very specific separation processes and molecular species, expanding the potential uses of the cyclic peptide nanotubes to other fields in materials science.

Meticulous control over the dimensions of the polymer covered cyclic peptide nanotubes is determined and achieved by a delicate balance between the enthalpic driving force promoting nanotube growth from the cyclic peptide backbone and the entropic penalty destabilizing the nanotube structure from the conjugated polymer chains. Thus, two separate approaches corresponding to the two contributions are designed and developed, in which both the monomer concentration and the degree of polymer conjugation can be used to form high aspect ratio nanotubes. This indeed allows one to have multiple handles to control the spatial organization of 1D nanostructures within the processing window.

Effective fabrication of membranes containing sub-nanometer channels can be achieved through guided growth of cyclic peptide nanotubes in polymeric matrix, in which the kinetic pathway the system takes is one of the ultimately critical factors in ensuring good membrane quality and integrity. Upon successful co-assembly of cyclic peptide-polymer conjugates within cylindrical block copolymer matrix, regularly spaced nanochannels with uniform length and pore diameter can be well-aligned normal to the surface, mimicking the structure of natural transport channels.

These research findings present exciting opportunities to explore the use of nanotubes in membrane technology at the scale of molecular separation and to develop further understanding on the structure-property relationship of sub-nanometer porous membranes. Preliminary studies on gas and ion transport validated the potential of using nanotubes as transport channels, which exhibit certain size exclusion and selectivity. This indeed establishes the foundation and guidelines for fabricating membranes based on cyclic peptide nanotubes and polymer matrix.

Using this platform, future developments will be focused on the interior functionalization of the nanotube surface to tailor the affinity for different permeating species, and hence achieving high selectivity with additional interactions coupled with size exclusion. These studies, coupled with comprehensive exploration and understanding of the transport phenomenon inside the cyclic peptide nanotubes both experimentally and theoretically, as well as the development of scalable processing techniques compatible with current membrane manufacturing infrastructure, will maximize the use of bio-mimicking cyclic peptide nanotubes as one of the key components for next generation chemical separation membranes.

## References

### Chapter 1

1. Nollet, A. Leçons de Physique Experimentale. *Leçons de Physique Experimentale* 1748.
2. Fick, A. Ueber Diffusion. *Annalen der Physik* 1855, 170, 59-86.
3. Graham, T. *W.G. Schmidt, Ann. Phys.* 1856, 49, 337.
4. Graham, T. On liquid transpiration in relation to chemical composition. *Phil. Trans. Roy. Soc.* 1861, 151, 1836.
5. Graham, T. *Phil. Mag.* 1866, 32, 402.
6. Pfeffer, W. Osmotische Untersuchungen. *Leipzig* 1877.
7. Traube, M. Physiologie und wissenschaftliche Medizin. *Reischert DuBoisReymond (Ed.), Archiv für Anatomie Leipzig* 1867.
8. van't Hoff, J. H. The role of osmotic pressure in the analogy between solutions and gases. *Z. Phys. Chem.* 1887, 1, 481-508.
9. van't Hoff, J. H. XII. The function of osmotic pressure in the analogy between solutions and gases. *Philosophical Magazine Series 5* 1888, 26, 81-105.
10. Zsigmondy, R.; Bachmann, W. Über neue Filter. *Zeitschrift für anorganische und allgemeine Chemie* 1918, 103, 119-128.
11. Manegold, E. Ueber Kollodiummembranen. III. *Kolloid-Zeitschrift* 1929, 49, 372-395.
12. Bechhold, H. Kolloidstudien mit der Filterationesmethode. *Z. Physik. Chem.* 1907, 60, 257-318.
13. Elford, J. W. A new series of graded collodion membranes suitable for general bacteriological use, especially in filterable virus studies. *J. Pathol. Bacteriol.* 1931, 34, 502-521.
14. Grabar, P. L'Ultrafiltration Fractionnée. *Hermann et Cie, Paris* 1943.
15. Baker, R. W. Membrane Technology. In *Encyclopedia of Polymer Science and Technology*, John Wiley & Sons, Inc.: 2002.
16. Lonsdale, H. K. The growth of membrane technology. *Journal of Membrane Science* 1982, 10, 81-181.
17. Baker, R. W. Future Directions of Membrane Gas Separation Technology. *Ind Eng Chem Res* 2002, 41, 1393-1411.
18. Baker, R. Future directions of membrane gas-separation technology. *Membrane Technology* 2001, 2001, 5-10.
19. Sidney, L.; Srinivasa, S. Sea Water Demineralization by Means of an Osmotic Membrane. In *Saline Water Conversion?II*, AMERICAN CHEMICAL SOCIETY: 1963; Vol. 38, pp 117-132.
20. Koros, W. J.; Fleming, G. K. Membrane-based gas separation. *Journal of Membrane Science* 1993, 83, 1-80.
21. Bernardo, P.; Drioli, E.; Golemme, G. Membrane Gas Separation: A Review/State of the Art. *Ind Eng Chem Res* 2009, 48, 4638-4663.
22. Pendergast, M. M.; Hoek, E. M. V. A review of water treatment membrane nanotechnologies. *Energy & Environmental Science* 2011, 4, 1946-1971.

23. Ismail, A. F.; David, L. I. B. A review on the latest development of carbon membranes for gas separation. *Journal of Membrane Science* 2001, 193, 1-18.
24. Ockwig, N. W.; Nenoff, T. M. Membranes for Hydrogen Separation. *Chemical Reviews* 2007, 107, 4078-4110.
25. Yampol'skii, Y. P.; Volkov, V. V. Studies in gas permeability and membrane gas separation in the Soviet Union. *Journal of Membrane Science* 1991, 64, 191-228.
26. Muruganandam, N.; Koros, W. J.; Paul, D. R. Gas sorption and transport in substituted polycarbonates. *Journal of Polymer Science Part B: Polymer Physics* 1987, 25, 1999-2026.
27. Li, Y.; Wang, X.; Ding, M.; Xu, J. Effects of molecular structure on the permeability and permselectivity of aromatic polyimides. *J Appl Polym Sci* 1996, 61, 741-748.
28. Kim, Y.-H.; Kim, H.-S.; Kwon, S.-K. Synthesis and Characterization of Highly Soluble and Oxygen Permeable New Polyimides Based on Twisted Biphenyl Dianhydride and Spirobifluorene Diamine. *Macromolecules* 2005, 38, 7950-7956.
29. Morisato, A.; Pinnau, I. Synthesis and gas permeation properties of poly(4-methyl-2-pentyne). *Journal of Membrane Science* 1996, 121, 243-250.
30. Merkel, T. C.; Freeman, B. D.; Spontak, R. J.; He, Z.; Pinnau, I.; Meakin, P.; Hill, A. J. Ultraporous, Reverse-Selective Nanocomposite Membranes. *Science* 2002, 296, 519-522.
31. Chung, T.-S.; Jiang, L. Y.; Li, Y.; Kulprathipanja, S. Mixed matrix membranes (MMMs) comprising organic polymers with dispersed inorganic fillers for gas separation. *Progress in Polymer Science* 2007, 32, 483-507.
32. Mahajan, R.; Koros, W. J. Factors Controlling Successful Formation of Mixed-Matrix Gas Separation Materials. *Ind Eng Chem Res* 2000, 39, 2692-2696.
33. Zimmerman, C. M.; Singh, A.; Koros, W. J. Tailoring mixed matrix composite membranes for gas separations. *Journal of Membrane Science* 1997, 137, 145-154.
34. Hu, Q.; Marand, E.; Dhingra, S.; Fritsch, D.; Wen, J.; Wilkes, G. Poly(amide-imide)/TiO<sub>2</sub> nano-composite gas separation membranes: Fabrication and characterization. *Journal of Membrane Science* 1997, 135, 65-79.
35. Holt, J. K.; Park, H. G.; Wang, Y.; Stadermann, M.; Artyukhin, A. B.; Grigoropoulos, C. P.; Noy, A.; Bakajin, O. Fast Mass Transport Through Sub-2-Nanometer Carbon Nanotubes. *Science* 2006, 312, 1034-1037.
36. Hinds, B. J.; Chopra, N.; Rantell, T.; Andrews, R.; Gavalas, V.; Bachas, L. G. Aligned Multiwalled Carbon Nanotube Membranes. *Science* 2004, 303, 62-65.
37. Majumder, M.; Chopra, N.; Andrews, R.; Hinds, B. J. Nanoscale hydrodynamics: Enhanced flow in carbon nanotubes. *Nature* 2005, 438, 44-44.
38. Yin, J.; Deng, B. Polymer-matrix nanocomposite membranes for water treatment. *Journal of Membrane Science* 2015, 479, 256-275.
39. Rubinstein, M.; Colby, R. H. *Polymer Physics*. OUP Oxford: 2003.
40. Bates, F. S. Polymer-Polymer Phase Behavior. *Science* 1991, 251, 898-905.
41. Bates, F. S.; Fredrickson, G. H. Block Copolymer Thermodynamics: Theory and Experiment. *Annual Review of Physical Chemistry* 1990, 41, 525-557.
42. Hashimoto, T.; Nagatosh, K.; Todo, A.; Hasegawa, H.; Kawai, H. Domain-Boundary Structure of Styrene-Isoprene Block Copolymer Films Cast from Toluene Solutions. *Macromolecules* 1974, 7, 364-373.

43. Hashimoto, T.; Todo, A.; Itoi, H.; Kawai, H. Domain-Boundary Structure of Styrene-Isoprene Block Copolymer Films Cast from Solutions .2. Quantitative Estimation of Interfacial Thickness of Lamellar Microphase Systems. *Macromolecules* 1977, 10, 377-384.
44. Todo, A.; Uno, H.; Miyoshi, K.; Hashimoto, T.; Kawai, H. Domain-Boundary Structure of Styrene-Isoprene Block Copolymer Films Cast from Solutions .3. Preliminary-Results on Spherical Microdomains. *Polym Eng Sci* 1977, 17, 587-597.
45. Hashimoto, T.; Fujimura, M.; Kawai, H. Domain-Boundary Structure of Styrene-Isoprene Block Co-Polymer Films Cast from Solutions .5. Molecular-Weight Dependence of Spherical Microdomains. *Macromolecules* 1980, 13, 1660-1669.
46. Hashimoto, T.; Shibayama, M.; Kawai, H. Domain-Boundary Structure of Styrene-Isoprene Block Co-Polymer Films Cast from Solution .4. Molecular-Weight Dependence of Lamellar Microdomains. *Macromolecules* 1980, 13, 1237-1247.
47. Hashimoto, H.; Fujimura, M.; Hashimoto, T.; Kawai, H. Domain-Boundary Structure of Styrene-Isoprene Block Co-Polymer Films Cast from Solutions .7. Quantitative Studies of Solubilization of Homopolymers in Spherical Domain Systems. *Macromolecules* 1981, 14, 844-851.
48. Fujimura, M.; Hashimoto, H.; Kurahashi, K.; Hashimoto, T.; Kawai, H. Domain-Boundary Structure of Styrene-Isoprene Block Co-Polymer Films Cast from Solutions .6. Effect of Temperature on Spherical Microdomain Structure. *Macromolecules* 1981, 14, 1196-1202.
49. Stewart-Sloan, C. R.; Thomas, E. L. Interplay of symmetries of block polymers and confining geometries. *Eur. Polym. J.* 2011, 47, 630-646.
50. Hillmyer, M. Nanoporous Materials from Block Copolymer Precursors. In *Block Copolymers II*, Abetz, V., Ed. Springer Berlin Heidelberg: 2005; Vol. 190, pp 137-181.
51. Olson, D. A.; Chen, L.; Hillmyer, M. A. Templating Nanoporous Polymers with Ordered Block Copolymers†. *Chemistry of Materials* 2008, 20, 869-890.
52. Hashimoto, T.; Tsutsumi, K.; Funaki, Y. Nanoprocessing based on bicontinuous microdomains of block copolymers: Nanochannels coated with metals. *Langmuir* 1997, 13, 6869-6872.
53. Okumura, A.; Nishikawa, Y.; Hashimoto, T. Nano-fabrication of double gyroid network structure via ozonolysis of matrix phase of polyisoprene in poly(2-vinylpyridine)-block-polyisoprene films. *Polymer* 2006, 47, 7805-7812.
54. Chen, L.; Phillip, W. A.; Cussler, E. L.; Hillmyer, M. A. Robust Nanoporous Membranes Templated by a Doubly Reactive Block Copolymer. *J Am Chem Soc* 2007, 129, 13786-13787.
55. Phillip, W. A.; Amendt, M.; O'Neill, B.; Chen, L.; Hillmyer, M. A.; Cussler, E. L. Diffusion and Flow Across Nanoporous Polydicyclopentadiene-Based Membranes. *ACS Applied Materials & Interfaces* 2009, 1, 472-480.
56. Uehara, H.; Yoshida, T.; Kakiage, M.; Yamanobe, T.; Komoto, T.; Nomura, K.; Nakajima, K.; Matsuda, M. Nanoporous Polyethylene Film Prepared from Bicontinuous Crystalline/Amorphous Structure of Block Copolymer Precursor. *Macromolecules* 2006, 39, 3971-3974.
57. Uehara, H.; Kakiage, M.; Sekiya, M.; Sakuma, D.; Yamanobe, T.; Takano, N.; Barraud, A.; Meurville, E.; Ryser, P. Size-Selective Diffusion in Nanoporous but Flexible Membranes for Glucose Sensors. *ACS Nano* 2009, 3, 924-932.



58. Zhou, N.; Bates, F. S.; Lodge, T. P. Mesoporous Membrane Templated by a Polymeric Bicontinuous Microemulsion. *Nano Lett* 2006, 6, 2354-2357.
59. Jackson, E. A.; Hillmyer, M. A. Nanoporous Membranes Derived from Block Copolymers: From Drug Delivery to Water Filtration. *Acs Nano* 2010, 4, 3548-3553.
60. Crossland, E. J. W.; Kamperman, M.; Nedelcu, M.; Ducati, C.; Wiesner, U.; Smilgies, D. M.; Toombes, G. E. S.; Hillmyer, M. A.; Ludwigs, S.; Steiner, U.; Snaith, H. J. A Bicontinuous Double Gyroid Hybrid Solar Cell. *Nano Lett* 2009, 9, 2807-2812.
61. Park, C.; La, Y.; An, T. H.; Jeong, H. Y.; Kang, S.; Joo, S. H.; Ahn, H.; Shin, T. J.; Kim, K. T. Mesoporous monoliths of inverse bicontinuous cubic phases of block copolymer bilayers. *Nat Commun* 2015, 6.
62. Dair, B. J.; Honeker, C. C.; Alward, D. B.; Avgeropoulos, A.; Hadjichristidis, N.; Fetters, L. J.; Capel, M.; Thomas, E. L. Mechanical Properties and Deformation Behavior of the Double Gyroid Phase in Unoriented Thermoplastic Elastomers. *Macromolecules* 1999, 32, 8145-8152.
63. Olayo-Valles, R.; Guo, S.; Lund, M. S.; Leighton, C.; Hillmyer, M. A. Perpendicular Domain Orientation in Thin Films of Polystyrene-Poly lactide Diblock Copolymers. *Macromolecules* 2005, 38, 10101-10108.
64. Crossland, E. J. W.; Ludwigs, S.; Hillmyer, M. A.; Steiner, U. Freestanding nanowire arrays from soft-etch block copolymer templates. *Soft Matter* 2007, 3, 94-98.
65. Rzaev, J.; Hillmyer, M. A. Nanochannel Array Plastics with Tailored Surface Chemistry. *J Am Chem Soc* 2005, 127, 13373-13379.
66. Guo, S.; Rzaev, J.; Bailey, T. S.; Zalusky, A. S.; Olayo-Valles, R.; Hillmyer, M. A. Nanopore and Nanobushing Arrays from ABC Triblock Thin Films Containing Two Etchable Blocks. *Chemistry of Materials* 2006, 18, 1719-1721.
67. Rzaev, J.; Hillmyer, M. A. Nanoporous Polystyrene Containing Hydrophilic Pores from an ABC Triblock Copolymer Precursor. *Macromolecules* 2005, 38, 3-5.
68. Phillip, W. A.; Rzaev, J.; Hillmyer, M. A.; Cussler, E. L. Gas and water liquid transport through nanoporous block copolymer membranes. *Journal of Membrane Science* 2006, 286, 144-152.
69. Phillip, W. A.; O'Neill, B.; Rodwogin, M.; Hillmyer, M. A.; Cussler, E. L. Self-Assembled Block Copolymer Thin Films as Water Filtration Membranes. *ACS Applied Materials & Interfaces* 2010, 2, 847-853.
70. Hawker, C. J.; Russell, T. P. Block Copolymer Lithography: Merging "Bottom-Up" with "Top-Down" Processes. *MRS Bulletin* 2005, 30, 952-966.
71. Thurn-Albrecht, T.; Steiner, R.; DeRouchey, J.; Stafford, C. M.; Huang, E.; Bal, M.; Tuominen, M.; Hawker, C. J.; Russell, T. P. Nanoscopic Templates from Oriented Block Copolymer Films. *Adv Mater* 2000, 12, 787-791.
72. Mansky, P.; Liu, Y.; Huang, E.; Russell, T. P.; Hawker, C. Controlling Polymer-Surface Interactions with Random Copolymer Brushes. *Science* 1997, 275, 1458-1460.
73. Huang, E.; Rockford, L.; Russell, T. P.; Hawker, C. J. Nanodomain control in copolymer thin films. *Nature* 1998, 395, 757-758.
74. Yang, S. Y.; Ryu, I.; Kim, H. Y.; Kim, J. K.; Jang, S. K.; Russell, T. P. Nanoporous Membranes with Ultrahigh Selectivity and Flux for the Filtration of Viruses. *Adv Mater* 2006, 18, 709-712.
75. Yang, S. Y.; Park, J.; Yoon, J.; Ree, M.; Jang, S. K.; Kim, J. K. Virus Filtration Membranes Prepared from Nanoporous Block Copolymers with Good Dimensional

Stability under High Pressures and Excellent Solvent Resistance. *Advanced Functional Materials* 2008, 18, 1371-1377.

76. Jeong, U.; Ryu, D. Y.; Kho, D. H.; Kim, J. K.; Goldbach, J. T.; Kim, D. H.; Russell, T. P. Enhancement in the orientation of the microdomain in block copolymer thin films upon the addition of homopolymer. *Adv Mater* 2004, 16, 533-+.

77. Jeong, U. Y.; Ryu, D. Y.; Kim, J. K.; Kim, D. H.; Wu, X. D.; Russell, T. P. Precise control of nanopore size in thin film using mixtures of asymmetric block copolymer and homopolymer. *Macromolecules* 2003, 36, 10126-10129.

78. Yang, S. Y.; Yang, J.-A.; Kim, E.-S.; Jeon, G.; Oh, E. J.; Choi, K. Y.; Hahn, S. K.; Kim, J. K. Single-File Diffusion of Protein Drugs through Cylindrical Nanochannels. *Acs Nano* 2010, 4, 3817-3822.

79. Peinemann, K.-V.; Abetz, V.; Simon, P. F. W. Asymmetric superstructure formed in a block copolymer via phase separation. *Nat Mater* 2007, 6, 992-996.

80. Zhang, M.; Yang, L.; Yurt, S.; Misner, M. J.; Chen, J. T.; Coughlin, E. B.; Venkataraman, D.; Russell, T. P. Highly Ordered Nanoporous Thin Films from Cleavable Polystyrene-block-poly(ethylene oxide). *Adv Mater* 2007, 19, 1571-1576.

81. Mao, H.; Hillmyer, M. A. Macroscopic samples of polystyrene with ordered three-dimensional nanochannels. *Soft Matter* 2006, 2, 57-59.

82. Joo, W.; Park, M. S.; Kim, J. K. Block Copolymer Film with Sponge-Like Nanoporous Structure for Antireflection Coating. *Langmuir* 2006, 22, 7960-7963.

83. Gin, D. L.; Noble, R. D. Designing the Next Generation of Chemical Separation Membranes. *Science* 2011, 332, 674-676.

84. Singer, S. J.; Nicolson, G. L. The Fluid Mosaic Model of the Structure of Cell Membranes. *Science* 1972, 175, 720-731.

85. Giorno, L.; Mazzei, R.; Drioli, E. 1.01 - Biological Membranes and Biomimetic Artificial Membranes. In *Comprehensive Membrane Science and Engineering*, Drioli, E.; Giorno, L., Eds. Elsevier: Oxford, 2010; pp 1-12.

86. McMahon, H. T.; Gallop, J. L. Membrane curvature and mechanisms of dynamic cell membrane remodelling. *Nature* 2005, 438, 590-596.

87. Steck, T. L. The band 3 protein of the human red cell membrane: A review. *Journal of Supramolecular Structure* 1978, 8, 311-324.

88. Steck, T. L. The organization of proteins in the human red blood cell membrane: A Review. *The Journal of Cell Biology* 1974, 62, 1-19.

89. King, L. S.; Kozono, D.; Agre, P. From structure to disease: the evolving tale of aquaporin biology. *Nat Rev Mol Cell Biol* 2004, 5, 687-698.

90. Nielsen, C. Biomimetic membranes for sensor and separation applications. *Anal Bioanal Chem* 2009, 395, 697-718.

91. Hansen, J. S.; Perry, M.; Vogel, J.; Vissing, T.; Hansen, C. R.; Geschke, O.; Emnéus, J.; Nielsen, C. H. Development of an automation technique for the establishment of functional lipid bilayer arrays. *Journal of Micromechanics and Microengineering* 2009, 19, 025014.

92. Preston, G. M.; Agre, P. Isolation of the cDNA for erythrocyte integral membrane protein of 28 kilodaltons: member of an ancient channel family. *Proceedings of the National Academy of Sciences* 1991, 88, 11110-11114.

93. Smith, B. L.; Agre, P. Erythrocyte Mr 28,000 transmembrane protein exists as a multisubunit oligomer similar to channel proteins. *Journal of Biological Chemistry* 1991, 266, 6407-6415.
94. Verbavatz, J. M.; Brown, D.; Sabolić, I.; Valenti, G.; Ausiello, D. A.; Van Hoek, A. N.; Ma, T.; Verkman, A. S. Tetrameric assembly of CHIP28 water channels in liposomes and cell membranes: a freeze-fracture study. *The Journal of Cell Biology* 1993, 123, 605-618.
95. Sui, H.; Han, B.-G.; Lee, J. K.; Walian, P.; Jap, B. K. Structural basis of water-specific transport through the AQP1 water channel. *Nature* 2001, 414, 872-878.
96. de Groot, B. L.; Grubmüller, H. Water Permeation Across Biological Membranes: Mechanism and Dynamics of Aquaporin-1 and GlpF. *Science* 2001, 294, 2353-2357.
97. Tajkhorshid, E.; Nollert, P.; Jensen, M. Ø.; Miercke, L. J. W.; O'Connell, J.; Stroud, R. M.; Schulten, K. Control of the Selectivity of the Aquaporin Water Channel Family by Global Orientational Tuning. *Science* 2002, 296, 525-530.
98. Nikaido, H.; Rosenberg, E. Y.; Foulds, J. Porin channels in *Escherichia coli*: studies with beta-lactams in intact cells. *Journal of Bacteriology* 1983, 153, 232-240.
99. Nikaido, H. Porins and specific channels of bacterial outer membranes. *Molecular Microbiology* 1992, 6, 435-442.
100. Schulz, G. E.  $\beta$ -Barrel membrane proteins. *Current Opinion in Structural Biology* 2000, 10, 443-447.
101. Popot, J.-L.; Engelman, D. M. Helical Membrane Protein Folding, Stability, and Evolution. *Annual Review of Biochemistry* 2000, 69, 881-922.
102. Wimley, W. C. The versatile  $\beta$ -barrel membrane protein. *Current Opinion in Structural Biology* 2003, 13, 404-411.
103. Schulz, G. E. Porins: general to specific, native to engineered passive pores. *Current Opinion in Structural Biology* 1996, 6, 485-490.
104. Faraldo-Gomez, J. D.; Sansom, M. S. P. Acquisition of siderophores in Gram-negative bacteria. *Nat Rev Mol Cell Biol* 2003, 4, 105-116.
105. Postle, K. Active transport by customized beta-barrels. *Nat Struct Biol* 1999, 6, 3-6.
106. Koronakis, V.; Sharff, A.; Koronakis, E.; Luisi, B.; Hughes, C. Crystal structure of the bacterial membrane protein TolC central to multidrug efflux and protein export. *Nature* 2000, 405, 914-919.
107. Song, L.; Hobaugh, M. R.; Shustak, C.; Cheley, S.; Bayley, H.; Gouaux, J. E. Structure of Staphylococcal  $\alpha$ -Hemolysin, a Heptameric Transmembrane Pore. *Science* 1996, 274, 1859-1865.
108. Bayley, H. Toxin structure: Part of a hole? *Current Biology* 1997, 7, R763-R767.
109. Snijder, H. J.; Ubarretxena-Belandia, I.; Blaauw, M.; Kalk, K. H.; Verheij, H. M.; Egmond, M. R.; Dekker, N.; Dijkstra, B. W. Structural evidence for dimerization-regulated activation of an integral membrane phospholipase. *Nature* 1999, 401, 717-721.
110. Skou, J. C. The Identification of the Sodium-Potassium Pump (Nobel Lecture). *Angewandte Chemie International Edition* 1998, 37, 2320-2328.
111. Skou, J. C. The Influence of Some Cations on an Adenosine Triphosphatase from Peripheral Nerves. *Biochim Biophys Acta* 1957, 23, 394-401.

112. Morth, J. P.; Pedersen, B. P.; Toustrup-Jensen, M. S.; Sorensen, T. L. M.; Petersen, J.; Andersen, J. P.; Vilsen, B.; Nissen, P. Crystal structure of the sodium-potassium pump. *Nature* 2007, 450, 1043-1049.
113. Kumar, M.; Grzelakowski, M.; Zilles, J.; Clark, M.; Meier, W. Highly permeable polymeric membranes based on the incorporation of the functional water channel protein Aquaporin Z. *Proceedings of the National Academy of Sciences* 2007, 104, 20719-20724.
114. Einholm, A. P.; Andersen, J. P.; Vilsen, B. Importance of Leu99 in Transmembrane Segment M1 of the Na<sup>+</sup>,K<sup>+</sup>-ATPase in the Binding and Occlusion of K<sup>+</sup>. *Journal of Biological Chemistry* 2007, 282, 23854-23866.
115. Fan, H. J.; Gösele, U.; Zacharias, M. Formation of Nanotubes and Hollow Nanoparticles Based on Kirkendall and Diffusion Processes: A Review. *Small* 2007, 3, 1660-1671.
116. Remškar, M. Inorganic Nanotubes. *Adv Mater* 2004, 16, 1497-1504.
117. Baughman, R. H.; Zakhidov, A. A.; de Heer, W. A. Carbon Nanotubes--the Route Toward Applications. *Science* 2002, 297, 787-792.
118. Dai, H. Carbon Nanotubes: Synthesis, Integration, and Properties. *Accounts of Chemical Research* 2002, 35, 1035-1044.
119. Coleman, J. N.; Khan, U.; Gun'ko, Y. K. Mechanical Reinforcement of Polymers Using Carbon Nanotubes. *Adv Mater* 2006, 18, 689-706.
120. Qian, H.; Greenhalgh, E. S.; Shaffer, M. S. P.; Bismarck, A. Carbon nanotube-based hierarchical composites: a review. *Journal of Materials Chemistry* 2010, 20, 4751-4762.
121. Park, S.; Vosguerichian, M.; Bao, Z. A review of fabrication and applications of carbon nanotube film-based flexible electronics. *Nanoscale* 2013, 5, 1727-1752.
122. Cao, Q.; Rogers, J. A. Ultrathin Films of Single-Walled Carbon Nanotubes for Electronics and Sensors: A Review of Fundamental and Applied Aspects. *Adv Mater* 2009, 21, 29-53.
123. Rouhi, N.; Jain, D.; Burke, P. J. High-Performance Semiconducting Nanotube Inks: Progress and Prospects. *Acs Nano* 2011, 5, 8471-8487.
124. Avouris, P. Molecular Electronics with Carbon Nanotubes. *Accounts of Chemical Research* 2002, 35, 1026-1034.
125. Ouyang, M.; Huang, J.-L.; Lieber, C. M. Fundamental Electronic Properties and Applications of Single-Walled Carbon Nanotubes. *Accounts of Chemical Research* 2002, 35, 1018-1025.
126. Wenrong, Y.; Pall, T.; Gooding, J. J.; Simon, P. R.; Filip, B. Carbon nanotubes for biological and biomedical applications. *Nanotechnology* 2007, 18, 412001.
127. Kam, N. W. S.; O'Connell, M.; Wisdom, J. A.; Dai, H. Carbon nanotubes as multifunctional biological transporters and near-infrared agents for selective cancer cell destruction. *Proceedings of the National Academy of Sciences of the United States of America* 2005, 102, 11600-11605.
128. Bianco, A.; Kostarelos, K.; Prato, M. Applications of carbon nanotubes in drug delivery. *Current Opinion in Chemical Biology* 2005, 9, 674-679.
129. Wang, J. Carbon-Nanotube Based Electrochemical Biosensors: A Review. *Electroanalysis* 2005, 17, 7-14.

130. Fornasiero, F.; Park, H. G.; Holt, J. K.; Stadermann, M.; Grigoropoulos, C. P.; Noy, A.; Bakajin, O. Ion exclusion by sub-2-nm carbon nanotube pores. *Proceedings of the National Academy of Sciences* 2008, 105, 17250-17255.
131. Thostenson, E. T.; Ren, Z.; Chou, T.-W. Advances in the science and technology of carbon nanotubes and their composites: a review. *Composites Science and Technology* 2001, 61, 1899-1912.
132. Gong, B.; Shao, Z. Self-Assembling Organic Nanotubes with Precisely Defined, Sub-nanometer Pores: Formation and Mass Transport Characteristics. *Accounts of Chemical Research* 2013, 46, 2856-2866.
133. Bong, D. T.; Clark, T. D.; Granja, J. R.; Ghadiri, M. R. Self-Assembling Organic Nanotubes. *Angewandte Chemie International Edition* 2001, 40, 988-1011.
134. Kameta, N.; Minamikawa, H.; Masuda, M. Supramolecular organic nanotubes: how to utilize the inner nanospace and the outer space. *Soft Matter* 2011, 7, 4539-4561.
135. Shimizu, T.; Masuda, M.; Minamikawa, H. Supramolecular Nanotube Architectures Based on Amphiphilic Molecules. *Chemical Reviews* 2005, 105, 1401-1444.
136. Zhang, S. Fabrication of novel biomaterials through molecular self-assembly. *Nat Biotech* 2003, 21, 1171-1178.
137. Percec, V.; Dulcey, A. E.; Balagurusamy, V. S. K.; Miura, Y.; Smidrkal, J.; Peterca, M.; Nummelin, S.; Edlund, U.; Hudson, S. D.; Heiney, P. A.; Duan, H.; Magonov, S. N.; Vinogradov, S. A. Self-assembly of amphiphilic dendritic dipeptides into helical pores. *Nature* 2004, 430, 764-768.
138. Moore, J. S. Shape-Persistent Molecular Architectures of Nanoscale Dimension. *Accounts of Chemical Research* 1997, 30, 402-413.
139. Zhong-can, O.-Y.; Ji-xing, L. Helical structures of tilted chiral lipid bilayers viewed as cholesteric liquid crystals. *Physical review letters* 1990, 65, 1679-1682.
140. Ou-Yang, Z.-c.; Liu, J. Theory of helical structures of tilted chiral lipid bilayers. *Physical Review A* 1991, 43, 6826-6836.
141. Schnur, J. M. Lipid Tubules: A Paradigm for Molecularly Engineered Structures. *Science* 1993, 262, 1669-1676.
142. Spector, M. S.; Selinger, J. V.; Schnur, J. M. Topics in Stereochemistry, Materials-Chirality. In *Topics in Stereochemistry, Materials-Chirality*, Green, M. M.; Nolte, R. J. M.; Meijer, E. W.; Denmark, S. E.; Siegel, J., Eds. Wiley: 2004; Vol. 24, pp 281-372.
143. Israelachvili, J. N. *Intermolecular and Surface Forces: With Applications to Colloidal and Biological Systems*. Academic Press: 1985.
144. Stewart, S.; Liu, G. Block Copolymer Nanotubes. *Angewandte Chemie International Edition* 2000, 39, 340-344.
145. Kim, Y.; Mayer, M. F.; Zimmerman, S. C. A New Route to Organic Nanotubes from Porphyrin Dendrimers. *Angewandte Chemie International Edition* 2003, 42, 1121-1126.
146. Huang, H.; Remsen, E. E.; Kowalewski, T.; Wooley, K. L. Nanocages Derived from Shell Cross-Linked Micelle Templates. *J Am Chem Soc* 1999, 121, 3805-3806.
147. Martin, C. R. Nanomaterials: A Membrane-Based Synthetic Approach. *Science* 1994, 266, 1961-1966.

148. Obare, S. O.; Jana, N. R.; Murphy, C. J. Preparation of Polystyrene- and Silica-Coated Gold Nanorods and Their Use as Templates for the Synthesis of Hollow Nanotubes. *Nano Lett* 2001, 1, 601-603.
149. Bognitzki, M.; Hou, H.; Ishaque, M.; Frese, T.; Hellwig, M.; Schwarte, C.; Schaper, A.; Wendorff, J. H.; Greiner, A. Polymer, Metal, and Hybrid Nano- and Mesotubes by Coating Degradable Polymer Template Fibers (TUFT Process). *Adv Mater* 2000, 12, 637-640.
150. Brumlik, C. J.; Martin, C. R. Template synthesis of metal microtubules. *J Am Chem Soc* 1991, 113, 3174-3175.
151. Steinhart, M.; Wendorff, J. H.; Greiner, A.; Wehrspohn, R. B.; Nielsch, K.; Schilling, J.; Choi, J.; Gösele, U. Polymer Nanotubes by Wetting of Ordered Porous Templates. *Science* 2002, 296, 1997.
152. Zhao, D.; Moore, J. S. Shape-persistent arylene ethynylene macrocycles: syntheses and supramolecular chemistry. *Chem Commun* 2003, 807-818.
153. Zhang, J.; Moore, J. S. Nanoarchitectures. 3. Aggregation of hexa(phenylacetylene) macrocycles in solution: a model system for studying  $\pi$ - $\pi$  interactions. *J Am Chem Soc* 1992, 114, 9701-9702.
154. Zhang, J.; Moore, J. S. Nanoarchitectures. 6. Liquid Crystals Based on Shape-Persistent Macrocyclic Mesogens. *J Am Chem Soc* 1994, 116, 2655-2656.
155. Hunter, C. A.; Sanders, J. K. M. The nature of  $\pi$ - $\pi$  interactions. *J Am Chem Soc* 1990, 112, 5525-5534.
156. Venkataraman, D.; Lee, S.; Zhang, J.; Moore, J. S. An organic solid with wide channels based on hydrogen bonding between macrocycles. *Nature* 1994, 371, 591-593.
157. Höger, S.; Meckenstock, A.-D.; Pellen, H. High-Yield Macrocyclization via Glaser Coupling of Temporary Covalent Templated Bisacetylenes. *The Journal of Organic Chemistry* 1997, 62, 4556-4557.
158. Höger, S.; Meckenstock, A.-D. Template-Directed Synthesis of Shape-Persistent Macrocyclic Amphiphiles with Convergently Arranged Functionalities. *Chemistry – A European Journal* 1999, 5, 1686-1691.
159. Höger, S. Highly efficient methods for the preparation of shape-persistent macrocyclics. *Journal of Polymer Science Part A: Polymer Chemistry* 1999, 37, 2685-2698.
160. Yuan, L.; Feng, W.; Yamato, K.; Sanford, A. R.; Xu, D.; Guo, H.; Gong, B. Highly Efficient, One-Step Macrocyclizations Assisted by the Folding and Preorganization of Precursor Oligomers. *J Am Chem Soc* 2004, 126, 11120-11121.
161. Yang, Y.; Feng, W.; Hu, J.; Zou, S.; Gao, R.; Yamato, K.; Kline, M.; Cai, Z.; Gao, Y.; Wang, Y.; Li, Y.; Yang, Y.; Yuan, L.; Zeng, X. C.; Gong, B. Strong Aggregation and Directional Assembly of Aromatic Oligoamide Macrocycles. *J Am Chem Soc* 2011, 133, 18590-18593.
162. Gao, X.; Matsui, H. Peptide-Based Nanotubes and Their Applications in Bionanotechnology. *Adv Mater* 2005, 17, 2037-2050.
163. Vauthey, S.; Santoso, S.; Gong, H.; Watson, N.; Zhang, S. Molecular self-assembly of surfactant-like peptides to form nanotubes and nanovesicles. *Proceedings of the National Academy of Sciences* 2002, 99, 5355-5360.
164. Hartgerink, J. D.; Beniash, E.; Stupp, S. I. Self-Assembly and Mineralization of Peptide-Amphiphile Nanofibers. *Science* 2001, 294, 1684-1688.

165. Matsui, H.; MacCuspie, R. Metalloporphyrin Nanotube Fabrication Using Peptide Nanotubes as Templates. *Nano Lett* 2001, 1, 671-675.
166. Reches, M.; Gazit, E. Casting Metal Nanowires Within Discrete Self-Assembled Peptide Nanotubes. *Science* 2003, 300, 625-627.
167. Cui, H.; Webber, M. J.; Stupp, S. I. Self-assembly of peptide amphiphiles: From molecules to nanostructures to biomaterials. *Peptide Science* 2010, 94, 1-18.
168. Sipe, J. D.; Cohen, A. S. Review: History of the Amyloid Fibril. *Journal of Structural Biology* 2000, 130, 88-98.
169. Harper, J. D.; Lansbury, P. T. MODELS OF AMYLOID SEEDING IN ALZHEIMER'S DISEASE AND SCRAPIE: Mechanistic Truths and Physiological Consequences of the Time-Dependent Solubility of Amyloid Proteins. *Annual Review of Biochemistry* 1997, 66, 385-407.
170. Legname, G.; Baskakov, I. V.; Nguyen, H.-O. B.; Riesner, D.; Cohen, F. E.; DeArmond, S. J.; Prusiner, S. B. Synthetic Mammalian Prions. *Science* 2004, 305, 673-676.
171. Lu, K.; Jacob, J.; Thiyagarajan, P.; Conticello, V. P.; Lynn, D. G. Exploiting Amyloid Fibril Lamination for Nanotube Self-Assembly. *J Am Chem Soc* 2003, 125, 6391-6393.
172. Wang, W.; Hecht, M. H. Rationally designed mutations convert de novo amyloid-like fibrils into monomeric  $\beta$ -sheet proteins. *Proceedings of the National Academy of Sciences* 2002, 99, 2760-2765.
173. Ryadnov, M. G.; Woolfson, D. N. Engineering the morphology of a self-assembling protein fibre. *Nat Mater* 2003, 2, 329-332.
174. Benedetti, E.; Di Blasio, B.; Pedone, C.; Lorenzi, G. P.; Tomasic, L.; Gramlich, V. A double-stranded [beta]-helix with antiparallel chains in a crystalline oligo-L-D-peptide. *Nature* 1979, 282, 630-630.
175. Ghadiri, M. R.; Granja, J. R.; Buehler, L. K. Artificial Transmembrane Ion Channels from Self-Assembling Peptide Nanotubes. *Nature* 1994, 369, 301-304.
176. Ghadiri, M. R.; Granja, J. R.; Milligan, R. A.; Mcree, D. E.; Khazanovich, N. Self-Assembling Organic Nanotubes Based on a Cyclic Peptide Architecture. *Nature* 1993, 366, 324-327.
177. Sisson, A. L.; Shah, M. R.; Bhosale, S.; Matile, S. Synthetic ion channels and pores (2004-2005). *Chemical Society Reviews* 2006, 35, 1269-1286.
178. Chui, J. K. W.; Fyles, T. M. Ionic conductance of synthetic channels: analysis, lessons, and recommendations. *Chemical Society Reviews* 2012, 41, 148-175.
179. Fyles, T. M. Synthetic ion channels in bilayer membranes. *Chemical Society Reviews* 2007, 36, 335-347.
180. De Santis, P.; Morosetti, S.; Rizzo, R. Conformational Analysis of Regular Enantiomeric Sequences. *Macromolecules* 1974, 7, 52-58.
181. Hartgerink, J. D.; Granja, J. R.; Milligan, R. A.; Ghadiri, M. R. Self-assembling peptide nanotubes. *J Am Chem Soc* 1996, 118, 43-50.
182. Clark, T. D.; Buriak, J. M.; Kobayashi, K.; Isler, M. P.; McRee, D. E.; Ghadiri, M. R. Cylindrical beta-sheet peptide assemblies. *J Am Chem Soc* 1998, 120, 8949-8962.
183. Ghadiri, M. R.; Kobayashi, K.; Granja, J. R.; Chadha, R. K.; McRee, D. E. The Structural and Thermodynamic Basis for the Formation of Self-Assembled Peptide Nanotubes. *Angewandte Chemie International Edition in English* 1995, 34, 93-95.

184. Ketchum, R. R.; Hu, W.; Cross, T. A. High-Resolution Conformation of Gramicidin-a in a Lipid Bilayer by Solid-State Nmr. *Science* 1993, 261, 1457-1460.
185. Montenegro, J.; Ghadiri, M. R.; Granja, J. R. Ion Channel Models Based on Self-Assembling Cyclic Peptide Nanotubes. *Accounts of Chemical Research* 2013, 46, 2955-2965.
186. White, C. J.; Yudin, A. K. Contemporary strategies for peptide macrocyclization. *Nat Chem* 2011, 3, 509-524.
187. Reiriz, C.; Brea, R. J.; Arranz, R.; Carrascosa, J. L.; Garibotti, A.; Manning, B.; Valpuesta, J. M.; Eritja, R.; Castedo, L.; Granja, J. R. alpha,gamma-Peptide Nanotube Templating of One-Dimensional Parallel Fullerene Arrangements. *J Am Chem Soc* 2009, 131, 11335-+.
188. Couet, J.; Jeyaprakash, J. D.; Samuel, S.; Kopyshchev, A.; Santer, S.; Biesalski, M. Peptide-polymer hybrid nanotubes. *Angew Chem Int Edit* 2005, 44, 3297-3301.
189. ten Cate, M. G. J.; Severin, N.; Borner, H. G. Self-assembling peptide-polymer conjugates comprising D-alt-L)-cyclopeptides as aggregator domains. *Macromolecules* 2006, 39, 7831-7838.
190. Danial, M.; My-Nhi Tran, C.; Young, P. G.; Perrier, S.; Jolliffe, K. A. Janus cyclic peptide-polymer nanotubes. *Nat Commun* 2013, 4.
191. Granja, J. R.; Ghadiri, M. R. Channel-Mediated Transport of Glucose across Lipid Bilayers. *J Am Chem Soc* 1994, 116, 10785-10786.
192. Khazanovich, N.; Granja, J. R.; McRee, D. E.; Milligan, R. A.; Ghadiri, M. R. Nanoscale Tubular Ensembles with Specified Internal Diameters. Design of a Self-Assembled Nanotube with a 13-ANG. Pore. *J Am Chem Soc* 1994, 116, 6011-6012.
193. Sanchez-Quesada, J.; Ghadiri, M. R.; Bayley, H.; Braha, O. Cyclic peptides as molecular adapters for a pore-forming protein. *J. Am. Chem. Soc.* 2000, 122, 11757-11766.
194. Fernandez-Lopez, S.; Kim, H.-S.; Choi, E. C.; Delgado, M.; Granja, J. R.; Khasanov, A.; Kraehenbuehl, K.; Long, G.; Weinberger, D. A.; Wilcoxon, K. M.; Ghadiri, M. R. Antibacterial agents based on the cyclic d,l-[alpha]-peptide architecture. *Nature* 2001, 412, 452-455.
195. Kienker, P. K.; DeGrado, W. F.; Lear, J. D. A helical-dipole model describes the single-channel current rectification of an uncharged peptide ion channel. *Proceedings of the National Academy of Sciences of the United States of America* 1994, 91, 4859-4863.
196. Clark, T. D.; Buehler, L. K.; Ghadiri, M. R. Self-Assembling Cyclic  $\beta$ 3-Peptide Nanotubes as Artificial Transmembrane Ion Channels. *J Am Chem Soc* 1998, 120, 651-656.
197. Fujimura, F.; Horikawa, Y.; Morita, T.; Sugiyama, J.; Kimura, S. Double Assembly Composed of Lectin Association with Columnar Molecular Assembly of Cyclic Tri- $\beta$ -peptide Having Sugar Units. *Biomacromolecules* 2007, 8, 611-616.
198. Amorin, M.; Castedo, L.; Granja, J. R. New cyclic peptide assemblies with hydrophobic cavities: The structural and thermodynamic basis of a new class of peptide nanotubes. *J Am Chem Soc* 2003, 125, 2844-2845.
199. Brea, R. J.; Reiriz, C.; Granja, J. R. Towards functional bionanomaterials based on self-assembling cyclic peptide nanotubes. *Chem Soc Rev* 2010, 39, 1448-56.



200. Hourani, R.; Zhang, C.; van der Weegen, R.; Ruiz, L.; Li, C. Y.; Keten, S.; Helms, B. A.; Xu, T. Processable Cyclic Peptide Nanotubes with Tunable Interiors. *J Am Chem Soc* 2011, 133, 15296-15299.
201. Horne, W. S.; Stout, C. D.; Ghadiri, M. R. A Heterocyclic Peptide Nanotube. *J Am Chem Soc* 2003, 125, 9372-9376.
202. Chapman, R.; Danial, M.; Koh, M. L.; Jolliffe, K. A.; Perrier, S. Design and properties of functional nanotubes from the self-assembly of cyclic peptide templates. *Chemical Society Reviews* 2012, 41, 6023-6041.
203. Ashkenasy, N.; Horne, W. S.; Ghadiri, M. R. Design of self-assembling peptide nanotubes with delocalized electronic states. *Small* 2006, 2, 99-102.
204. Reiriz, C.; Amorin, M.; Garcia-Fandino, R.; Castedo, L.; Granja, J. R. alpha,gamma-Cyclic peptide ensembles with a hydroxylated cavity. *Org Biomol Chem* 2009, 7, 4358-4361.
205. Montenegro, J.; Vázquez-Vázquez, C.; Kalinin, A.; Geckeler, K. E.; Granja, J. R. Coupling of Carbon and Peptide Nanotubes. *J Am Chem Soc* 2014, 136, 2484-2491.
206. Xu, T.; Zhao, N. N.; Ren, F.; Hourani, R.; Lee, M. T.; Shu, J. Y.; Mao, S.; Helms, B. A. Subnanometer Porous Thin Films by the Co-assembly of Nanotube Subunits and Block Copolymers. *Acs Nano* 2011, 5, 1376-1384.
207. Chapman, R.; Jolliffe, K. A.; Perrier, S. Multi-shell Soft Nanotubes from Cyclic Peptide Templates. *Adv Mater* 2013, 25, 1170-1172.
208. Couet, J.; Biesalski, M. Polymer-wrapped peptide nanotubes: Peptide-grafted polymer mass impacts length and diameter. *Small* 2008, 4, 1008-1016.
209. Chapman, R.; Jolliffe, K. A.; Perrier, S. Modular design for the controlled production of polymeric nanotubes from polymer/peptide conjugates. *Polym Chem-Uk* 2011, 2, 1956-1963.
210. Chapman, R.; Jolliffe, K. A.; Perrier, S. Synthesis of Self-assembling Cyclic Peptide-polymer Conjugates using Click Chemistry. *Aust J Chem* 2010, 63, 1169-1172.
211. Chapman, R.; Koh, M. L.; Warr, G. G.; Jolliffe, K. A.; Perrier, S. Structure elucidation and control of cyclic peptide-derived nanotube assemblies in solution. *Chem Sci* 2013, 4, 2581-2589.
212. Chapman, R.; Bouten, P. J. M.; Hoogenboom, R.; Jolliffe, K. A.; Perrier, S. Thermoresponsive cyclic peptide - poly(2-ethyl-2-oxazoline) conjugate nanotubes. *Chem Commun* 2013, 49, 6522-6524.

## Chapter 2

1. Gin, D. L.; Noble, R. D. Designing the Next Generation of Chemical Separation Membranes. *Science* 2011, 332, 674-676.
2. Jirage, K. B.; Hulteen, J. C.; Martin, C. R. Nanotubule-Based Molecular-Filtration Membranes. *Science* 1997, 278, 655-658.
3. Zhang, S. Fabrication of novel biomaterials through molecular self-assembly. *Nat Biotech* 2003, 21, 1171-1178.
4. Wang, J. Carbon-Nanotube Based Electrochemical Biosensors: A Review. *Electroanalysis* 2005, 17, 7-14.
5. Chen, R. J.; Bangsaruntip, S.; Drouvalakis, K. A.; Wong Shi Kam, N.; Shim, M.; Li, Y.; Kim, W.; Utz, P. J.; Dai, H. Noncovalent functionalization of carbon nanotubes for highly specific electronic biosensors. *Proceedings of the National Academy of Sciences* 2003, 100, 4984-4989.
6. Ding, W.; Wada, M.; Kameta, N.; Minamikawa, H.; Shimizu, T.; Masuda, M. Functionalized organic nanotubes as tubular nonviral gene transfer vector. *Journal of Controlled Release* 2011, 156, 70-75.
7. Hentschel, J.; Borner, H. G. Blendable Peptide-Polymer Nanofibers to Modulate Mechanical Properties of Polymers. *Macromol Biosci* 2009, 9, 187-194.
8. Baughman, R. H.; Zakhidov, A. A.; de Heer, W. A. Carbon Nanotubes--the Route Toward Applications. *Science* 2002, 297, 787-792.
9. Coleman, J. N.; Khan, U.; Gun'ko, Y. K. Mechanical Reinforcement of Polymers Using Carbon Nanotubes. *Adv Mater* 2006, 18, 689-706.
10. Cao, Q.; Rogers, J. A. Ultrathin Films of Single-Walled Carbon Nanotubes for Electronics and Sensors: A Review of Fundamental and Applied Aspects. *Adv Mater* 2009, 21, 29-53.
11. Rouhi, N.; Jain, D.; Burke, P. J. High-Performance Semiconducting Nanotube Inks: Progress and Prospects. *Acs Nano* 2011, 5, 8471-8487.
12. Ouyang, M.; Huang, J.-L.; Lieber, C. M. Fundamental Electronic Properties and Applications of Single-Walled Carbon Nanotubes. *Accounts of Chemical Research* 2002, 35, 1018-1025.
13. Wenrong, Y.; Pall, T.; Gooding, J. J.; Simon, P. R.; Filip, B. Carbon nanotubes for biological and biomedical applications. *Nanotechnology* 2007, 18, 412001.
14. Kam, N. W. S.; O'Connell, M.; Wisdom, J. A.; Dai, H. Carbon nanotubes as multifunctional biological transporters and near-infrared agents for selective cancer cell destruction. *Proceedings of the National Academy of Sciences of the United States of America* 2005, 102, 11600-11605.
15. Bianco, A.; Kostarelos, K.; Prato, M. Applications of carbon nanotubes in drug delivery. *Current Opinion in Chemical Biology* 2005, 9, 674-679.
16. Holt, J. K.; Park, H. G.; Wang, Y.; Stadermann, M.; Artyukhin, A. B.; Grigoropoulos, C. P.; Noy, A.; Bakajin, O. Fast Mass Transport Through Sub-2-Nanometer Carbon Nanotubes. *Science* 2006, 312, 1034-1037.
17. Majumder, M.; Chopra, N.; Andrews, R.; Hinds, B. J. Nanoscale hydrodynamics: Enhanced flow in carbon nanotubes. *Nature* 2005, 438, 44-44.
18. Park, S.; Vosguerichian, M.; Bao, Z. A review of fabrication and applications of carbon nanotube film-based flexible electronics. *Nanoscale* 2013, 5, 1727-1752.

19. Dai, H. Carbon Nanotubes: Synthesis, Integration, and Properties. *Accounts of Chemical Research* 2002, 35, 1035-1044.
20. Hu, L.; Hecht, D. S.; Grüner, G. Carbon Nanotube Thin Films: Fabrication, Properties, and Applications. *Chemical Reviews* 2010, 110, 5790-5844.
21. Zhang, W.; Moore, J. S. Shape-Persistent Macrocycles: Structures and Synthetic Approaches from Arylene and Ethynylene Building Blocks. *Angewandte Chemie International Edition* 2006, 45, 4416-4439.
22. Moore, J. S. Shape-Persistent Molecular Architectures of Nanoscale Dimension. *Accounts of Chemical Research* 1997, 30, 402-413.
23. Shimizu, T.; Masuda, M.; Minamikawa, H. Supramolecular Nanotube Architectures Based on Amphiphilic Molecules. *Chemical Reviews* 2005, 105, 1401-1444.
24. Kameta, N.; Minamikawa, H.; Masuda, M. Supramolecular organic nanotubes: how to utilize the inner nanospace and the outer space. *Soft Matter* 2011, 7, 4539-4561.
25. Bong, D. T.; Clark, T. D.; Granja, J. R.; Ghadiri, M. R. Self-Assembling Organic Nanotubes. *Angewandte Chemie International Edition* 2001, 40, 988-1011.
26. Percec, V.; Dulcey, A. E.; Balagurusamy, V. S. K.; Miura, Y.; Smidrkal, J.; Peterca, M.; Nummelin, S.; Edlund, U.; Hudson, S. D.; Heiney, P. A.; Duan, H.; Magonov, S. N.; Vinogradov, S. A. Self-assembly of amphiphilic dendritic dipeptides into helical pores. *Nature* 2004, 430, 764-768.
27. Gao, X.; Matsui, H. Peptide-Based Nanotubes and Their Applications in Bionanotechnology. *Adv Mater* 2005, 17, 2037-2050.
28. Gong, B.; Shao, Z. Self-Assembling Organic Nanotubes with Precisely Defined, Sub-nanometer Pores: Formation and Mass Transport Characteristics. *Accounts of Chemical Research* 2013, 46, 2856-2866.
29. Yang, Y.; Feng, W.; Hu, J.; Zou, S.; Gao, R.; Yamato, K.; Kline, M.; Cai, Z.; Gao, Y.; Wang, Y.; Li, Y.; Yang, Y.; Yuan, L.; Zeng, X. C.; Gong, B. Strong Aggregation and Directional Assembly of Aromatic Oligoamide Macrocycles. *J Am Chem Soc* 2011, 133, 18590-18593.
30. Schnur, J. M. Lipid Tubules: A Paradigm for Molecularly Engineered Structures. *Science* 1993, 262, 1669-1676.
31. Ghadiri, M. R.; Granja, J. R.; Milligan, R. A.; Mcree, D. E.; Khazanovich, N. Self-Assembling Organic Nanotubes Based on a Cyclic Peptide Architecture. *Nature* 1993, 366, 324-327.
32. Ghadiri, M. R.; Granja, J. R.; Buehler, L. K. Artificial Transmembrane Ion Channels from Self-Assembling Peptide Nanotubes. *Nature* 1994, 369, 301-304.
33. Ghadiri, M. R.; Kobayashi, K.; Granja, J. R.; Chadha, R. K.; Mcree, D. E. The Structural and Thermodynamic Basis for the Formation of Self-Assembled Peptide Nanotubes. *Angewandte Chemie-International Edition in English* 1995, 34, 93-95.
34. Brea, R. J.; Reiriz, C.; Granja, J. R. Towards functional bionanomaterials based on self-assembling cyclic peptide nanotubes. *Chem Soc Rev* 2010, 39, 1448-56.
35. Chapman, R.; Danial, M.; Koh, M. L.; Jolliffe, K. A.; Perrier, S. Design and properties of functional nanotubes from the self-assembly of cyclic peptide templates. *Chemical Society Reviews* 2012, 41, 6023-6041.

36. Hourani, R.; Zhang, C.; van der Weegen, R.; Ruiz, L.; Li, C. Y.; Keten, S.; Helms, B. A.; Xu, T. Processable Cyclic Peptide Nanotubes with Tunable Interiors. *J Am Chem Soc* 2011, 133, 15296-15299.
37. Couet, J.; Jeyaprakash, J. D.; Samuel, S.; Kopyshv, A.; Santer, S.; Biesalski, M. Peptide-polymer hybrid nanotubes. *Angew Chem Int Edit* 2005, 44, 3297-3301.
38. Couet, J.; Biesalski, M. Polymer-wrapped peptide nanotubes: Peptide-grafted polymer mass impacts length and diameter. *Small* 2008, 4, 1008-1016.
39. ten Cate, M. G. J.; Severin, N.; Borner, H. G. Self-assembling peptide-polymer conjugates comprising D-alt-L)-cyclopeptides as aggregator domains. *Macromolecules* 2006, 39, 7831-7838.
40. Chapman, R.; Koh, M. L.; Warr, G. G.; Jolliffe, K. A.; Perrier, S. Structure elucidation and control of cyclic peptide-derived nanotube assemblies in solution. *Chem Sci* 2013, 4, 2581-2589.
41. Xu, T.; Zhao, N. N.; Ren, F.; Hourani, R.; Lee, M. T.; Shu, J. Y.; Mao, S.; Helms, B. A. Subnanometer Porous Thin Films by the Co-assembly of Nanotube Subunits and Block Copolymers. *Acs Nano* 2011, 5, 1376-1384.
42. Chapman, R.; Jolliffe, K. A.; Perrier, S. Multi-shell Soft Nanotubes from Cyclic Peptide Templates. *Adv Mater* 2013, 25, 1170-1172.
43. Danial, M.; My-Nhi Tran, C.; Young, P. G.; Perrier, S.; Jolliffe, K. A. Janus cyclic peptide-polymer nanotubes. *Nat Commun* 2013, 4.
44. Alexander, S. Polymer adsorption on small spheres. A scaling approach. *J. Phys. France* 1977, 38, 977-981.
45. de Gennes, P. G. Conformations of Polymers Attached to an Interface. *Macromolecules* 1980, 13, 1069-1075.
46. Milner, S. T.; Witten, T. A.; Cates, M. E. Theory of the grafted polymer brush. *Macromolecules* 1988, 21, 2610-2619.
47. Chapman, R.; Jolliffe, K. A.; Perrier, S. Modular design for the controlled production of polymeric nanotubes from polymer/peptide conjugates. *Polym Chem-Uk* 2011, 2, 1956-1963.
48. Lund, R.; Shu, J.; Xu, T. A Small-Angle X-ray Scattering Study of  $\alpha$ -helical Bundle-Forming Peptide-Polymer Conjugates in Solution: Chain Conformations. *Macromolecules* 2013, 46, 1625-1632.
49. Israelachvili, J. N.; Mitchell, D. J.; Ninham, B. W. Theory of self-assembly of hydrocarbon amphiphiles into micelles and bilayers. *Journal of the Chemical Society, Faraday Transactions 2: Molecular and Chemical Physics* 1976, 72, 1525-1568.
50. Ruiz, L.; Keten, S. Directing the self-assembly of supra-biomolecular nanotubes using entropic forces. *Soft Matter* 2014, 10, 851-861.
51. Lautié, A.; Froment, F.; Novak, A. Relationship Between NH Stretching Frequencies and N...O Distances of Crystals Containing NH...O Hydrogen Bonds. *Spectroscopy Letters* 1976, 9, 289-299.

### Chapter 3

1. Gin, D. L.; Noble, R. D. Designing the Next Generation of Chemical Separation Membranes. *Science* 2011, 332, 674-676.
2. Shannon, M. A.; Bohn, P. W.; Elimelech, M.; Georgiadis, J. G.; Marinas, B. J.; Mayes, A. M. Science and technology for water purification in the coming decades. *Nature* 2008, 452, 301-310.
3. Ghadiri, M. R.; Granja, J. R.; Milligan, R. A.; Mcree, D. E.; Khazanovich, N. Self-Assembling Organic Nanotubes Based on a Cyclic Peptide Architecture. *Nature* 1993, 366, 324-327.
4. Ghadiri, M. R.; Granja, J. R.; Buehler, L. K. Artificial Transmembrane Ion Channels from Self-Assembling Peptide Nanotubes. *Nature* 1994, 369, 301-304.
5. Granja, J. R.; Ghadiri, M. R. Channel-Mediated Transport of Glucose across Lipid Bilayers. *J Am Chem Soc* 1994, 116, 10785-10786.
6. Khazanovich, N.; Granja, J. R.; McRee, D. E.; Milligan, R. A.; Ghadiri, M. R. Nanoscale Tubular Ensembles with Specified Internal Diameters. Design of a Self-Assembled Nanotube with a 13- $\text{\AA}$  Pore. *J Am Chem Soc* 1994, 116, 6011-6012.
7. Hartgerink, J. D.; Granja, J. R.; Milligan, R. A.; Ghadiri, M. R. Self-assembling peptide nanotubes. *J Am Chem Soc* 1996, 118, 43-50.
8. Clark, T. D.; Buriak, J. M.; Kobayashi, K.; Isler, M. P.; McRee, D. E.; Ghadiri, M. R. Cylindrical beta-sheet peptide assemblies. *J Am Chem Soc* 1998, 120, 8949-8962.
9. Amorin, M.; Castedo, L.; Granja, J. R. New cyclic peptide assemblies with hydrophobic cavities: The structural and thermodynamic basis of a new class of peptide nanotubes. *J Am Chem Soc* 2003, 125, 2844-2845.
10. Horne, W. S.; Stout, C. D.; Ghadiri, M. R. A Heterocyclic Peptide Nanotube. *J Am Chem Soc* 2003, 125, 9372-9376.
11. Hourani, R.; Zhang, C.; van der Weegen, R.; Ruiz, L.; Li, C. Y.; Keten, S.; Helms, B. A.; Xu, T. Processable Cyclic Peptide Nanotubes with Tunable Interiors. *J Am Chem Soc* 2011, 133, 15296-15299.
12. Xu, T.; Zhao, N. N.; Ren, F.; Hourani, R.; Lee, M. T.; Shu, J. Y.; Mao, S.; Helms, B. A. Subnanometer Porous Thin Films by the Co-assembly of Nanotube Subunits and Block Copolymers. *Acs Nano* 2011, 5, 1376-1384.
13. Rzayev, J.; Hillmyer, M. A. Nanoporous polystyrene containing hydrophilic pores from an ABC triblock copolymer precursor. *Macromolecules* 2005, 38, 3-5.
14. Yang, S. Y.; Ryu, I.; Kim, H. Y.; Kim, J. K.; Jang, S. K.; Russell, T. P. Nanoporous Membranes with Ultrahigh Selectivity and Flux for the Filtration of Viruses. *Adv Mater* 2006, 18, 709-712.
15. Peinemann, K.-V.; Abetz, V.; Simon, P. F. W. Asymmetric superstructure formed in a block copolymer via phase separation. *Nat Mater* 2007, 6, 992-996.
16. Jackson, E. A.; Hillmyer, M. A. Nanoporous Membranes Derived from Block Copolymers: From Drug Delivery to Water Filtration. *Acs Nano* 2010, 4, 3548-3553.
17. Wang, Y.; Li, F. An Emerging Pore-Making Strategy: Confined Swelling-Induced Pore Generation in Block Copolymer Materials. *Adv Mater* 2011, 23, 2134-2148.
18. Holt, J. K.; Park, H. G.; Wang, Y.; Stadermann, M.; Artyukhin, A. B.; Grigoropoulos, C. P.; Noy, A.; Bakajin, O. Fast Mass Transport Through Sub-2-Nanometer Carbon Nanotubes. *Science* 2006, 312, 1034-1037.

19. Hinds, B. J.; Chopra, N.; Rantell, T.; Andrews, R.; Gavalas, V.; Bachas, L. G. Aligned Multiwalled Carbon Nanotube Membranes. *Science* 2004, 303, 62-65.
20. Chapman, R.; Koh, M. L.; Warr, G. G.; Jolliffe, K. A.; Perrier, S. Structure elucidation and control of cyclic peptide-derived nanotube assemblies in solution. *Chem Sci* 2013, 4, 2581-2589.
21. Thompson, R. B.; Ginzburg, V. V.; Matsen, M. W.; Balazs, A. C. Predicting the mesophases of copolymer-nanoparticle composites. *Science* 2001, 292, 2469-2472.
22. Balazs, A. C.; Emrick, T.; Russell, T. P. Nanoparticle Polymer Composites: Where Two Small Worlds Meet. *Science* 2006, 314, 1107-1110.
23. Bockstaller, M. R.; Mickiewicz, R. A.; Thomas, E. L. Block Copolymer Nanocomposites: Perspectives for Tailored Functional Materials. *Adv Mater* 2005, 17, 1331-1349.
24. Jia, M.-D.; Pleinemann, K.-V.; Behling, R.-D. Preparation and characterization of thin-film zeolite-PDMS composite membranes. *Journal of Membrane Science* 1992, 73, 119-128.
25. Chung, T.-S.; Jiang, L. Y.; Li, Y.; Kulprathipanja, S. Mixed matrix membranes (MMMs) comprising organic polymers with dispersed inorganic fillers for gas separation. *Progress in Polymer Science* 2007, 32, 483-507.
26. Couet, J.; Jeyaprakash, J. D.; Samuel, S.; Kopyshev, A.; Santer, S.; Biesalski, M. Peptide-polymer hybrid nanotubes. *Angew Chem Int Edit* 2005, 44, 3297-3301.
27. Couet, J.; Biesalski, M. Polymer-wrapped peptide nanotubes: Peptide-grafted polymer mass impacts length and diameter. *Small* 2008, 4, 1008-1016.
28. ten Cate, M. G. J.; Severin, N.; Borner, H. G. Self-assembling peptide-polymer conjugates comprising D-alt-L)-cyclopeptides as aggregator domains. *Macromolecules* 2006, 39, 7831-7838.
29. Chapman, R.; Jolliffe, K. A.; Perrier, S. Multi-shell Soft Nanotubes from Cyclic Peptide Templates. *Adv Mater* 2013, 25, 1170-1172.
30. Danial, M.; My-Nhi Tran, C.; Young, P. G.; Perrier, S.; Jolliffe, K. A. Janus cyclic peptide-polymer nanotubes. *Nat Commun* 2013, 4.
31. Jeong, U.; Ryu, D. Y.; Kho, D. H.; Lee, D. H.; Kim, J. K.; Russell, T. P. Phase behavior of mixtures of block copolymer and homopolymers in thin films and bulk. *Macromolecules* 2003, 36, 3626-3634.
32. Khurana, E.; Nielsen, S. O.; Ensing, B.; Klein, M. L. Self-Assembling Cyclic Peptides: Molecular Dynamics Studies of Dimers in Polar and Nonpolar Solvents†. *The Journal of Physical Chemistry B* 2006, 110, 18965-18972.
33. Engels, M.; Bashford, D.; Ghadiri, M. R. Structure and Dynamics of Self-Assembling Peptide Nanotubes and the Channel-Mediated Water Organization and Self-Diffusion. A Molecular Dynamics Study. *J Am Chem Soc* 1995, 117, 9151-9158.
34. Brandrup, J.; Immergut, E. H. *Polymer handbook*. Interscience Publishers: 1966.
35. Chapman, R.; Jolliffe, K. A.; Perrier, S. Synthesis of Self-assembling Cyclic Peptide-polymer Conjugates using Click Chemistry. *Aust J Chem* 2010, 63, 1169-1172.
36. Mansky, P.; Liu, Y.; Huang, E.; Russell, T. P.; Hawker, C. Controlling Polymer-Surface Interactions with Random Copolymer Brushes. *Science* 1997, 275, 1458-1460.

## Chapter 4

1. Baker, R. Future directions of membrane gas-separation technology. *Membrane Technology* 2001, 2001, 5-10.
2. Gin, D. L.; Noble, R. D. Designing the Next Generation of Chemical Separation Membranes. *Science* 2011, 332, 674-676.
3. Shannon, M. A.; Bohn, P. W.; Elimelech, M.; Georgiadis, J. G.; Marinas, B. J.; Mayes, A. M. Science and technology for water purification in the coming decades. *Nature* 2008, 452, 301-310.
4. Bernardo, P.; Drioli, E.; Golemme, G. Membrane Gas Separation: A Review/State of the Art. *Ind Eng Chem Res* 2009, 48, 4638-4663.
5. Pendergast, M. M.; Hoek, E. M. V. A review of water treatment membrane nanotechnologies. *Energy & Environmental Science* 2011, 4, 1946-1971.
6. Sui, H.; Han, B.-G.; Lee, J. K.; Walian, P.; Jap, B. K. Structural basis of water-specific transport through the AQP1 water channel. *Nature* 2001, 414, 872-878.
7. Tajkhorshid, E.; Nollert, P.; Jensen, M. Ø.; Miercke, L. J. W.; O'Connell, J.; Stroud, R. M.; Schulten, K. Control of the Selectivity of the Aquaporin Water Channel Family by Global Orientational Tuning. *Science* 2002, 296, 525-530.
8. King, L. S.; Kozono, D.; Agre, P. From structure to disease: the evolving tale of aquaporin biology. *Nat Rev Mol Cell Biol* 2004, 5, 687-698.
9. de Groot, B. L.; Grubmüller, H. Water Permeation Across Biological Membranes: Mechanism and Dynamics of Aquaporin-1 and GlpF. *Science* 2001, 294, 2353-2357.
10. Amorin, M.; Castedo, L.; Granja, J. R. New cyclic peptide assemblies with hydrophobic cavities: The structural and thermodynamic basis of a new class of peptide nanotubes. *J Am Chem Soc* 2003, 125, 2844-2845.
11. Kubik, S.; Goddard, R. A new cyclic pseudopeptide composed of (L)-proline and 3-aminobenzoic acid subunits as a ditopic receptor for the simultaneous complexation of cations and anions. *Journal of Organic Chemistry* 1999, 64, 9475-9486.
12. Amorin, M.; Castedo, L.; Granja, J. R. Self-assembled peptide tubelets with 7 angstrom pores. *Chemistry-a European Journal* 2005, 11, 6543-6551.
13. Hourani, R.; Zhang, C.; van der Weegen, R.; Ruiz, L.; Li, C. Y.; Keten, S.; Helms, B. A.; Xu, T. Processable Cyclic Peptide Nanotubes with Tunable Interiors. *J Am Chem Soc* 2011, 133, 15296-15299.
14. Ghadiri, M. R.; Granja, J. R.; Buehler, L. K. Artificial Transmembrane Ion Channels from Self-Assembling Peptide Nanotubes. *Nature* 1994, 369, 301-304.
15. Ghadiri, M. R.; Granja, J. R.; Milligan, R. A.; Mcree, D. E.; Khazanovich, N. Self-Assembling Organic Nanotubes Based on a Cyclic Peptide Architecture. *Nature* 1993, 366, 324-327.
16. Bong, D. T.; Clark, T. D.; Granja, J. R.; Ghadiri, M. R. Self-Assembling Organic Nanotubes. *Angewandte Chemie International Edition* 2001, 40, 988-1011.
17. Hartgerink, J. D.; Granja, J. R.; Milligan, R. A.; Ghadiri, M. R. Self-assembling peptide nanotubes. *J Am Chem Soc* 1996, 118, 43-50.
18. Couet, J.; Jeyaprakash, J. D.; Samuel, S.; Kopyshov, A.; Santer, S.; Biesalski, M. Peptide-polymer hybrid nanotubes. *Angew Chem Int Edit* 2005, 44, 3297-3301.
19. Couet, J.; Biesalski, M. Polymer-wrapped peptide nanotubes: Peptide-grafted polymer mass impacts length and diameter. *Small* 2008, 4, 1008-1016.

20. ten Cate, M. G. J.; Severin, N.; Borner, H. G. Self-assembling peptide-polymer conjugates comprising D-alt-L)-cyclopeptides as aggregator domains. *Macromolecules* 2006, 39, 7831-7838.
21. Chapman, R.; Koh, M. L.; Warr, G. G.; Jolliffe, K. A.; Perrier, S. Structure elucidation and control of cyclic peptide-derived nanotube assemblies in solution. *Chem Sci* 2013, 4, 2581-2589.
22. Chapman, R.; Danial, M.; Koh, M. L.; Jolliffe, K. A.; Perrier, S. Design and properties of functional nanotubes from the self-assembly of cyclic peptide templates. *Chemical Society Reviews* 2012, 41, 6023-6041.
23. Mansky, P.; Liu, Y.; Huang, E.; Russell, T. P.; Hawker, C. Controlling Polymer-Surface Interactions with Random Copolymer Brushes. *Science* 1997, 275, 1458-1460.



## Chapter 5

1. Baker, R. Future directions of membrane gas-separation technology. *Membrane Technology* 2001, 2001, 5-10.
2. Baker, R. W. Membrane Technology. In *Encyclopedia of Polymer Science and Technology*, John Wiley & Sons, Inc.: 2002.
3. Baker, R. W. Future Directions of Membrane Gas Separation Technology. *Ind Eng Chem Res* 2002, 41, 1393-1411.
4. Gin, D. L.; Noble, R. D. Designing the Next Generation of Chemical Separation Membranes. *Science* 2011, 332, 674-676.
5. Mulder, J. *Basic Principles of Membrane Technology*. Springer Netherlands: 1996.
6. Lonsdale, H. K. The growth of membrane technology. *Journal of Membrane Science* 1982, 10, 81-181.
7. D'Alessandro, D. M.; Smit, B.; Long, J. R. Carbon Dioxide Capture: Prospects for New Materials. *Angewandte Chemie International Edition* 2010, 49, 6058-6082.
8. Koros, W. J.; Fleming, G. K. Membrane-based gas separation. *Journal of Membrane Science* 1993, 83, 1-80.
9. Yampolskii, Y. Polymeric Gas Separation Membranes. *Macromolecules* 2012, 45, 3298-3311.
10. Freeman, B. D. Basis of Permeability/Selectivity Tradeoff Relations in Polymeric Gas Separation Membranes. *Macromolecules* 1999, 32, 375-380.
11. Chung, T.-S.; Jiang, L. Y.; Li, Y.; Kulprathipanja, S. Mixed matrix membranes (MMMs) comprising organic polymers with dispersed inorganic fillers for gas separation. *Progress in Polymer Science* 2007, 32, 483-507.
12. Lai, Z.; Bonilla, G.; Diaz, I.; Nery, J. G.; Sujaoti, K.; Amat, M. A.; Kokkoli, E.; Terasaki, O.; Thompson, R. W.; Tsapatsis, M.; Vlachos, D. G. Microstructural Optimization of a Zeolite Membrane for Organic Vapor Separation. *Science* 2003, 300, 456-460.
13. Davis, M. E. Ordered porous materials for emerging applications. *Nature* 2002, 417, 813-821.
14. Bloch, E. D.; Queen, W. L.; Krishna, R.; Zadrozny, J. M.; Brown, C. M.; Long, J. R. Hydrocarbon Separations in a Metal-Organic Framework with Open Iron(II) Coordination Sites. *Science* 2012, 335, 1606-1610.
15. Li, J.-R.; Kuppler, R. J.; Zhou, H.-C. Selective gas adsorption and separation in metal-organic frameworks. *Chemical Society Reviews* 2009, 38, 1477-1504.
16. Holt, J. K.; Park, H. G.; Wang, Y. M.; Stadermann, M.; Artyukhin, A. B.; Grigoropoulos, C. P.; Noy, A.; Bakajin, O. Fast mass transport through sub-2-nanometer carbon nanotubes. *Science* 2006, 312, 1034-1037.
17. Ordoñez, M. J. C.; Balkus Jr, K. J.; Ferraris, J. P.; Musselman, I. H. Molecular sieving realized with ZIF-8/Matrimid® mixed-matrix membranes. *Journal of Membrane Science* 2010, 361, 28-37.
18. Ismail, A. F.; Goh, P. S.; Sanip, S. M.; Aziz, M. Transport and separation properties of carbon nanotube-mixed matrix membrane. *Separation and Purification Technology* 2009, 70, 12-26.

19. Shimizu, T.; Masuda, M.; Minamikawa, H. Supramolecular Nanotube Architectures Based on Amphiphilic Molecules. *Chemical Reviews* 2005, 105, 1401-1444.
20. Bong, D. T.; Clark, T. D.; Granja, J. R.; Ghadiri, M. R. Self-Assembling Organic Nanotubes. *Angewandte Chemie International Edition* 2001, 40, 988-1011.
21. Kameta, N.; Minamikawa, H.; Masuda, M. Supramolecular organic nanotubes: how to utilize the inner nanospace and the outer space. *Soft Matter* 2011, 7, 4539-4561.
22. Gong, B.; Shao, Z. Self-Assembling Organic Nanotubes with Precisely Defined, Sub-nanometer Pores: Formation and Mass Transport Characteristics. *Accounts of Chemical Research* 2013, 46, 2856-2866.
23. Xu, T.; Zhao, N. N.; Ren, F.; Hourani, R.; Lee, M. T.; Shu, J. Y.; Mao, S.; Helms, B. A. Subnanometer Porous Thin Films by the Co-assembly of Nanotube Subunits and Block Copolymers. *Acs Nano* 2011, 5, 1376-1384.
24. Hourani, R.; Zhang, C.; van der Weegen, R.; Ruiz, L.; Li, C. Y.; Keten, S.; Helms, B. A.; Xu, T. Processable Cyclic Peptide Nanotubes with Tunable Interiors. *J Am Chem Soc* 2011, 133, 15296-15299.
25. Chapman, R.; Danial, M.; Koh, M. L.; Jolliffe, K. A.; Perrier, S. Design and properties of functional nanotubes from the self-assembly of cyclic peptide templates. *Chemical Society Reviews* 2012, 41, 6023-6041.
26. Brea, R. J.; Reiriz, C.; Granja, J. R. Towards functional bionanomaterials based on self-assembling cyclic peptide nanotubes. *Chem Soc Rev* 2010, 39, 1448-56.
27. Matsen, M. W. Phase-Behavior of Block-Copolymer Homopolymer Blends. *Macromolecules* 1995, 28, 5765-5773.
28. Robeson, L. M. Correlation of separation factor versus permeability for polymeric membranes. *Journal of Membrane Science* 1991, 62, 165-185.
29. Kentish, S. E.; Scholes, C. A.; Stevens, G. W. Carbon Dioxide Separation through Polymeric Membrane Systems for Flue Gas Applications. *Recent Patents on Chemical Engineering* 2008, 1, 52-66.
30. Alexander Stern, S. Polymers for gas separations: the next decade. *Journal of Membrane Science* 1994, 94, 1-65.
31. Bernardo, P.; Drioli, E.; Golemme, G. Membrane Gas Separation: A Review/State of the Art. *Ind Eng Chem Res* 2009, 48, 4638-4663.
32. Koresh, J.; Soffer, A. Study of molecular sieve carbons. Part 1.-Pore structure, gradual pore opening and mechanism of molecular sieving. *Journal of the Chemical Society, Faraday Transactions 1: Physical Chemistry in Condensed Phases* 1980, 76, 2457-2471.
33. Koresh, J. E.; Sofer, A. Molecular Sieve Carbon Permselective Membrane. Part I. Presentation of a New Device for Gas Mixture Separation. *Separation Science and Technology* 1983, 18, 723-734.
34. Rao, M. B.; Sircar, S. Nanoporous carbon membranes for separation of gas mixtures by selective surface flow. *Journal of Membrane Science* 1993, 85, 253-264.
35. Keizer, K.; Uhlhorn, R. J. R.; Van vuren, R. J.; Burggraaf, A. J. Gas separation mechanisms in microporous modified  $\gamma$ - $\text{Al}_2\text{O}_3$  membranes. *Journal of Membrane Science* 1988, 39, 285-300.

36. Holt, J. K.; Park, H. G.; Wang, Y.; Stadermann, M.; Artyukhin, A. B.; Grigoropoulos, C. P.; Noy, A.; Bakajin, O. Fast Mass Transport Through Sub-2-Nanometer Carbon Nanotubes. *Science* 2006, 312, 1034-1037.
37. Fornasiero, F.; Park, H. G.; Holt, J. K.; Stadermann, M.; Grigoropoulos, C. P.; Noy, A.; Bakajin, O. Ion exclusion by sub-2-nm carbon nanotube pores. *Proceedings of the National Academy of Sciences* 2008, 105, 17250-17255.
38. Hinds, B. J.; Chopra, N.; Rantell, T.; Andrews, R.; Gavalas, V.; Bachas, L. G. Aligned Multiwalled Carbon Nanotube Membranes. *Science* 2004, 303, 62-65.
39. Li, H.; Song, Z.; Zhang, X.; Huang, Y.; Li, S.; Mao, Y.; Ploehn, H. J.; Bao, Y.; Yu, M. Ultrathin, Molecular-Sieving Graphene Oxide Membranes for Selective Hydrogen Separation. *Science* 2013, 342, 95-98.
40. Berens, A. R.; Hopfenberg, H. B. Diffusion of organic vapors at low concentrations in glassy PVC, polystyrene, and PMMA. *Journal of Membrane Science* 1982, 10, 283-303.
41. Pye, D. G.; Hoehn, H. H.; Panar, M. Measurement of gas permeability of polymers. II. Apparatus for determination of permeabilities of mixed gases and vapors. *J Appl Polym Sci* 1976, 20, 287-301.
42. Robeson, L. M. The upper bound revisited. *Journal of Membrane Science* 2008, 320, 390-400.
43. Park, H. B.; Jung, C. H.; Lee, Y. M.; Hill, A. J.; Pas, S. J.; Mudie, S. T.; Van Wagner, E.; Freeman, B. D.; Cookson, D. J. Polymers with Cavities Tuned for Fast Selective Transport of Small Molecules and Ions. *Science* 2007, 318, 254-258.
44. Merkel, T. C.; Gupta, R. P.; Turk, B. S.; Freeman, B. D. Mixed-gas permeation of syngas components in poly(dimethylsiloxane) and poly(1-trimethylsilyl-1-propyne) at elevated temperatures. *Journal of Membrane Science* 2001, 191, 85-94.
45. Wiebe, R.; Gaddy, V. L. The Solubility of Carbon Dioxide in Water at Various Temperatures from 12 to 40° and at Pressures to 500 Atmospheres. *Critical Phenomena\**. *J Am Chem Soc* 1940, 62, 815-817.
46. Aroon, M. A.; Ismail, A. F.; Matsuura, T.; Montazer-Rahmati, M. M. Performance studies of mixed matrix membranes for gas separation: A review. *Separation and Purification Technology* 2010, 75, 229-242.
47. Bouma, R. H. B.; Checchetti, A.; Chidichimo, G.; Drioli, E. Permeation through a heterogeneous membrane: the effect of the dispersed phase. *Journal of Membrane Science* 1997, 128, 141-149.
48. Petropoulos, J. H. A comparative study of approaches applied to the permeability of binary composite polymeric materials. *Journal of Polymer Science: Polymer Physics Edition* 1985, 23, 1309-1324.
49. Maxwell, J. C. *A Treatise on Electricity and Magnetism*. OUP Oxford: 1998.
50. Cong, H.; Zhang, J.; Radosz, M.; Shen, Y. Carbon nanotube composite membranes of brominated poly(2,6-diphenyl-1,4-phenylene oxide) for gas separation. *Journal of Membrane Science* 2007, 294, 178-185.
51. Vu, D. Q.; Koros, W. J.; Miller, S. J. Mixed matrix membranes using carbon molecular sieves: II. Modeling permeation behavior. *Journal of Membrane Science* 2003, 211, 335-348.
52. Zimmerman, C. M.; Singh, A.; Koros, W. J. Tailoring mixed matrix composite membranes for gas separations. *Journal of Membrane Science* 1997, 137, 145-154.

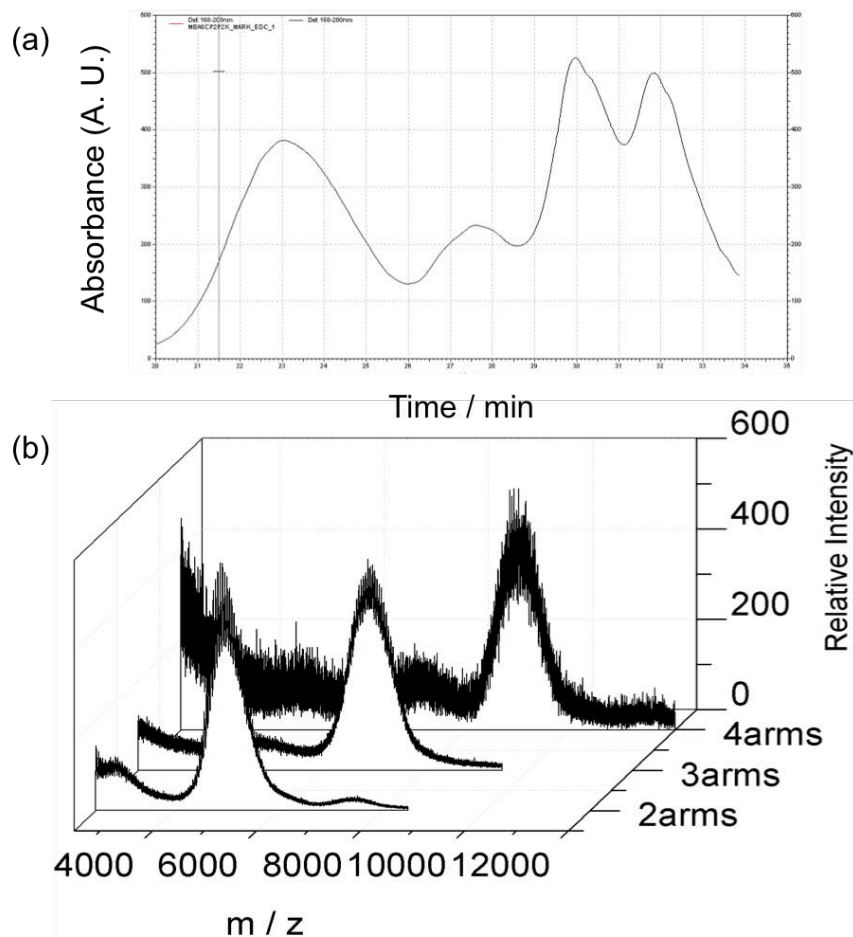
53. Moore, T. T.; Mahajan, R.; Vu, D. Q.; Koros, W. J. Hybrid membrane materials comprising organic polymers with rigid dispersed phases. *AIChE Journal* 2004, 50, 311-321.
54. Mahajan, R.; Koros, W. J. Mixed matrix membrane materials with glassy polymers. Part 1. *Polymer Engineering & Science* 2002, 42, 1420-1431.
55. Mahajan, R.; Koros, W. J. Mixed matrix membrane materials with glassy polymers. Part 2. *Polymer Engineering & Science* 2002, 42, 1432-1441.
56. Ghadiri, M. R.; Granja, J. R.; Buehler, L. K. Artificial Transmembrane Ion Channels from Self-Assembling Peptide Nanotubes. *Nature* 1994, 369, 301-304.
57. Ghadiri, M. R.; Granja, J. R.; Milligan, R. A.; Mcree, D. E.; Khazanovich, N. Self-Assembling Organic Nanotubes Based on a Cyclic Peptide Architecture. *Nature* 1993, 366, 324-327.
58. Sanchez-Quesada, J.; Ghadiri, M. R.; Bayley, H.; Braha, O. Cyclic peptides as molecular adapters for a pore-forming protein. *J. Am. Chem. Soc.* 2000, 122, 11757-11766.
59. Clark, T. D.; Buehler, L. K.; Ghadiri, M. R. Self-Assembling Cyclic  $\beta$ 3-Peptide Nanotubes as Artificial Transmembrane Ion Channels. *J Am Chem Soc* 1998, 120, 651-656.
60. Granja, J. R.; Ghadiri, M. R. Channel-Mediated Transport of Glucose across Lipid Bilayers. *J Am Chem Soc* 1994, 116, 10785-10786.

## Appendix

|   |     |
|---|-----|
| Appendix.....   | 128 |
| Appendix 1: Supporting Information for Chapter 2..... | 129 |
| Appendix 2: Supporting Information for Chapter 3..... | 139 |
| Appendix 3: Supporting Information for Chapter 4..... | 143 |
| Appendix 4: Supporting Information for Chapter 5..... | 149 |

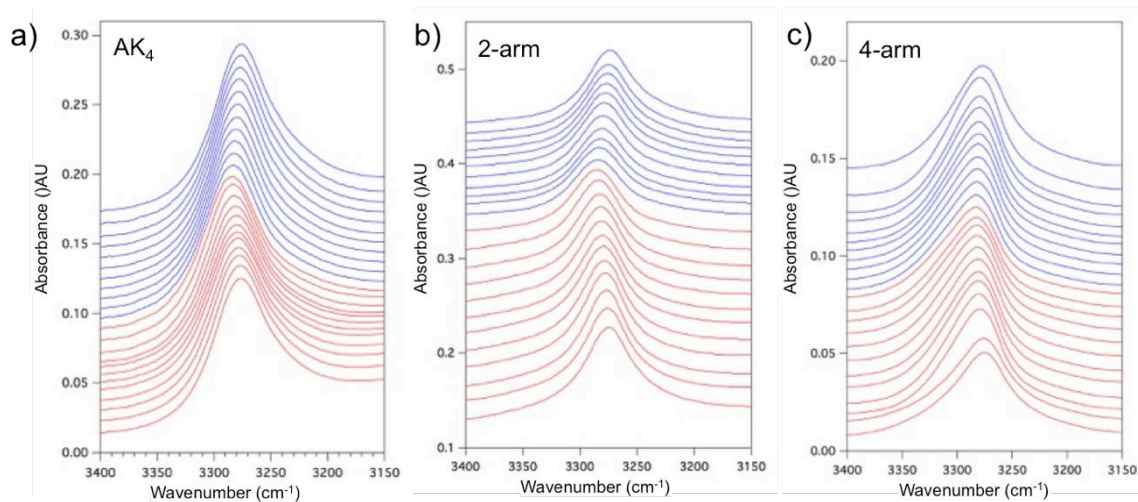
## Appendix 1: Supporting Information for Chapter 2

### Appendix 1.1



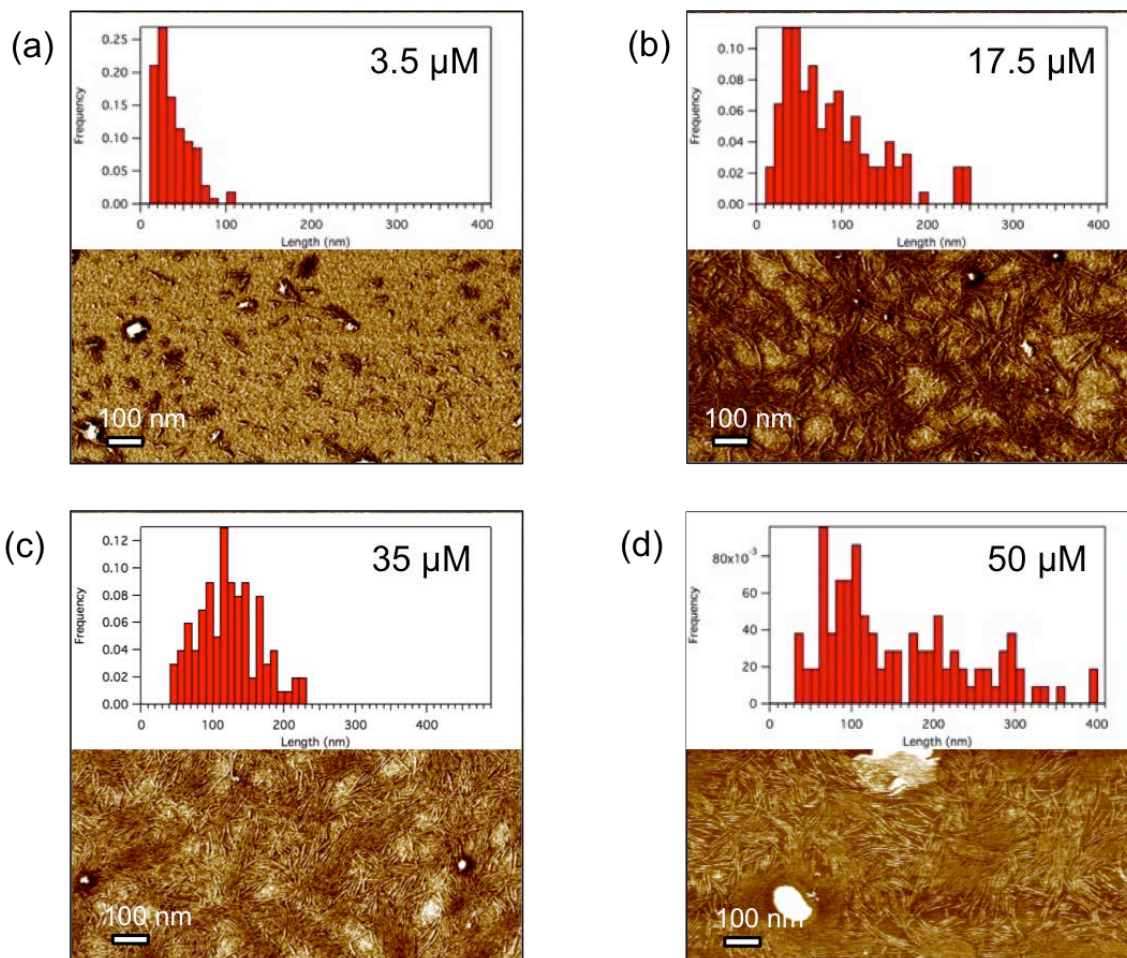
**A. 1.1.** (a) RP-HPLC spectrum of AK<sub>4</sub>-PEG conjugates with different degrees of conjugation in which the 4 peaks correspond to 1-arm with free PEG, 2-arm, 3-arm, and 4-arm conjugates respectively. (b) MALDI-TOF spectra of 2-, 3- and 4-arm conjugates collected, confirming the purity of materials used in this study.

## Appendix 1.2



**A. 1.2.** FTIR temperature studies showing the amide A region of a) bare CP (AK<sub>4</sub>), b) 2-arm conjugates, and c) 4-arm conjugates. Red traces and blue traces correspond to heating from 30 °C to 250 °C to cooling back to 30 °C at 20 °C interval.

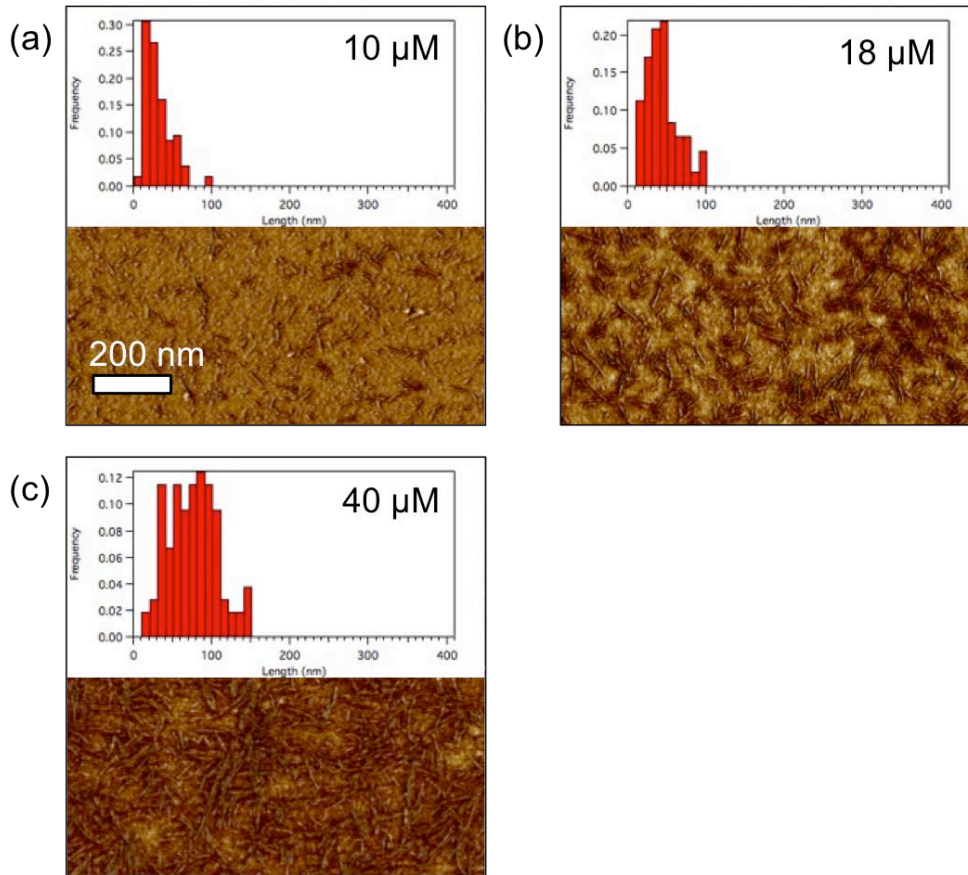
## Appendix 1.3



**A. 1.3.** Phase contrast AFM images and statistical length analysis of the 2-arm pc-CPNs spin-casted from toluene solutions at a) 3.5  $\mu\text{M}$ , b) 17.5  $\mu\text{M}$ , c) 35  $\mu\text{M}$ , and d) 50  $\mu\text{M}$ . The average length of the 2-arm CPNs is directly correlated to the solution concentration below 35  $\mu\text{M}$ . The growth of pc-CPNs is limited by the available space and therefore no significant increase in pc-CPN length is seen at high concentration. Due to fast rate of solvent removal by spin casting, only one layer of pc-CPNs is observed. Due to fast rate of solvent removal by spin casting, only one layer of pc-CPNs is observed.

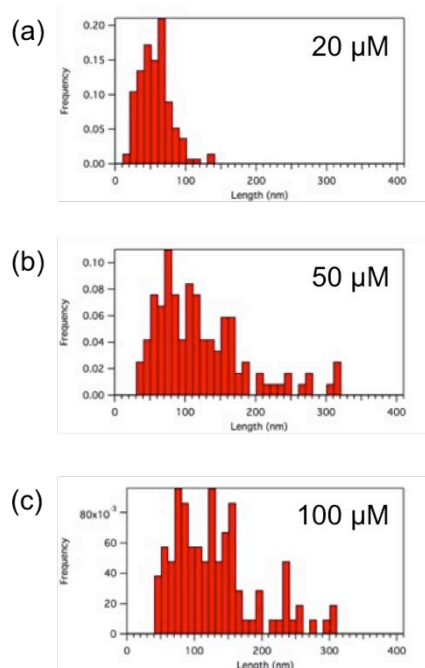


## Appendix 1.4



**A. 1.4.** Phase contrast AFM images and statistical analysis of the 3-arm pc-CPNs spin-casted from toluene solutions with different solution concentrations. A direct correlation between the pc-CPN length with solution concentration is observed.

## Appendix 1.5



**A. 1.5.** Statistical analysis of the 4-arm pc-CPNs spin-casted from toluene solutions with different solution concentrations at a) 20  $\mu\text{M}$ , b) 50  $\mu\text{M}$ , and c) 100  $\mu\text{M}$ . At high concentrations  $> 50 \mu\text{M}$ , the substrate is fully covered by pc-CPNs and thus limits the growth of longer nanotubes.

## Appendix 1.6

| 2-arm              |                 | 3-arm            |                | 4-arm             |                 |
|--------------------|-----------------|------------------|----------------|-------------------|-----------------|
| Concentration      | Length          | Concentration    | Length         | Concentration     | Length          |
| 3.5 $\mu\text{M}$  | 36 $\pm$ 19 nm  | 10 $\mu\text{M}$ | 31 $\pm$ 16 nm | 10 $\mu\text{M}$  | 14 $\pm$ 7 nm   |
| 10 $\mu\text{M}$   | 64 $\pm$ 42 nm  | 16 $\mu\text{M}$ | 45 $\pm$ 20 nm | 20 $\mu\text{M}$  | 50 $\pm$ 21 nm  |
| 17.5 $\mu\text{M}$ | 88 $\pm$ 54 nm  | 40 $\mu\text{M}$ | 102 $\pm$ 30nm | 50 $\mu\text{M}$  | 121 $\pm$ 60 nm |
| 35 $\mu\text{M}$   | 154 $\pm$ 86 nm |                  |                | 100 $\mu\text{M}$ | 126 $\pm$ 64 nm |
| 50 $\mu\text{M}$   | 161 $\pm$ 90 nm |                  |                |                   |                 |

**A. 1.6.** Summary of the lengths of pc-CPNs with different degrees of conjugation at various solution concentrations.

## Appendix 1.7 Theory Framework

The experimental observations suggest that both the binding energy and bending rigidity of the CPNs must be reduced as the degree and length of the conjugate arms increase. Here, we hypothesize that the PEG conjugated side arms effectively destabilize the nanotubes by introducing a free energy penalty ( $\Delta F_{PEG}$ ) into the binding free energy of the cyclic peptides ( $\Delta F_{CP}$ ). The axial free energy landscape of a unconjugated CP dimer has been studied in a previous work.<sup>1</sup> Here we use the basic features of this landscape and simplify it slightly without loss of generality. The most relevant feature of the energy landscape is the softening (decrease in the Young's modulus) as the intersubunit distance is increased.

The total free energy of the system ( $\Delta F$ ) can be written as:

$$\Delta F = \Delta F_{CP} - \Delta F_{PEG} \quad [1]$$

Due to steric repulsions and excluded volume interactions experienced by the polymer side arms under confinement, a tensile force is exerted on the cyclic peptide (CP) nanotube core stabilized by hydrogen bonds, which increases the intersubunit distance between the CPs. Since the characteristic free energy landscape of peptide assemblies involve van der Waals and electrostatics interactions that diminish (i.e. soften) with increasing intersubunit spacing,<sup>1</sup> this effectively leads to a decrease in the axial stiffness ( $E$ ) of the CPN core, which is directly correlated to its persistence length ( $l_p = EI / k_B T$ ). This observation is contrary to what's known for molecular brushes, which are known to stiffen by conjugation. This is a main difference between *supramolecules* vs. *macromolecules*, where the latter have a relatively inextensible, covalently bonded backbone and stiffen due to backbone tension. The energy landscapes for the 0-arm and 4-arm conjugated CPs are shown in Figure A.1.7a) and exhibit this reduction in the binding energy, shifting of the equilibrium spacing, as well as softening which characterized by the curvature near the equilibrium spacing.

To estimate the free energy penalty introduced by the conjugated polymer side arms, we approximate the conjugated CP confined between two subunits to that of a star polymer confined in a slit. Subsequently, we employ a simple Flory approach to express the entropic penalty term of the free energy expression.<sup>2</sup> Considering the slit spacing as an evolving parameter during the self-assembly process (initially infinite and decreasing until reaching equilibrium value during self-assembly), the entropic penalty of self-assembly is:

$$\Delta F_{PEG} = k_B T \left[ \frac{v(nN)^2}{R^2 d_s} + n \frac{Na^2}{d_s^2} \right] \quad [2]$$

where  $k_b$  is the Boltzmann constant,  $T$  is the temperature,  $v$  is the excluded volume coefficient,  $n$  is the number of arms,  $N$  is the number of monomers per arm,  $a$  is the monomer size,  $d_s$  is the slit separation, and  $R$  is the star radius. In Eq. 2, the first term in the right hand side is the contribution from the excluded volume interactions, and the second term is the compression energy of the arms. The effective slit spacing depends on the confinement degree of the arms that in turn depends on the number of arms. This is taken into account probabilistically, by considering that it will become increasingly difficult to avoid overlap as  $N$  is increased, which translates into greater entropic penalty for systems with greater  $N$ . The values for the excluded volume parameter, the monomer length and the monomer to molecular weight proportion have been extracted from a previous computational study of PEG.<sup>3</sup> The theory predicts a non-linear decrease in the binding free energy with the conjugation density, shown in the inset of Figure A.1.7a). The effective outcome of this finding is that conjugation should: *i*) reduce the stability of CPNs, *ii*) soften the CP-CP interactions and thereby reduce bending rigidity and as a results of (*i*) and *iii*) lead to CPs with lower propensity to assemble into longer tubes.

Assuming that the binding free energy of the unconjugated CPs ( $\Delta F_{CP}$ ) is not directly dependent on the arm size  $R$ , we can propose scaling laws and quantitative predictions that can explain the experimental observations. To calculate the equilibrium  $R$ , we minimized the free energy of the conjugated polymer  $\Delta F_{PEG}$ :

$$\frac{\partial \Delta F_{PEG}}{\partial R} = 0 \rightarrow R : n^{1/4} N^{3/4} d^{-1/4} \quad [3]$$

This result shows a strong dependence of  $R$  on the molecular weight of the side arms. However, the effect of the number of arms on  $R$  is very weak for the 2k Da system, suggesting minimal extension for short polymer conjugates.

As observed experimentally, and explained with simple theoretical concepts, increasing conjugation density progressively decrease the binding energy between polymer-peptide conjugates in nanotubes. This therefore opens possibilities for controlling the insertion of intruding polymer-peptide conjugates of lower polymer conjugation density within the nanotube self-assembled sequence. An example system would be mixed nanotubes consisting of 0-arm and  $n$ -arm conjugates. These intruding conjugates lower the overall energy of the nanotube and stabilize the system by increasing the local entropy at the locations of insertion. A mixed CPN is one that contains CPs with two different degrees of conjugation. This system can be modeled as a binary mixture of a-arm and b-arm conjugate CPs and the free energy of the system can be written as:

$$F_{ab} = k_B T \left[ N_a \ln \left( \frac{N_a}{N} \right) + N_b \ln \left( \frac{N_b}{N} \right) \right] + \frac{u_{ab}}{2} N_a + \frac{u_{bb}}{2} N_b + \left( u_{ab} - \frac{u_{aa} + u_{bb}}{2} \right) n_{ab} \quad [4]$$

where  $N_i$  is the number of  $i$ -arms conjugated CPs,  $N$  is the total number of CPs in the CPN,  $u_{ij}$  is the interaction energy between  $i$ -arm and  $j$ -arm conjugated CPs, and  $n_{ab}$  is the number of contacts between CPs with different conjugation. The first term on the right hand side of Eq. (7) corresponds to the mixing entropy and the last three terms correspond to the internal energy. In the following discussion we would consider  $a < b$  meaning that  $u_{aa} < u_{ab} < u_{bb}$  (the lower the number of conjugated arms the stronger the binding is).

The self-assembly sequence offers two possible extreme cases: (1)  $n_{ab} = 1$ , the system is segregated in two major domains of composed of all  $a$ -arms and all  $b$ -arms respectively, and (2)  $n_{ab} = N - 1$ , the  $a$ -arms and  $b$ -arms conjugated CPs self-assembly in an alternating fashion. The internal energy of both cases is a simple summation over the nanotube, yielding:

$$U^{(1)} = (u_{aa} + u_{bb}) \frac{(N-2)}{2} + u_{ab} \quad [5]$$

$$U^{(2)} = (N-1)u_{ab} \quad [6]$$

In order to find out which configuration is more energetically favorable, we look at the asymptotic limit for infinitely long nanotubes ( $N \rightarrow \infty$ ) of the quotient  $U^{(1)} / U^{(2)}$ :

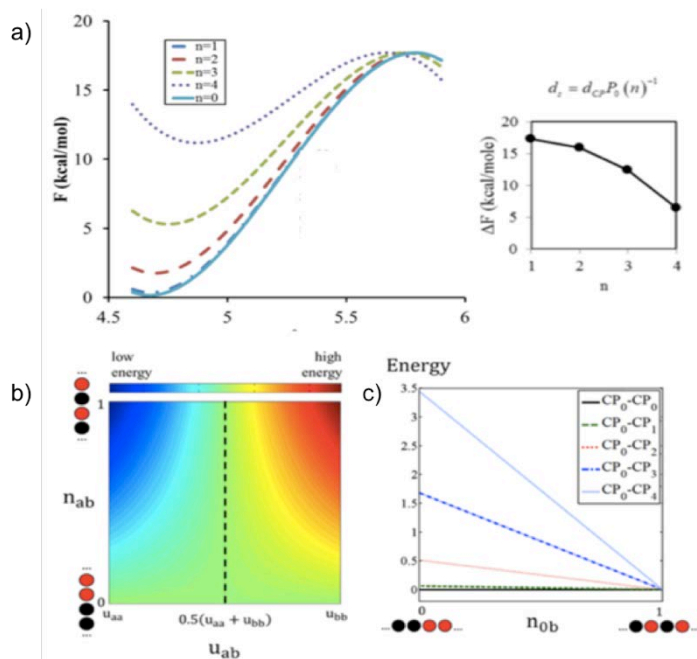
$$\lim_{N \rightarrow \infty} \left( \frac{U^1}{U^2} \right) = \lim_{N \rightarrow \infty} \left( \frac{(u_{aa} + u_{bb})}{2u_{ab}} \cdot \frac{(N-2)}{(N-1)} + \frac{1}{(N-1)} \right) = \frac{1}{2} \frac{(u_{aa} + u_{bb})}{u_{ab}} \quad [7]$$

The critical case where both configurations are equally favorable ( $U^{(1)} = U^{(2)}$ ) yields:

$$\lim_{N \rightarrow \infty} \left( \frac{U^1}{U^2} \right) = 1 \rightarrow u_{ab} = \frac{1}{2}(u_{aa} + u_{bb}) \quad [8]$$

If  $u_{ab}$  is larger than this arithmetic average threshold value (closer to  $u_{bb}$ ) then the system would tend to self-assembly into a CPN with two segregated domains, while if it is lower (closer to  $u_{aa}$ ) the system would form a CPN of alternating  $a$ -arms and  $b$ -arms conjugated CPs. The final configuration of a mixed CPN therefore depends on the cross interaction energy term ( $u_{ab}$ ) with respect to the self-interaction terms ( $u_{aa}, u_{bb}$ ). Figure 6B shows the free energy landscape of a CPN as a function of  $u_{ab}$  and the number of a-b contacts ( $n_{ab}$ );  $n_{ab} = 1$  corresponds to alternating sequences,  $n_{ab} = 0$  to phase segregation. The following parameters were used ( $N_a = N_b = 1000, u_{aa} = \Delta F_{00}, u_{bb} = \Delta F_{44}$ , where the

subindexes indicate the number of arms of the conjugated CPs used in the mix. The energy landscape resembles half of a hyperbolic paraboloid (horse saddle) and displays the same features as predicted in the theoretical analysis. For  $u_{ab} = 0.5(u_{aa} + u_{bb})$  the free energy difference between a phase segregated system ( $n_{ab} = 0$ ) and one with alternating sequence ( $n_{ab} = 1$ ) is negligible. However, the system would tend towards the alternating sequence configuration if  $u_{ab} \sim u_{aa}$  and towards the phase segregated system if  $u_{ab} \sim u_{bb}$ . We studied all possible cases of mixed nanotubes containing 0-arm and  $n$ -arm conjugated CPs. The self-interaction terms have been calculated previously for homogeneous nanotubes ( $u_{ii} = \Delta F_{ii}$ ). To calculate the cross interaction terms ( $u_{0b}$ ), we use the same methodology described to CPNs composed of alternating 0-arms and  $b$ -arms conjugated CPs. Specifically, introduction of a 0-arm CP effectively increases the slit spacing and reduces conjugation density along the length of the nanotube. All of the calculated values of  $u_{0b}$  lay closer to  $u_{00}$  than  $u_{bb}$ . According to our theoretical derivation this implies that alternating sequences are preferred by these systems. The free energy of the different mixed systems as a function of the self-assembled sequence ( $n_{0b}$ ) is shown in Figure A 1.7 c). We only considered the free energy differences between two extreme cases for different mixed systems; accordingly the free energies (Figure A 1.7c) were normalized (energy per CP) and shifted to facilitate visualization. An alternating sequence is always more favorable than segregation into two domains. The free energy difference between the two extreme scenarios increases as we increase the conjugation density of the insertion into the 0-arm CPs. The higher the difference between  $u_{aa}$  and  $u_{bb}$ , the stronger is the tendency of the system to self-assemble into an alternating sequence. This observation should generally hold for self-assembling systems with binary mixtures. By modifying conjugation order and conjugate chain length, it is possible to generate nanotubes with controlled distribution of subunits along the length of the nanotube.

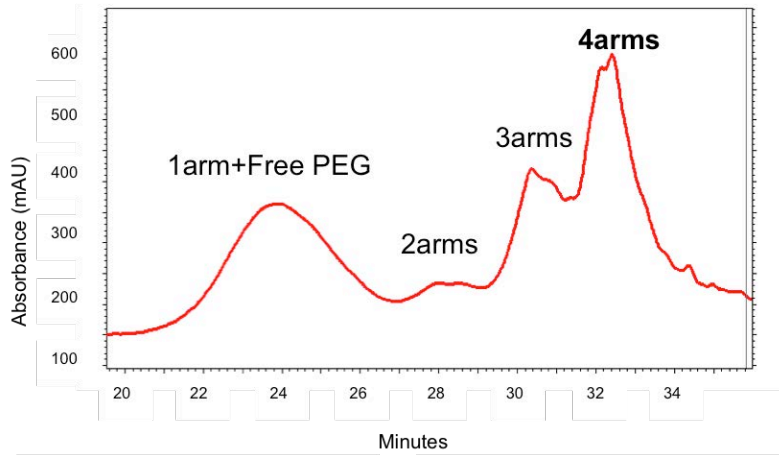


**A. 1.7.** a) Free energy as a function of sub-unit separation distance. b) Energy landscape and self-assembly sequences from mixtures of a-b arm polymer-cyclic peptides conjugates. Contour plot of the free energy surface of a mixed CPN. The number of a-b interfaces in the nanotube  $n_{ab}$  is normalized:  $n_{ab} = 0$  for phase segregated sequence,  $n_{ab} = 1$  for alternating sequence. c) Normalized free energy from mixtures of 0-arm and  $n$ -arm ( $n=1, 2, 3, 4$ ) conjugates.

- (1) Ruiz, L.; Keten, S. Multi-Scale Modeling of Elasticity and Fracture in Organic Nanotubes. *Journal of Engineering Mechanics*, 0, 371.
- (2) Sevick, E. M. Compression and Escape of a Star Polymer. *Macromolecules* 2000, 33, 5743-5746.
- (3) Lee, H.; de Vries, A. H.; Marrink, S.-J.; Pastor, R. W. A Coarse-Grained Model for Polyethylene Oxide and Polyethylene Glycol: Conformation and Hydrodynamics. *The Journal of Physical Chemistry B* 2009, 113, 13186-13194.

## Appendix 2: Supporting Information for Chapter 3

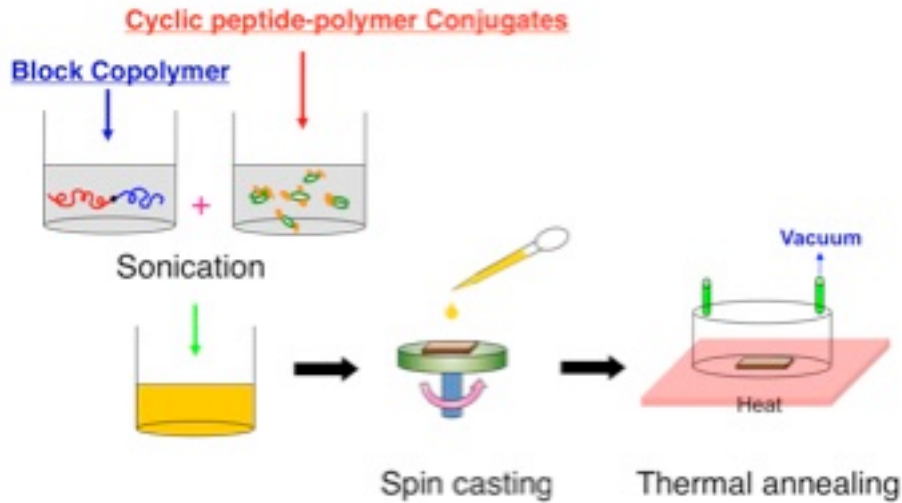
### Appendix 2.1



**A. 2.1.** Purification and characterization of AK<sub>4</sub>-PEG conjugates showing the RP-HPLC trace of PEG conjugation reaction mixtures, where 4 peaks are observed corresponding to AK<sub>4</sub>-PEG conjugates with 1, 2, 3, and 4 PEG chains attached respectively. The fraction collected between 32-34 min corresponds to AK<sub>4</sub>-4P2k (4arms), whose purify is confirmed via MALDI-TOF (Figure 2.1a) and RP-HPLC (Figure 2.1b).

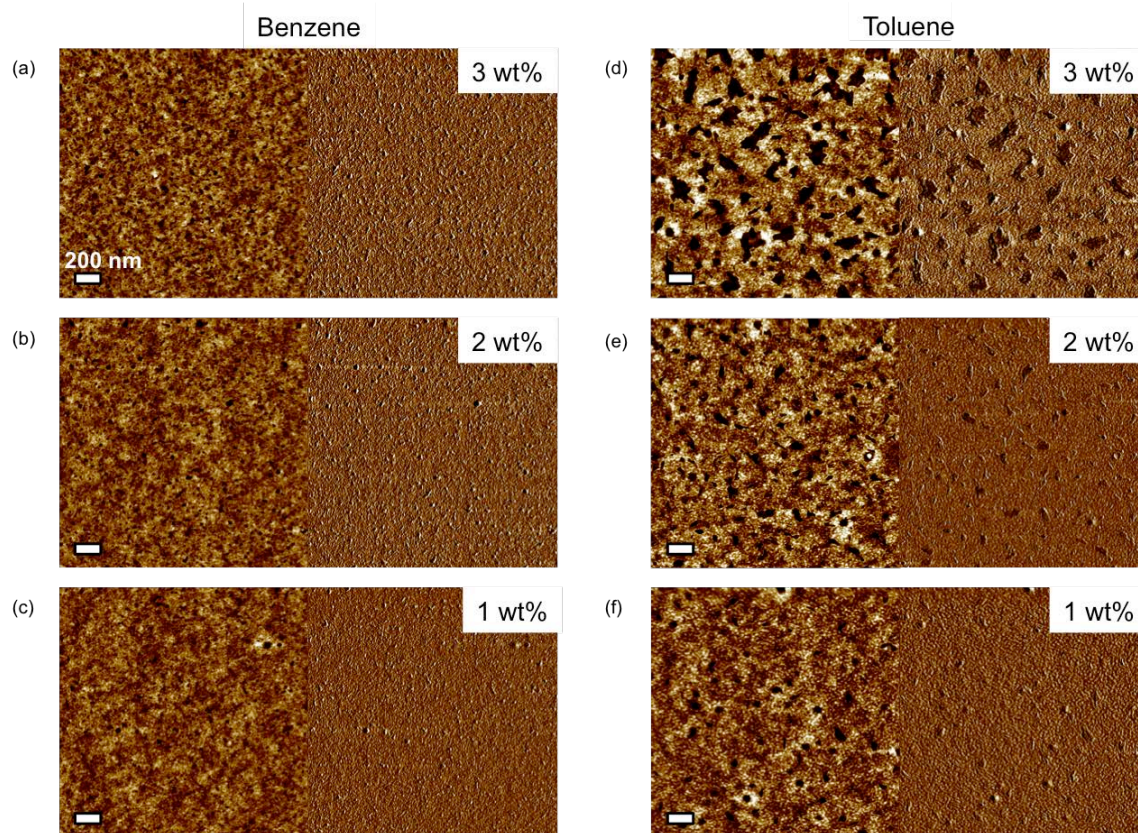


## Appendix 2.2



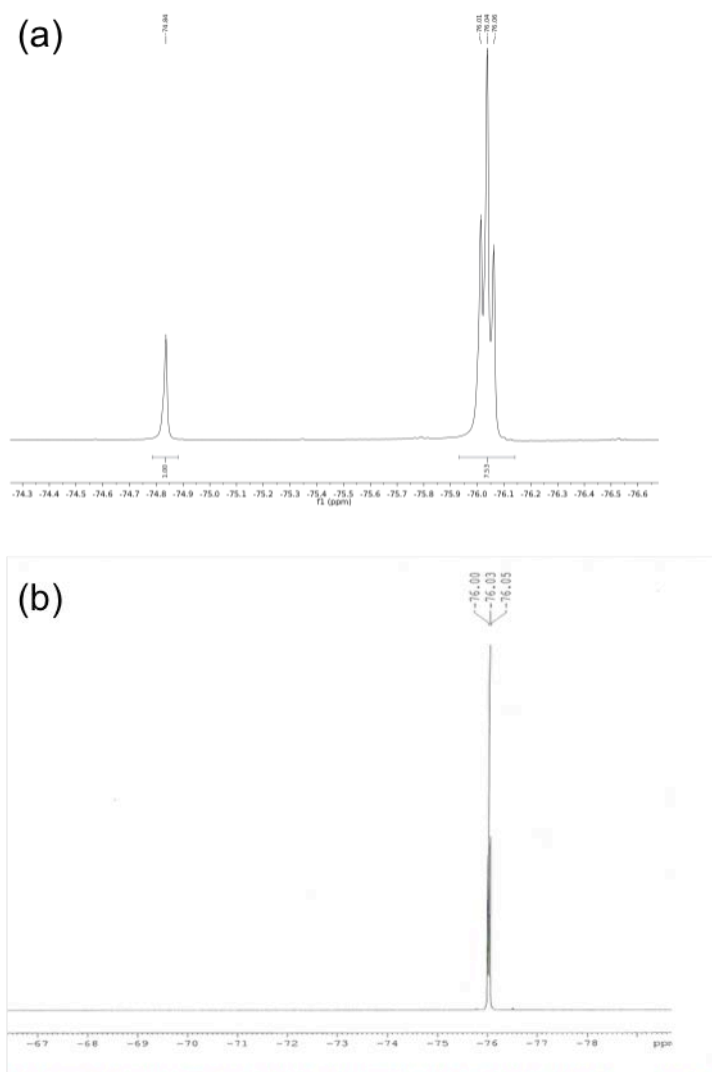
**A. 2.2.** Schematic showing the thin film fabrication process. PS-*b*-PMMA is pre-dissolved in selected solvent to make a stock solution at 10 mg/mL. Freshly lyophilized cyclic peptide-polymer conjugate (AK<sub>4</sub>-4P2k) powder is dissolved in the same selected solvent in a separate vial, and the stock solution is then slowly added to the AK<sub>4</sub>-4P2k solution. The combined mixture is then sonicated for 30 minutes, and then spin casted onto Si wafer surface modified with neutral brush layer ~ 12 nm at desired spinning speed. The samples are transferred to a vacuum oven for thermal annealing and slowly cooled afterwards.

## Appendix 2.3



**A. 2.3** Characterization of as-casted thin films from benzene and toluene solution. For good solvent benzene, no large aggregates are observed for  $f = 1-3 \text{ wt}\%$  as shown in Figure S2 a-c). In contrast, aggregates shown as darker regions in the phase images are observed for films casted from toluene (Figure S2 d-f). Moreover, the sizes of the aggregates are correlated to the value of  $f$ , demonstrating a concentration dependence of self-aggregation of AK<sub>4</sub>-4P2k conjugates in toluene solution.

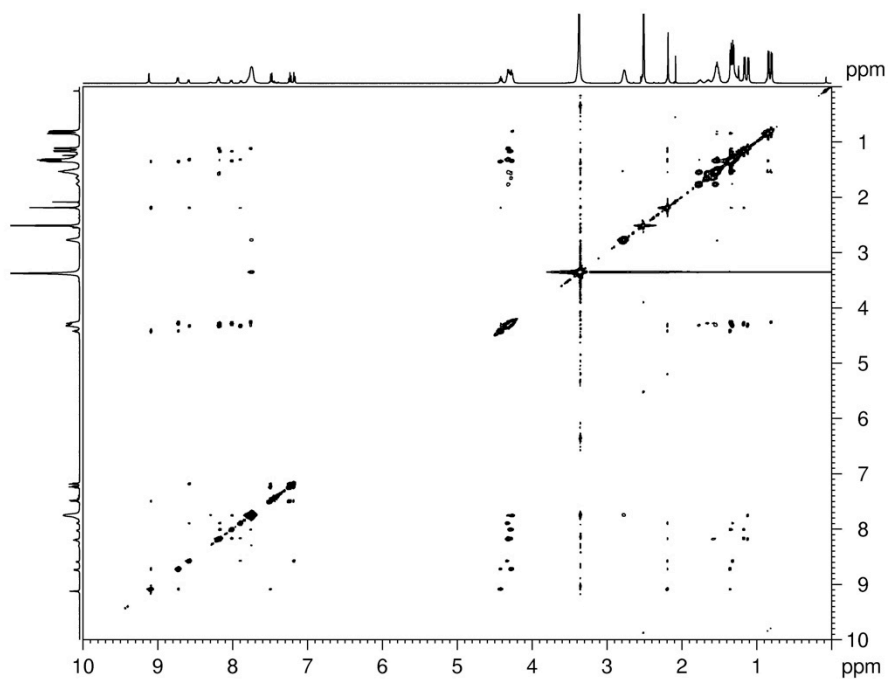
## Appendix 2.4



**A. 2.4.** <sup>19</sup>F NMR spectra of AK<sub>4</sub>-4P2k conjugates (a) post TFA vapor treatment and (b) first treated with TFA vapor and then thermally heated at 180 °C for 4 hours in vacuum. The triplet peak ~ -76 ppm corresponds to TFE and the single -74 ppm peak corresponds to TFA. The lack of the peak around ~ -74 ppm in (b) indicates that TFA molecules are mostly removed during thermal treatment to the level below the detection limit of the NMR. From the integrated areas of TFA and TFE in (a), the amount of TFA in the sample can be estimated.

## Appendix 3: Supporting Information for Chapter 4

### Appendix 3.1



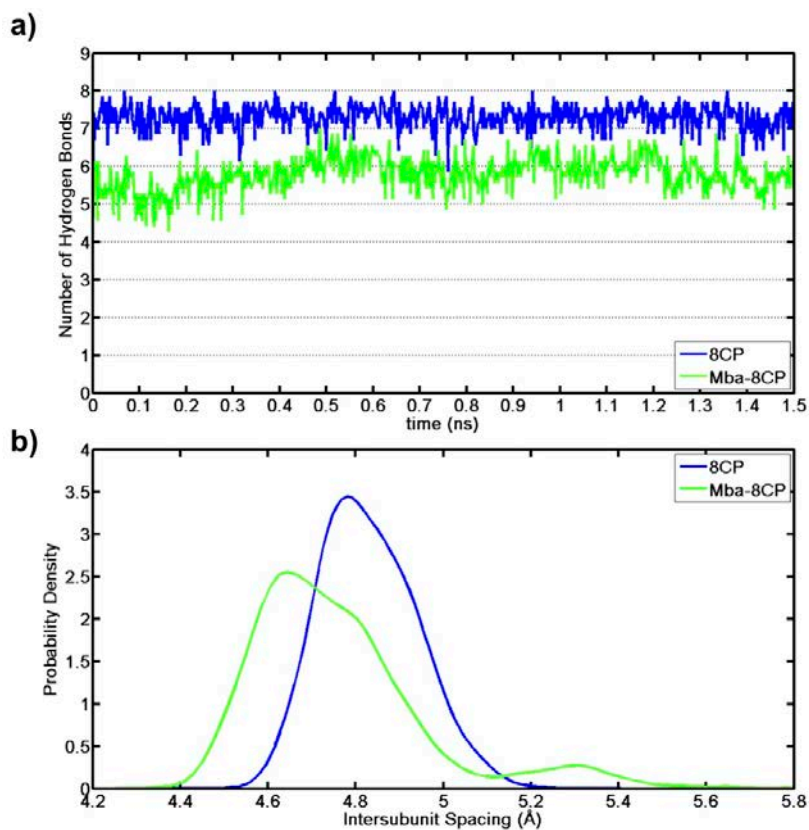
**A. 3.1.** 2D NOESY spectra in  $d_6$ -DMSO of molecularly dissolved Mba-8CP ( $\sim 4\text{mg/mL}$ ). Experiment was run at room temperature for 1 hour.

### Appendix 3.2 Molecular Dynamics Simulations

Molecular Dynamics Simulations: In previous studies, different computational approaches such as MD3 or computational quantum mechanics methods<sup>4</sup> have been successfully applied to the study of CPNs presenting excellent agreement with structural parameters of the nanotubes obtained from experimental studies, such as intersubunit distance, backbone hydrogen bond lengths or unit cell parameters. For this study, we selected molecular dynamics as the preferred approach for several reasons, namely: (i) the suitability of the MD protocol as evidenced by widespread application of this technique in earlier studies of CPNs for structural characterization and stability assessment (ii) ability to obtain longer time scale dynamical data in explicit solvent conditions, providing insight into overall self-assembly metrics and stability of the CPNs arising from long-range interactions (iii) excellent overall agreement of earlier MD studies with experimental evidence, including measurements of pore size, intersubunit distances, and crystal structure lattice constants (iv) the flexibility in examining CPN structure in non-periodic conditions, which are more relevant for self-assembly in solution as opposed to crystal formation.

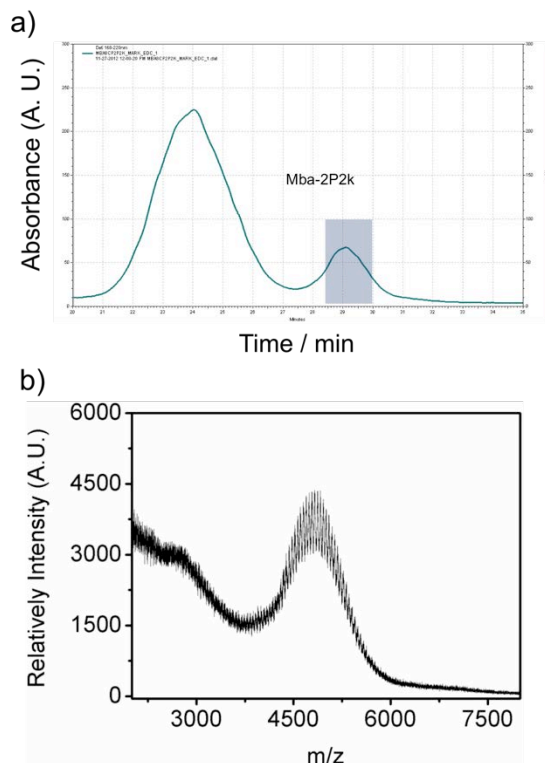
Initial coordinates for the CP subunit structures were taken from optimized geometries calculated using MM+ force field in HyperChem. Molecular Dynamics simulations were carried out in Materials Studio using the *ab-initio* based COMPASS<sup>1</sup> force field. In order to explore the conformational space and find the minimum energy configuration of the CP monomers in the tubular morphology, three subunits were stacked and subjected to five annealing cycles with a temperature range of 298K to 600K in the NVT ensemble, where each cycle was followed by minimization calculations. The final configuration of the central subunit was selected to build the CPNs used for equilibration simulations. The structures computed from these final equilibration runs were used for the comparative analysis. CPNs were composed of eight subunits stacked in an antiparallel fashion. These simulations were carried out in an isothermal-isobaric ensemble (NPT) with the Berendsen method and the Nose thermostat to control pressure and temperature at 1 atm and 298 K respectively. The system is solvated in explicit water and periodic boundary conditions are employed for a cubic box that is 50Åx30Åx30Å. To calculate the electrostatic interactions and the Van der Waals forces, we use the Ewald summation method with a repulsive cutoff of 6 Å and a cutoff distance of 12.5 Å. The time-step is fixed to 1 fs and the total duration of the simulations is 1.5 ns. Post-processing was done using Visual Molecular Dynamics (VMD)<sup>2</sup> and .tcl scripts. The cutoff distance for the hydrogen bonds was 3.4 Å and the minimum D-H-A angle for bond formation is taken as 130°. The inter-subunit distance was calculated as the center of mass distance between the alpha-carbon atoms of each subunit. For all calculations, measurements are taken every 2 ps, excluding the first 200 ps of the equilibration runs.

### Appendix 3.3



**A. 3.3** Time history of the average number of interring backbone hydrogen bonds. The number of H-bonds remains stable during the simulation for both cases, with a lower average value for Mba-8CP than the 8CP nanotubes. Intersubunit distance distribution (b) is comparable in both cases and agree with reported experimental values (4.7-4.8 Å) for CPNs.

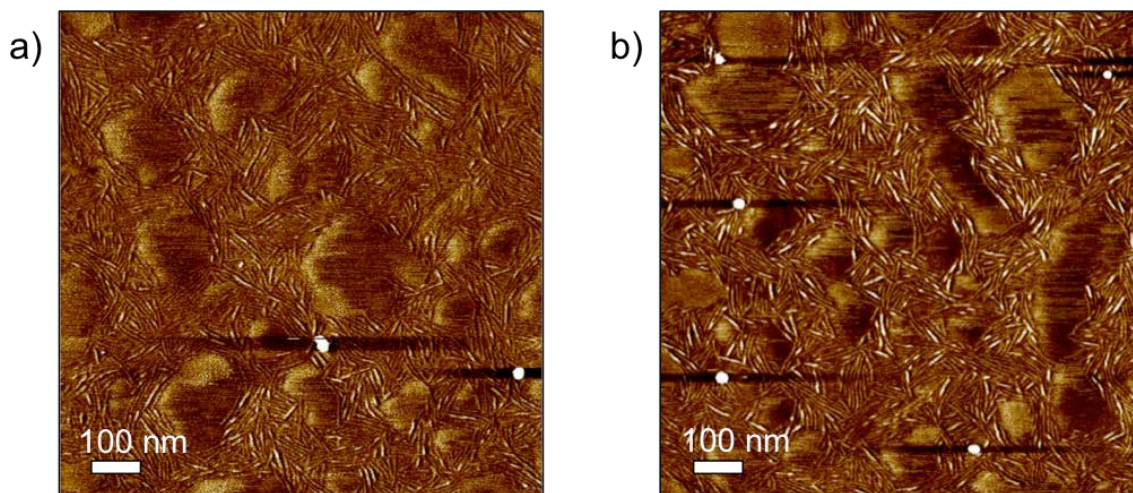
### Appendix 3.4.



**A. 3.4.** a) RP-HPLC of PEG and Mba-8CP conjugation reaction mixture using acetonitrile and water mixing solvent containing 0.1 % TFA as eluent. The spectrum is separated into two independent peaks, corresponding to Mba-8CP conjugates with different numbers of PEG chains attached per Mba-8CP. The first coming out peak is assigned to free PEG and Mba-8CP attached one PEG chain. The second peak is confirmed to be Mba-8CP with two PEG chains. In order to guarantee the purity of Mba-2P2k conjugate, we only collect fractions of the second peak as indicated by the highlighted rectangle. b) MALDI-TOF mass spectrum of Mba-2P2k used in present study, confirming the purity of the material.



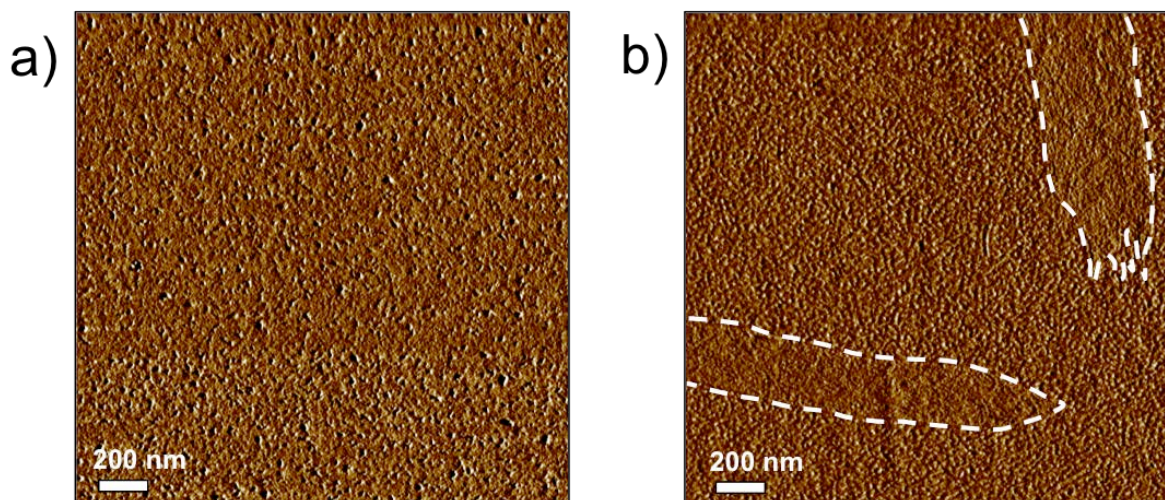
### Appendix 3.5.



**A. 3.5.** AFM phase images of Mba-pc-CPNs formed from 50  $\mu\text{M}$  THF solution spin casted at a) 500 rpm; and b) 5000 rpm, respectively. No obvious differences in the length of the nanotubes can be seen between the two samples due to high evaporation rate of the casting solvent, tetrahydrofuran (THF). Thus, all the samples were spin-casted at 500 rpm under ambient condition.



### Appendix 3.6

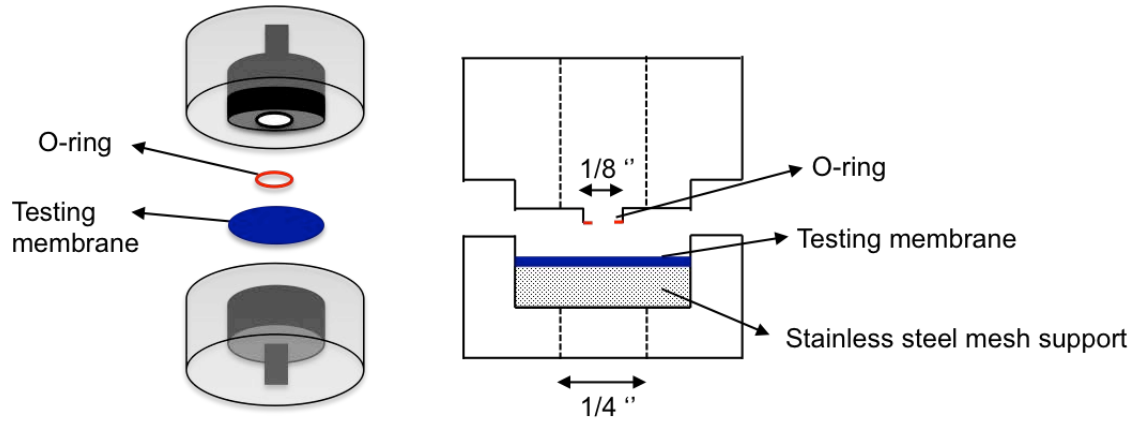


**A. 3.6.** AFM phase images of 1 wt% Mba-2P2k conjugates and PS-*b*-PMMA blends casted from a) chloroform; and b) toluene, respectively. The highlighted regions in b) are large aggregates of Mba-2P2k pre-formed in solution.

- (1) Sun, H. COMPASS: An ab Initio Force-Field Optimized for Condensed-Phase Applications Overview with Details on Alkane and Benzene Compounds. *The Journal of Physical Chemistry B* **1998**, *102*, 7338-7364.
- (2) Humphrey, W.; Dalke, A.; Schulten, K. VMD: Visual molecular dynamics. *Journal of Molecular Graphics* **1996**, *14*, 33-38.

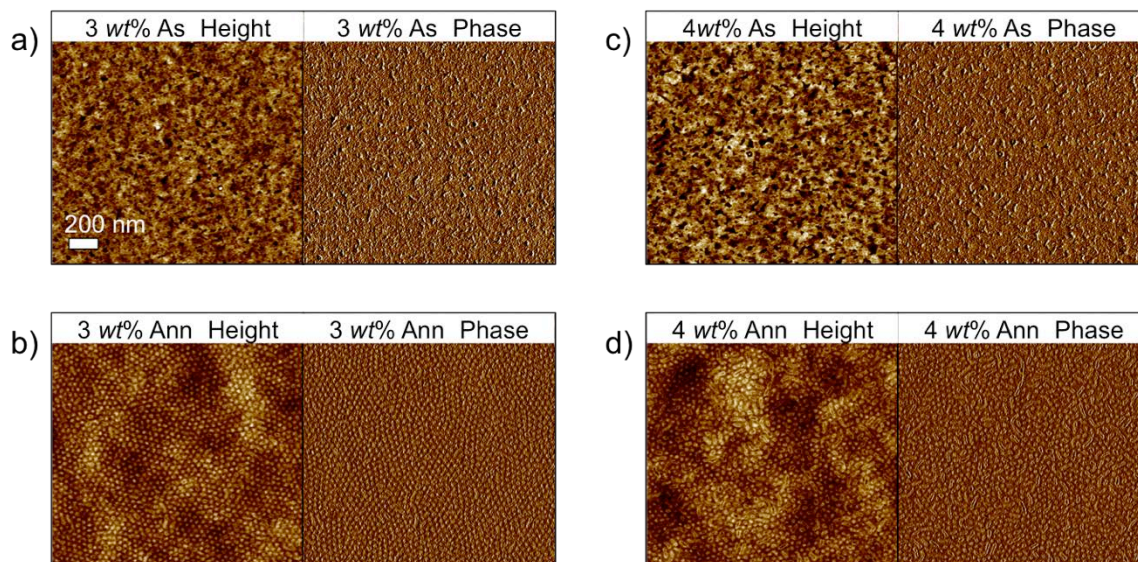
## Appendix 4: Supporting Information for Chapter 5

### Appendix 4.1



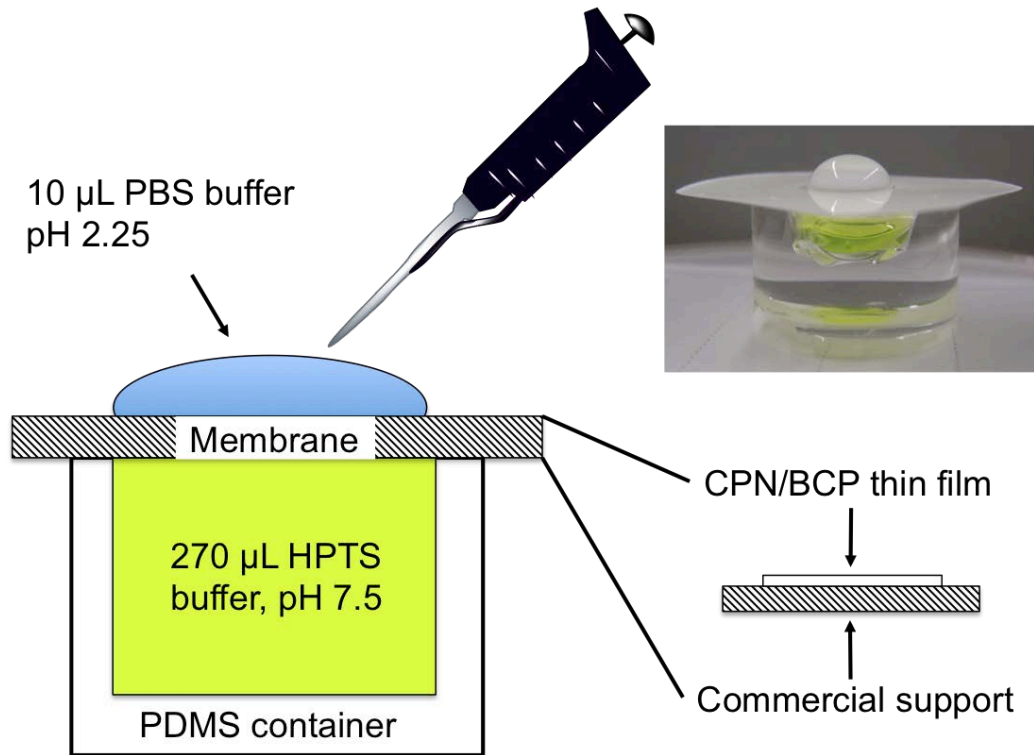
**A. 4.1.** Schematic representation of the internal structure of the customized membrane holder (not to scale). Polytetrafluoroethylene (PTFE, “Teflon”) is used to construct the holder body while the stainless steel is used for tubings and clamping screws (not shown). The diameter for the input/output fitting and adapter is 1/4 ” and the actual testing area is set by the o-ring with external diameter 1/8 ” and internal diameter 0.12 ”.

## Appendix 4.2



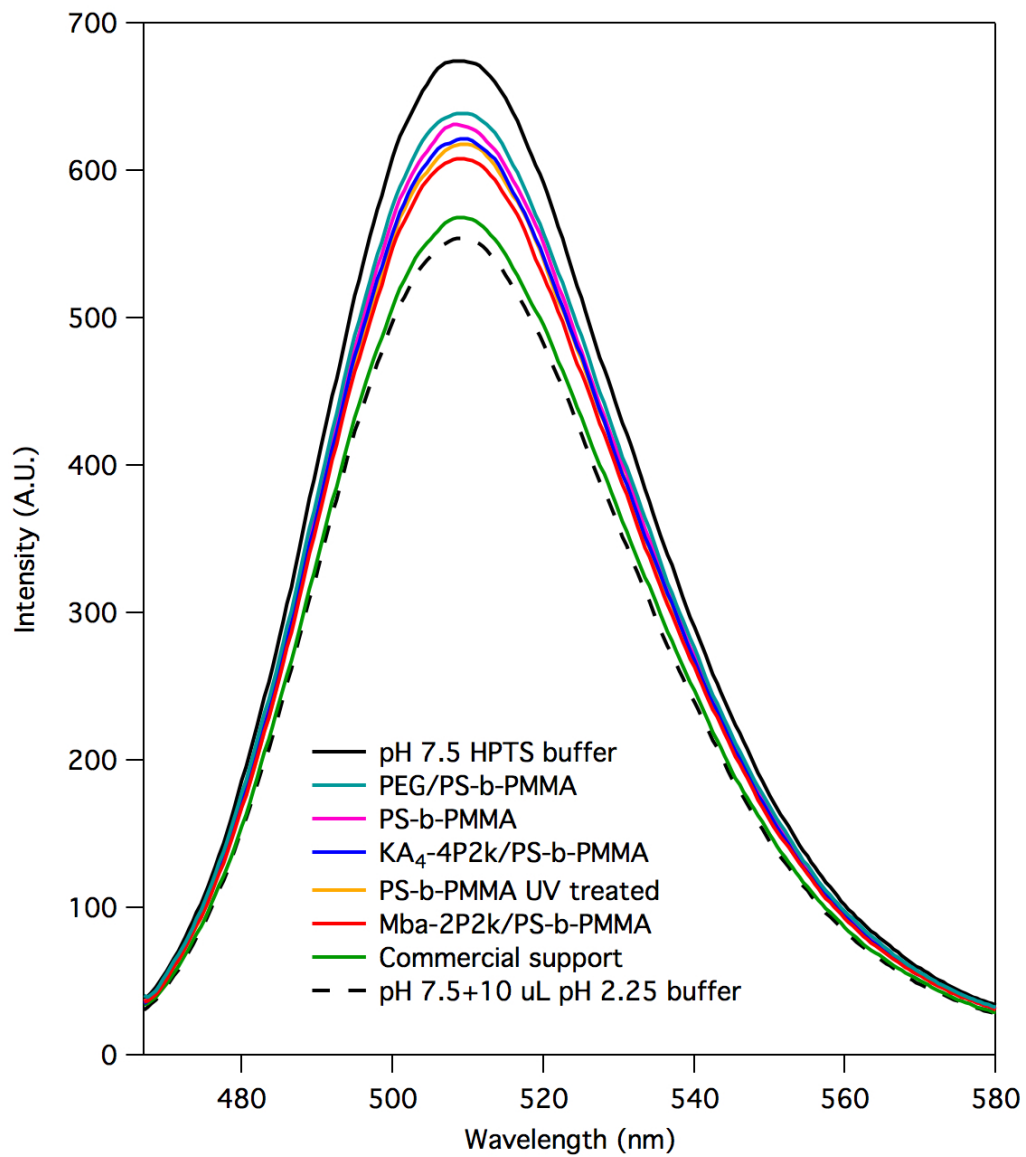
**A. 4.2** AFM images of blends of unmodified CPN, AK<sub>4</sub>-4P2k, and PS-*b*-PMMA matrix at different loading amounts after spin casting (“As”) and after thermal annealing (“Ann”). No obvious morphological difference is observed for the as-prepared samples as shown in a) and c). However, overloading of the conjugates results in excessive nanotubes lay parallel at the polymer/air interface.

### Appendix 4.3



**A. 4.3.** Schematic representation of the ion transport setup. Due to the hydrophobic nature of the CPN/BCP thin film, the pH 2.25 PBS buffer has a high contact angle when placed on top of our membrane. This simple method can be used to assess the integrity of the tested membrane. If defects are present, the PBS buffer droplet will spread out quickly.

## Appendix 4.4



**A. 4.4.** Fluorescence intensity of the HEPES buffer 5 minutes after treatments with different membranes.